COMPUTER-AIDED-DESIGN OF SATURATED MAGNETIC LENSES FOR ELECTRON MICROSCOPES

A THESIS SUBMITTED FOR THE DEGREE
OF
DOCTOR OF PHILOSOPHY

AT THE
UNIVERSITY OF ASTON

BY

ANAM SAMI AL-NAKESHLI, B.Sc., M.Sc.

DEPARTMENT OF MATHEMATICS AND PHYSICS

FEBRUARY 1986

COMPUTER-AIDED-DESIGN OF SATURATED MAGNETIC LENSES FOR ELECTRON MICROSCOPES

PhD THESIS,1985

UNIVERSITY OF ASTON IN BIRMINGHAM, UK

BY

ANAM SAMI AL-NAKESHLI

Summary

In the last few years, there has been considerable interest in using saturated magnetic objective lenses in high resolution electron microscopes. Such lenses, in present commercial electron microscopes, are energized either by conventional or superconducting coils. Very litle work, however, has been reported on the use of conventional coils in saturated magnetic electron lenses. The present investigation has been concerned with the design of high flux density saturated objective lenses of both single and double polepiece types which may be energized by conventional coils and in some cases by superconducting coils. Such coils have the advantage of being small and capable of carrying high current densities. The present work has been carried out with the aid of several computer programs based on the finite element method. The effect of the shape and position of the energizing coil on the electron optical parameter has been investigated. Electron optical properties such as chromatic and spherical aberration have been studies in detail for saturated single and double polepiece lenses. Several high flux density coils of different shapes have been investigated. The choice of the most favourable coil shape and position subject to the operational requirements, has been studied in some detail. The focal properties of such optimised lenses have been computed and compared .

Key words

Saturated magnetic lenses, Finite element method, Axial flux density, High voltage electron microscopy, Superconducting lenses.

ACKNOWLEDGMENTS

I am greatly indebted to Professor T. Mulvey for his supervision, useful suggestions and patient guidance throughout my work. I am particularly most grateful to Mrs. B. Lencova of the Institute of Scientific Instruments, Czechoslovak Academy of Sciences, Brno, Czechoslovakia for invaluable assistance and permission to use her computer program. The helpful discussions, continuous encouragement and reading of manuscript of this thesis by Dr. S. M. Juma are deeply appreciated. I am also very grateful to Mrs. H. C. Yin for the useful discussions and for her permission to use her computations. My sincere thanks are due to my colleagues, Mrs. K. Tahir, Mr. A. Al-Amir and Dr. G. L. Mair for the stimulating comments and consultations on various aspects of the project. I acknowledge the help given to me at various stages of my work by Mr. A. E. Marriott-Reynolds and the technical staff of the Physics Department, Computer Centre and Photography Unit in Aston University. Finally, I would like to thank the University of Al-Mustansiriyah in Baghdad, Iraq for the financial support during the course of this work.

CONTENTS

LIST OF TABLES

Table Title Page

LIST OF FIGURES

Figure Title Page

Figure Title Page

LIST OF SYMBOLS

A	Cross-sectional area of the energizing coil (m^2)
A'	Conducting cross-sectional area of one turn of the coil (m^2)
a	Radius of a spherical polepiece
B	Magnetic flux density (Tesla T)
B_{coil}	Axial flux density due to exciting coil (Tesla T)
B_{Fe}	Axial flux density due to iron magnetization (Tesla T)
B_m	Maximum (peak) flux density (Tesla T)
B_{pf}	Flux density at the poleface (Tesla T)
B_z	Axial flux density (Tesla T)
C_c	Chromatic aberration coefficient
C_s	Spherical aberration coefficient
D	Axial bore diameter of a polepiece
D_1, D_2	Axial bore diameters in asymmetrical double polepiece lens
D_m	Mean axial bore diameter of asymmetrical double polepiece lens [$D_m = (D_1 + D_2)/2$]
d_1	Inner diameter of a coil
d_2	Outer diameter of a coil
d_m	Mean diameter of a coil [$d_m = (d_1 + d_2)/2$]
F	Focal point
f_o	Objective focal length
H	Magnetic field strength (A/m)
I	Electric current (ampere A)
k	Scaling factor
L	Geometrical parameter of a double polepiece lens
N	Number of turns of a coil
NI	Excitation of energizing coil (ampere-turns A-t)
P	Power (watt W)

S	Air gap width separating two polepieces
s	Axial thickness of a coil
V	Accelerating voltage (Volt V)
V_r	Relativistically corrected accelerating voltage (Volt V)
$NI/V_r^{\frac{1}{2}}$	Lens excitation parameter
W	Halfwidth of the axial field
z	Optical axis
z_F	Focal distance
λ	Electron wavelength
σ	Current density (= I/A')
ρ	Electrical resistivity (m)
δ	Spatial resolution [$\delta = 0.7(C_s \lambda^3)^{1/4}$]
γ	Packing factor
μ_o	Permeability in vacuum ($4\pi \times 10^{-7}$ H/m)
μ_r	Relative permeability
θ	Polepiece taper angle
ϕ	Magnetic flux
η	Ratio of charge e to rest-mass m_o of the electron ($e = 1.60 \times 10^{-19}$ C, $m_o = 9.11 \times 10^{-31}$ kg, $\eta = 1.76 \times 10^{11}$ C/kg)

1. INTRODUCTION

Various kinds of electron-optical instruments are now common and necessary tools in almost all contemporary technical areas. The electron microscope is possibly the most important electron-optical instrument and is manufactured in different types such as the conventional transmission electron microscope (TEM), high voltage electron microscope (HVEM), scanning electron microscope (SEM) and the scanning transmission electron microscope (STEM). There has been considerable interest in the last few years, in using high flux density magnetic electron lenses particularly in HVEM.

1.1 MAGNETIC ELECTRON LENSES

Magnetic lenses are chiefly used in two ways, to form focused electron beam or "probes", namely a demagnified image of a distant electron source, or to form a highly magnified image of a small object placed near the focal point of the lens. The most critical component in any electron microscope is usually the objective lens. The design and focal properties of the objective lens determine the main characteristics of the electron microscope. The principal defect of electron objective lenses, spherical aberration, has the effect of limiting the resolution. With the increasing need for powerful analytical electron-optical instruments the design of magnetic lenses of low aberration coefficients is of considerable interest. To improve the resolution of an electron microscope, its objective lens must have very small aberration coefficients and, mechanically, meet high tolerances. As a general rule, a high resolution magnetic objective lens requires an axial field of high peak flux density and narrow field distribution i.e. small halfwidth. The following is a brief account of the various types of magnetic electron lenses.

1.1.1 IRON-FREE LENSES

The iron-free coil is the simplest form of a magnetic electron lens. It consists of either a wire or a tape winding. In the early days of electron optics and electron microscopy, iron-free solenoids were in fairly common use. Interest in the properties and advantages of iron-free magnetic lenses has revived as increased demands are being placed on superconducting coils (Dietrich 1976) and water-cooled mini-lenses (Mulvey 1974a) for conventional forms of electron-optical systems.

The magnetic field generated by a coil depends on its shape and excitation. The main factor that limits the field of the coil is the current density σ that can be supported in the windings. The electron-optical properties of the various lenses discussed in the present work have therefore been investigated in terms of σ . The high flux density lenses under consideration can be operated at high current densities which can be achieved by suitably cooled conventional coils and in some cases by superconducting coils.

Suitably water cooled coils can be neither bulky nor costly. The coolant should be in direct contact with the windings which are isolated both thermally and mechanically from the surrounding magnetic structure and hence from the electron-optical column. Wire coils are wound with a metallic conductor, usually copper, surrounded by an insulating coating. The term "insulating" refers to both thermal and electrical properties. Tape coils made from copper insulated by a thin Mylar tape can be constructed with high symmetry and produce high flux densities when operated at current densities in the order of 10^4 A/cm^2 (Mulvey 1974a, 1982). These considerable benefits are obtained largely at the cost of increased power input to the coil. In order to understand this, consider a coil of rectangular cross-section, d_1 and d_2 being its inner and outer diameter respectively and of axial thickness s. The electrical power P in Watt required to energize the coil is given by

$$P = \pi \rho \, d_m \sigma \, (NI) \tag{1.1}$$

where ρ = electrical resistivity of the conductor in Ω m; $d_m = (d_1 + d_2)/2$, the mean diameter in m; σ = current density in A/m^2; NI = coil excitation in ampere-turns (A-t), N being the number of turns of the coil and I the current passing through it. The packing factor, γ can be defined as the ratio of NA' the current-carrying cross-sectional area to $(d_2 - d_1)s/2$ the total cross-sectional area i.e.

$$\gamma = NA'/[(d_2 - d_1)s/2] \tag{1.2}$$

where A' is the conducting cross-sectional area of one turn. Therefore, it follows from equation (1.2) that the current density σ (= I/A') in a coil can be written in the following form ,

$$\sigma = NI/NA' = NI/ \gamma \, [(d_2 - d_1)s/2] \tag{1.3}$$

It is seen from equation (1.3) that for a fixed lens excitation NI, by decreasing the size of the lens so as to reduce the focal length and aberrations the current density σ will be increased. In terms of the packing factor γ, the total power P is given by

$$P = \pi \rho (d_2 + d_1)(NI)^2/(d_2 - d_1)s\gamma \qquad (1.4)$$

Typical values of γ are 0.65 and 0.9 for wire and tape coil respectively. Thus a tape coil reduces the power required to produce a specific excitation. Equations (1.1) and (1.4) have been used in this investigation for determining the power required to energize the coils.

The flat-helical coils are an important class of solenoidal lenses which are of great theoretical and practical interest. Calculations of Bassett and Mulvey (1969) indicated that the axial field distribution produced by a flat thin helical coil (pancake lenses) can lead to an appreciably low spherical aberration coefficient C_s. However, there are many difficulties in the practical realisation of such a lens. The design of flat-helical iron-free coils have been investigated by Marai (1977) and Mulvey and Wallington (1973) for absolute minimum spherical aberration parameter $C_sB_m/V_r^{\frac{1}{2}}$ i.e. for a constant maximum flux density B_m; V_r being the relativistically corrected accelerating voltage. Under these conditions a coil ratio of axial thickness s to mean diameter d_m, $s/d_m = 0.1$ and outer to inner diameter d_2/d_1 = infinity appears to be an optimum. For larger values of s/d_m, the spherical aberration parameter rises rapidly. The main difficulty in the practical realisation of such a coil is that it requires a very high current density. It should be noted that the analyses of Marai (1977) and of Mulvey and Wallington (1973) assume that the current density in the windings is not limited. In the present work however, the computations have been carried out for a given limiting current density in practical coils. It can be shown for example that for a given excitation parameter $NI/V_r^{\frac{1}{2}}$, the maximum flux density B_m at the centre-plane of an iron-free coil, operated at a constant current density σ , varies with $V_r^{1/4}$.

Some metals (eg. lead Pb, tin Sn, niobium Nb, indium In, vanadium V and zinc Zn), alloys (eg. niobium-zirconium, Nb-Zr, niobium-titanium, Nb-Ti) and compounds (eg. niobium-tin, Nb_3Sn) possess the interesting property of losing all electrical resistance (zero-resistance state) below a certain critical temperature, typically a few degrees Kelvin. Coils wound of superconducting wire or tape can produce very high fields when immersed in a liquid helium bath (4 K). The coils can be operated at current densities, of the order of 10^6 A/cm^2; a very high value compared with the current densities (200 A/cm^2) at which conventional lenses are operated. However, in the present investigation attention has been concentrated on the use of suitably cooled tape-coils operated at a current density of 20000 A/cm^2, i.e. at the beginning of the range of current density where superconducting coils would certainly be needed.

1.1.2 DOUBLE POLEPIECE LENSES

The most common form of magnetic lens is the conventional symmetrical double polepiece lens. Since the invention of the electron microscope in the 1930's, the main features of the conventional double polepiece magnetic electron lenses have remained basically the same.

A typical design of a conventional symmetrical double polepiece magnetic electron lens is shown in figure 1.1a. It consists of a large coil of N turns usually wound with insulated copper wire carrying a stabilized current I, an iron circuit and two polepieces of axial symmetry made of ferromagnetic material. An axial field is created in the air gap S, separating the two polepieces of plane parallel faces, by means of the coil. The coil is usually kept away from the polepieces to reduce the dependence of the lens properties on imperfections in the coil. The air gap S is usually small so as to produce a high local flux density. Coaxial circular holes are bored in the two polepieces with their axis perpendicular to the faces to allow passage for the electron beam. The lens geometry is usually defined by the width S of the air gap and the diameter D of each bore.

The iron circuit is continuous except for the air gap where the field is concentrated. The otherwise uniform axial magnetic field in the air gap S (figure 1.1b) is disturbed near the axial bores; this gives rise to a lens action, the properties of which are expressed in terms of the gap-bore diameter ratio, S/D. When the axial bores in the two accurately machined polepieces are equal, the axial field of the lens is symmetrical about the mid plane of the gap and the peak field B_m occurs in the middle of the gap.

The design parameters and the focal properties of unsaturated conventional lenses are well known; see, for example, the surveys of Lenz (1982) and of Riecke (1982). Dugas et al (1961), Durandeau and Fert (1957), Fert and Durandeau (1967), Mulvey (1953) and Mulvey and Wallington

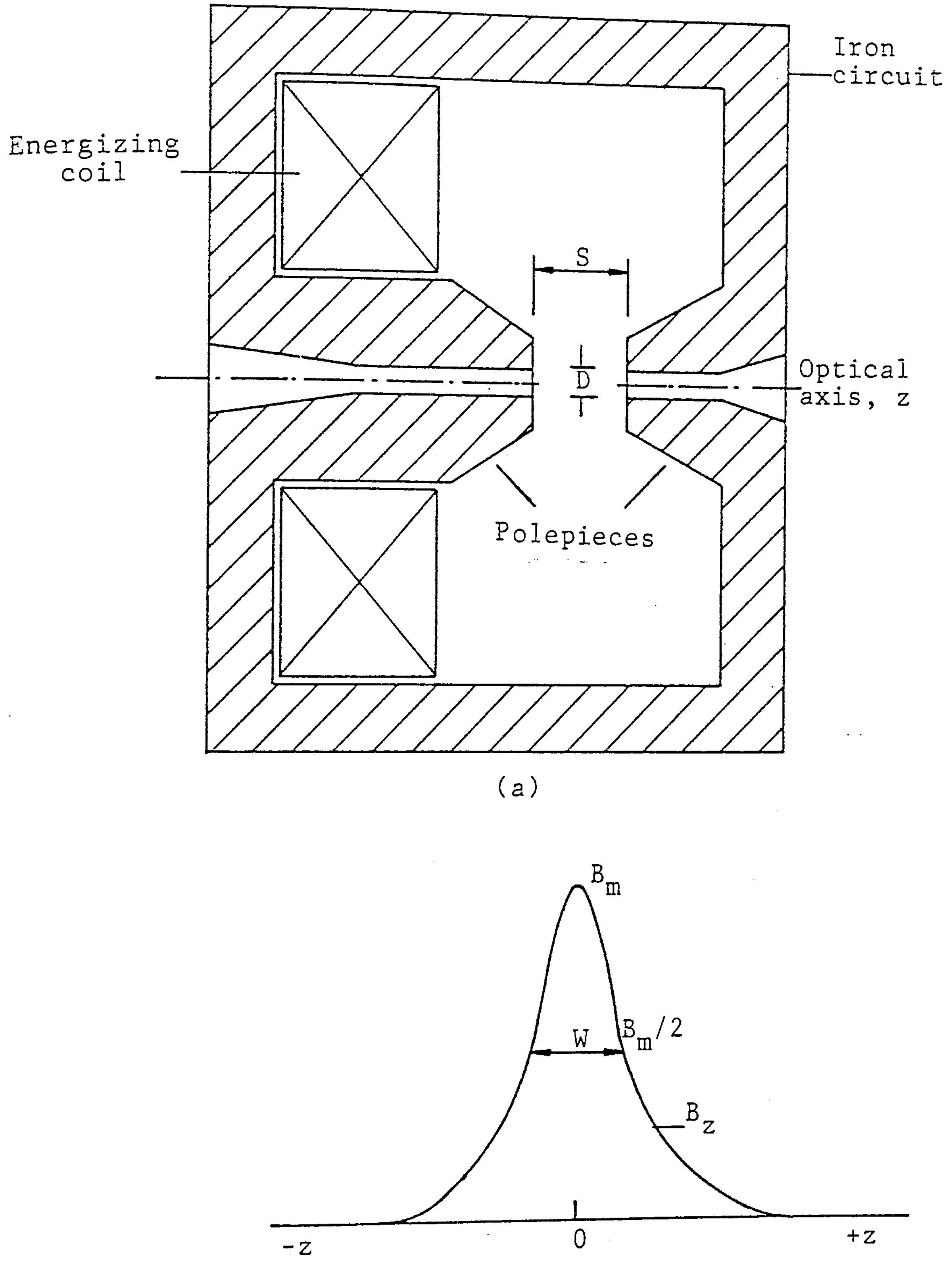

(a)

(b)

Figure 1.1 (a) Cross-section of a conventional symmetrical double polepieces lens. (b) The axial flux density distribution. S = air gap width, D = axial bore diameter, B_m = maximum axial flux density, W = halfwidth at $B_z = B_m/2$.

(1973) deduced the principles for the correct design of the magnetic circuit of an electron lens from their extensive measurements on models and actual lenses. The ferromagnetic material of the polepieces will not saturate provided $NI/S < 1100$ ampere-turns mm^{-1}. Under non-saturation conditions, the peak flux density, B_m in Tesla is given by the following approximate equation,

$$B_m = \mu_o \, NI/L \qquad (1.5)$$

where $\mu_o = 4\pi \times 10^{-7}$ H m^{-1} is the permeability in vacuum, NI is the number of ampere-turns producing the field and L in metres is a geometrical parameter given by

$$L = (S^2 + 0.45D^2)^{\frac{1}{2}} \qquad (1.6)$$

The halfwidth W is related to the parameter L by the following equation,

$$W = 0.97L \qquad (1.7)$$

Fert and Durandeau (1967) claimed the accuracy of equations (1.5) and (1.7) to be better than 5% and 3% respectively.

The variation of the electron-optical properties of magnetic lenses can be described in terms of the maximum flux density B_m and the halfwidth, W. For example, under non-saturation conditions, both the spherical and chromatic aberration coefficients C_s and C_c respectively increase approximately linearly with the halfwidth W and are inversely proportional to the peak flux density B_m.

In unsaturated double polepiece lenses the values of B_m and W are functions of S and D as shown in equations (1.5) and (1.7). Therefore, the values of C_s and C_c depend on, among other factors, the ratio of S/D. The specimen position for minimum C_s operation mode is near the centre of the air gap so that a lens of minimum C_s is usually a variant of the single-field condenser-objective lens of Riecke and Ruska (1966) whose ray paths are essentially telescopic (see, for example, Riecke 1982). The lowest value of C_c that can be achieved is that of a lens of infinite S/D ratio (Schiske 1956); for this lens the quotient C_c/f_o is $\pi/4$, f_o being the objective focal length. The field of such lenses is represented by the square-top field which has a constant flux density B_m along the air gap width and zero value outside it. In Chapter 4 saturated double pole-piece condenser-objective lenses characterized by the large S/D ratio have been investigated in detail.

Under saturation conditions, additional factors may affect lens aberrations. These include polepiece shape and position and shape of the energizing coil and the current density σ that may be supported by the windings.

Another conventional form of magnetic electron lens is the asymmetrical lens, shown schematically in cross-section in figure 1.2. The two polepieces are bored axially with holes of different diameter D_1 and D_2. The electron-optical properties of asymmetrical lenses are usually evaluated as functions of the geometrical ratios D_1/D_2 and S/D_m where $D_m = (D_1 + D_2)/2$ is the mean bore diameter of the two polepieces. The axial flux density distribution B_z in the vicinity of the two unsaturated polepieces is similar to that shown in figure 1.2, except that it is asymmetrical about the peak flux density B_m. The decrease of the field away from the peak is steeper on the side where the axial bore diameter is smaller. The important properties of the unsaturated asymmetrical double polepiece

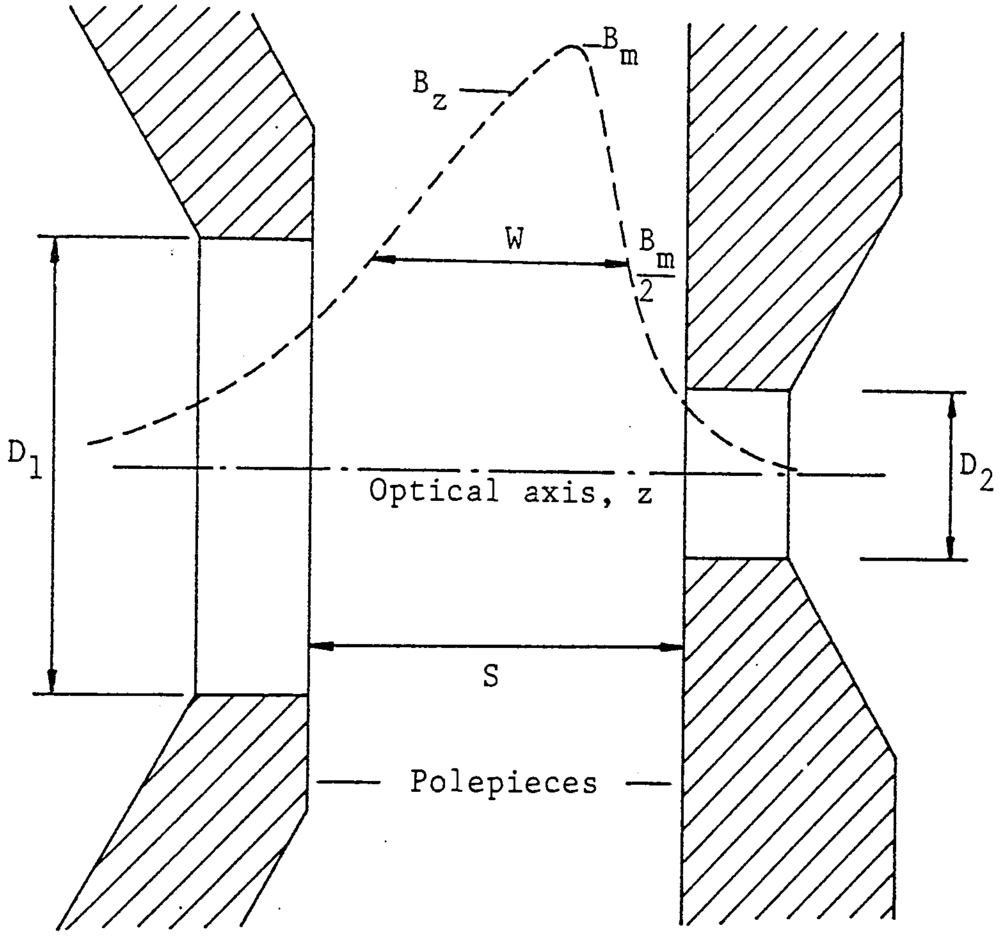

Figure 1.2 Schematic cross-section through typical asymmetrical polepieces of a magnetic double polepiece electron lens. S = air gap width, D_1 and D_2 = axial bore diameters, B_m = maximum axial flux density, W = halfwidth at $B_z = B_m/2$.

lenses were discussed by several authors (Juma and Yahya 1984, Liebmann 1955a, b, Riecke 1982). Apart from the C_s value, the electron-optical parameters of asymmetrical lenses are similar to those of symmetrical lenses when the bore D of the symmetrical lens is replaced by the mean diameter D_m of the asymmetrical lens in equations (1.5)-(1.7).

Asymmetrical objective lenses have the advantage of permitting the specimen holder to enter the large bore on the electron source side (top-entry) since in some analytical electron-optical instruments, quite a large volume of space is required in the vicinity of the specimen for extracting x-rays, secondary electrons and other emissions from the specimen at large solid angles without loss of resolution. The large bore provides the possibility of inserting analytical accessories such as x-ray and electron spectrometers and secondary electron collecting devices close to the specimen. In the limiting case this large polepiece may be removed altogether; this introduces the concept of the single polepiece magnetic electron lens.

1.1.3 THE SINGLE POLEPIECE LENS

An important development in the design of electron lenses was the introduction of the single polepiece lens by Mulvey (1972). In the double polepiece magnetic lenses, it is necessary to distort the parallel field between the two polepieces by means of the bore to produce a lens action. In the single polepiece lens, the second polepiece is dispensed with.

Figure 1.3 shows a cross-section of a typical single polepiece lens with no axial bore through its pole. It has an open construction so that the flux lines concentrated at the poleface, diverge widely before re-entering the iron circuit. Thus the axial magnetic field is strong in the vicinity of the poleface but decays outside the lens structure in a manner depending on the pole's profile which can be designed in different geometrical shapes. In general, for a given NI, the flux density at the poleface will increase as the lens is made smaller. The use of the term "single polepiece" is considered to be justified in this case since the magnetic flux emerging from the polepiece returns to a semi-infinite plate which would not normally be described as a "polepiece" (Mulvey 1982).

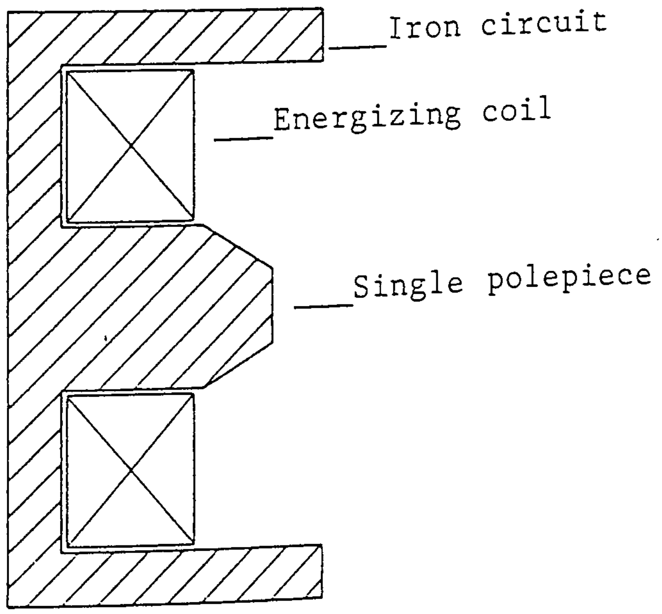

Figure 1.3 Cross-section of a zero-bore single polepiece lens.

The advantages of single polepiece lenses arise from their essentially different axial flux density distribution from those of normal double polepiece lenses. Hence, their electron-optical properties cannot be predicted from the data of conventional lenses. The factors that affect the electron-optical properties of the single polepiece lens are the shape, size and axial bore diameter of its pole (Hill and Smith 1982, Juma et al 1983a, b, Lenc and Lencová 1984). However, the lens axial bore is not always necessary when it is used as a probe-forming lens. The absence of the axial bore in the single polepiece makes fabrication of the lens easier and the entire lens can be situated outside the vacuum chamber. If a small hole is bored along the axis of the single polepiece, the lens may be used as an objective in TEM and STEM (Mulvey 1974a, b; Mulvey and Newman 1973) or as a projector in TEM (Al-Hilly and Mulvey 1982) and HVEM (Mulvey and Newman 1974). A single polepiece lens combined with a triode field emission gun has many practical advantages as an electron source. The use of single polepiece lenses in electron guns has been reviewed by Mulvey (1984). A full account of the developments of the single polepiece and the iron-free lens has been given in detail by Mulvey (1982). In the present investigation attention has been paid to the design of both single and double polepiece lenses operating at high flux densities i.e., greater than 2 Tesla.

1.2 HIGH FLUX DENSITY LENSES

For polepiece flux density less than 2 Tesla, the axial flux density distribution of a well-designed conventional lens increases almost linearly with increasing excitation NI and depends very little on the profile of the poleface (Fert and Durandeau 1967). At higher flux densities in the lens gap, the peak axial flux density B_m does not increase linearly with excitation NI and the halfwidth W of the axial field distribution broadens considerably as NI increased (Fert and Durandeau 1967).

Several papers have been published concerning the electron-optical properties of both symmetrical and asymmetrical double polepiece lenses operated under saturation conditions. Conventional lenses (Riecke 1972) and the smaller superconducting lenses (Dietrich 1976, Lefranc et al 1982) have been investigated at flux densities higher than 2 Tesla for high voltage and high resolution electron microscopes. The small size lenses lead to a reduction in the height of the electron microscope column which also reduces the sensitivity to stray magnetic fields and the effect of mechanical vibrations.

Several types of superconducting lenses reported in the literature have been reviewed by Dietrich (1976). Iron-free, iron-shrouded and iron polepiece lenses excited by superconducting windings at current densities in the order of 5×10^4 A/cm^2 can produce peak flux densities of more than 4 Tesla and are capable of operating at electron beam voltages higher than 1 MV. The ring lens of Dietrich et al (1972) operated at a current density σ of 4×10^5 A/cm^2 for a beam voltage of 1300 kV can produce a peak flux density of 7 Tesla. Furthermore, the design proposed by Dietrich et al (1975) of a superconducting shielding lens (S = 7 mm, D = 3 mm) as an objective for a proposed 3 MV electron microscope should be capable of producing a peak flux density B_m of 6 Tesla. A superconducting asymmetrical double polepiece lens for microprobe analysis has been reported by Dietrich et al (1977) operating at 150 kV electron beam. The lens was excited by a superconducting winding (d_1 = 10 mm, d_2 = 60 mm) at a current density of 1.5×10^4 A/cm^2 and produced a peak flux density of 1.4 Tesla.

The above figures indicate that different types of superconducting lenses have been operated at relatively low current densities compared with what can be achieved in practice. In the present work computations have shown that, by careful design, high flux density single and double polepiece soft iron lenses excited at current densities that can be obtained from suitably cooled copper tape coils, may be fabricated for 1 MV electron microscopes. It should be mentioned that, up to now, superconducting coils have not been investigated computationally or experimentally for energizing single polepiece lenses to achieve high flux densities under saturation conditions.

Different types of saturated conventional double polepiece lenses based on computational and experimental investigations have been reported in the literature. In his computations, Cleaver (1980) compared symmetrical and asymmetrical double polepiece lenses of various pole shapes. As far as the peak axial flux density B_m of the lenses under consideration is concerned, the symmetrical condenser-objective lens with Permendur polepieces of gap S = 5 mm and axial bore diameter D = 3 mm (i.e. S/D = 1.66) produced a peak axial flux density B_m of about 3.5 Tesla at excitation NI = 40000 ampere-turns, adequate for operation at a relativistically corrected accelerating voltage V_r = 2 MV. The computations of Kamminga (1976) on saturated condenser-objective lens with soft iron polepieces of S = 5 mm and D = 2.5 mm (i.e. S/D = 2) has a value of B_m = 3.5 Tesla at NI = 40000 ampere-turns and V_r = 2 MV. In the experimental 200 kV saturated condenser-objective lens (S = 2.5 mm, D = 2 mm, S/D = 1.25) of Kunath et al (1966), a flux density of 3.1 Tesla was achieved at the polepiece surface. The 1 MV experimental asymmetrical objective lens of Tsuno and Honda (1983) has a peak flux density B_m of 2.5 Tesla at NI = 32000 ampere-turns.

The above figures indicate that the values of B_m achieved in saturated double polepiece lenses of conventional designs are not very far above the saturation flux density of the ferromagnetic material of the polepieces. Although, at high voltages, superconducting lenses should be superior to conventional lenses in size and weight some technological problems are still involved (Hawkes and Valdre' 1977) and they have not made an impact in high resolution electron microscopy. In the present work high flux density objective lenses of smaller sizes than conventional ones are investigated for use in high resolution and high voltage electron microscopes.

1.3 HIGH VOLTAGE ELECTRON MICROSCOPY

High (atomic) resolution and observation of thick specimens are the main aspects of electron microscopy which require operation at high accelerating voltages. Electron-optically, most conventional high voltage electron microscopes are just scaled-up versions of conventional 100 kV instruments (Hawkes 1972) rather than designed expressly for high voltages. The lenses are simply built on a larger scale to accommodate the increased number of ampere-turns since the lens focal properties are determined essentially by $NI/V_r^{\frac{1}{2}}$; to avoid saturation, the yoke is made bigger and the gap S wider.

The use of high voltage in the transmission electron microscope has proved to be the best way to improve resolution. The parameter $(C_s\ \lambda^3)^{1/4}$ is a measure for the resolving power of an objective lens. This resolution parameter is a function of the spherical aberration coefficient C_s and the electron wavelength λ ; the latter being strongly dependent on the relativistically corrected accelerating voltage, V_r i.e.

$$\lambda = 1.23/V_r^{\frac{1}{2}} \quad \text{nm} \tag{1.8}$$

where

$$V_r = V\ (1 + 0.978 \times 10^{-6}V) \tag{1.9}$$

V being the accelerating voltage in volts, or

$$V_r = V + 0.978\ V^2 \tag{1.10}$$

when V is in MV. Equation (1.8) indicates that as V increases, λ decreases. Although the increase in V, in general, leads to an increase in C_s and the focal length of the objective lens, the increase in C_s in the resolution parameter is as more than counterbalanced by the decrease in λ as shown in table 1.1. The C_s values were taken from Dupouy (1968), Ozasa et al (1970), Tsuno and Harada (1983) and Tsuno and Honda (1983).

Table 1.1 The resolution parameter $(C_s \lambda^3)^{1/4}$ at different accelerating voltages.

V (kV)	λ (nm)	C_s (mm)	$(C_s \lambda^3)^{1/4}$ (nm)
100	0.00370	3.2	0.635
200	0.0025	0.8	0.336
400	0.00165	1.2	0.271
1000	0.000872	6.5	0.256
2000	0.00050	8.2	0.179
3000	0.000355	17.9	0.168

Therefore, the resolving power of the microscope improves considerably when the voltage is made appreciably higher. The observation of thick specimens is essential when properties typical of the bulk material are to be studied or when thin specimens are very difficult to prepare (as in the case of rocks and minerals, for example). The observable specimen thickness increases with increasing accelerating voltage (Sugata et al 1970). Therefore, thicker specimens and higher densities can be studied. With thicker specimens the chromatic aberration caused by inelastic scattering and its accompanying energy losses suffered by the electrons, decreases when the electron energy is very high.

Due to the above advantages of high voltage electron microscopy, attention has been concentrated in this investigation on the possibility of using improved designs of magnetic objective lenses in high resolution and high voltage electron microscopes.

1.4 SCALING OF LENSES

Kelvin's Rule (Thomson 1872) states that if a magnetic electron lens with coordinates z and y is scaled by a factor k i.e. the coordinates of the scaled lens are kz and ky respectively and if in addition the excitation $(NI)_o$ of the original lens is also scaled by a factor k i.e. $(NI)_s = k(NI)_o$ where $(NI)_s$ is the excitation of the scaled lens, the flux density B at corresponding points in the two lenses is the same, provided that B-H magnetization characteristics of the magnetic material in the original and scaled lenses are identical. This means that even if any part of the magnetic circuit is saturated, it is still possible to scale the lens, i.e. increase or reduce its dimensions without any loss of accuracy in determining the flux density $B_{kz,ky}$, provided the above conditions are satisfied.

1.4.1 LENS PROPERTIES IN A SCALED LENS

Figure 1.4a shows the trajectory of the electron beam accelerated at a relativistic voltage $(V_r)_o$ through the field of a given lens. The beam intersects the optical axis at a certain point p at which the focal properties e.g. objective focal length $(f_o)_o$, spherical aberration coefficient $(C_s)_o$ and chromatic aberration coefficient $(C_c)_o$ can be calculated. Figure 1.4b shows the axial field distribution of the given lens scaled in size by a factor k, so that the axial distance kz is also scaled by a factor k. In addition the excitation $(NI)_s$ has also been scaled by a factor k so that the flux density at corresponding points on the original and the scaled lenses are the same. If the relativistically corrected accelerating voltage is $(V_r)_s$ in the scaled lens (figure 1.4b) is made equal to $k^2(V_r)_o$ i.e. $(V_r)_s/(NI)_s^2 = k^2(V_r)_o/[k(NI)_o]^2 = (V_r)_o/(NI)_o^2$ is unchanged then the trajectory and hence all focal properties will be scaled by a factor k in the z direction i.e. the height of the trajectory at corresponding points in the original and scaled lens is the same. The objective focal length $(f_\circ)_s$, the spherical aberration coefficient $(C_s)_s$ and the chromatic aberration coefficient $(C_c)_s$ of the scaled lens are related to those of the original lens by the following equations

$$\left.\begin{aligned} (f_\circ)_s &= k(f_\circ)_o \\ (C_s)_s &= k(C_s)_o \\ (C_c)_s &= k(C_c)_o \end{aligned}\right] \qquad (1.11)$$

The current density σ_s (defined as the current per unit cross-sectional area of the conductor) in the scaled lens is 1/k times σ_o in the original lens. This is clear from the fact that in the scaled lens the cross-sectional area

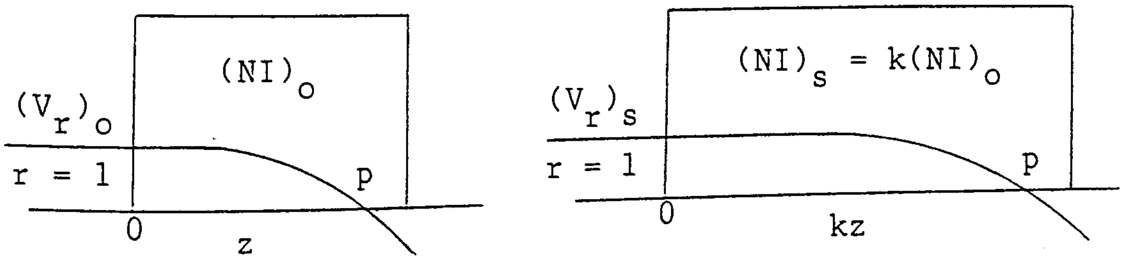

(a) (b)

Figure 1.4 The electron beam trajectory in the field of (a) the original lens and (b) the scaled lens.

is multiplied by k^2 whilst the current I (or excitation NI) is multiplied by k only. This means that the focal properties of a family of scaled lenses from a given magnetic lens and its computed focal properties can be determined directly by simple scaling operations.

In the present investigatigation, the axial flux density distributions B_z of a given lens were computed at different excitations NI. For each value of NI, the B_z data were used in computing the focal properties. The values of C_s, C_c, f_o and the focal distance z_F were computed as functions of the relativistic voltage V_r at constant NI. Hence the electron-optical parameters of a lens of the same shape, but not of the same size can be determined at any accelerating voltage and specimen position. The value of flux density at corresponding points in the original and scaled lenses, of course, remains the same. Throughout the present work the above method of scaling was followed.

1.5 DESIGN CONCEPTS

In order to reduce aberration, the magnetic electron lens should produce the highest possible flux density peak consistent with the smallest halfwidth of the axial flux density distribution. Reduced size and weight of lens may also be important.

At any point on the axis of a magnetic lens the total flux density B_z is a function of the flux density produced by the current in the coil windings and that produced by the magnetization in the iron elements. Thus

$$B_z = B_{coil} + B_{Fe} \tag{1.12}$$

where B_{coil} is the axial flux density due to the energizing coil and B_{Fe} is that due to iron magnetization. Figure 1.5 shows a schematic B-H curve for a soft iron. There are three regions of the iron magnetization depending on the magnetic field strength H. In the linear region, up to H = 350 A/m magnetic flux density, B_{Fe} due to the iron increases linearly with increasing magnetic field strength H. For a further increse in H, B_{Fe} deviates from linearity (intermediate region) until it reaches a limiting value ($\simeq$ 2 Tesla for soft iron). In this region the iron is said to be saturated. The value of saturation flux density depends on the material; for example, for soft iron it varies from 1.8 to 2 Tesla and is 2.37 Tesla for Permendur. Soft iron or Permendur are commonly used in electron lenses. The effect of the iron magnetization curve on the design parameters of single and double polepiece lenses is investigated in Chapters 2, 3 and 4.

It is seen from equation (1.12) that once the iron is saturated, any further increase in the flux density must come from the coil. The contribution of B_{coil} to the axial flux density B_z can be increased, for example, by placing the coil in the region of the lens gap, instead of in the conventional position. The effect of the exciting coil shape and position on the electron-optical properties appears to have been neglected by the designers of magnetic lenses in commercial microscopes, so this point has been investigated in some detail in Chapters 2, 3 and 4 for single and double polepiece lenses.

In the present work, computations have been concentrated on determining a favourable combination of the polepiece and the energizing coil in order to achieve

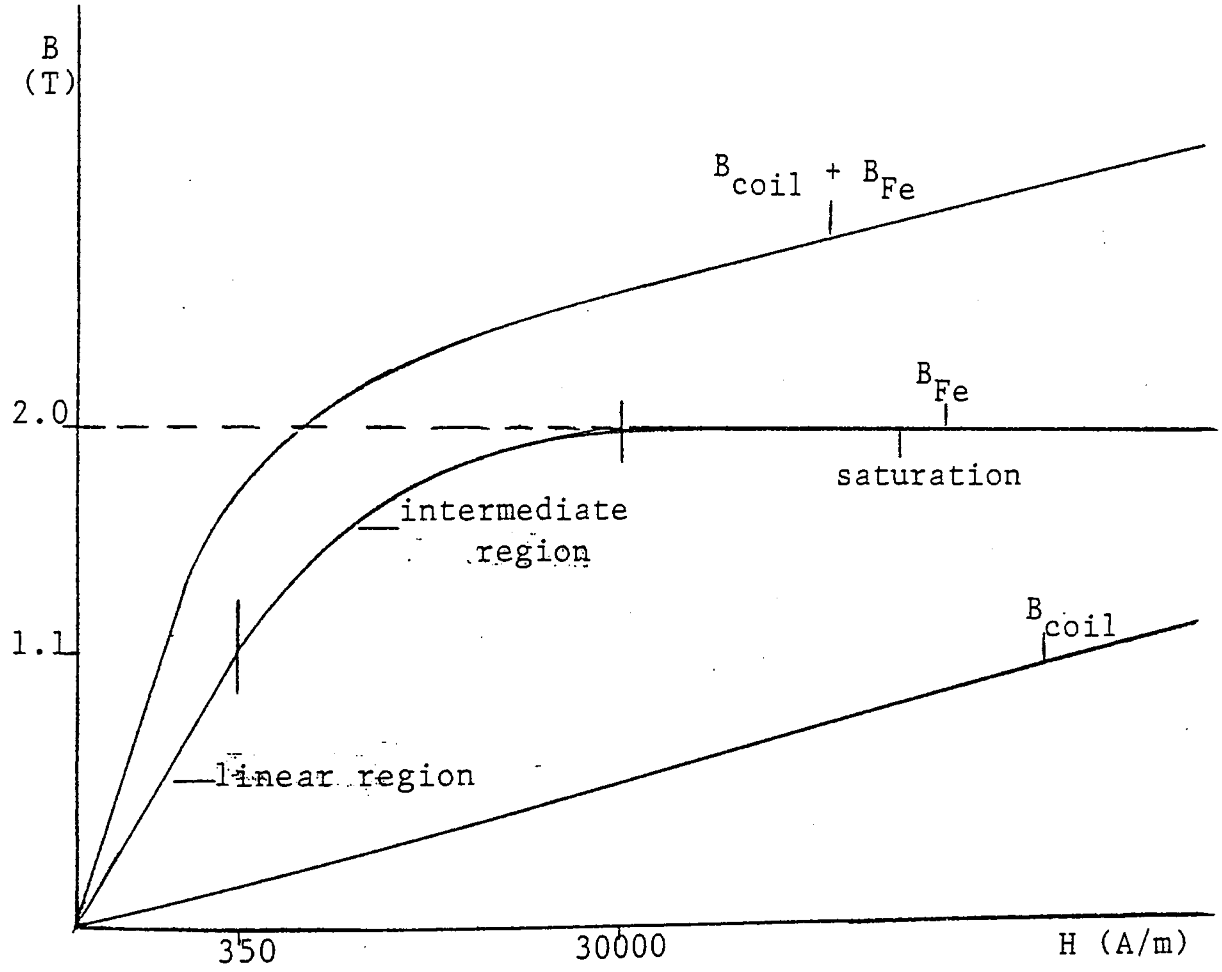

Figure 1.5 Schematic B-H curves for a typical ferromagnetic material.

high flux density magnetic electron lenses for high voltage and high resolution electron microscopes. In a conventional lens the energizing coil makes a negligible contribution to the axial field distribution, nearly all of which is produced by the magnetization of the iron polepieces. As the lens excitation is increased these polepieces and often other parts of the magnetic circuit begin to saturate. Further increase of lens excitation leads to a broadening of the field distribution, and an effective limitation to the maximum flux density that can be achieved. Many of these effects can be avoided or at least reduced if careful consideration is given to the shape and position of the energizing coil.

The present work is mainly concerned with the design concepts of high flux density lenses. Such lenses may be used in high voltage and high resolution electron microscopes. The main aim of this thesis, therefore, is to calculate the total field distribution in saturated single and double polepiece lenses operating at gap flux densities greatly in excess of 2 Tesla and subsequently to determine the electron-optical properties. From these calculations, it should be possible to deduce, among other things, the limiting performance of saturated objective lenses for high voltage and high resolution electron microscopes (Al-Nakeshli et al 1984a and b, Al-Nakeshli and Juma 1986; see Appendix 1).

2. THE COMPUTER PROGRAMS

The work described in this thesis is mainly computational, based on the use of several computer programs of different origin. The most important factor which decides the properties of a magnetic lens is its axial flux density distribution. The axial flux density distribution of each lens investigated in present work has been computed by means of the finite element method which was first introduced in electron optics by Munro (1971) who applied it to computation of the magnetic field in round lenses (Munro 1973, 1976).

The axial flux density distribution was computed using the computer programs set up by Munro (1975) and program AMAG of Lencová (1984); the latter has been recently discussed by Lencová and Lenc (1984). Munro's programs (Munro 1975), written in Fortran 4, were run on the ICL 1904S computer (storage of 256 kilo-bytes) at Aston University. Four of the programs of Munro (1975), namely programs M12, M13, M21 and M31 were used in this investigation. The axial flux density distributions of most of the lenses investigated were first computed with the aid of programs M12 and M13 using the maximum finite element mesh number of 50 mesh points in the axial direction and 25 in the radial direction. These field distributions were then used for computing the lens focal properties by means of program M21. Programs M12 and M13 also compute the flux density and flux values in the magnetic circuit. The computed flux values at each mesh point were then used for plotting tubes of constant flux in the magnetic lenses with the aid of program M31 (Munro 1975).

Program AMAG (Lencová 1984), as received, was written in Fortran 4 by Mrs. B. Lencová of the Institute of Scientific Instruments at Brno, Czechoslovakia. It was supplied to the Electron-Optics Group of Aston University as part of the scientific exchange between the Institute of Scientific Instruments in Czechoslovakia and the University of Aston. Since program AMAG needs more storage than that available in the ICL computer at Aston University it was, therefore, adapted to Fortran 77 and compiled in the Harris 800 computer (storage of 8 mega-bytes) at Aston University. The axial flux density distributions of all the lenses under investigation were recomputed by program AMAG; their focal properties were then recomputed with the aid of program M21 of Munro (1975).

The magnetic field produced by the lens energizing coil alone has been computed with the aid of the program set up by Nasr (1981) based on Biot-Savart law. The program Area (Nasr 1981) was also used for computing the area under the axial field distribution.

For reference purposes, the following is a brief description of these programs mentioned above. It should be emphasised, however, that these programs were used mainly as tools; some of the finer details of these programs is the subject of a Ph.D. thesis by Tahir (1985).

2.1 THE FINITE ELEMENT METHOD

The finite element method is a numerical technique for solving magnetic field problems in electron lenses. The lens or, in general, the region to be analysed is divided by a mesh into a large number of small sub-regions called finite elements. These finite elements may be triangles, quadrilaterals or more complicated shapes.

Figure 2.1 shows an example of a mesh of triangular finite elements. Triangular mesh grids are used instead of rectangular ones since arbitrary triangles are the most elementary kinds of elements (Kasper 1982). Where an interface occurs between two media (e.g. at the surface of a polepiece), the mesh lines are chosen to coincide with the interface. A potential value is assigned to each mesh point, and the potential is assumed to vary linearly across each triangular finite element. The differential equation of the system is replaced by an appropriate "functional" in an arbitrary triangle. The minimization of this functional with respect to changes in the potentials at each mesh point corresponds to the solution of the original differential equation. The functional must have a stationary value with respect to small changes in the potential of each mesh point. This condition makes it possible to set up a nodal equation for each mesh point, relating the potential at that node to the potentials at adjacent nodes. The set of algebraic nodal equations thus obtained is solved by a matrix method, to yield the vector potential value at every nodal point.

The use of the finite element method in electron optics has many advantages which may be summarized as follows:

(a) Lenses with polepieces of any shape can be analysed.

(b) The finite permeability of the polepieces can be taken into account.

(c) The flux distribution through the magnetic circuit, including the coil windings can be computed. The finite element method can calculate the flux density in all parts of the lens, including parts where it would be difficult to

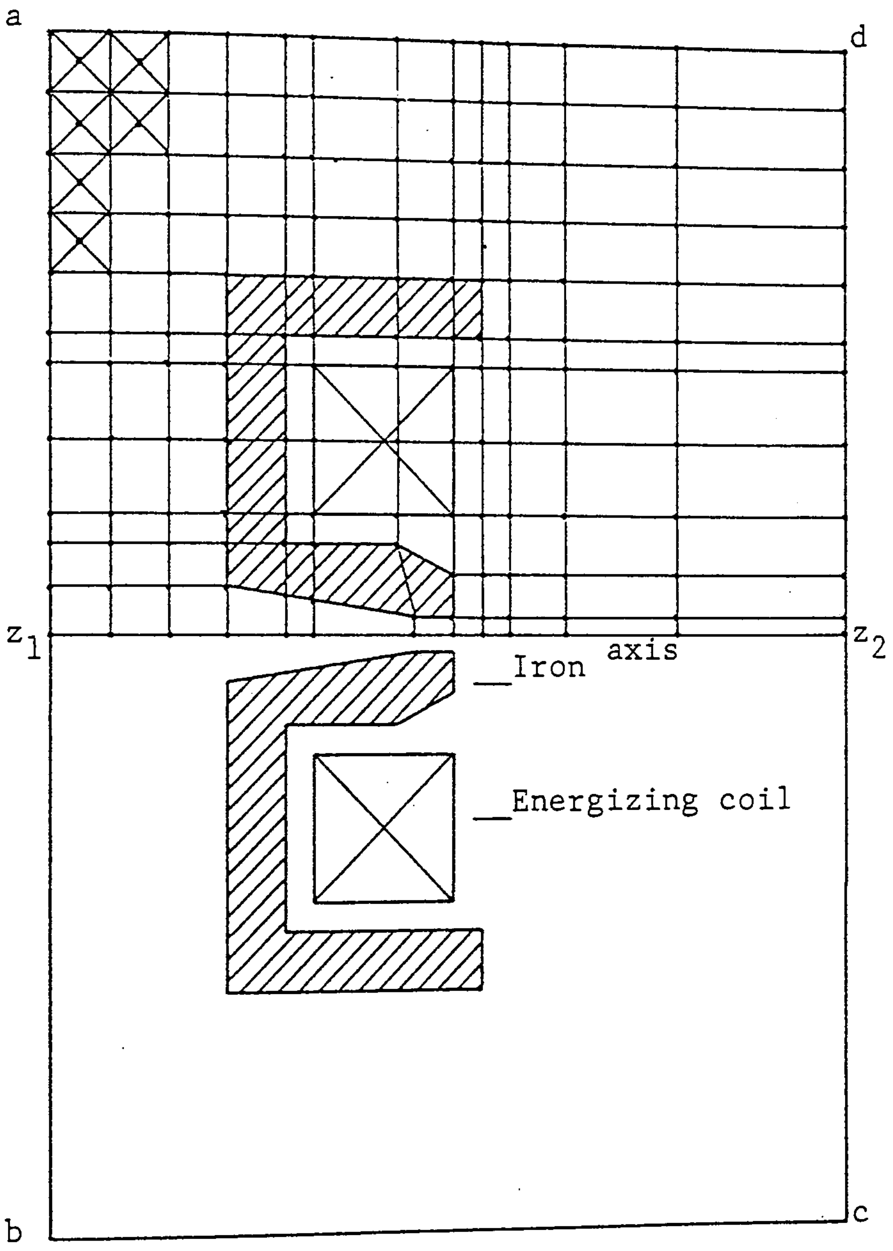

Figure 2.1 Cross-section of an axially symmetric magnetic structure; this includes the energizing coil, the magnetic material and the space around it within the rectangular boundary abcd. The finite element boundary is az_1z_2d, dividing the structure into quadrilaterals and triangular finite elements.

be measured experimentally.

(d) Magnetic lenses can be analysed under saturation conditions, taking the non-linearity of the magnetization characteristic into account.

(e) Lenses with superconducting shielding cylinders, and iron-free mini-lenses, can be dealt with.

2.2 MUNRO'S PROGRAMS

2.2.1 PROGRAM M12: Program For Computing Vector Potential Distributions And Flux Density Distributions Throughout The Magnetic Circuit And Coil Windings Of Unsaturated Magnetic Lenses

This program computes the distributions of the vector potential A and the flux density B throughout the magnetic circuit and coil windings of any unsaturated rotationally-symmetric magnetic lens. The magnetic circuit is assumed to have a constant finite permeability. The axial flux density distribution can be used by program M21 for computing the focal properties. The flux pattern through the magnetic circuit and coil windings can be plotted using program M31. The flux density is computed at points throughout the magnetic circuit; the result can be used to discover parts of the iron circuit operating at high flux density, and which may therefore require further computation using the B-H curve of the ferromagnetic material in use.

2.2.2 PROGRAM M13: Program For Computing Vector Potential Distributions And Flux Density Distributions Throughout The Magnetic Circuit And Coil Windings Of Saturated Magnetic Lenses

This program computes the distributions of the vector potential A and flux density B throughout the magnetic circuit and coil windings of a rotationally-symmetric lens for a given B-H curve. This program is therefore suitable in calculations with saturated magnetic lenses, in which the non-linear part of the B-H curve of the magnetic materials must be taken into account. The program can handle composite magnetic circuits, i.e. circuits constructed from up to five different magnetic materials. The magnetization curve for each magnetic material must be specified. As in program M12, the axial flux density distribution and the flux density values throughout the magnetic circuit and the flux values throughout the two-dimensional mesh system within the boundary conditions are computed.

2.2.3 PROGRAM M21: Program For Computing The Objective Properties Of Any Magnetic Lens

This program computes the objective focal properties of any magnetic electron lens of a known axial flux density distribution B_z. The axial field may be either an experimentally measured or a computed one at a known excitation NI. For a given range of relativistically corrected beam voltages V_r, the B_z data at excitation NI are supplied to the program. Program M21 then computes the excitation parameter $NI/V_r^{\frac{1}{2}}$, the object or image plane, the objective principal plane, the objective focal length f_o, the spherical aberration coefficient C_s, the chromatic aberration coefficient C_c, the axial flux density at object plane and magnification of a probe or image forming lens. For details of the computation see Appendix 2.

2.2.4 PROGRAM M31: Program For Plotting Tubes Of Constant Flux In Magnetic Lenses

This program plots as a function of z, the radii R through which a given flux ϕ passes using the relationship

$$A = \phi/(2\pi R) \qquad (2.1)$$

It can do this since the vector potential distribution has been computed beforehand using program M12 or M13. For each specified ϕ value, the program finds, by linear interpolation between the computed vector potential values at points on the finite element mesh, a set of radii enclosing the required flux ϕ. The plotter then joins these points together with a series of straight-line segments. A set of such curves of different ϕ values gives a strong visual impression of the flux density in the magnetic circuit since the lines crowd together in regions of high flux density.

2.3 PROGRAM BIOT

This program computes the axial flux density distribution of any rotationally symmetric iron-free magnetic electron lens, using Biot-Savart's law (see e.g. Nasr 1981). The importance of this program is that it makes it possible to determine the flux density B_{coil} contributed directly by the coil to the axial field distribution, B_z of a saturated lens, for example. The axial magnetic field, B_z which is computed with the aid of programs M12 and M13 of Munro, is the sum of the contributions from the coil, B_{coil} and the magnetized iron, B_{Fe}. Thus, the flux density due to the magnetized iron, B_{Fe} can be determined from equation (1.12), i.e.

$$B_{Fe} = B_z - B_{coil} \qquad (2.2)$$

This simple additional calculation provides useful information about the state of magnetization of the polepiece tip in a saturated lens. In addition, the axial flux density distribution B_{Fe} due to iron itself, will be known in both saturated and unsaturated lenses. The variation of B_{Fe} with the axial distance, z can also be used as a check on the accuracy of the computations. Since the iron circuit does not contribute additional ampere-turns to the magnetic circuit, the integral $\int_{-\infty}^{+\infty} B_{Fe}\, dz$ must equal to zero. This suggests that the total area under the B_{Fe}-z distribution must be zero. In general, this is not the case with the finite element method with a finite boundary, since it tends to underestimate the magnetization of the iron in the open part of the magnetic circuit of a single polepiece lens (Mulvey and Nasr 1981).

2.4 PROGRAM AREA: Program For Computing The Area Under Axial Magnetic Flux Density Distribution

This program computes the area under the axial magnetic flux density distribution by means of the trapezoidal rule. The area under the axial magnetic flux density distribution is given by Ampere's law,

$$\int_{-\infty}^{+\infty} \frac{B_z}{\mu_r}\, dz = \mu_o NI \qquad (2.3)$$

where $\mu_o = 4\pi \times 10^{-7}$ H/m is the permeability in vacuum and NI is the number of ampere-turns producing the magnetic field along the axis, z. The computation of the area under the axial field distribution can be used as a check on the accuracy of the computations.

2.5 SOME COMPUTATIONAL INVESTIGATIONS USING MUNRO'S PROGRAMS

2.5.1 ACCURACY OF THE COMPUTED FIELDS

In the finite element method, the number of the meshes and the mesh distribution are very important factors. To investigate this subject, several test lenses have been devised to check the accuracy of Munro's programs.

Figure 2.2 shows a section of a symmetrical double polepiece lens studied by Munro (1975) according to his mesh distribution shown in the figure at an excitation of 480 ampere-turns i.e. under non-saturation conditions. The lens has a gap width, S equal to the bore diameter, D of 10mm. Applying equation (1.5), the maximum flux density, B_m at the centre of the air gap is 0.0501 T. However, the computed value of B_m according to Munro's mesh distribution is 0.0519 T, i.e. 3.6% higher than that calculated from equation (1.5). From equation (1.7), the halfwidth W of the lens field is 11.7 mm while that determined by Munro is 11.5 mm, i.e. 1.7% less than the calculated value. It is seen that the mesh distribution of figure 2.2 produced high peak and narrow field. By keeping the mesh distribution in the

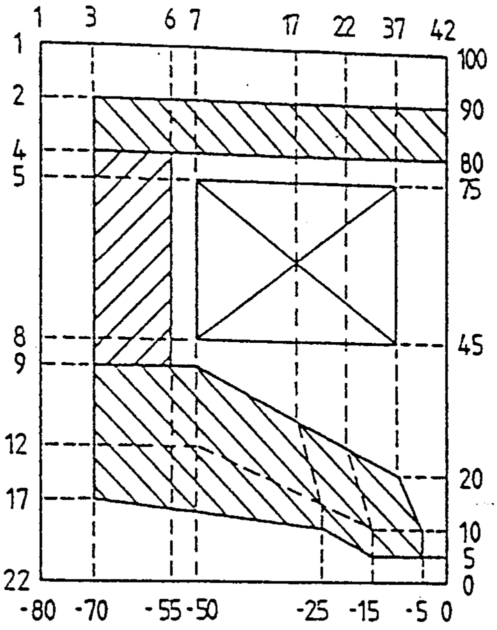

Figure 2.2 Cross-section of the upper quarter of Munro's symmetrical double polepiece lens (S = 10 mm, D = 10 mm) showing his original mesh distribution (22 x 42).

z direction unaltered and slightly increasing and rearranging the mesh distribution in the R direction (figure 2.3), the computed value of B_m became 0.0501 T which is in agreement with that calculated from equation (1.5). The new halfwidth is in agreement with that calculated from equation (1.7). Figure 2.4 shows the two computed axial fields, one according to the mesh distribution of Munro shown in figure 2.2 and the other according to the new mesh distribution shown in figure 2.3. For convenience, the negative half of the field has not been plotted due to the axial symmetry of the flux density distribution. The area under the curve, computed with the aid of Program Area

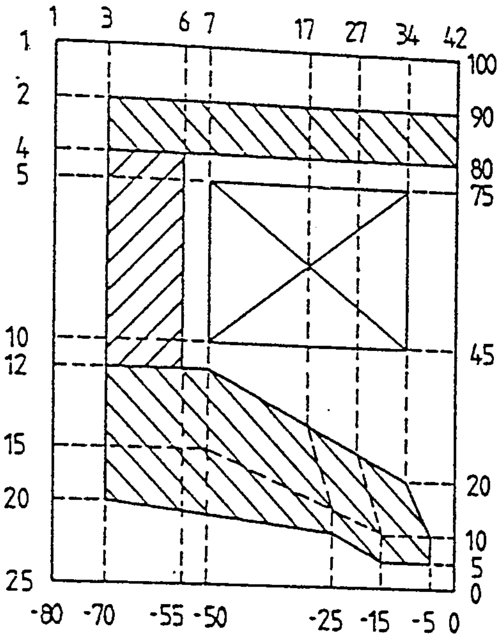

Figure 2.3 Cross-section of the upper quarter of Munro's symmetrical double polepiece lens (S = 10 mm, D = 10 mm) showing the new mesh distribution (25 x 42).

according to the new mesh distribution, is in excellent agreement with the value of μ_o NI, while that of Munro is about 1% higher.

Another example on this subject is the symmetrical double polepiece lens described by Cleaver (1978) and shown in figure 2.5. The lens (S = 10 mm, D = 5 mm) is excited by a solenoid and has a shroud of very high permeability (μ_r = 50000) and Permendur polepiece, as suggested by Cleaver. The advantage of having a very high permeability shroud is to eliminate any loss in ampere-turns due to flux leakage. Cleaver (1978) used Munro's programs (Munro 1975) for computing the lens axial field distributions

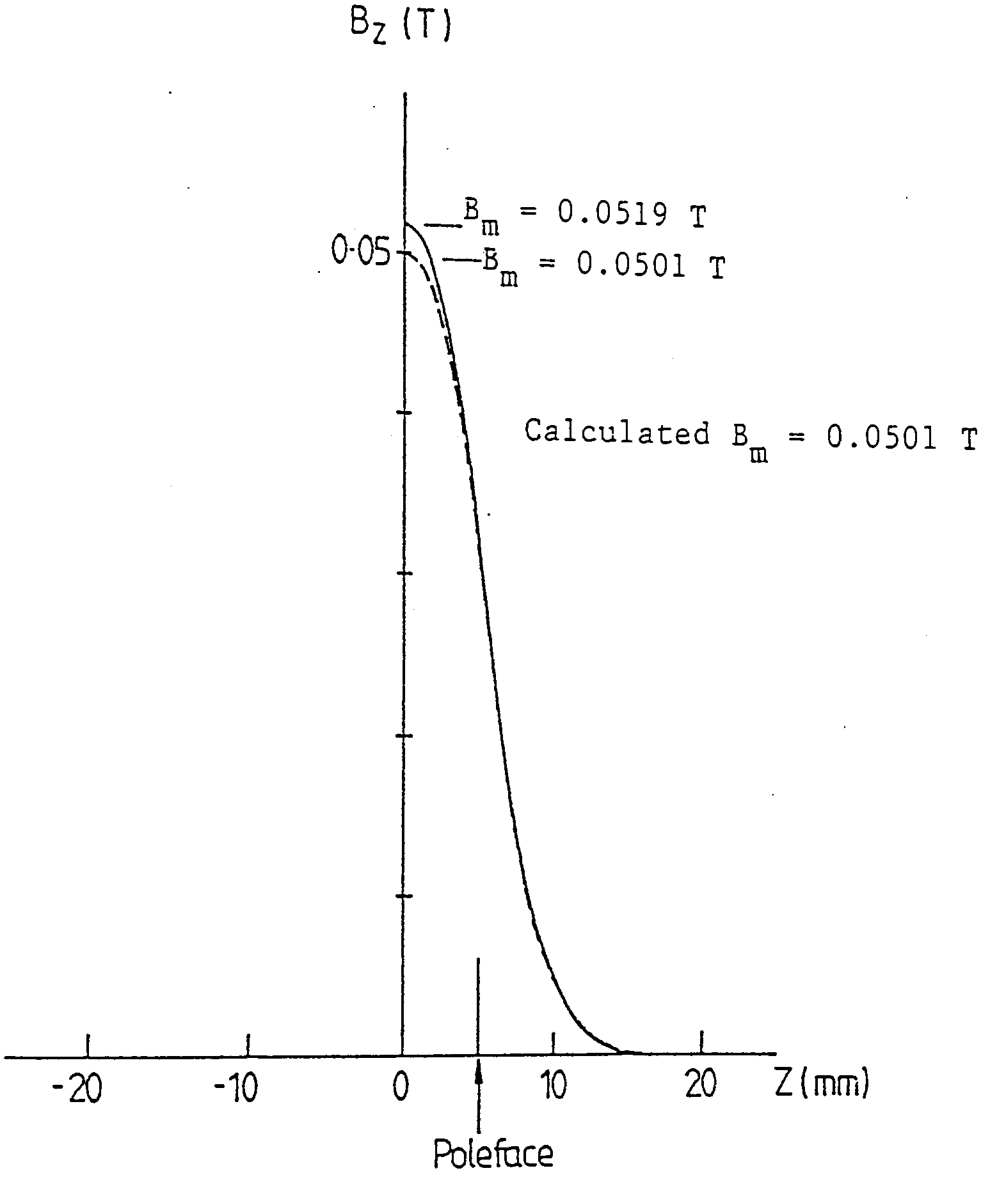

Figure 2.4 The positive half of the two axial magnetic fields computed at 480 ampere-turns using Munro's mesh distribution shown in figure 2.2 (solid curve) and the new mesh distribution shown in figure 2.3 (dotted curve).

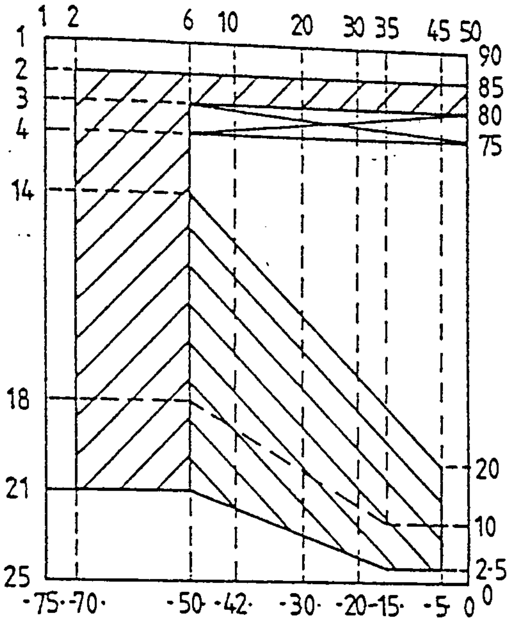

Figure 2.5 Cross-section of the upper quarter of Cleaver's symmetrical double polepiece lens (S = 10 mm, D = 5 mm) showing the mesh distribution used for computing its axial field distribution at NI = 10000 ampere-turns and μ_r = 50000.

under both saturation and non-saturation conditions. In his paper Cleaver, unfortunately, did not show the mesh distribution. However, in his computations under non-saturation conditions at 10^4 ampere-turns, the computed value of B_m is 1.29 T which is 8.4% higher than the value of 1.19 T calculated from equation (1.5). With the aid of Program M12 of Munro, the axial field of Cleaver's lens was computed at the same excitation of 10^4 ampere-turns using the mesh distribution shown in figure 2.5. This mesh distribution has given B_m = 1.2 T; a value only 0.8% higher than that calculated from equation (1.5).

Figure 2.6 shows the axial field computed by Cleaver (1978) and that computed according to the new mesh distribution shown in figure 2.5. The area under the new axial field is in excellent agreement with the value of μ_0 NI. The steeply inclined edges of the polepieces have also been converted into steps of a "staircase" i.e. the meshes in the "staircase" polepiece were rectangular. Computations were carried out by using this steps method for comparison. Figure 2.6 shows a plot of the field computed for a polepiece in which the inclined edges were replaced by a series of rectangular steps. It is seen from the accuracy of the B_m and W values that the steps method can be usefully employed as an alternative at steeply inclined edges even though it does not represent accurately the actual shape of the polepiece.

Using the same excitation and the new mesh distribution of figure 2.5 in Munro's saturation program M13, the computed field was found to be the same as that determined from the non-saturation program, M12. This suggests that there is no problem in the arithmetics of the programs and the main factor that makes the computations differ from those of Cleaver is the mesh distribution. The above investigation also suggests that in order to compute the axial field distribution under saturation conditions, it is advisable to find out first under non-saturation conditions the proper mesh distribution giving accurate enough values of both B_m and the area under the axial field distribution.

These examples indicate that the difference in the computed fields of a specific lens using different distribution and number of meshes, is mainly significant in

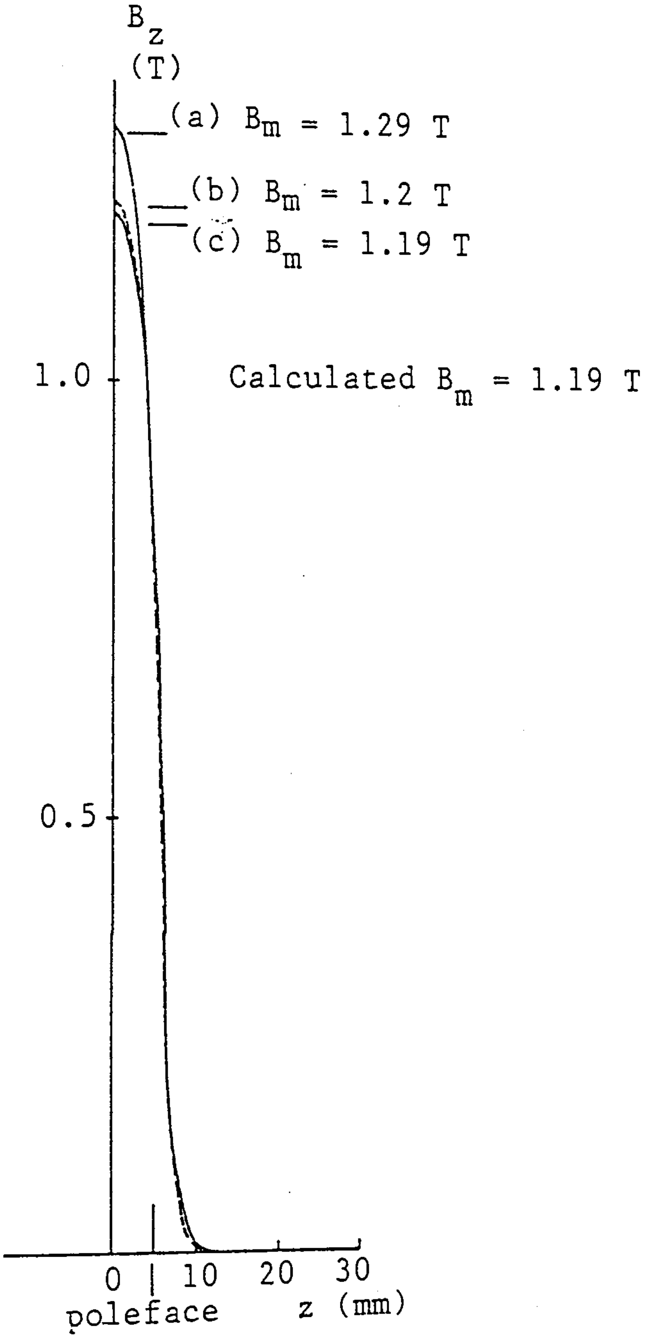

Figure 2.6 The positive half of the three axial field distributions computed at NI = 10000 ampere-turns and μ_r = 50000. (a) Original field of Cleaver (1978), (b) Computed field using the mesh distribution of figure 2.5, (c) Computed field using the stepped polepiece method.

the peak region of the axial field; this would have considerable effect on the computed focal properties. To obtain high accuracy the mesh length should change gradually rather than in very abrupt steps, keeping in mind to use many mesh points near the two polepieces. In fact, for very high accuracy a large computer store will be required. Therefore, the difference in the computations concerning the lenses of both Munro (1975) and Cleaver (1978) was mainly due to their mesh arrangements, i.e. the mesh distribution was concentrated in the polepiece region on the expense of the other parts in the lens.

Under saturation conditions, the effect of mesh arrangements was also clear. Consider the mesh distribution shown in figure 2.5 which was used under non-saturation conditions in Cleaver's lens of very high permeability shroud and Permendur polepieces. With the aid of Munro's saturation program, M13, which was also used by Cleaver, the axial field distribution has been computed at 90000 ampere-turns and plotted together with Cleaver's axial field as shown in figure 2.7. It is seen that the difference between the two fields is confined to the peak region within the air gap separating the two polepieces. Figure 2.7 shows that, according to Cleaver's computation, B_m is 3.58 Tesla which is 5.4% higher than the value of B_m (3.4 Tesla) computed according to the new mesh distribution shown in figure 2.5. The area under the curve of the axial field distribution (figure 2.7) computed according to the mesh distribution of figure 2.5 is equal to the value of μ_0 NI while that of Cleaver's field is slightly higher. This result suggests again that in order to compute the

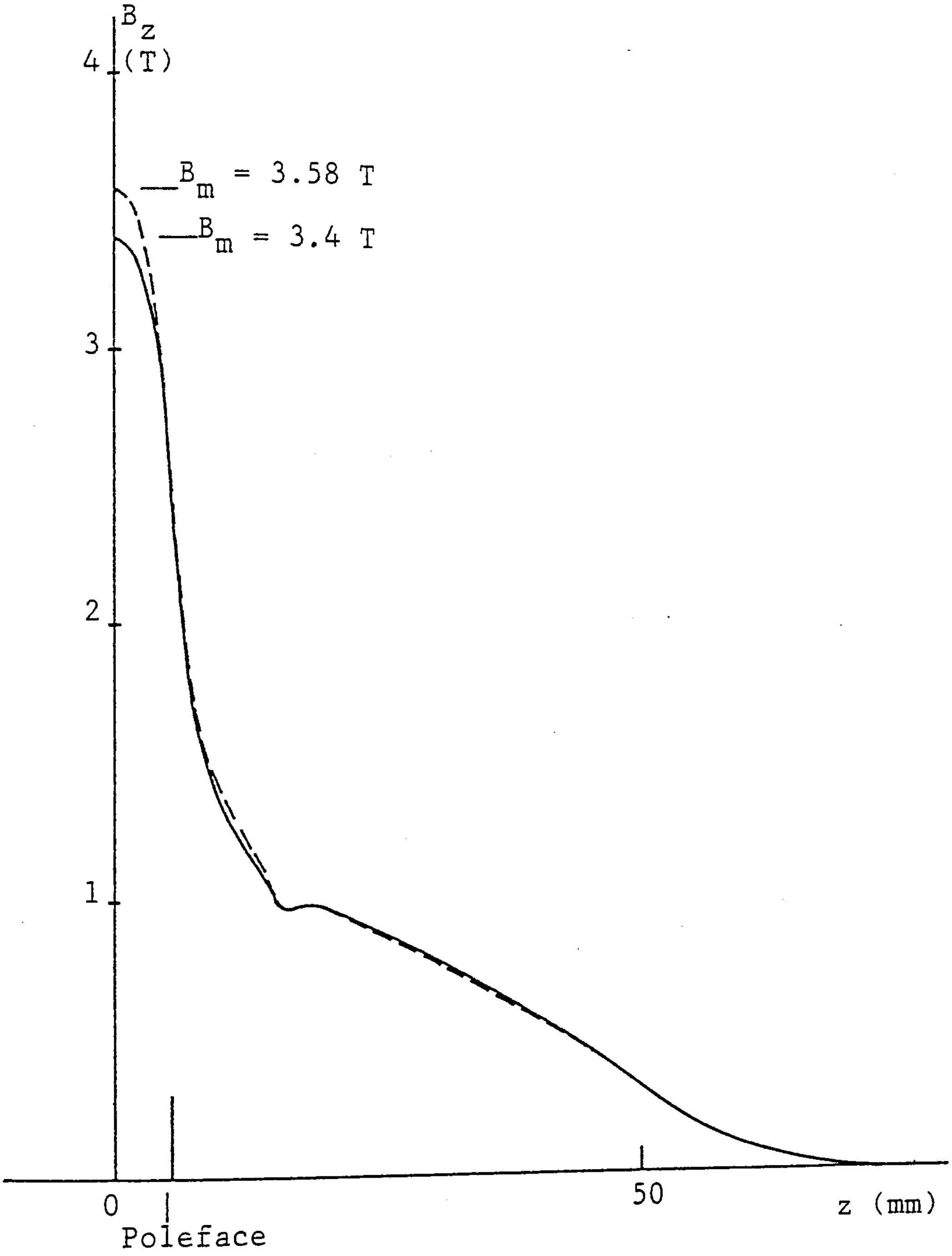

Figure 2.7 The positive half of the axial magnetic field distribution of the lens shown in figure 2.5 computed at 90000 ampere-turns according to Cleaver (1978) (dotted curve) and by using the mesh distribution shown in figure 2.5 (solid curve). The lens has a high permeability shroud (μ_r = 50000) and Permendur polepieces.

axial field distribution under saturation conditions, it is important to determine first the proper mesh distribution that gives accurate enough results under non-saturation conditions.

2.5.2 EFFECT OF POLEPIECE PROFILE

An investigation on a series of double polepiece lenses has been carried out to study the effect of polepiece profile on the axial field using Munro's non-saturation program, M12. Figure 2.8 shows sections of the four double polepiece test lenses which, for simplicity, have no axial bore i.e. $D = 0$. In each lens, the width of the air gap S separating the flat parallel faces of its two polepieces is equal to 10 mm, hence the geometrical length L (equation (1.6)) is also equal to 10 mm. Each lens is excited by a long thin coil of axial thickness 10 mm and inner and outer diameter of 3.4 and 160 mm respectively, thus the ratio of its axial thickness s to mean diameter d_m is 0.12. The thickness of the coil fills the air gap S and hence it is in contact with the flat parallel faces of the two polepieces.

The axial flux density distribution has been computed for high permeability iron ($\mu_r = 50000$) under non-saturation conditions at an excitation of 10000 ampere-turns. Figure 2.9 shows half the computed axial flux density distribution in the air gap and inside the iron polepieces. Due to the absence of an axial bore in the polepieces, the axial field will not be distorted and thus the magnetic flux lines along the air gap S are parallel to each other and normal to the flat face of the polepieces. It is seen that the flux density along the air gap is constant and equal

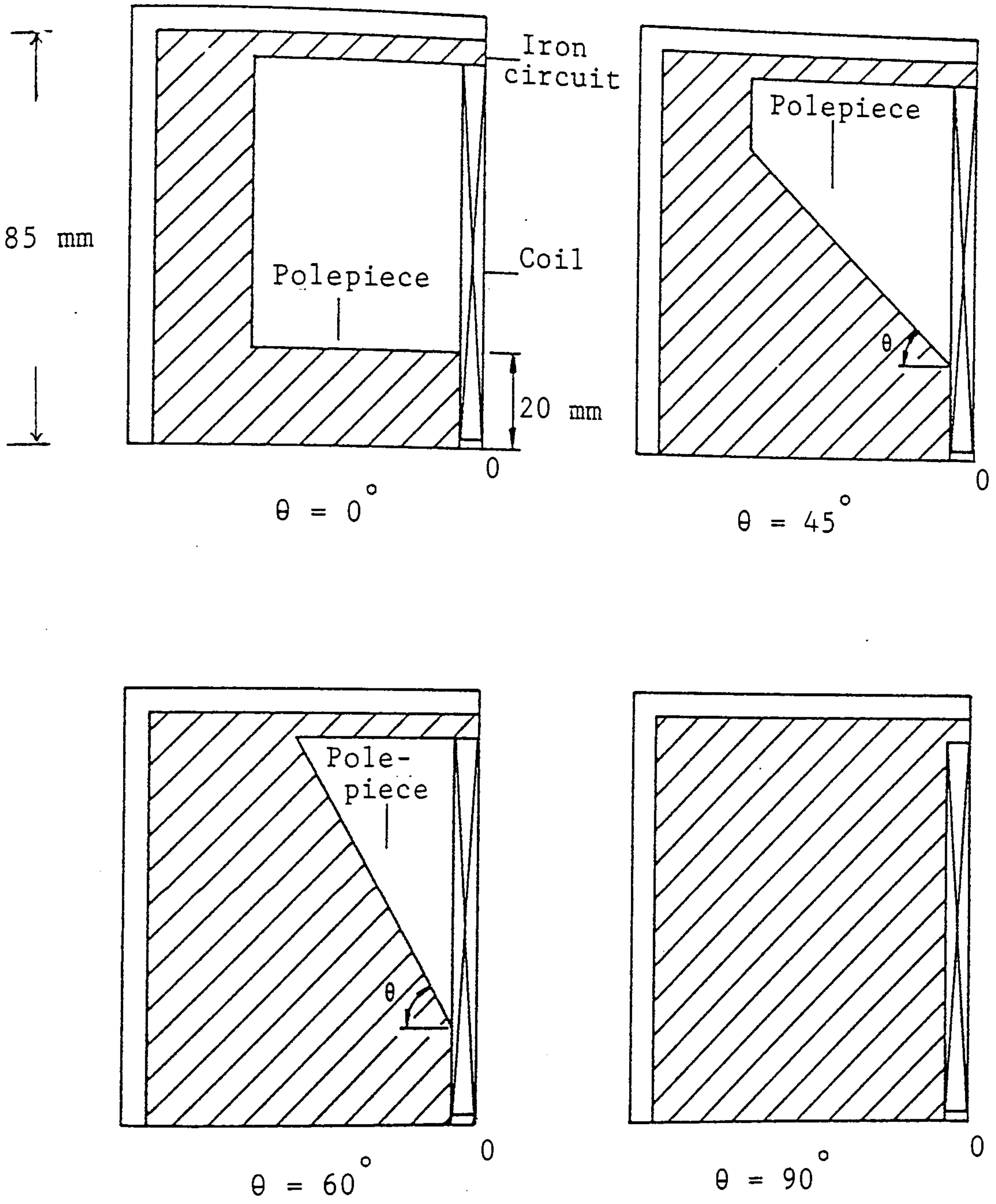

$\theta = 0^\circ$ $\theta = 45^\circ$

$\theta = 60^\circ$ $\theta = 90^\circ$

Figure 2.8 Cross-section of the upper quarter of four zero-bore symmetrical double polepiece lenses (S = 10 mm) with different polepiece taper angles ($\theta = 0^\circ$, 45°, 60° and 90°) excited by a thin flat helical coil of axial thickness s = 10 mm, inner diameter d_1 = 3.4 mm and outer diameter d_2 = 160 mm.

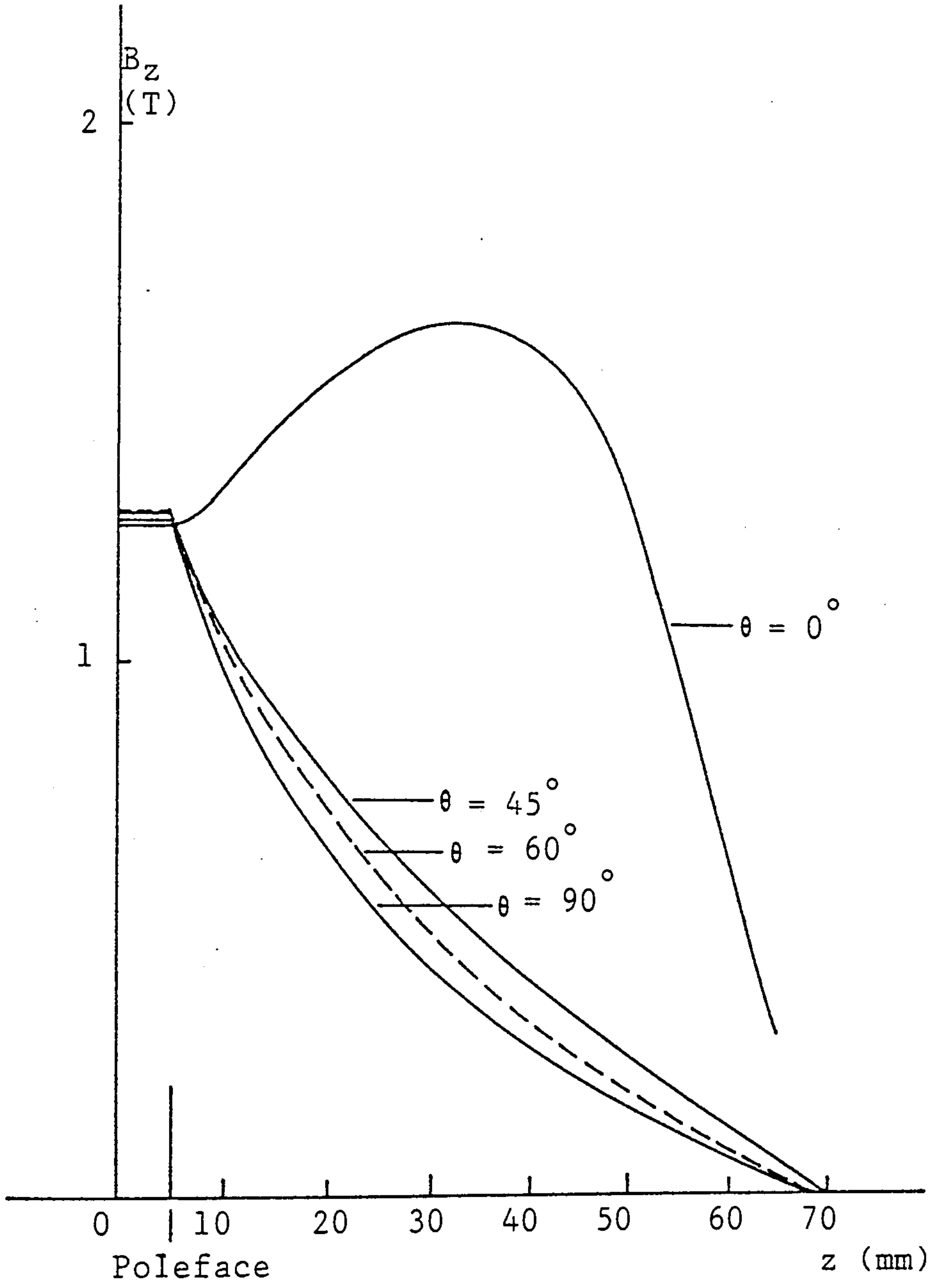

Figure 2.9 The positive half of the computed axial flux density distributions of the four zero-bore lenses shown in figure 2.8 excited by thin flat helical coil under non-saturation conditions at NI = 10000 ampere-turns and $\mu_r = 50000$.

Calculated $B_m = 1.257$ T (equation 1.5)

$\theta = 0^\circ$, $B_m = 1.2526$ T

$\theta = 45^\circ$, $B_m = 1.2746$ T

$\theta = 60^\circ$, $B_m = 1.2963$ T

$\theta = 90^\circ$, $B_m = 1.26454$ T

to B_m. The area, B_mS under the field distribution in the air gap is consistent with the calculated value, μ_o NI. According to equation (1.5), the maximum flux density, B_m (= μ_o NI/S) in the air gap is 1.257 Tesla. Within 1% accuracy in comparison with the calculated value, figure 2.9 shows that by varying the taper angle θ of the polepiece, the maximum flux density B_m is not affected by the profile of the polepiece. However, as one would expect, the taper angle θ has a considerable effect on the flux density inside the iron polepiece. Figure 2.9 shows that the cylindrical polepiece (i.e. $\theta = 0^{o}$) has a peak flux density inside it. This peak disappeared as the polepiece was tapered. Figure 2.9 suggests that in a saturated lens it is important to taper the polepiece at a taper angle of about 60^{o}; a flat-face pole will thus have the shape of a truncated cone.

Another example on the effect of polepiece profile in unsaturated double polepiece lenses is shown in figure 2.10 where sections of three lenses are drawn. Each lens has an axial bore, D of 10 mm and air gap S separating the two polepieces of 10 mm also, i.e. S/D ratio is unity. An objective lens of gap-bore ratio S/D = 1 was considered a good practical compromise (Riecke 1982). The profile of the polepieces has been varied by varying the taper angle θ as shown in figure 2.10. Each lens is excited by a long thin coil of axial thickness 8 mm and inner and outer diameter of 10 and 160 mm respectively, situated within the air gap. The flux density distribution has been computed for high permeability iron (μ_r = 50000) under non-saturation conditions at an excitation of 1000 ampere-turns.

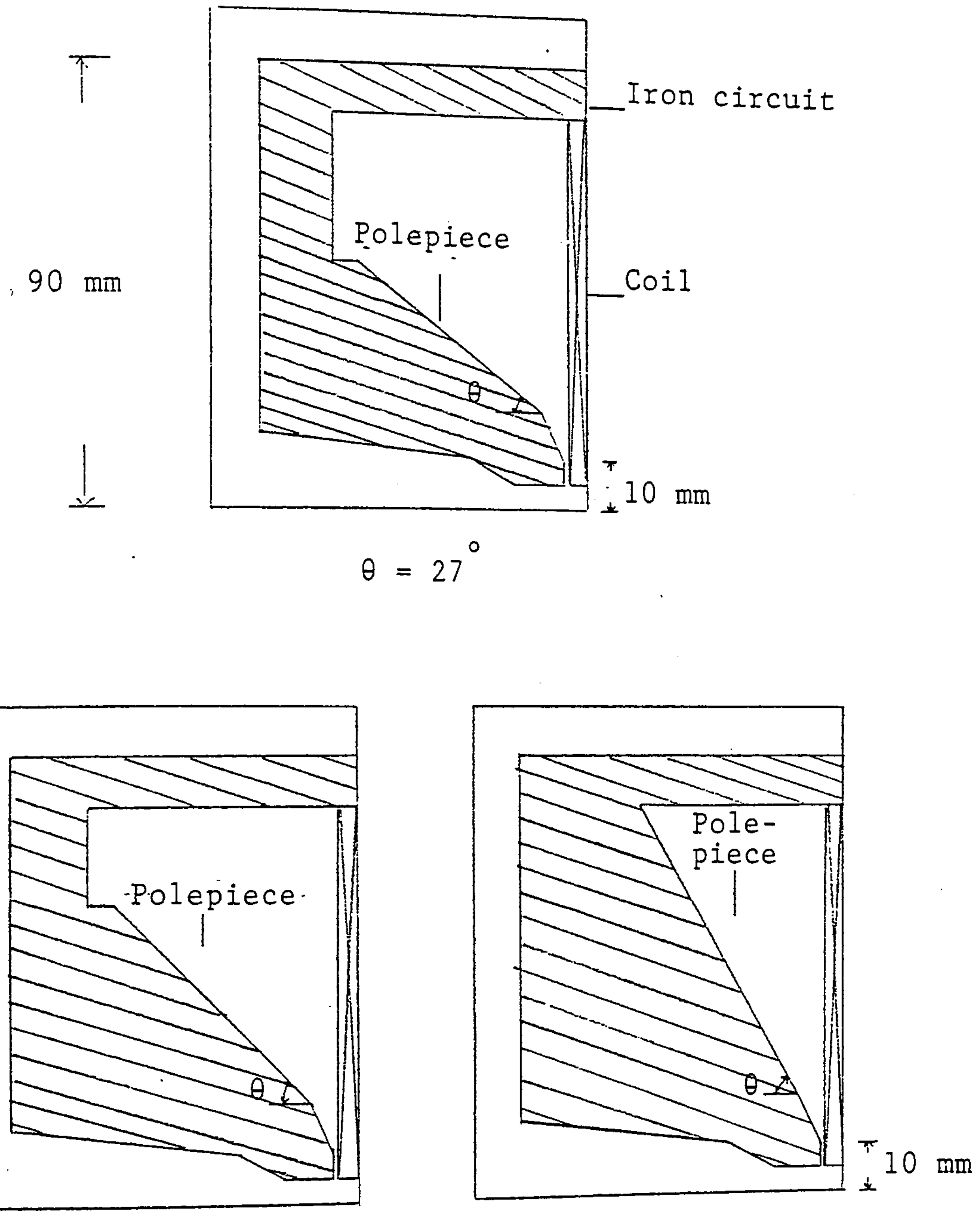

$\theta = 27^\circ$

$\theta = 45^\circ$

$\theta = 60^\circ$

Figure 2.10 Cross-section of the upper quarter of three symmetrical double polepiece lenses (S = 10 mm, D = 10 mm) with different polepiece taper angles ($\theta = 27^\circ$, 45° and 60°) excited by a thin flat helical coil of axial thickness s = 8 mm, inner diameter d_1 = 10 mm and outer diameter d_2 = 160 mm.

According to equations (1.5) and (1.7), the maximum flux density, B_m and the halfwidth W are 0.1044 Tesla and 11.68 mm respectively. Computations have shown that B_m and W of the field in each lens are within an accuracy of 0.5% in comparison with the above values. In addition, the area under the field distribution in each lens is consistent with the value of μ_0 NI.

As in the previous example, this demonstrates the very small effect of polepiece profile and shape, size and position of the energizing coil on the electron-optical parameters of unsaturated lenses with two polepieces of plane parallel faces. Similar results were deduced experimentally by Fert and Durandeau (1967) with unsaturated lenses excited by a bulk coil situated in the conventional position away from the air gap and the faces of the two polepieces.

2.5.3 EFFECT OF THE RELATIVE PERMEABILITY

Three double polepiece lenses, shown in figure 2.11, have been devised to investigate the effect of the relative permeability, μ_r of the iron circuit and the polepiece ferromagnetic material on the axial field under non-saturation conditions. The lenses have different polepiece taper angles, θ. Each lens is energized by a long thin coil of axial thickness 6 mm and inner and outer diameter of 4 and 124 mm respectively i.e. its thickness s to mean diameter d_m ratio is about 0.1 and it is positioned within the air gap separating the two polepieces. The lenses have the same air gap S of 8 mm and axial bore diameter D of 4 mm i.e. the ratio S/D = 2. The value of the maximum flux

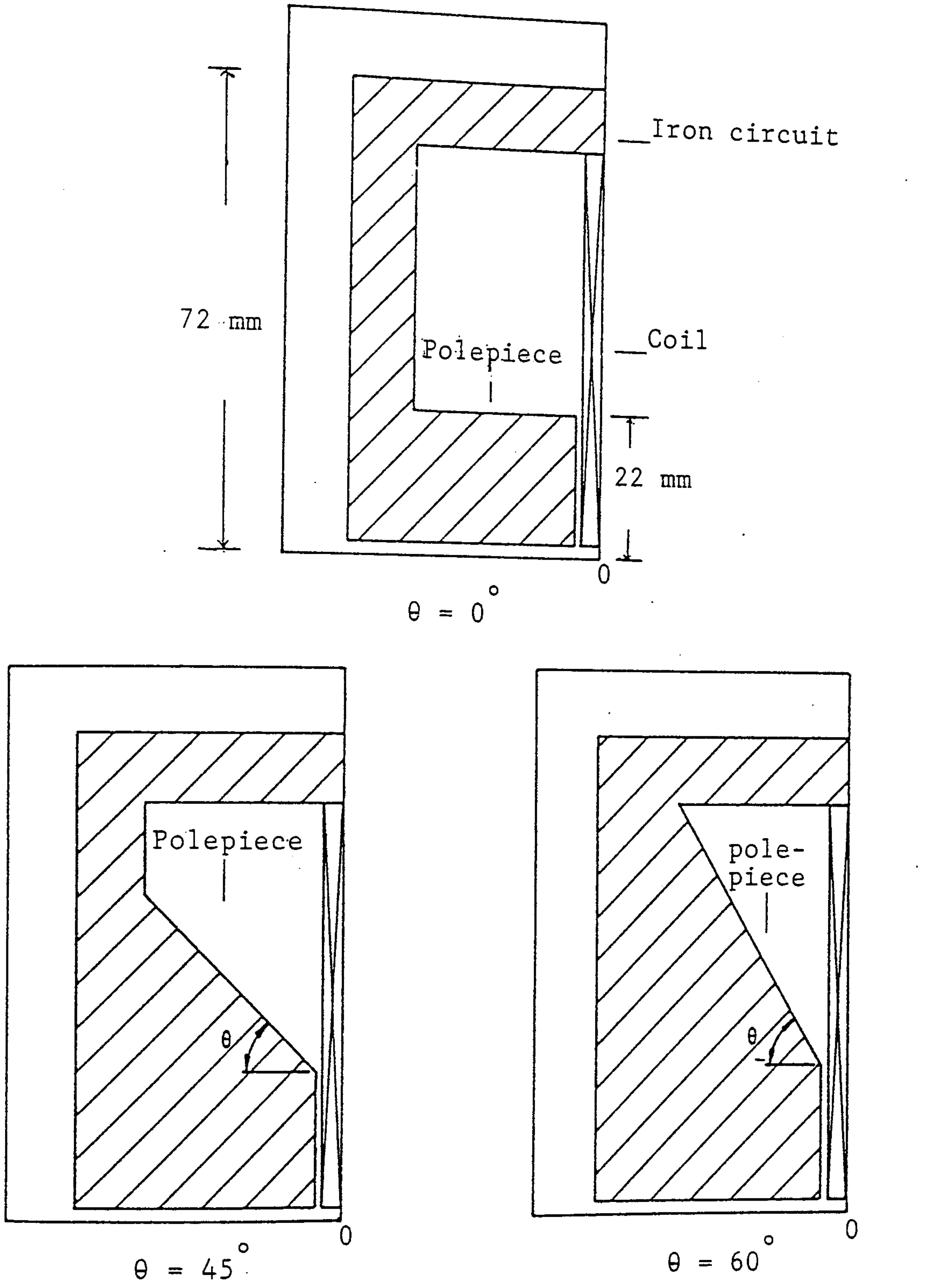

$\theta = 0^\circ$

$\theta = 45^\circ$ $\theta = 60^\circ$

Figure 2.11 Cross-section of the upper quarter of three symmetrical double polepiece lenses ($S = 8$ mm, $D = 4$ mm) with different polepiece taper angles ($\theta = 0^\circ$, 45° and 60°) excited by a thin helical coil of axial thickness $s = 6$ mm, inner diameter $d_1 = 4$ mm and outer diameter $d_2 = 124$ mm.

density at the centre of the air gap, calculated from equation (1.5) is 1.49 Tesla at an excitation of 10000 ampere-turns. The halfwidth W calculated from equation (1.7) is 8.2 mm.

The axial flux density distribution of each lens has been computed at two values of μ_r, 1000 and 50000 using the same excitation of 10000 ampere-turns with the aid of Program M12 of Munro under non-saturation conditions. It was found that the halfwidth W was very little affected by μ_r; it was within 0.5% accuracy compared with the calculated one. However, μ_r has some effect on the maximum flux density B_m as shown in table 2.1

Table 2.1 Effect of the relative permeability μ_r on the maximum flux density B_m of the lenses shown in figure 2.11.

θ°	B_m	
	$\mu_r = 1000$	$\mu_r = 50000$
0	1.4677	1.495
45	1.479	1.499
60	1.483	1.506

At low μ_r, the computed B_m is always lower than the calculated value by about 1% while at high μ_r it becomes about 0.5% higher. By comparison with the calculated value of the area under the axial field curve and that of B_m, the above results indicate that the accuracy is better as μ_r becomes higher due to the elimination in flux leakage at high μ_r. In an untapered (cylindrical) polepiece (i.e. $\theta = 0^\circ$), the flux leakage at low μ_r is higher than that in a tapered one which stresses on the importance of tapering the polepiece.

2.5.4 DISCUSSION

From the results of these computations, it may be deduced that:

(a) The shape, size and position of the energizing coil have little effect on the axial field of unsaturated double polepiece lenses of high permeability.

(b) The use of a stepped edge at the radial boundary of the polepiece to determine the axial field seems to be justified particularly at steeply inclined edges even though it does not model the exact shape of the polepiece.

(c) For a proper choice of meshes, the use of too sharp angles of the coarse quadrilaterals should be avoided. If one, however, is forced to have sharp angles, then a sufficiently dense mesh should be used. The density of mesh lines should not change too abruptly. The mesh must be sufficiently dense in the regions of the polepieces and the coil.

(d) In both Munro's and Lencová's programs the mesh distribution can have a considerable effect on the computed axial field. In general all errors in a finite element program decrease with increasing number of meshes. It was therefore decided to increase the number of meshes available. Fortunately the "AMAG" program of Lencová (with maximum finite element mesh number of 120 mesh points in the axial direction and 51 in the radial direction) became available and so it was decided to repeat some of the calculations with the same mesh arrangement but with a greater number of meshes. The computer program "AMAG" (Lencová 1984) is discussed briefly in the next section.

2.6 LENCOVÁ'S PROGRAM "AMAG"

AMAG is a program for the computation of vector potential distribution in rotationally symmetric magnetic electron lenses (Lencová 1984). It is based on the finite element method, and uses essentially the same algorithm as the program of Munro in the linear B-H mode. In the saturation case, however, it uses the Cholesky decomposition method combined with the conjugate gradient method (or "preconditioned conjugate gradient method") of Meijerink and Van der Vorst as described by Lencová (1977, 1984) and Lencová and Lenc (1984). The program can handle composite magnetic circuits constructed from either one or two magnetic materials with different B-H curves. The program prints and checks the input data, prints the distribution of materials in the mesh, evaluates the axial flux density, prints the value of flux, flux density and mesh coordinates, maps the flux density in the iron circuit, evaluates the flux density in a given region, evaluates the lens excitation from the axial flux density distribution and the flux from the vector potential distribution. It can deal with up to ten excitations using the same input data.

Program AMAG which requires 276 kilo-bytes was run on the Harris 800 of large computer storage at Aston University. It enables one to find the vector potential in a mesh with up to 6500 points including the points on the boundary where the vector potential is zero, and at 6000 points with unknown potential; the maximum number of points in the z axial direction is 120.

The advantages of Lencová's program AMAG may be summarized as follows:

(a) The AMAG program can run with up to 6500 mesh points while that of Munro runs with 1250 mesh points. However, in computing the axial flux density distribution, both programs take the same time and produce identical results if the same layout and number of meshes are used. This fact is very useful in assessing finite element calculations carried out with the two programs and gives useful hints to the operator.

(b) The AMAG program is largely self-checking.

(c) The number of excitations dealt with in this program are up to ten. Usually the current densities in the coil are arranged in ascending order. The program starts first with linear (non-saturation) computations at the lowest excitation and then proceeds with non-linear (saturation) computations.

(d) The program can determine, if it is required, the axial flux density in an infinitesimally small bore along the axis. With a special subroutine designated "AMULV", the axial flux density B_z in the iron is divided by the relevant relative permeability μ_r at the point in question. This is mathematically equivalent to finding the axial flux density distribution in a bore of vanishingly small size.

(e) The program also evaluates numerically by trapezoidal rule the integral of the axial flux density (B_z/μ_r) to determine and print the effective excitation NI of the lens; thus allowing for the presence of a polepiece with zero bore; this may be checked against the excitation given originally. Any discrepancy between these values of NI indicates the presence of an error caused by the selected boundary position.

(f) The program prints out the distribution of materials in the mesh and hence one may check the correct input of the lens materials (iron, copper, vacuum).

Accurate computation of the axial field distribution can also be ensured by the method of linear extrapolation suggested by Lencová (1984). If the axial field distribution, is calculated for two values n_1 and n_2 of the total number of meshes used, a linear extrapolation may be made for the corresponding value for an infinite number of meshes. The simplest method is to plot the value of B_z as a function of 1/n as shown for example in figure 2.12. The inset diagram in figure 2.12 shows the upper half of a zero-bore lens with a single spherical-face truncated-cone polepiece excited at 161465 ampere-turns by a thin flat coil of large ratio d_2/d_1 of outer to inner diameter (38.7). Initially 25 x 50 meshes were employed, and the axial flux density distribution was computed for a soft iron circuit. The number of meshes was then increased to 63 x 92, and the axial flux density distribution was re-computed. From the two computed fields, the axial flux density at any point on the lens axis can be chosen and plotted as a function of 1/n. As an example, in figure 2.12 the peak flux density B_m at 3 mm from the poletip and the two values for the two mesh numbers are plotted as function of 1/n. The line joining these two points has been extrapolated to the value for $1/n = 0$ i.e. the value of the axial flux density for an infinite number of meshes. By replacing the smooth conical sides and the spherical face of the pole-

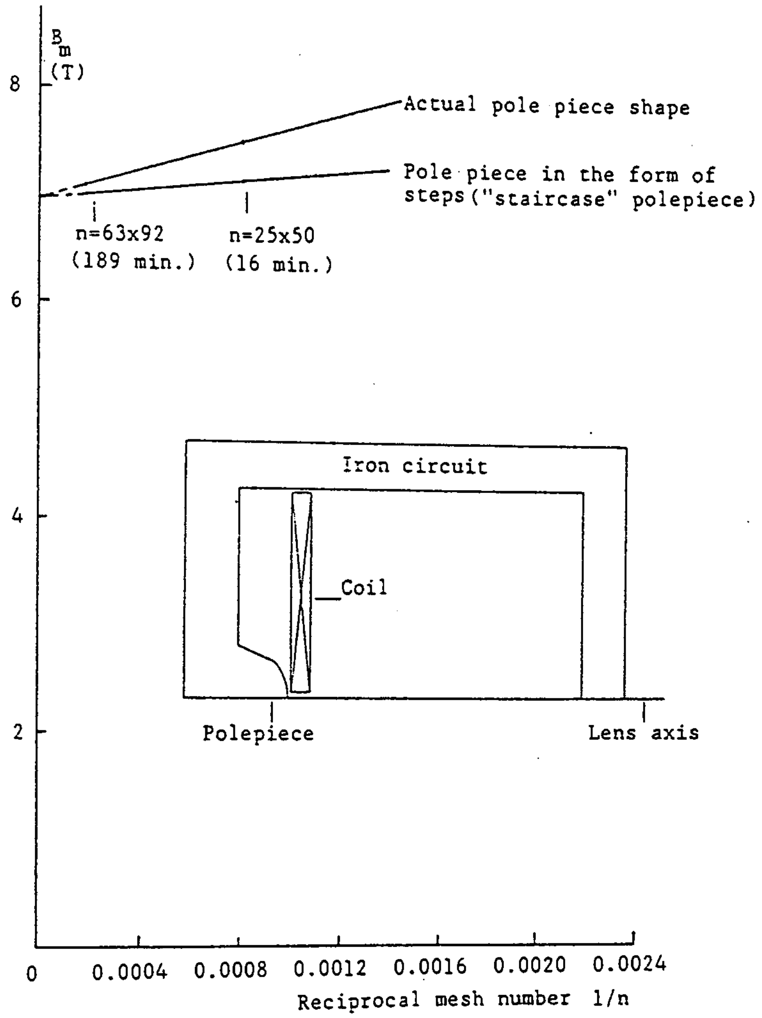

Figure 2.12 Extrapolation procedure to an infinite number of meshes. Two values of the peak flux density B_m computed at NI = 161465 ampere-turns using two different meshes n (25 x 50 and 63 x 92) plotted as a function of 1/n. The two points are extrapolated to 1/n = 0 to determine the value of the peak flux density for an infinite number of meshes.

Note: For the layout of the mesh distribution of the lens with the actual polepiece and the "staircase" polepiece see Appendix 3.

piece by a series of small steps (i.e. "staircase" polepiece), the above method of extrapolation produced the same value of the peak flux density at the point $1/n = 0$. The extrapolation method thus indicates that the greater the number of meshes n (i.e. smaller $1/n$) used the more accurate the computed field will be but time can be saved by the extrapolation method. Furthermore, the larger the number of meshes, the less sensitive will be the calculated result to the choice of mesh layout. On the other hand the computer storage requirements go up rapidly with increasing n. The chief advantage of the extrapolation method therefore is that it gives a good indication of the probable result for $n = \infty$ without the need for excessive computer storage.

2.7 THE B-H CURVES

The polepieces of magnetic electron lenses can be made of soft iron or Permendur. The B-H curves for soft iron and Permendur, used in the programs Munro and Lencová, are shown in figure 2.13 where B is the magnetic flux density and H is the magnetic field strength.

The relative permeability μ_r may be deduced from the B-H curve since

$$\mu_r = B/(\mu_o H) \qquad (2.4)$$

where μ_o is the permeability of vacuum ($4\pi \times 10^{-7}$ H/m). The value of μ_r is dependent on the material concerned (Kamminga 1976, Cleaver 1980).

Program M13 of Munro (1975) uses an iterative method to take into account the B-H characteristic of the iron circuit. Up to five data inputs allow for magnetization

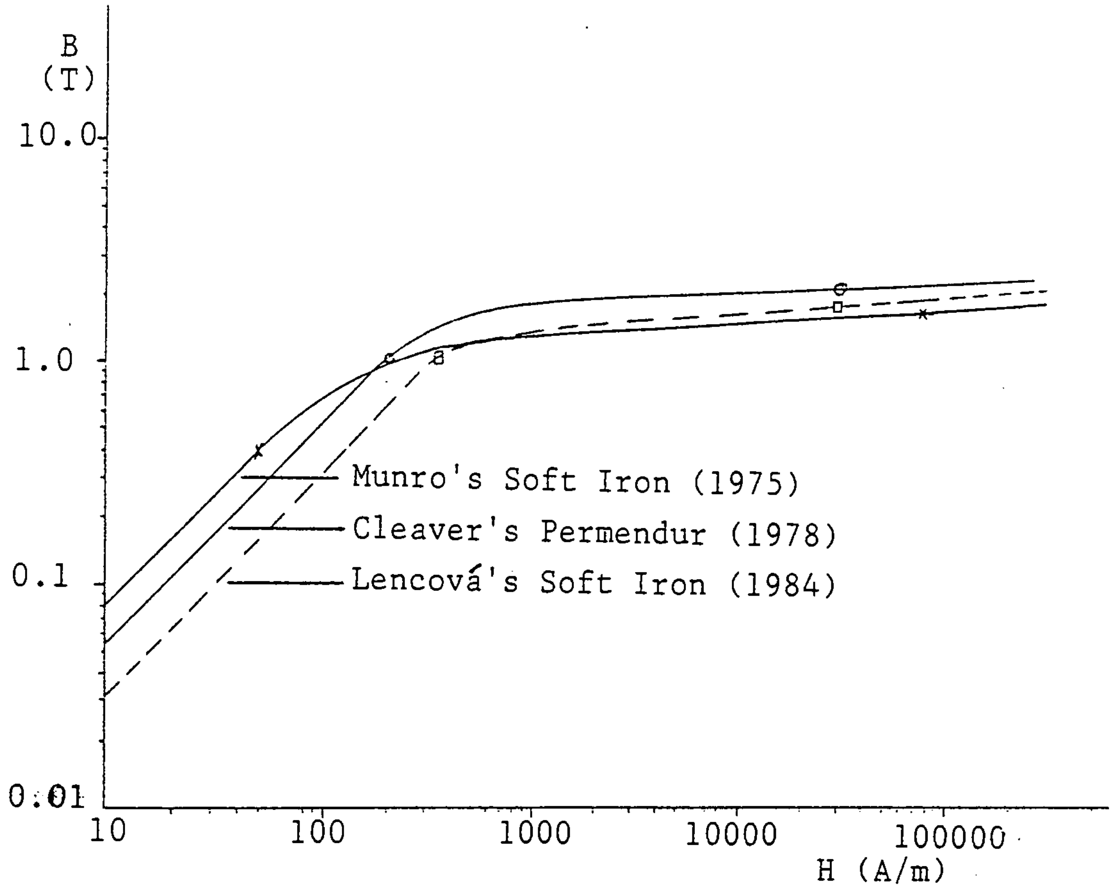

Figure 2.13 Magnetization curves for soft iron (Munro 1975, Lencová 1984) with Permendur (Cleaver 1978). The first point on each curve represents the limiting value of the linear region. The second point represents the beginning of the saturation region.

curves in the form of a B-H table for each magnetic material. In this investigation the B-H curves for soft iron of Munro (1975) and Lencová (1984) were used but for Permendur only the B-H curve of Cleaver (1978) was used.

In Munro's program the B-H curve of soft iron is assumed to be linear up to a flux density of 0.4 Tesla with a constant relative permeability μ_r of 6366.2. This region is therefore called the linear region. For a flux density B greater than 0.4 Tesla and less than 1.9 Tesla the actual values of B-H are used. This region is called the intermediate region. For values of B greater than 1.9 Tesla the B-H curve is represented by a straight line. This region is called the saturation region since the increase in B with H is due entirely to the increase in H and not to the magnetization of the iron.

The B-H curve for Permendur (Cleaver 1978) shown in figure 2.13 is assumed to be linear up to a flux density of 1.07 Tesla with constant μ_r of 4257.4. In the intermediate region, B has values greater than 1.07 Tesla and less than 2.4 Tesla.

In program AMAG of Lencová (1984), up to two kinds of iron may be handled (as opposed to five in program M13 of Munro); these are represented by two B-H magnetization curves or tables. Each B-H curve may have maximum of 20 B-H points. The lowest (B-H) values specify the linear region of constant relative permeability and the highest value specifies the onset of the saturation region. This is essentially the same procedure therefore as in Munro's program. Likewise, the whole mesh area is divided into quadrilaterals which are further subdivided into triangles.

Each small triangle may contain only one type of material (iron,coil or non-magnetic material). If the triangle lies in the magnetic material and a first approximation is required in the non-linear mode, the value of the two permeabilities μ_r and μ_d can be determined from the magnetization curve to a linear approximation given by $\mu_r \approx \mu_d \approx \mu_{ro}$ where μ_r is the relative permeability, μ_o the permeability of vacuum and μ_d the differential permeability given by

$$\mu_d = \left(\frac{\partial B}{\partial H}\right)/\mu_o \tag{2.5}$$

In the linear approximation, the iron has a constant initial relative permeability μ_{ro} given by

$$\mu_{ro} = \left(\frac{BM(1,I)}{H(1,I)}\right) /\mu_o \tag{2.6}$$

where BM(1,I) and H(1,I) are the first listed value of magnetic flux density and magnetic field strength respectively.

In Lencová's program therefore, with her B-H curve, the value of μ_{ro} for soft iron is constant and equal to 2478.3. For the non-linear computation, the values of μ_r and μ_d are evaluated from the magnetization curve with the help of the following formulae.

Here BC means the flux density value at the centre of the triangle and BM(J,I) means the listed value of magnetic flux density.

(a) If BC $\leqslant$ BM(1,I), then $\mu_r = \mu_d = \mu_{ro}$ = constant.

In the intermediate region,

(b) if BM(J,I) < BC $\leqslant$ BM(J+1,I), then

$$\mu_d = \frac{BM(J+1,I) - BM(J,I)}{\mu_o\ [\ H(J+1,I) - H(J,I)\ ]} \tag{2.7}$$

and

$$\mu_r = \frac{BC}{\mu_o\ H(J,I) + [\ BC - BM(J,I)\ ]/\mu_d} \qquad (2.8)$$

(c) If BC > BM(J,I), i.e. BM(J,I) is the last value in the table, then $\mu_d = 1$ and μ_r is defined as follows

$$\mu_r = \frac{BC}{\mu_o\ H(J,I) + [\ BC - BM(J,I)\ ]} \qquad (2.9)$$

Figure 2.14 shows the variation of relative permeability μ_r with flux density B for soft iron (Munro 1975, Lencová 1984) and Permendur (Cleaver 1978) in the linear and intermediate regions of the B-H curves shown in figure 2.13. It is seen that in the assumed linear region of each B-H curve the value of μ_r remains constant with increasing B. However, in the intermediate region, μ_r decreases with increasing B and its initial and final values depend on the material in use. Table 2.2 shows typical values of B, H and μ_r for soft iron and Permendur in the linear region and at the beginning of the saturation region deduced from figures 2.13 and 2.14.

In the following section an example is given in which six different lenses are computed with aid of the programs of Munro and Lencová. In all cases polepieces were made of Permendur and the iron shroud was made of high permeability iron (μ_r = 50000).

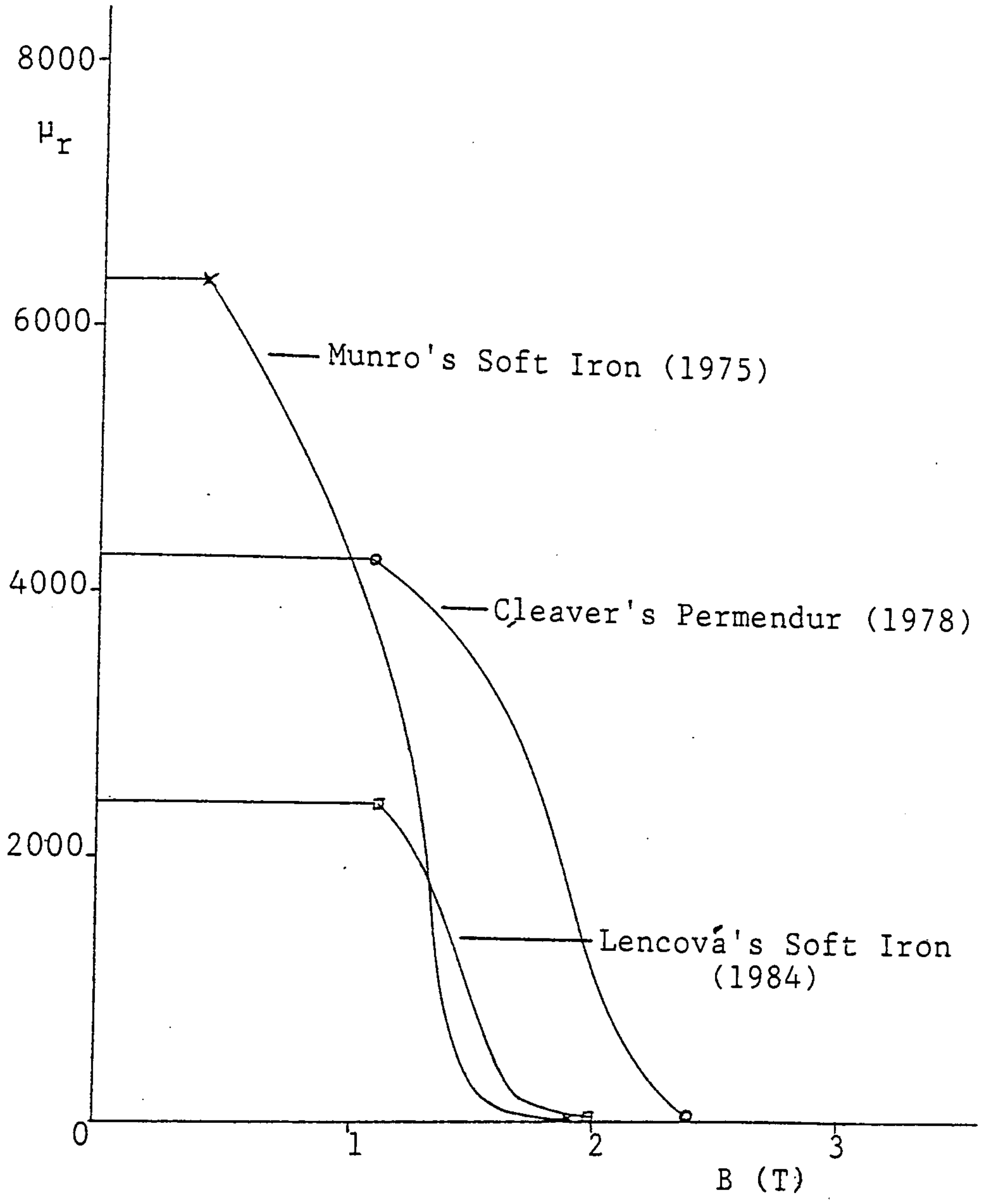

Figure 2.14 Relative permeability μ_r as a function of flux density B in the linear and intermediate regions of the B-H magnetization curves shown in figure 2.13 for soft iron (Munro 1975, Lencová 1984) and Permendur (Cleaver 1978). The horizontal part of each curve represents the constant value of μ_r in the linear region. The first point on each curve shows μ_r value at the start of intermediate region. The second point indicates the start of the saturation region.

Table 2.2 Typical B-H parameters for Munro and Lencová programs.

Curve	Linear region			Saturation starts at		
	up to		Constant			
	B (T)	H (A/m)	μ_{ro}	B (T)	H(A/m)	μ_r
Soft iron (Munro 1975)	0.4	50	6366.2	1.9	77421	19.5
Soft iron (Lencová 1984)	1.09	350	2478.3	1.99	30000	52.8
Permendur (Cleaver 1978)	1.07	200	4257.4	2.4	30000	63.7

2.8 COMPARISON BETWEEN MUNRO AND AMAG PROGRAMS

In order to compare the Munro and AMAG programs under practical conditions it was decided to compute a number of test lenses based on designs that have been reported in the literature, such as those of Cleaver (1978), Riecke (1962) and Ruska (1962). These test lenses follow the idea put forward by Cleaver (1978) for saving meshes. Since the modelling of the lens shroud is a separate design issue from the modelling of the polepieces it is possible to replace the normal bulky shroud by a much thinner iron sheet of high permeability. It should be remembered however, that once the best polepiece shape has been arrived at, a further field calculation is needed on the actual shroud to check that no appreciable external leakage flux is being generated.

The three lenses designated TL1, TL2 and TL3 are shown in figure 2.15. TL1 is based on Cleaver's test lens (Cleaver 1978), TL2 is based on the lens of Riecke and Ruska (1962). Lens TL3 with poipiece taper angle of 60° was devised by the author. Following Cleaver (1978) the polepieces of the test lenses were of Permendur, whilst the external shroud was of soft iron with a fixed permeability (μ_r = 50000). The test lenses TL1-TL3 are excited by long energizing coils (inner diameter d_1 = 150 mm. outer diameter d_2 = 160 mm and axial thickness s = 84 mm) similar to conventional coils as used by Cleaver and Ruska. Another group of test lenses TL4-TL6 shown in figure 2.16 have similar shapes to the TL1-Tl3 group but the arrangement of the coil is unconventional, being in the form of thin flat helical windings (inner diameter d_1 = 3.4 mm, outer diameter d_2 = 160 mm and axial thickness s = 10 mm) filling the lens gap S. Since the lens is symmetric the diagrams shown in figures 2.15 and 2.16 show only a quarter of the magnetic circuit.

The programs of Munro and Lencová were used for computing the axial flux density of the six test lenses. With the 25 x 50 mesh size of Munro's programs, and using the same mesh size and arrangement in the Lencová program it was found that the results were always identical. However, with the higher mesh numbers at which the program of Lencová can be operated, the results were slightly, but systematically different. In the following computations, the programs were operated at their maximum mesh number, using a suitable mesh distribution. The increase in the mesh number allowed by the Lencová program was usually

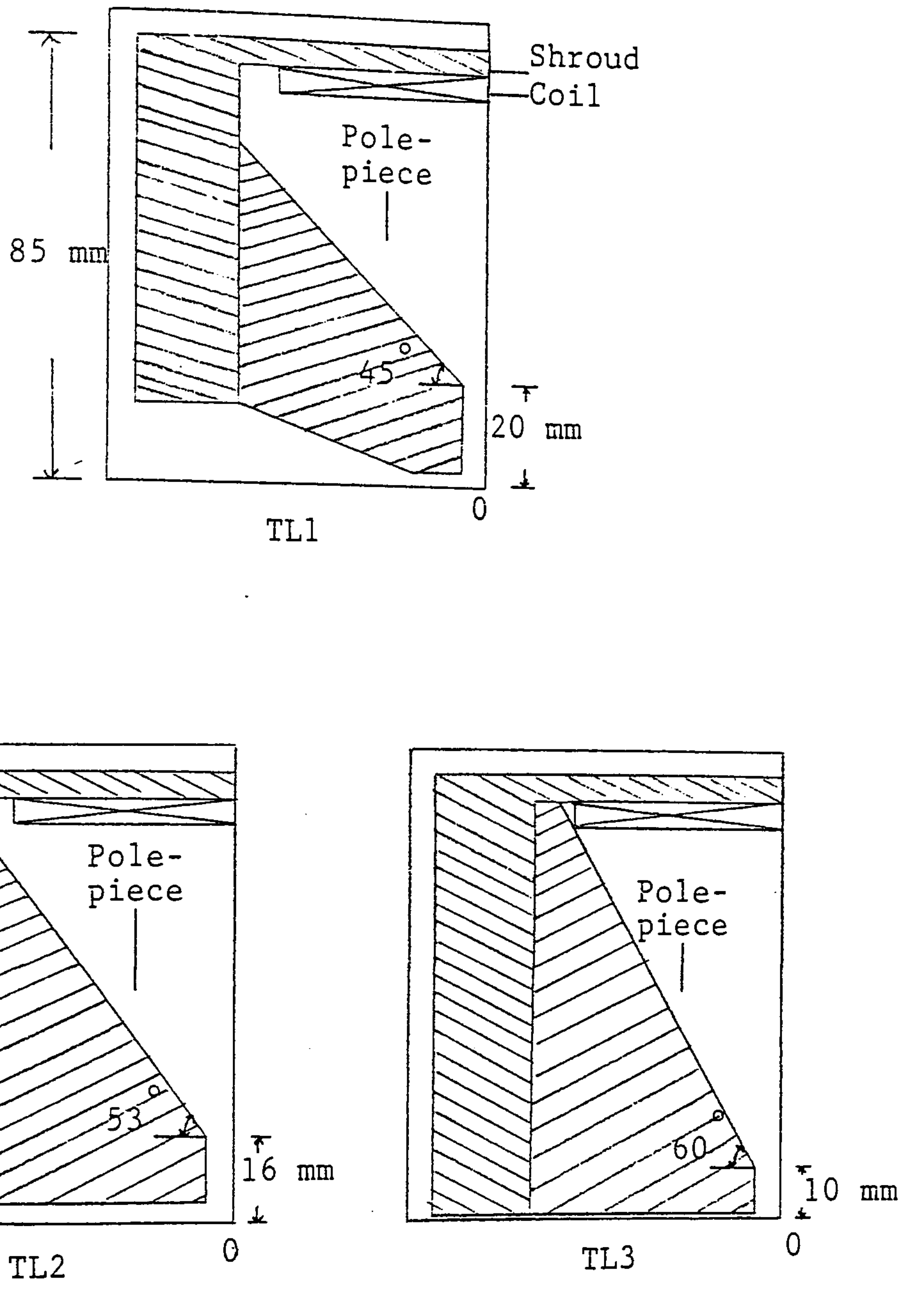

TL1

TL2

TL3

Figure 2.15 Cross-section of upper quarter of three symmetrical double polepiece test lenses excited by a solenoid coil of axial thickness s = 84 mm, inner diameter d_1 = 150 mm and outer diameter d_2 = 160 mm.

Test lens TL1. Gap S = 10 mm, axial bore diameter D = 5 mm.

Test lens TL2. Gap S = 10 mm, axial bore diameter D = 8 mm.

Test lens TL3. Gap S = 10 mm, axial bore diameter D = 1.7 mm.

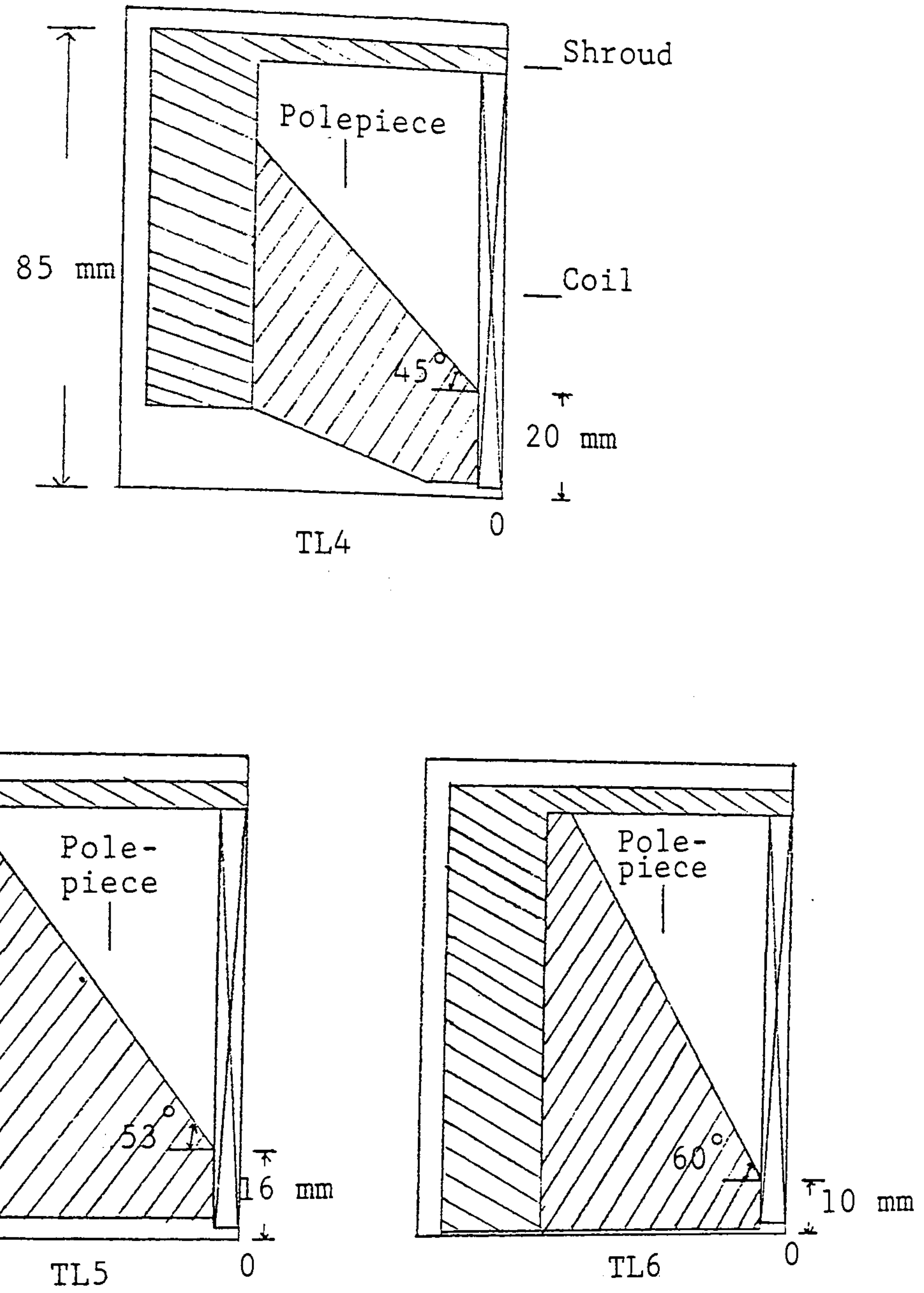

TL4

TL5

TL6

Figure 2.16 Cross-section of the upper quarter of three symmetrical double polepiece test lenses excited by the same thin flat helical coil of axial thickness $s = 10$ mm, inner diameter $d_1 = 3.4$ mm and outer diameter $d_2 = 160$ mm.

Test lens TL4. Gap $S = 10$ mm, axial bore diameter $D = 5$ mm.

Test lens TL5. Gap $S = 10$ mm, axial bore diameter $D = 8$ mm.

Test lens TL6. Gap $S = 10$ mm, axial bore diameter $D = 1.7$ mm.

employed in the polepiece region since it is the most sensitive part of a magnetic lens.

In the linear B-H region of the polepieces the values, calculated from Fert and Durandeau (1967), of the maximum flux density ($B_m = \mu_o NI/L$), in the lens gap, at 10000 ampere-turns and the halfwidth ($W = 0.97L$) of the six test lenses were as follows: Lenses TL1 and TL4, 1.19 Tesla and 10.23 mm; Lenses TL2 and TL5, 1.107 Tesla and 11 mm; Lenses TL3 and TL6, 1.25 Tesla and 9.8 mm respectively.

The area under the axial flux density distribution (figure 2.17) computed by Lencová's program (using 63 x 92 meshes) of each lens is in excellent agreement with the theoretical value $\mu_o NI$ as shown directly by the Lencová program. The accuracy of the area of the field computed by Munro's program was checked by program Area and agreed within 1%. This self checking of the program of Lencová with regard to the area under the curve is an advantage over that of Munro which requires more efforts to check. From the axial fields computed with the aid of the two programs, the following results were obtained for B_m and W as shown in table 2.3. The table also includes the relevant values predicted by the equations of Fert and Durandeau (1967). The results shown in table 2.3 indicate that the computed and the values according to Fert and Durandeau (1967) of B_m and W are, in general, within an accuracy of 1-2%. A comparison between the results computed by the two programs suggests that, in the linear region, an increase in the mesh number affects both the peak height and the halfwidth of the axial flux density distribution; systematic changes of both quantities up to 1% in fact occur. However, both

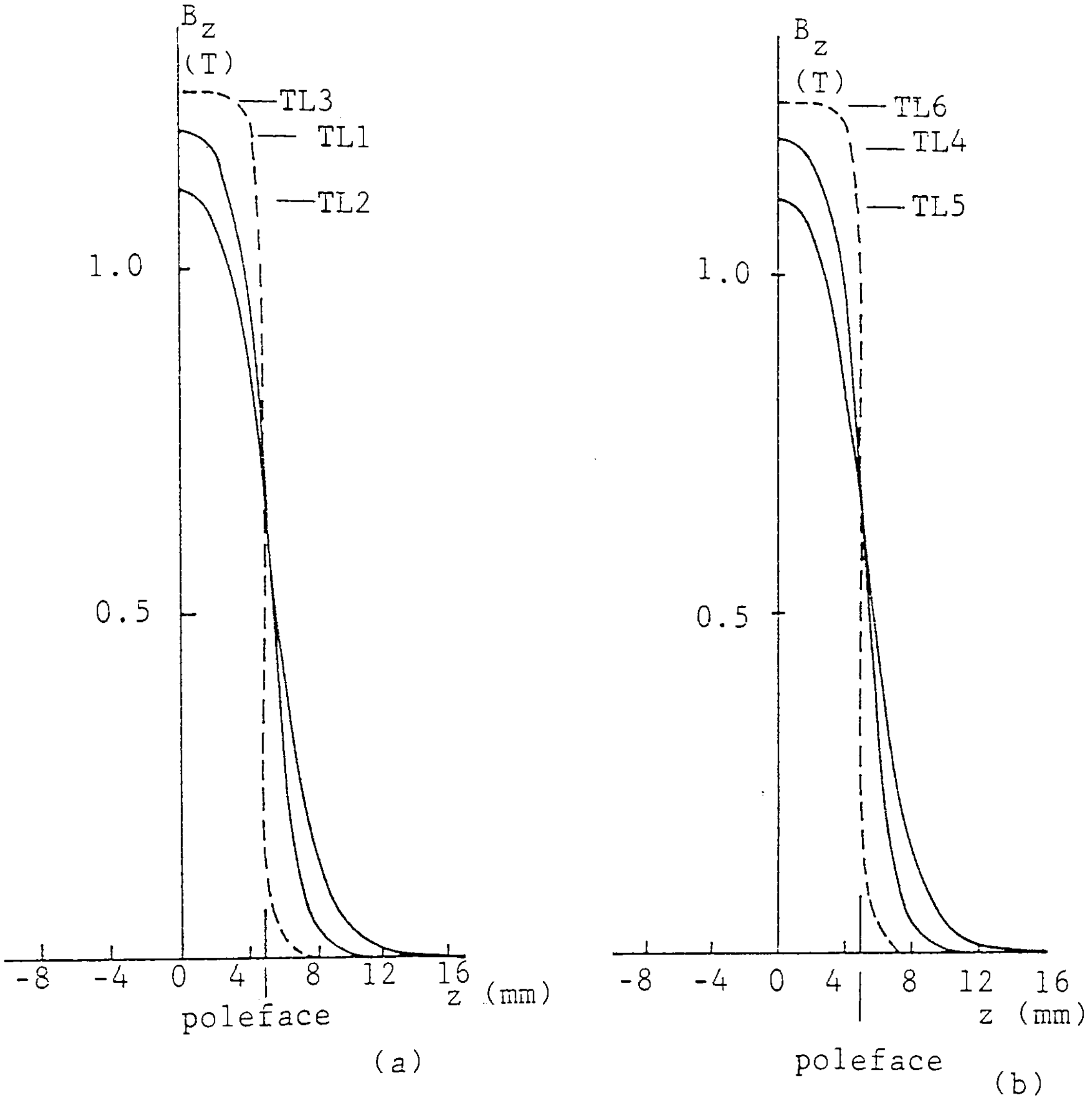

Figure 2.17 The positive half of the axial flux density distributions computed with the Lencová program at NI = 10000 ampere-turns, Permendur polepieces and high permeability shroud (μ_r = 50000).

(a) Fields of the lenses shown in figure 2.15 using a long solenoid coil.

(b) Fields of the lenses shown in figure 2.16 using a thin flat coil.

Table 2.3 The maximum flux density B_m and the halfwidth W of the axial field of the test lenses shown in figures 2.15 and 2.16 excited at NI = 10000 ampere-turns (linear program). Munro program 25x50 meshes, Lencová program 63x92 meshes and * Fert and Durandeau equations (1967).

Maximum flux density, B_m in Tesla at $NI=10^4$ ampere-turns				
Coil	Program	Test lenses		
		TL1 and TL4	TL2 and TL5	TL3 and TL6
Solenoid	Munro	1.203	1.099	1.245
	Lencová	1.2025	1.115	1.257
Thin	Munro	1.207	1.11	1.258
	Lencová	1.204	1.117	1.258
Fert and Durandeau equation		1.19*	1.107*	1.25*

Halfwidth W in mm				
Coil	Program	Test lenses		
		TL1 and TL4	TL2 and TL5	TL3 and TL6
Solenoid	Munro	10.3	11.0	9.85
	Lencová	10.4	10.9	9.85
Thin	Munro	10.3	11.0	9.85
	Lencová	10.4	10.9	9.85
Fert and Durandeau equation		10.23*	11.0*	9.8*

programs are sufficiently accurate for computations in the linear region. As one would expect under non-saturation conditions, the above results show that the values of B_m and W are independent of the shape of the energizing coil. This is due to the negligible contribution of the coil field, B_{coil} to the lens field B_z compared with that of B_{Fe} due to the iron.

The results show that the effect of the bore is an important factor for determining the peak flux density and halfwidth.

When the computations were carried out under saturation conditions, the permeability of the shroud was kept constant at $\mu_r = 50000$ but the appropriate B-H curve (Cleaver 1978) of Permendur polepieces was used. Excitations of 30000, 50000, 70000 and 90000 ampere-turns were used for each lens. Figure 2.18 shows an example of the shape of the axial flux density distributions, computed by the Lencová program, of the test lenses TL1, TL2 and TL3 fitted with long solenoids excited at 90000 ampere-turns. Since the field of each lens is symmetrical, only half of the curve is drawn for simplicity. Figure 2.19 shows the corresponding axial field distributions for the lenses TL4, TL5 and TL6 i.e. the same magnetic circuits of TL1, TL2 and TL3 but with a thin flat coil located in the lens gap. It was found that the area under the field distribution curve of each lens, computed directly by the program of Lencová, was consistent, in all cases, with the value of the applied excitation NI irrespective of the coil shape. The area of the fields computed by Munro's program was checked by program Area and was found to be 3% higher than the theoretical value μ_0 NI.

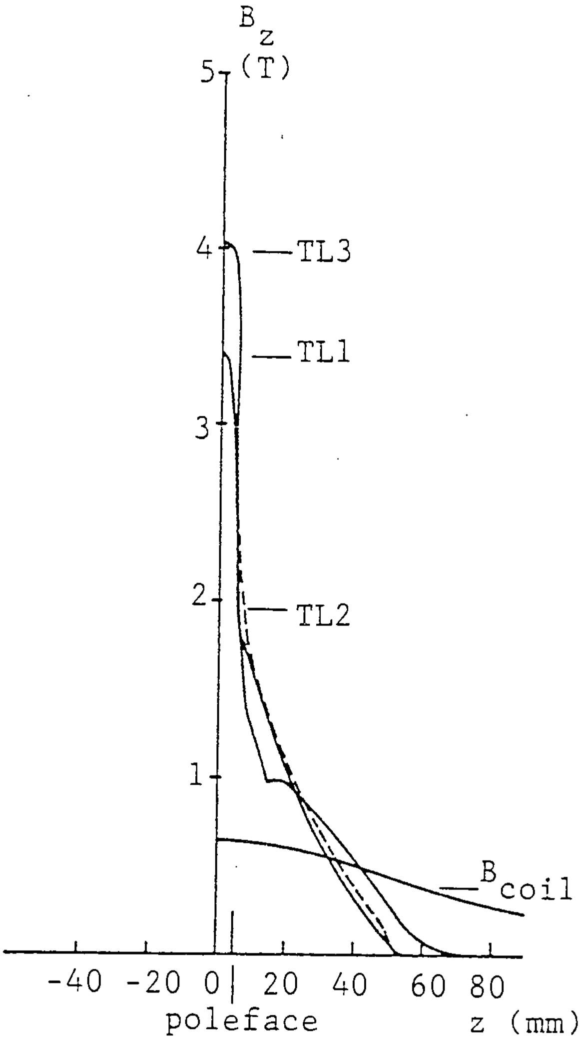

Figure 2.18 Axial flux density distributions, computed by the Lencová program at NI = 90000 ampere-turns, (μ_r of the shroud = 50000) of the three test lenses TL1, TL2 and TL3 shown in figure 2.15 with Permendur polepieces and excited by a long solenoid coil. Only the positive half of the axial fields is shown.

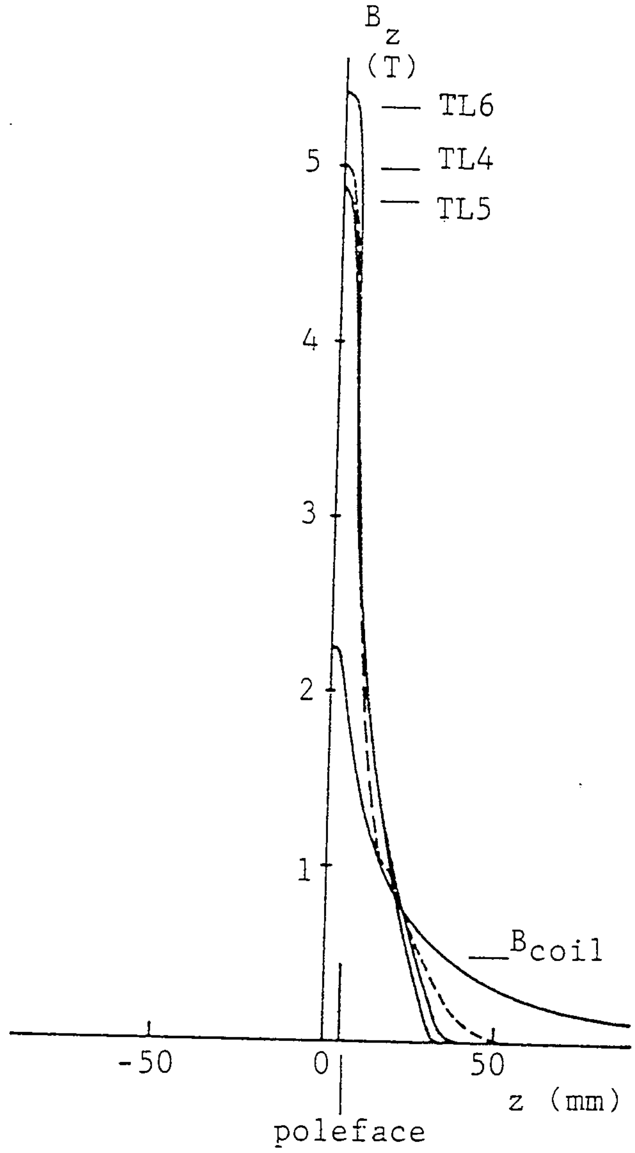

Figure 2.19 Axial flux density distributions, computed by the Lencová program at NI = 90000 ampere-turns, (μ_r of the shroud = 50000) of the three test lenses TL4, TL5 and TL6 shown in figure 2.16 with Permendur polepieces and excited by a thin flat coil positioned within the air gap. Only the positive half of the axial fields is shown.

The reason for this is not entirely clear, but it could be caused by the limited number of meshes available in the Munro program. In addition the Lencová program uses a gradual increase of excitation rather than the abrupt change from the linear to saturation employed by Munro.

At the various excitations used in the computations under saturation conditions the two programs gave different values of the lens field parameters such as peak flux density and halfwidth. Tables 2.4-2.6 which show the computed parameters of the axial field at 90000 ampere-turns give an example of the results obtained by the two programs. Table 2.4 shows that the values of the maximum axial flux density B_m at the centre of the test lenses excited by a thin coil are higher than those in the lenses excited by a solenoid due to the considerable contribution of the thin

Table 2.4 The maximum flux density B_m at the centre of the test lenses shown in figures 2.15 and 2.16 excited at NI = 90000 ampere-turns (saturation program). Munro program 25x50 meshes, Lencová program 63x92 meshes.

Maximum flux density, B_m in Tesla at 90000 ampere-turns				
Coil	Program	Test lenses		
		TL1 and TL4	TL2 and TL5	TL3 and TL6
Solenoid	Munro	3.42	3.35	3.92
	Lencová	3.43	3.43	4.03
Thin	Munro	5.01	4.86	5.37
	Lencová	5.02	4.89	5.42

coil in the air gap region at high excitations. The values of B_m computed by the program of Munro are consistently lower (0.2-3%) than those computed by the program of Lencová.

Figure 2.20 shows an example of the shape of the axial field B_{Fe} due to iron magnetization, for thin and solenoid coils respectively at 90000 ampere-turns. Magnetization by a solenoid coil leads to more axial broadening of the B_{Fe} field inside the bore than that of the thin coil. Since the effective total number of ampere-turns contributed by the iron circuit is zero, then according to Ampere's law a negative magnetic field must inevitably appear in the axis of the lens. The area under the negative half of the B_{Fe} curve must be equal to the area under the positive half of the curve. It is found, however, that with both types of coil and in both programs the positive part of the B_{Fe} field was consistently higher than the negative part. For example in Munro's program with 25 x 50 meshes this error could perhaps amount to 3%. The same sort of error would also be expected in the Lencová program with the same number of meshes. However, if the larger mesh (63 x 92) of the Lencová program is used, this error was found to drop to just below 1%.

At the poleface the value of B_{Fe} cannot exceed the saturation flux density (2.37 Tesla) of the Permendur polepiece. Since the flux lines due to the iron converge at the centre of the gap, the effective contribution of the iron can rise to about 3.4 Tesla (figure 2.20). Table 2.5 shows the values of B_{Fe} at the poleface of the six test lenses.

It is seen in table 2.5 that when the lenses are

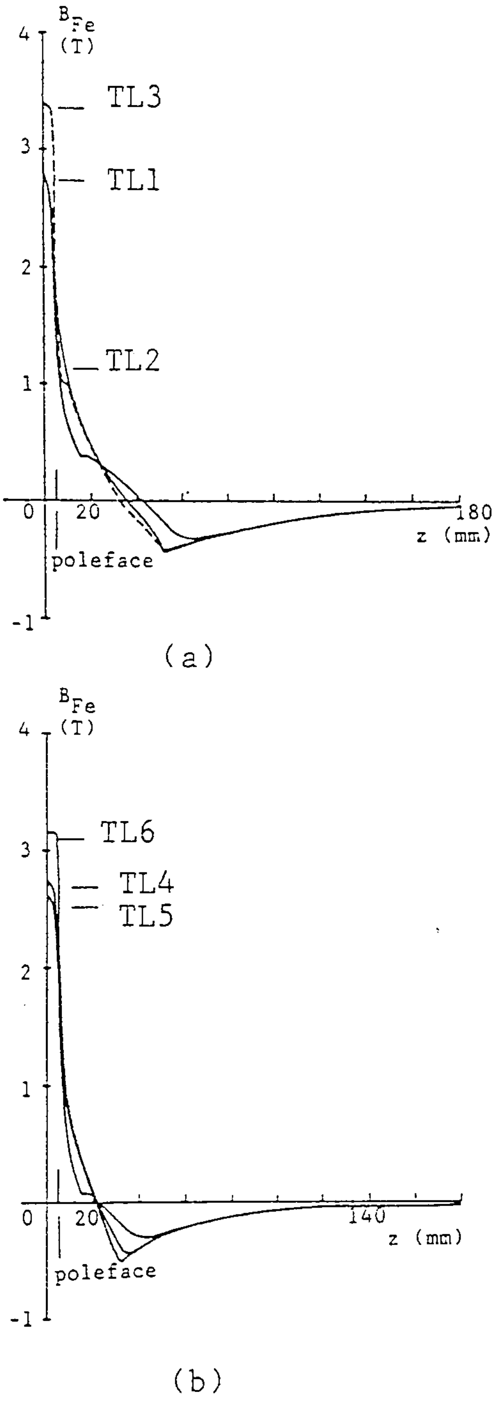

(a)

(b)

Figure 2.20 Axial fields B_{Fe} due to iron magnetization computed by the Lencova´ program at 90000 ampere-turns, (μ_r of the shroud = 50000) of the six test lenses with Permendur polepieces shown in (a) figure 2.15 which are energized by a solenoid coil and (b) figure 2.16 which are energized by a thin flat coil. Only the positive half of the axial fields is shown.

Table 2.5 Poleface flux density due to iron magnetization B_{Fe} of the test lenses shown in figures 2.15 and 2.16 excited at NI = 90000 ampere-turns (saturation program). Munro program 25x50 meshes, Lencová program 63x92 meshes.

Poleface field B_{Fe} due to iron in Tesla at 90000 A-t				
Coil	Program	Test lenses		
		TL1 and TL4	TL2 and TL5	TL3 and TL6
Solenoid	Munro	1.93	1.97	2.32
	Lencová	1.86	2.03	2.36
Thin	Munro	1.91	1.84	2.18
	Lencová	1.83	1.87	2.19

energized by a solenoid, the value of B_{Fe} at the poleface is higher (1-8%) than that by a thin coil. This indicates that the solenoid is a better magnetizer than the thin coil. However the peak flux density B_m at the centre of the lenses energized by a thin coil (figure 2.19) is higher than those energized by the solenoid coil (figure 2.18) as shown in table 2.4; this is due to the considerable contribution of the thin coil field to the total field B_z. The poleface of the test lenses TL3 and TL6 reaches the value of saturation flux density of Permendur before the other test lenses. This can be attributed to the small poleface and small bore diameter compared with those of the other test lenses. Figure 2.21a,b shows plots of flux lines in the six lenses at 90000 ampere-turns. The figure demonstrates the high density of flux

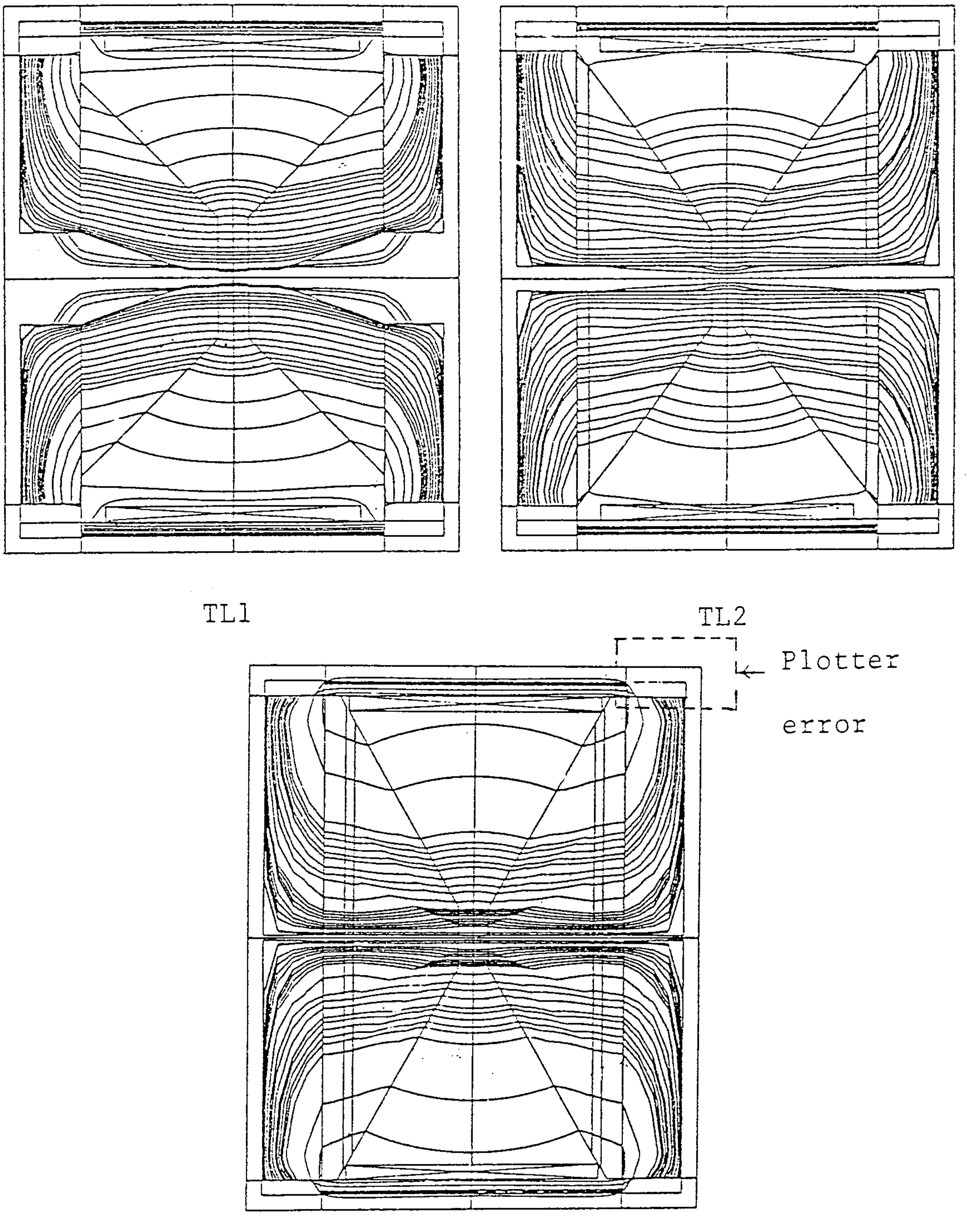

TL1

TL2

Plotter error

TL3

Figure 2.21(a) Plots of the magnetic flux lines computed at NI = 90000 ampere-turns (μ_r of the shroud = 50000) in the three test lenses with Permendur polepieces which are excited by a solenoid coil.

Test lens TL1 (S = 10 mm, D = 5 mm).

Test lens TL2 (S = 10 mm, D = 8 mm).

Test lens TL3 (S = 10 mm, D = 1.7 mm).

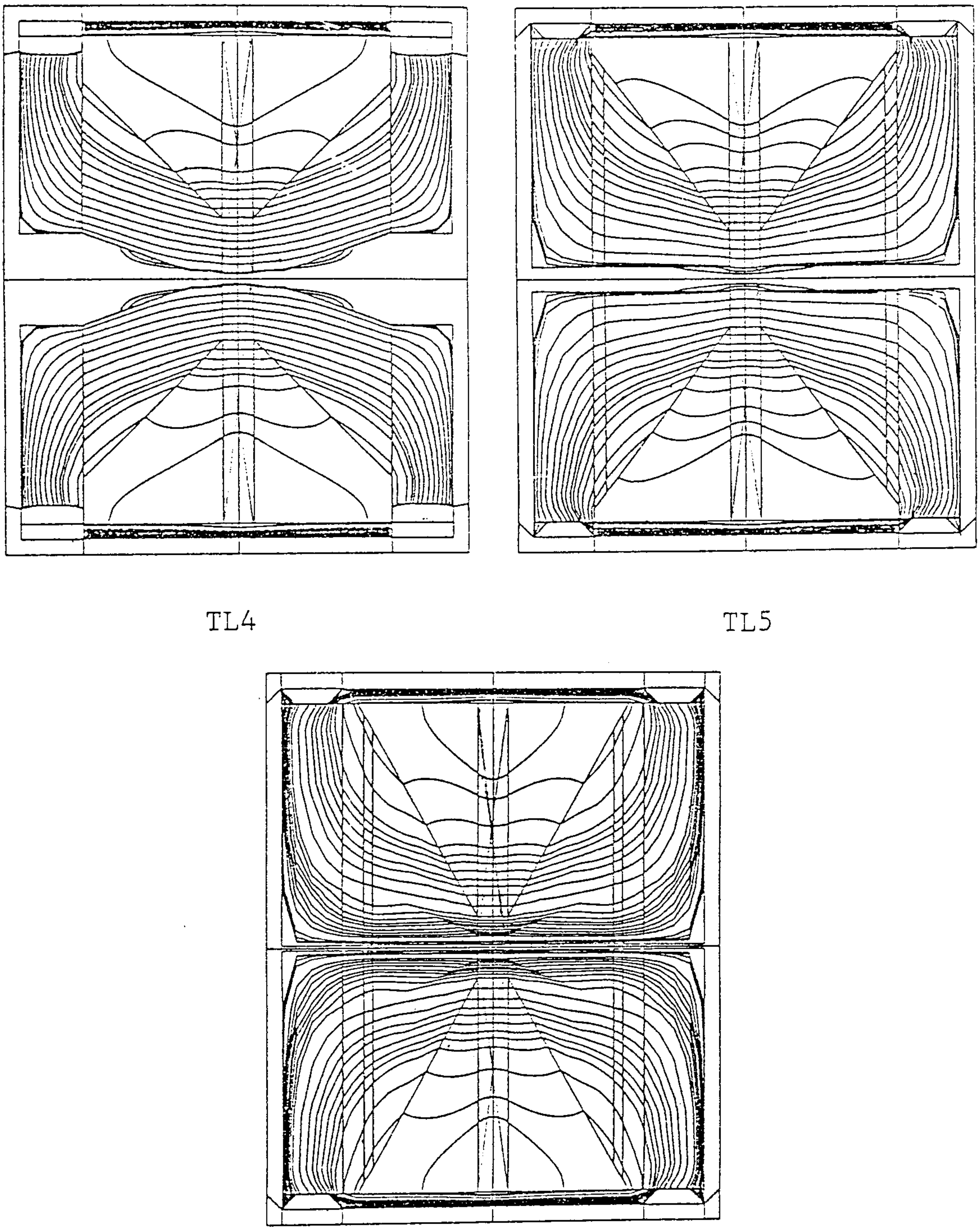

TL4

TL5

TL6

Figure 2.21(b) Plots of the magnetic flux lines computed at NI = 90000 ampere-turns (μ_r of the shroud = 50000) in the three test lenses with Permendur polepieces which are excited by a flat thin coil.

Test lens TL4 (S = 10 mm, D = 5 mm).

Test lens TL5 (S = 10 mm, D = 8 mm).

Test lens TL6 (S = 10 mm, D = 1.7 mm).

lines at the poleface region of the test lenses TL3 and TL6. Thus as far as magnetization and high peak flux density are concerned, it is preferrable to have a small face area and small bore diameter.

The effect of the programs, coil shape and the dimensions of the polepiece on the halfwidth W of the axial field of a saturated lens is demonstrated by the results shown in table 2.6. The values of W computed by the program of Munro with 25 x 50 meshes are 0.2-5.2% higher in comparison with those computed by the program of Lencová with 63 x 92 meshes.

Table 2.6 indicates that the test lenses TL3 and TL6 have the smallest halfwidth even at high excitation and as a comparison with its halfwidth in the linear region shows that the field broadening of those two lenses is not so high as in the case of the other test lenses.

Table 2.6 Halfwidth W of the axial field of the test lenses shown in figures 2.15 and 2.16 excited at NI = 90000 ampere-turns (saturation program). Munro program 25x50 meshes, Lencová program 63x92 meshes.

Halfwidth, W in mm computed at 90000 ampere-turns				
Coil	Program	Test lenses		
		TL1 and TL4	TL2 and TL5	TL3 and TL6
Solenoid	Munro	14.0	18.04	11.1
	Lencová	13.6	18.0	10.65
Thin	Munro	14.25	16.4	12.04
	Lencová	14.0	16.35	11.45

Figures 2.22(a) and 2.22(b) show the variation of B_m, B_{Fe} and B_{coil} at the centre of test lenses TL1-TL6 of figures 2.15 and 2.16 and the halfwidth W of the axial field B_z with the excitation NI produced by a solenoid and thin coil respectively. The program of Lencová was used to compute the parameters plotted in figures 2.22(a) and 2.22(b).

Figures 2.22(a) and 2.22(b) show that:

(a) the deviation from linearity of B_m-NI curve occurs at about 20000 ampere-turns,

(b) the peak of the coil field at the centre of the air gap due to the thin coil is always higher than that of the solenoid for a given excitation,

(c) the test lenses TL3 and TL6 have the highest B_m and B_{Fe}, at the centre of the air gap, and the smallest halfwidth which indicate that their focal properties are better than those of the other test lenses.

Comparing the two programs, it can be concluded that with same number and layout of meshes both programs produce similar results. However, if the large mesh number of the Lencová program is used, the error usually found in the area under the axial flux density distribution curve for example, drops well below that of Munro. The area under the curve of the axial field computed by the program of Lencová is more consistent with theoretical value μ_o NI. This indicates the importance and the advantage of having large number of meshes in use. In addition, the direct check of the area by the program of Lencová is an advantage over that of Munro since it saves time and effort. The larger number of meshes that can be used in the program of Lencová has an advantage

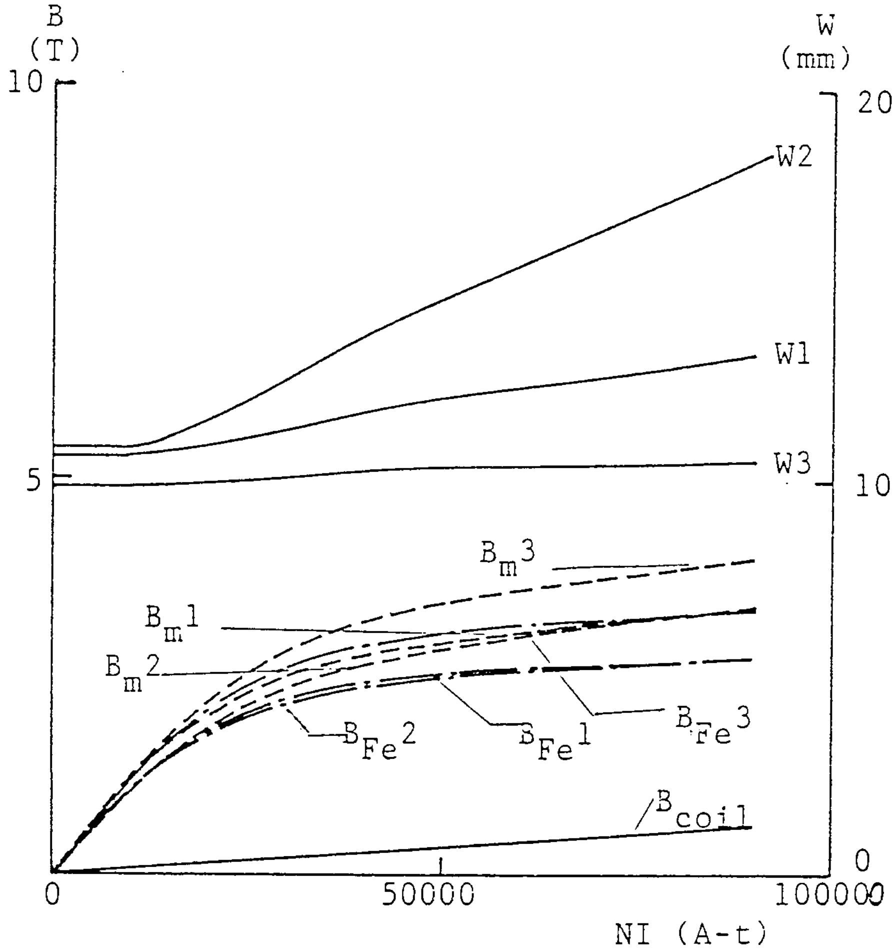

Figure 2.22(a) The halfwidth W of the axial field B_z computed by the Lencová program and the values of B_m, B_{Fe} and B_{coil} at the centre of the test lenses TL1, TL2 and TL3 shown in figure 2.15, as a function of the excitation NI. The lenses are excited by a long solenoid.

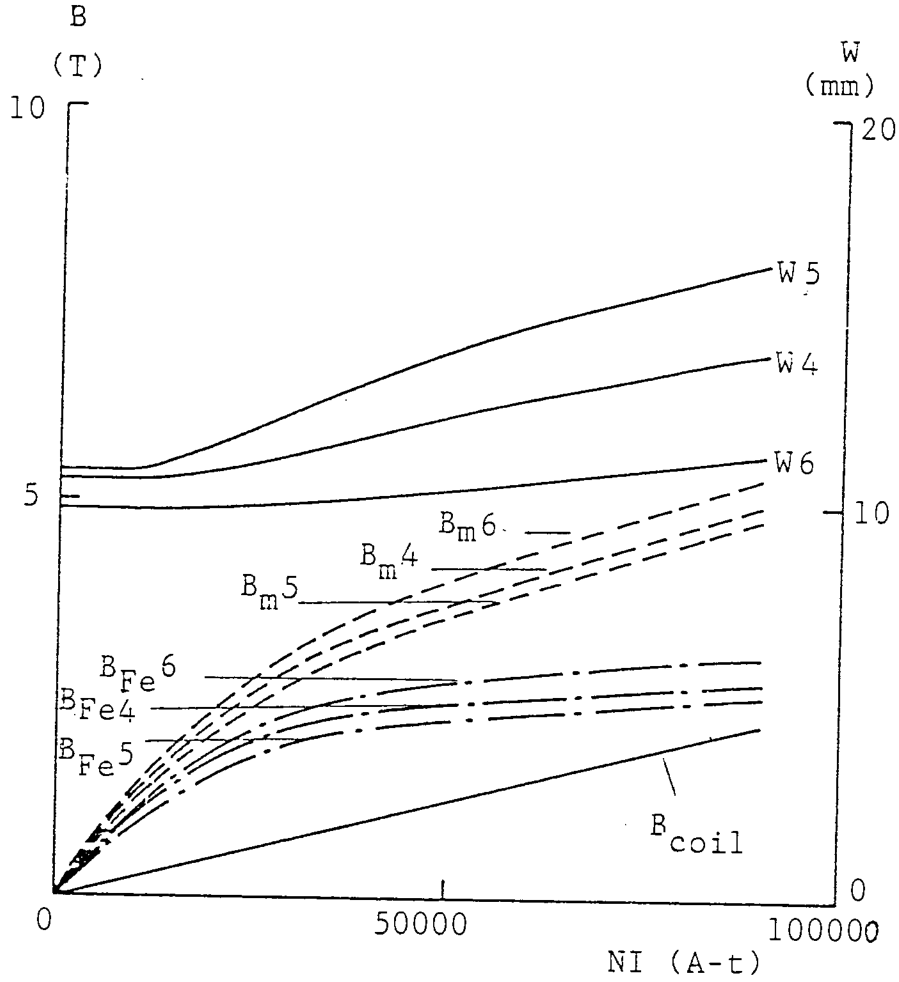

Figure 2.22(b) The halfwidth W of the axial field B_z computed by the Lencová program and the values of B_m, B_{Fe} and B_{coil} at the centre of the test lenses TL4, TL5 and TL6 shown in figure 2.16 as a function of the excitation NI. The lenses are excited by a thin coil.

when investigating the field of lenses where the polepieces are either large in size or complicated in shape. In these cases the fields computed with aid of the program of Lencová are more accurate than those computed by Munro's program. However, this does not imply that the fields computed by Munro's program are not sufficient for computer-aided-design considerations.

3. DESIGN OF SATURATED SINGLE POLEPIECE OBJECTIVE LENS

In objective lenses, aberration coefficients must be small to achieve high resolution and if possible a large space should be available around the specimen to allow freedom for specimen manipulation. The single polepiece lens can satisfy these requirements. It provides a large solid angle around the poletip and low spherical aberration coefficient compared with its polepiece dimensions at both SEM and TEM modes of operation (Mulvey 1974b). As with all lenses, the electron-optical properties of the single polepiece lens depend on the shape of the axial magnetic field.

3.1 EFFECT OF SHAPE OF POLEPIECE AND COIL

One may imagine that the factors involved in controlling the the electron-optical parameters of the single polepiece lens are the polepiece shape, and the design of the energizing coil. The size of the axial bore in the polepiece will alter the axial field distribution and hence the electron-optical properties. However, in the present work attention has been concentrated on lenses of zero or infinitesimally small bore.

Figure 3.1 shows the various shapes of soft iron zero-bore polepieces and flat helical energizing coils which have been employed in a series of test lenses. The following four shapes of polepiece were studied:

(a) Flat-face cylindrical polepiece.
(b) Flat-face truncated-cone polepiece.
(c) Hemispherical polepiece.
(d) Spherical-face truncated-cone polepiece.

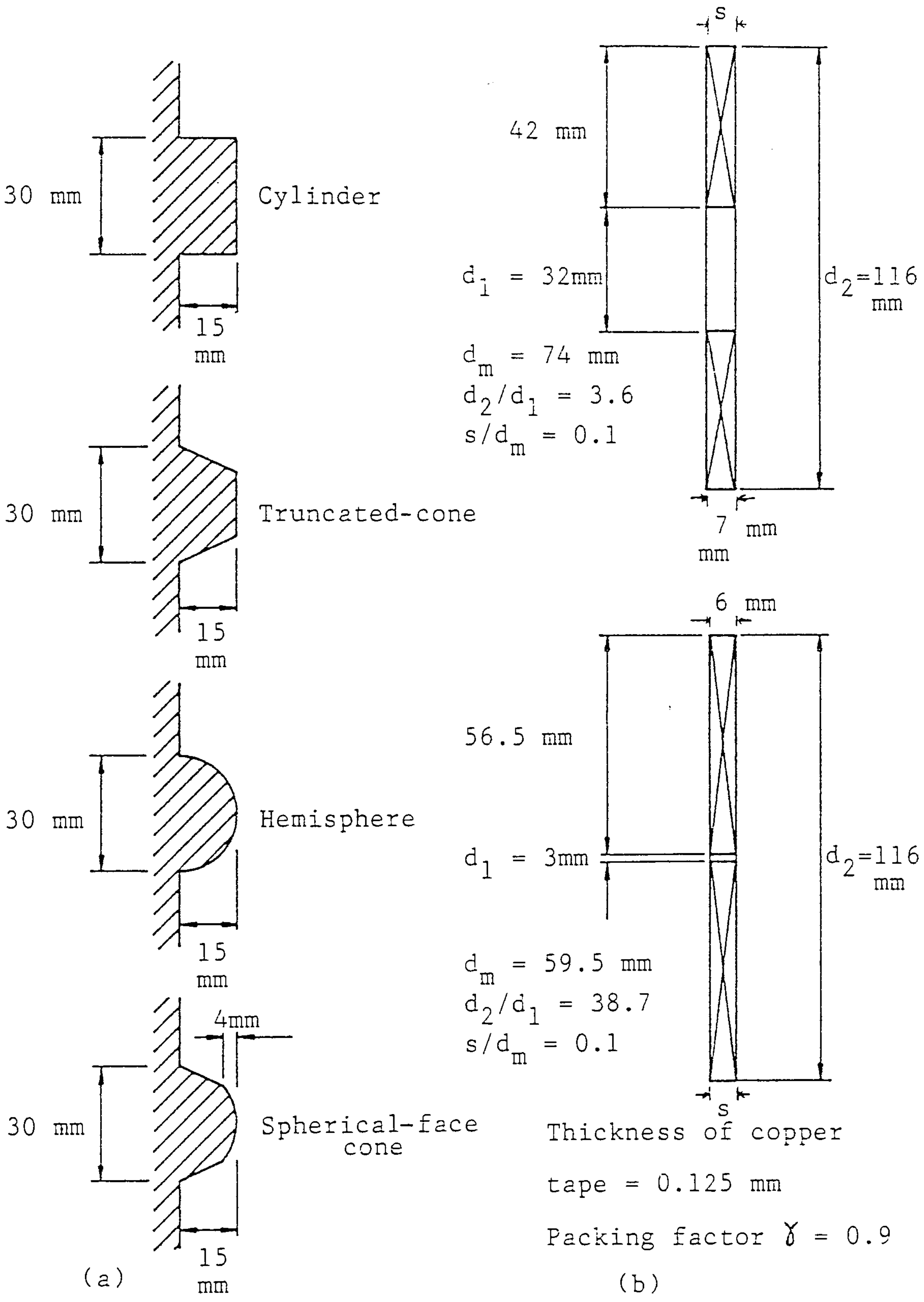

(a) (b)

Figure 3.1 Diagram of the various shapes and dimensions of the zero-bore polepieces and thin flat helical coils considered in the different types of magnetic electron lenses. (a) four polepieces, (b) two flat copper tape coils.

The dimensions of each thin flat coil were chosen such that the value of the ratio of its axial thickness s to the mean diameter d_m was maintained at about 0.1 in order to produce a high flux density and a small halfwidth axial field. However, it should be remembered that the optimum shape of the coil ($s/d_m = 0.1$) described above, assumes that the current density in the coil is not a limiting factor. Since the actual current density in a given lens is known only after the lens properties have been calculated, it was decided to calculate the current density σ in the coil as well as the focal properties. The relevant σ values are shown in subsequent diagrams. The current density σ in each coil under consideration was calculated from equation (1.3) for a copper tape winding of packing factor $\gamma = 0.9$ and thickness 0.125 mm (figure 3.1b). A value of $\sigma = 20000$ A/cm^2 has been adopted in this thesis as the point above which the use of superconducting windings cannot be avoided. Computations were carried out using Munro's M13 saturation program and also by Lencová's program.

3.1.1 SINGLE POLEPIECE LENS WITH A FLAT-FACE CYLINDRICAL POLE

The investigation was begun by considering a test lens SP1 (figure 3.2) with a single flat-face cylindrical polepiece, since the cylinder represents the simplest pole design that can be made. The lens is enclosed in a complete iron shell to define its magnetic boundary in a precise manner. Figure 3.2 shows two examples of the computed axial flux density distributions at two different positions of the coil with respect to the poleface. The coil has an inner bore

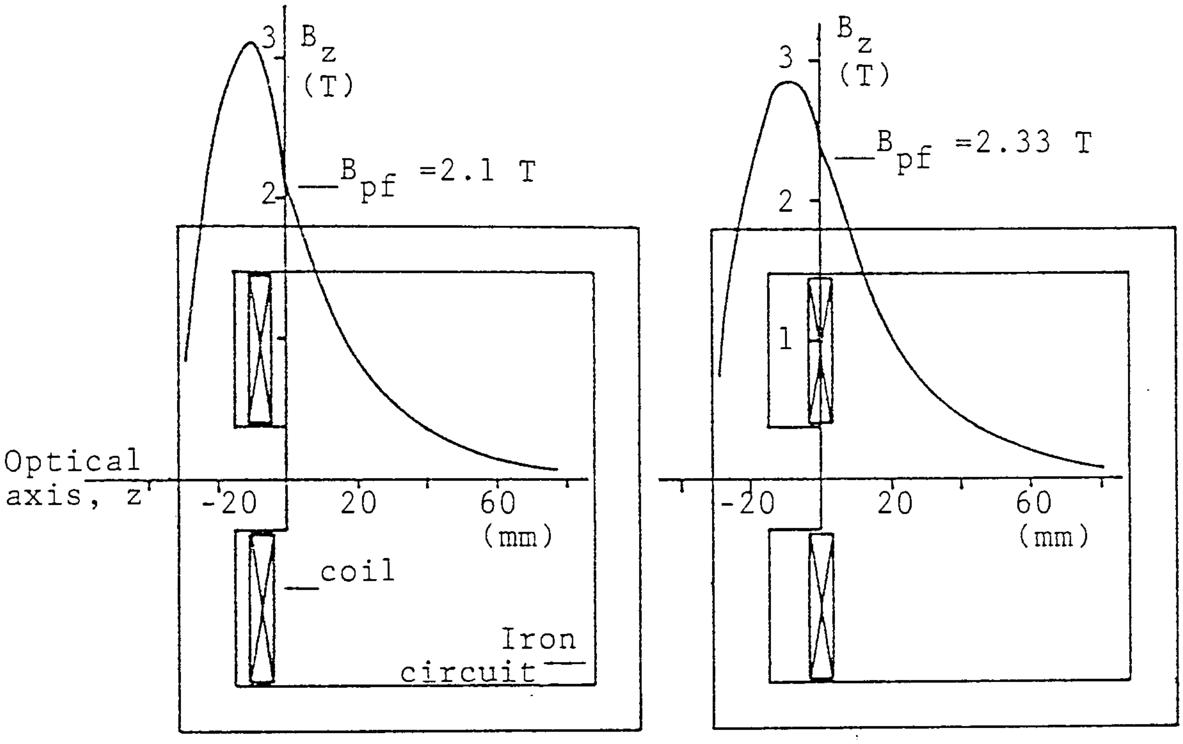

(a)

(b)

Test lens SP1

Figure 3.2 Axial flux density distributions in a zero-bore single polepiece test lens SP1 with a soft iron flat-face cylindrical pole, computed at NI = 60000 ampere-turns and current density $\sigma = 22700\ \mathrm{A/cm^2}$ for two positions of the energizing coil ($s = 7$ mm, $d_1 = 32$ mm and $d_2 = 116$ mm). Lens outer diameter = 144 mm.

(a) Coil is placed in the conventional position.

(b) Centre-plane of coil coincides with the poleface.

which allows the coil to slide over the polepiece. The field distributions of figure 3.2 (and those computed at other positions of the coil) have shown that a flux density peak is always situated inside the iron polepiece. An example of the plots of magnetic flux lines in this type of lens for the two positions of the coil is shown in figure 3.3. The presence of the peak inside the soft iron polepiece is further demonstrated by the convergence of the flux lines inside the polepiece. It is seen that at the poleface region the flux lines in the vicinity of the lens axis are nearly normal to the poleface but converge once they enter the iron polepiece.

Therefore, an arrangement of a cylindrical polepiece magnetized by a coil which is situated in the conventional position creates a flux density peak inside the iron cylinder, rather than at the poleface. A lens of such simple design operated in the linear region of the B_{Fe}-H magnetization curve can be used as an objective in SEM and generally as a probe-forming lens which may be placed outside the vacuum system or with a small axial bore in the polepiece, it can be used successfully as a projector in TEM. However, for an objective lens it would be desirable to see if the peak flux density could be made to occur at the poleface.

The variation of the poleface flux density B_{pf} with the position of the centre-plane of the coil is shown in figure 3.4 computed at a constant excitation NI of 60000 ampere-turns and current density σ of 22700 A/cm^2. It is seen that the highest B_{pf} occurs when the centre-plane of the coil coincides with the poleface as might be expected.

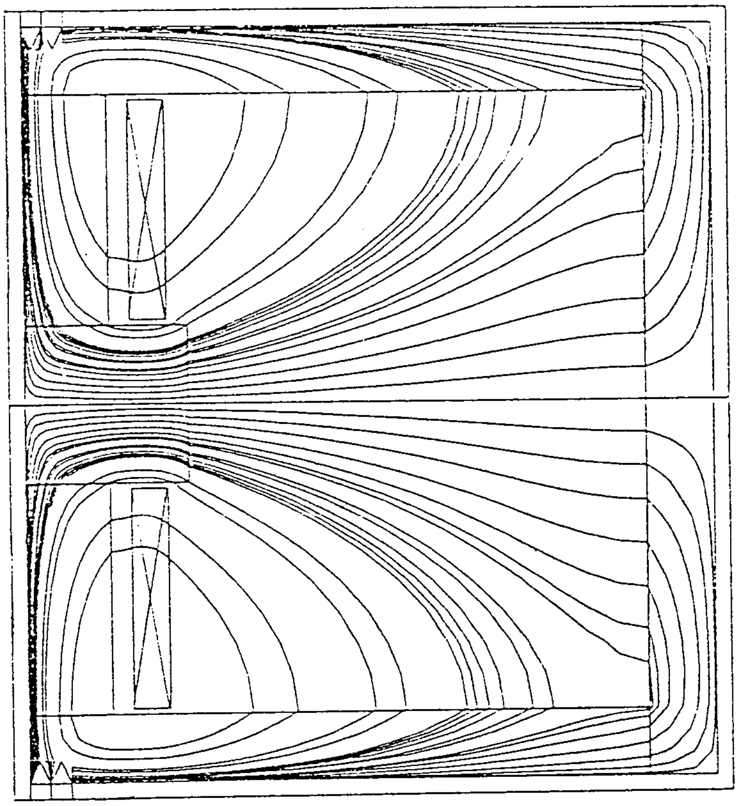

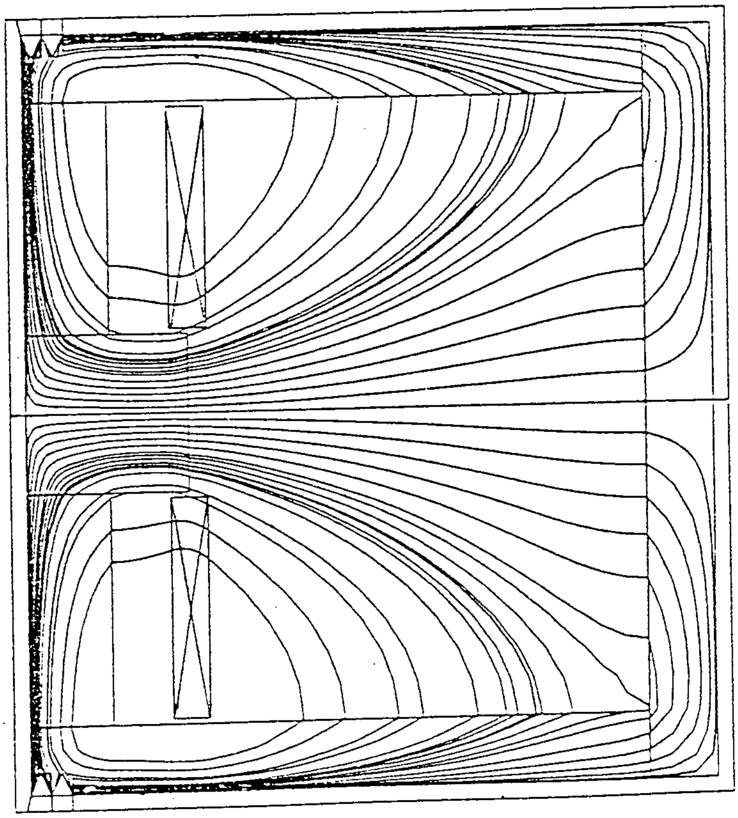

Figure 3.3 Plots of the magnetic flux lines in the zero-bore test lens SP1 shown in figure 3.2 with external iron shroud of diameter 144 mm computed at 60000 ampere-turns.

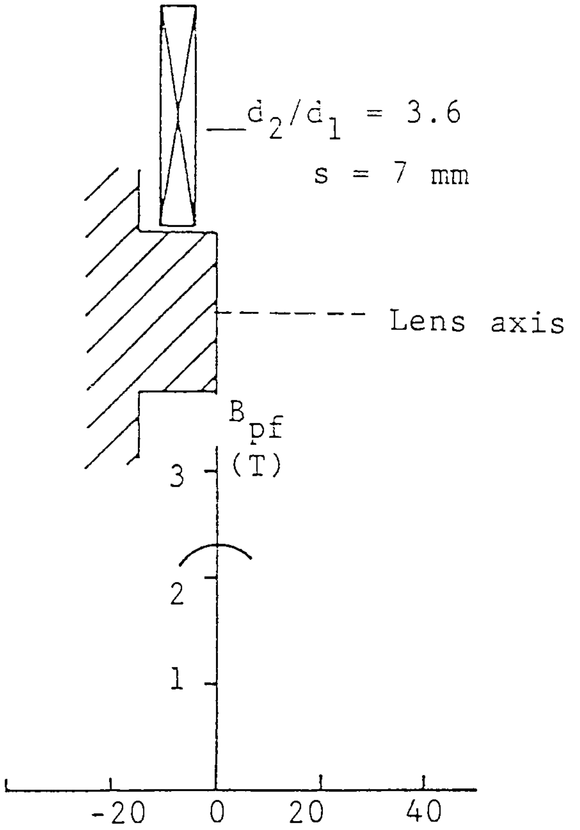

Distance between centre-plane of coil and poleface (mm)

Figure 3.4 The flux density B_{pf} at the poleface of the zero-bore single polepiece test lens SP1 with a cylindrical pole (figure 3.2) as a function of the distance between the coil centre-plane and the poleface. NI = 60000 ampere-turns and $\sigma = 22700\ A/cm^2$. Only the upper half of the tape coil is shown.

The field at the poleface due to the magnetization of the iron is therefore added to the peak of the coil field. However, this position does not lead to the smallest effective halfwidth of the axial field distribution in air as shown in figure 3.5. Here the effective halfwidth W is the axial distance from the poleface to where the peak of the lens axial flux density distribution in air has fallen to half its peak value. The effective halfwidth increases as the coil is moved further away from the lens structure, due to the considerable contribution from the field of the coil which causes the broadening of the lens field in air. However, it seems possible that such an unpromising polepiece shape could work reasonably well under saturation conditions if the position of the coil were set to the optimum position.

Energizing the lens with a thin narrow coil ($d_2/d_1 = 38.7$) of large outer to inner diameter ratio (test lens SP2 of figure 3.6) by the same excitation of 60000 ampere-turns ($\sigma = 19700$ A/cm^2), produces an interesting effect; although the flux density peak still occurs inside the iron polepiece the flux density just outside the polepiece is much higher than that in the polepiece. This is due to the position of the energizing coil outside the effective lens structure, giving considerable contribution from the coil field on the axial field B_z of the lens. It can be seen that the peak field occurs in the region of the centre-plane of the coil. These peaks are demonstrated by the convergence of the flux lines plotted in figure 3.7.

The variation of the flux density B_{pf} at the poleface with the position of the centre-plane of the thin narrow

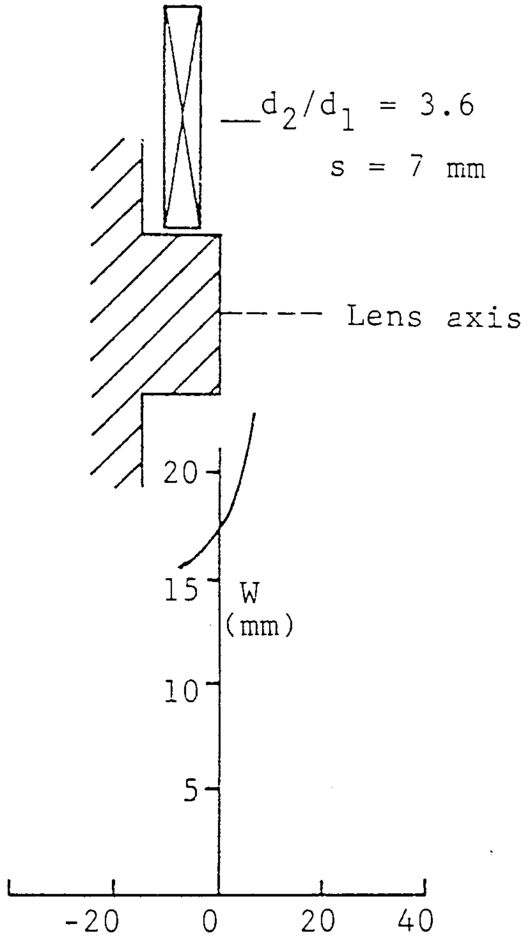

Distance between centre-plane of coil and poleface (mm)

Figure 3.5 Variation of the halfwidth W of the axial flux density distribution B_z of the zero-bore single flat-face cylindrical polepiece test lens SP1 with the distance between the centre-plane of the energizing coil and the poleface. Total halfwidth W of the coil field = 47 mm, NI = 60000 ampere-turns and σ = 22700 A/cm^2. Only the upper half of the tape coil is shown.

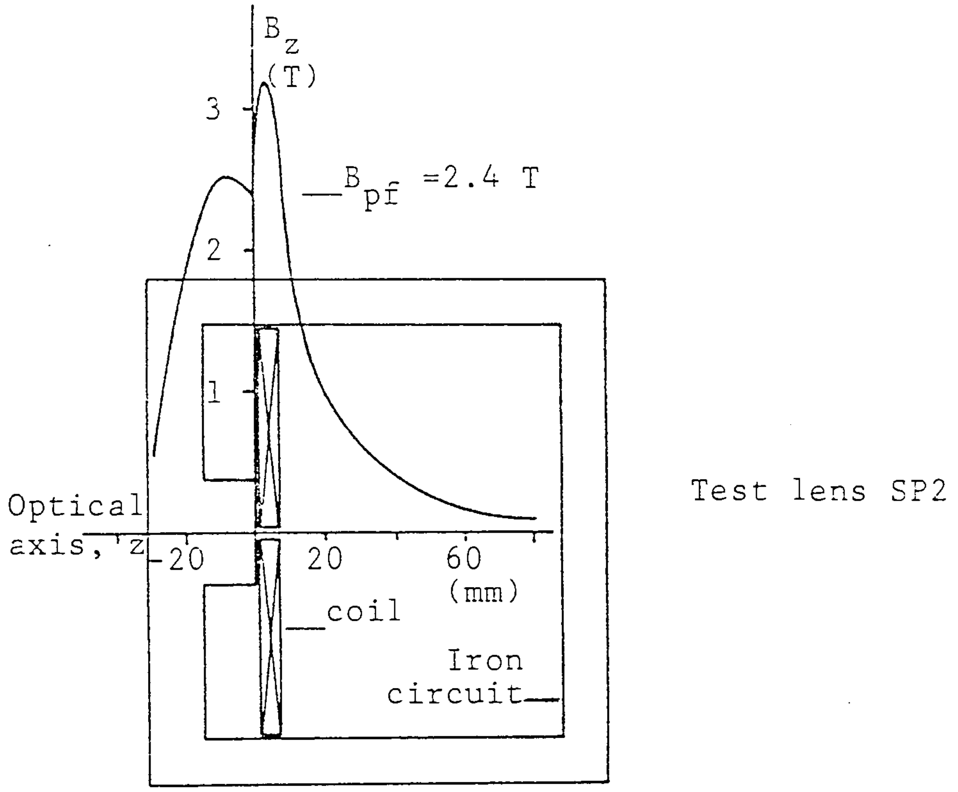

Figure 3.6 Axial flux density distribution of zero-bore single flat-face cylindrical polepiece test lens SP2 with narrow magnetizing coil close up to the poleface. NI = 60000 ampere-turns and σ = 19700 A/cm^2. Lens outer diameter = 144 mm.

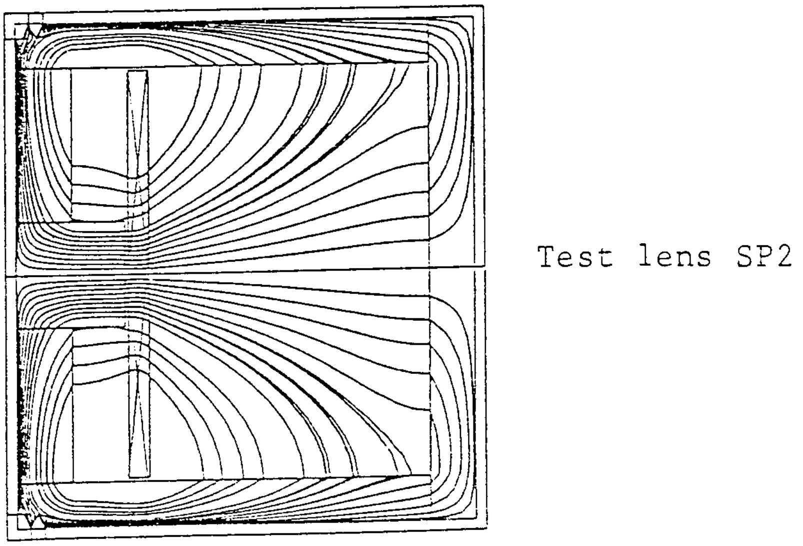

Figure 3.7 Plot of the magnetic flux lines in the zero-bore test lens SP2 with external iron shroud of diameter 144 mm (NI = 60000 ampere-turns).

coil is shown in figure 3.8 computed at a constant excitation NI of 60000 ampere-turns and current density σ of 19700 A/cm^2. The figure shows that B_{pf} decreases rather steeply as the coil is shifted away from the poleface.

A comparison between figures 3.4 and 3.8 shows that, for a given position of the energizing coil away from the poleface, there is little effect of coil shape on the value of the flux density at the poleface. This suggests that the poleface flux density depends mainly on the excitation NI of the flat helical coil in question and not on its outer to inner diameter ratio. The coil field leads to a considerable broadening of the lens field B_z as shown in figure 3.9 where the halfwidth W increases with the increase of the distance of separation between the coil centre-plane and the flat poleface. The field broadening is due to the dominant contribution to B_z of B_{coil} over that due to B_{Fe} at large distances of the coil from the poleface. Hence such a thin narrow coil should be placed as close to the poleface as possible. It can therefore be deduced from the above results that the thin narrow coil placed as close to the poleface as possible has the advantage over the large inner diameter coil in producing a field of small halfwidth and high peak flux density just outside the polepiece.

3.1.2 SINGLE POLEPIECE LENS WITH A FLAT-FACE TRUNCATED-CONE POLE

Conventional lenses usually have two polepieces in the form of a flat-face truncated-cone. This is to ensure that the

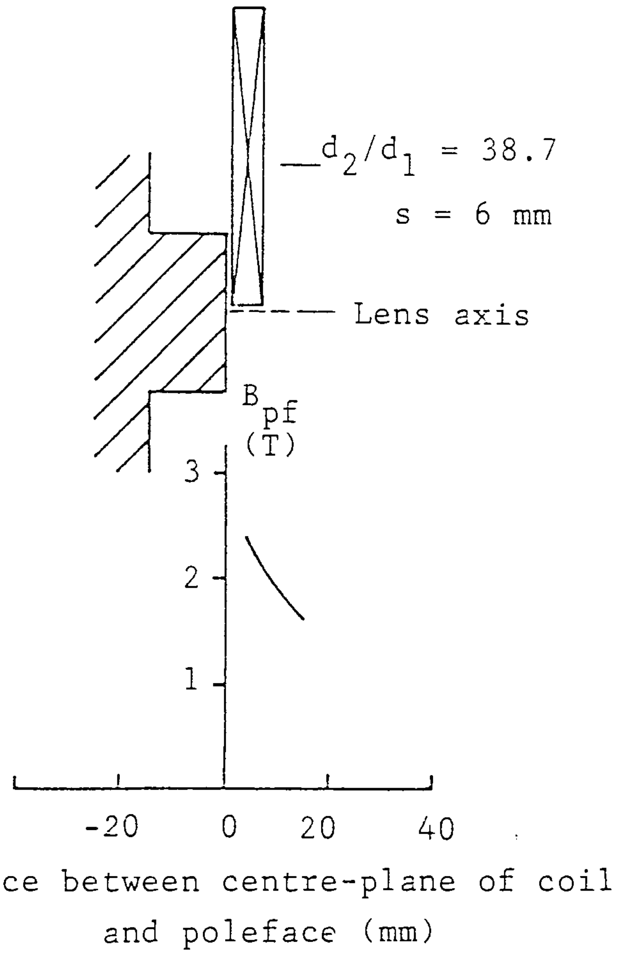

Figure 3.8 The flux density B_{pf} at the flat-face of the zero-bore single polepiece test lens SP2 as a function of the distance between the coil centre-plane and the poleface. NI = 60000 ampere-turns and $\sigma = 19700\ A/cm^2$. Only the upper half of the tape coil is shown.

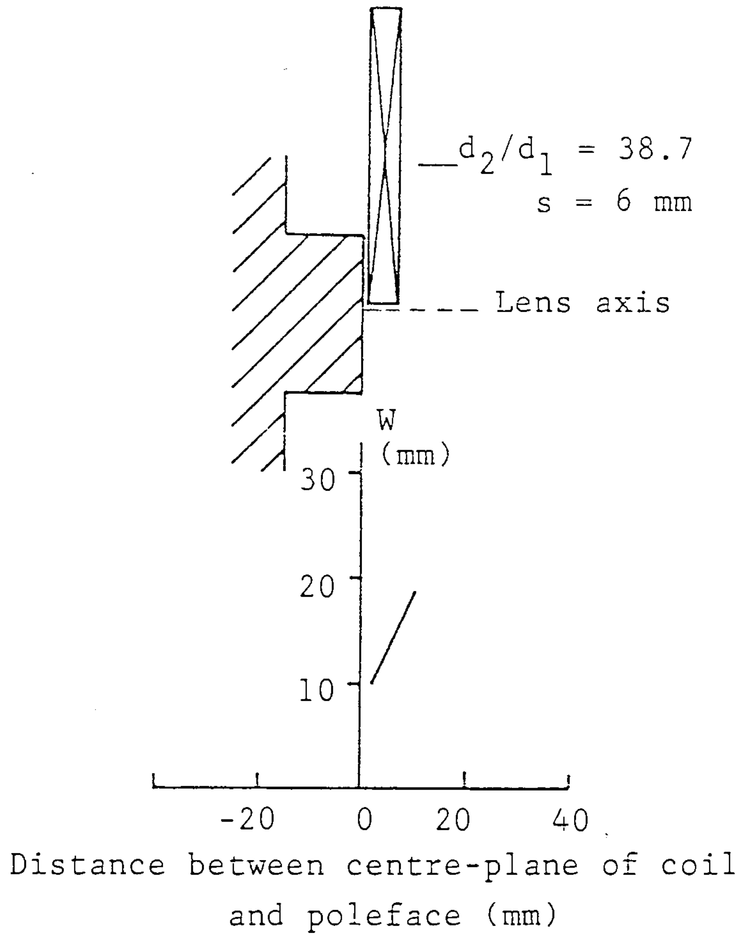

Figure 3.9 The halfwidth W of the axial flux density distribution B_z of the zero-bore test lens SP2 as a function of the distance between the centre-plane of the narrow magnetizing coil and the poleface. Total halfwidth of the coil field = 18 mm, NI = 60000 ampere-turns and $\sigma = 19700\ A/cm^2$. Only the upper half of the tape coil is shown.

flux density in the polepiece decreases from the tip to the base of the cone. Therefore, a truncated-cone polepiece might be superior to a cylindrical polepiece under saturation conditions.

Consider the test lens SP3 shown in figure 3.10 with an iron truncated-cone polepiece. The diameter of the base of the truncated-cone is equal to that of the cylinder (30 mm) in lens SP2 while the diameter of its flat-face is 17 mm i.e. the polepiece taper angle θ is 23° (see also figure 3.1a). The axial length of the truncated-cone polepiece was kept equal (15 mm) to that of the previous cylindrical one. To study the properties of the axial flux density distribution, computations were carried out using the coils (as shown previously in figure 3.1b) excited at 60000 ampere-turns. When the energizing coil of large inner diameter ($d_2/d_1 = 3.6$) was placed close to the base of the truncated-cone polepiece (i.e. surrounding the polepiece which protrudes through the coil axis), it was found that a flux density peak occurs inside the polepiece similar to that produced in the cylindrical polepiece. However, the value of the flux density peak inside the iron drops when the coil is moved nearer to the poleface. The maximum value of poleface flux density is achieved when the centre-plane of the coil coincides with the poleface.

When the lens is energized by a thin flat coil ($d_2/d_1 = 38.7$) placed in close proximity to the poleface, the value of the flux density peak inside the polepiece becomes less than B_{pf} at the poleface at excitations higher than 40000 ampere-turns. Due to the considerable contribution of the coil field at higher excitations the lens field B_z will have a peak just outside the polepiece in the region of the centre-plane of the coil.

Figure 3.10 shows an example of the axial flux density inside and outside the zero-bore single truncated-cone polepiece test lens SP3 computed at 60000 ampere-turns. It is seen that the peak inside the iron polepiece has disappeared unlike that in the cylindrical polepiece shown in figure 3.6. Although the halfwidth W and the value of the peak B_m of the axial field B_z of the test lenses SP2 and SP3 shown in figures 3.6 and 3.10 are the same (12.3 mm and 3.2 Tesla respectively), the value of the flux density B_{pf} at the poleface of the truncated-cone (3.07 Tesla) is higher than that at the poleface of the cylinder (2.4 Tesla).

3.1.3 MAGNETIC LENSES WITH SINGLE SPHERICAL-FACE POLEPIECE

The sphere is a particular case of an ellipsoid polepiece which is amenable to analytical treatment (Alshwaikh 1979, Alshwaikh and Mulvey 1977). The importance of the polepiece with a spherical face lies in the higher flux density that can be achieved at its tip than that of flat face under non-saturation conditions for a given NI (Juma et al 1983b).

A spherical-face polepiece can be designed either in the form of a simple hemisphere or a truncated-cone with a spherical cap. The latter is a more practical design for an electron microscope. To compare these two spherical-tip polepieces the cylindrical polepiece of the lenses SP1 and SP2 shown in figures 3.2 and 3.6 have been replaced firstly by the hemispherical polepiece and secondly by a spherical-face truncated-cone polepiece shown in figure 3.1a.

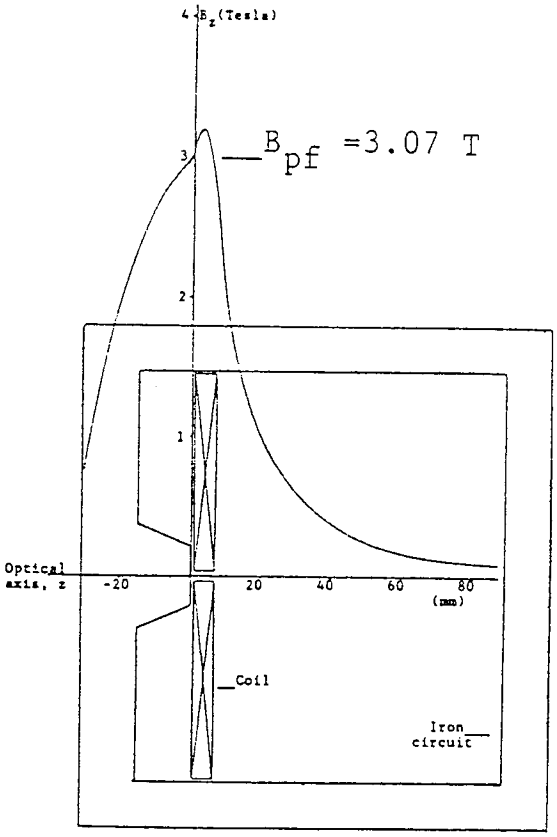

Test lens SP3

Figure 3.10 Axial flux density distribution in a zero-bore single polepiece test lens SP3 with a soft iron flat-face truncated-cone pole, computed at NI = 60000 ampere-turns and current density $\sigma = 19700$ A/cm^2. The lens is energized by a thin flat coil of s = 6 mm, d_1 = 3 mm and d_2 = 116 mm. Lens outer diameter = 144 mm.

A series of computations carried out by the author concerning the magnetic field have shown that under similar excitations both the hemispherical polepiece and the truncated-cone polepiece with a spherical cap of an equal radius produced similar axial flux density distributions. For these reasons, the truncated-cone polepiece with a spherical face shown in figure 3.1a was chosen for detailed investigations. The coils previously shown in figure 3.1b were used for energizing the lens with single spherical-face polepiece at 60000 ampere-turns. The radius of curvature of the spherical cap is equal to the outer radius of the cylindrical polepiece (15 mm) as shown in figure 3.1a.

The effect of the position of the magnetizing coil with large inner diameter ($d_2/d_1 = 3.6$) on the flux density distribution inside and outside the single truncated-cone spherical-face polepiece test lens SP4 of zero bore is shown in figure 3.11. With the coil situated in the conventional position where it surrounds the conical part of the polepiece (figure 3.11a), it is seen that a flux density peak appears inside the conical section. However, when the centre-plane of the coil coincides with the polepiece tip (figure 3.11b), the axial flux density peak inside the conical section shifts to the poleface. The position of the peak flux density situated at the polepiece tip is not affected by shifting the coil further away from the poleface (figure 3.11c). The maximum value of the poleface flux density appears when the centre-plane of the coil coincides with polepiece tip due to the combination of the B_{Fe} peak at the poleface and the maximum value of B_{coil} at the coil centre-plane.

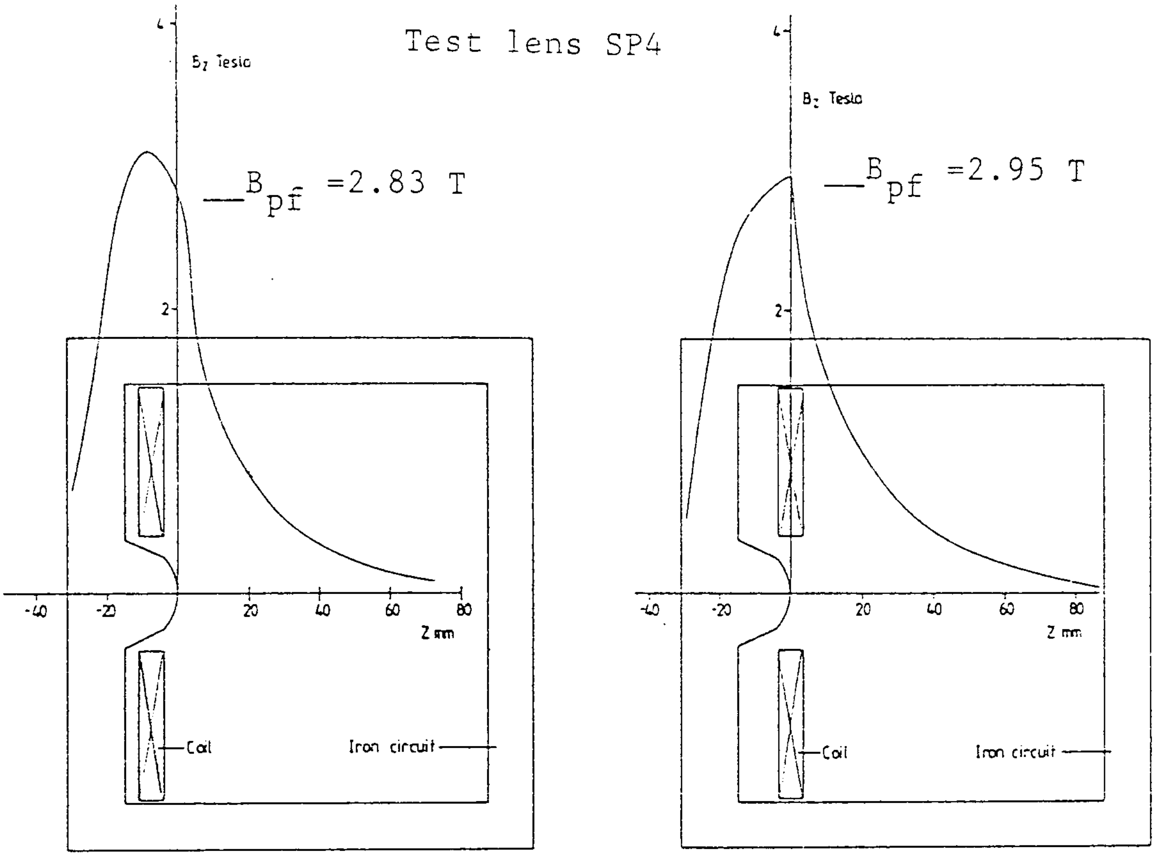

(a) Coil in conventional position.

(b) Centre-plane of coil coincides with poletip.

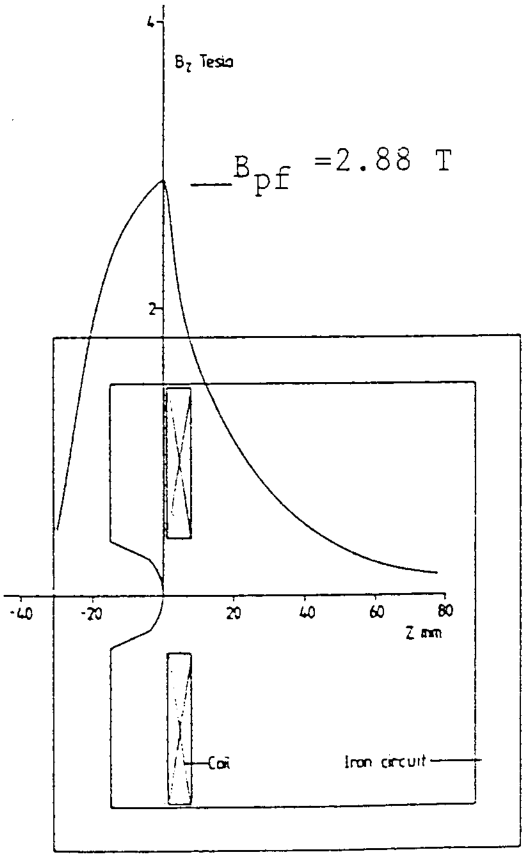

(c) Coil before poletip.

Figure 3.11 Axial flux density distributions in a zero-bore single polepiece test lens SP4 with a soft iron spherical-face truncated-cone pole, computed at NI = 60000 ampere-turns and current density σ = 22700 A/cm^2 for three positions of the energizing coil (s = 7 mm, d_1 = 32 mm and d_2 = 116 mm). Lens outer diameter = 144 mm.

Figure 3.12 demonstrates the distribution of the magnetic flux lines in the zero-bore test lens SP4 shown in figure 3.11. The flux lines are, of course, concentrated and converge at the point where the flux density peak appears.

If the coil is placed in the region of the tip, the effect of the coil position on the poleface flux density is non-critical as shown in figure 3.13. However, the effect of the coil position on the halfwidth of the lens axial flux density distribution in air, measured from the poletip, is more serious as shown in figure 3.14. The halfwidth W increases rapidly as the coil is shifted away from the poletip. This is due to the effect of the coil field which leads to the broadening of the lens axial field B_z. The least effect of the coil field on the halfwidth W of B_z in air occurs, as one would expect, when the coil is placed in the conventional position, but that would of course reduce the poleface flux density.

Figure 3.15 shows the axial flux density distribution B_z of the zero-bore test lens SP5 with a single spherical-face truncated-cone polepiece when it is magnetized by the narrow coil ($d_2/d_1 = 38.7$) at 60000 ampere-turns ($\sigma = 19700$ A/cm^2). The coil is placed in close proximity to the poletip. The axial peak flux density is also situated at the poletip. This is demonstrated in figure 3.16 by the high concentration and convergence of the magnetic flux lines at the spherical surface of the pole where a flux density peak appears.

Although the thin energizing coil of $d_2/d_1 = 38.7$ is operated at a current density lower than that of the coil

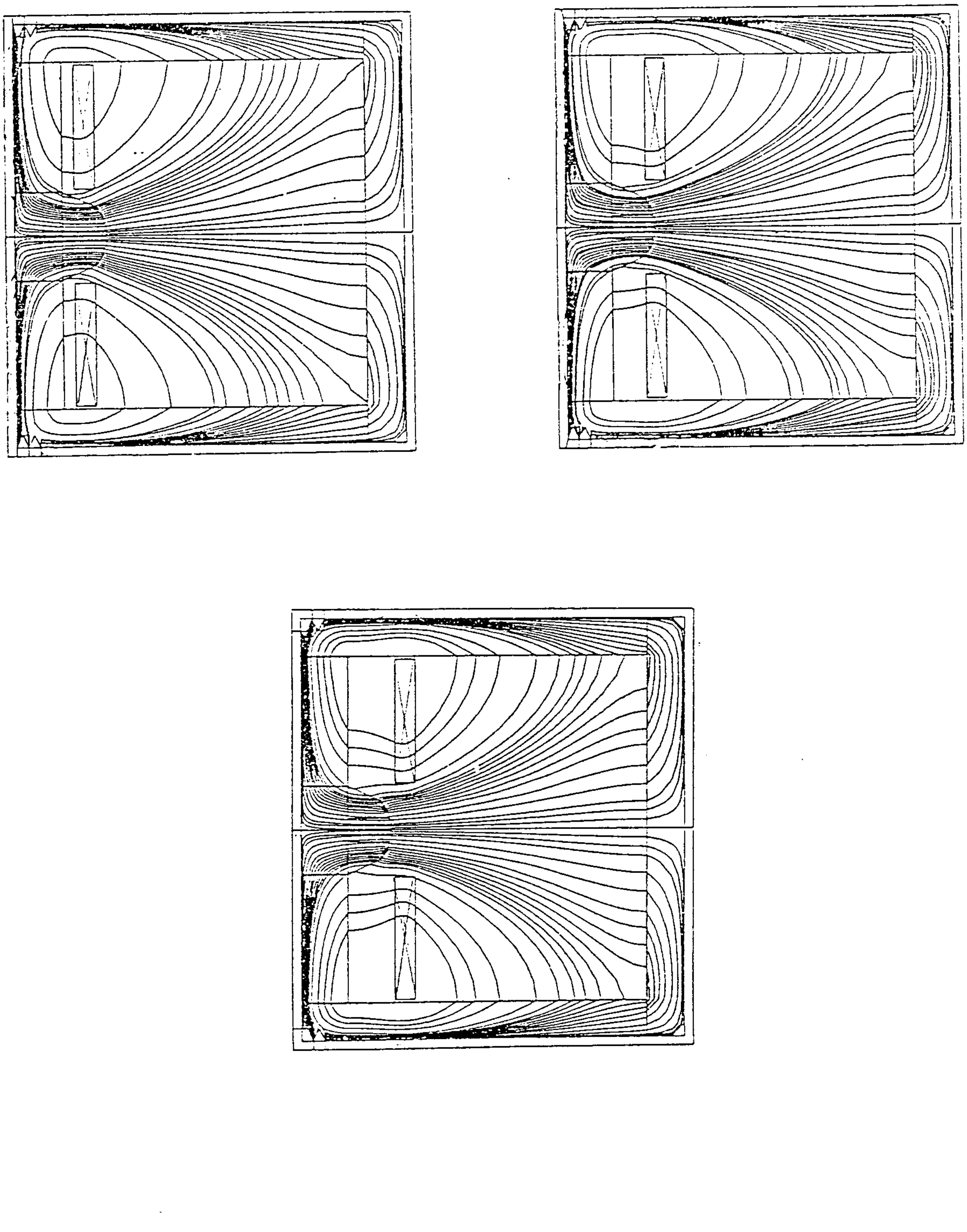

Figure 3.12 Plots of the magnetic flux lines in the zero-bore test lens SP4 with external iron shroud of diameter 144 mm (NI = 60000 ampere-turns).

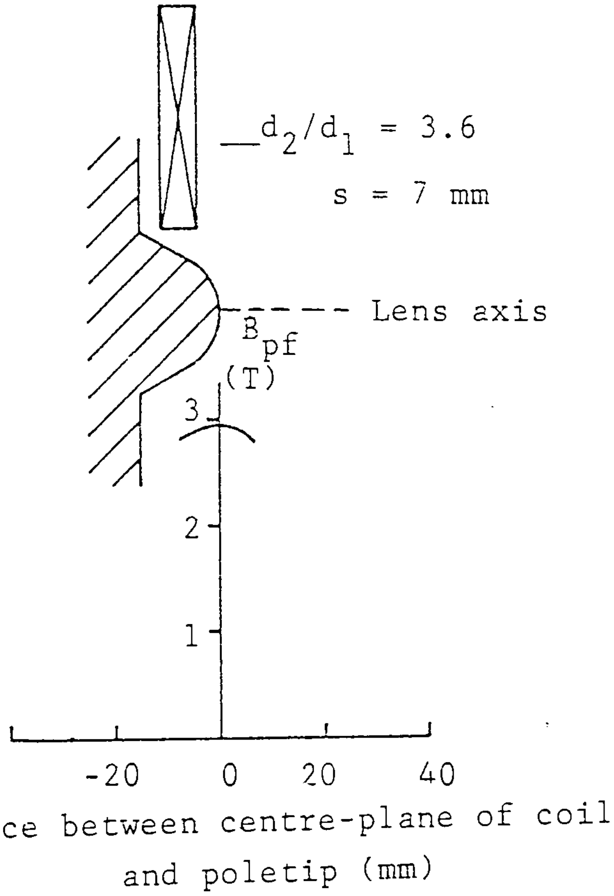

Figure 3.13 The flux density B_{pf} at the spherical poleface of the zero-bore single polepiece test lens SP4 as a function of the distance between the coil centre-plane and the poletip. Only the upper half of the tape coil is shown. NI = 60000 ampere-turns and σ = 22700 A/cm^2.

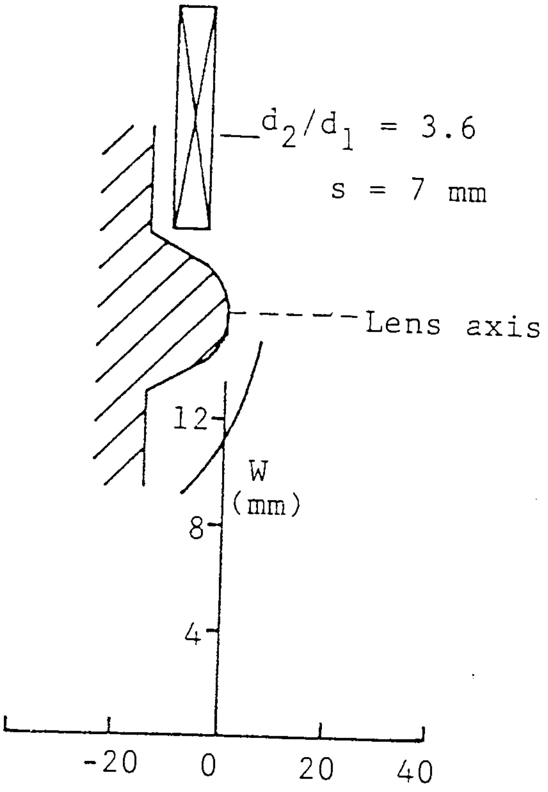

Distance between centre-plane of coil and poletip (mm)

Figure 3.14 Variation of the halfwidth W of the axial flux density distribution B_z of the zero-bore single spherical-face truncated-cone polepiece test lens SP4 with the distance between the coil centre-plane and the poletip. Total halfwidth of the coil field = 47 mm, NI = 60000 ampere-turns and σ = 22700 A/cm^2. Only the upper half of the tape coil is shown.

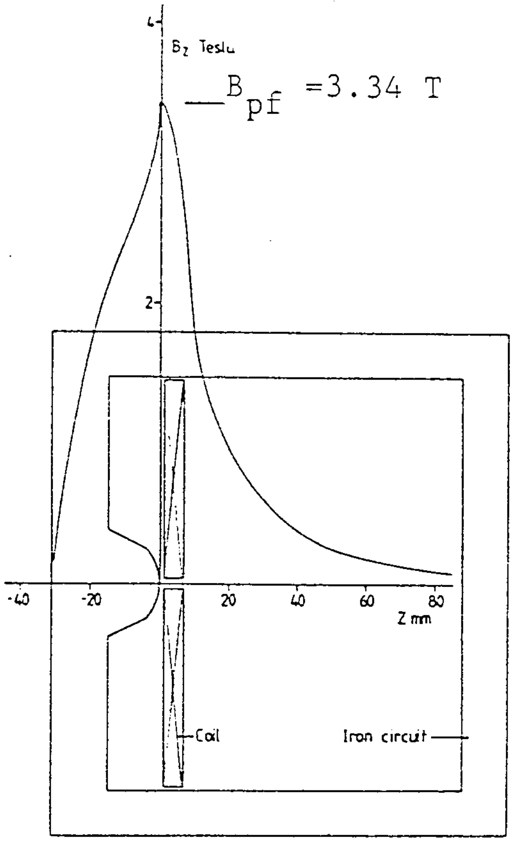

Test lens SP5

Figure 3.15 Axial flux density distribution computed at NI = 60000 ampere-turns and σ = 19700 A/cm^2 in a zero-bore single polepiece test lens SP5 with soft iron spherical-face truncated-cone pole excited by a thin flat coil of s = 6 mm, d_1 = 3 mm and d_2 = 116 mm. Lens outer diameter = 144 mm.

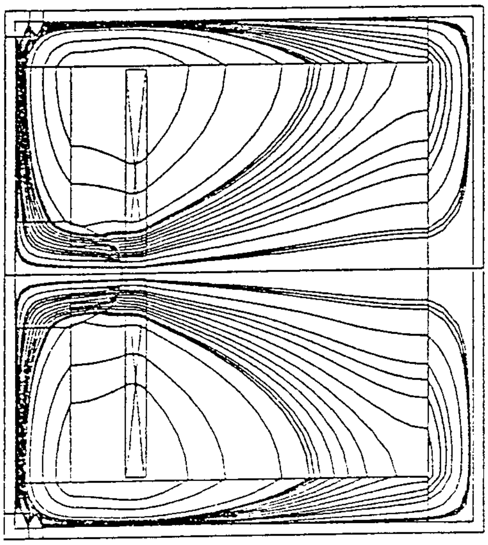

Test lens SP5

Figure 3.16 Plots of the magnetic flux lines in the test lens SP5 with external iron shroud of diameter 144 mm computed at 60000 ampere-turns..

whose d_2/d_1 = 3.6 the value of the axial flux density peak in figure 3.15 is higher than the best value obtained with the other coil of d_2/d_1 = 3.6 (figure 3.11b) due to the high field of this thin coil for the same excitation NI. The halfwidth W of the axial field B_z in air of the test lens SP5 energized by the coil of d_2/d_1 = 38.7 (figure 3.15) is 1 mm higher than that of the test lens SP4 of smallest halfwidth (9.2 mm) energized by the coil of d_2/d_1 = 3.6 (figure 3.11a). However, for the same excitation and position of the coil centre-plane, the halfwidth W of the lens in figure 3.15 is 3 mm smaller than that of the lens in figure 3.11c.

The variation of the flux density B_{pf} at the poleface with the position of the thin coil centre-plane measured from the poletip (figure 3.17) indicates that by placing the coil in close proximity to the poleface, the highest flux density at the poletip will be obtained, for a given excitation (NI = 60000 ampere-turns). At this position of close proximity of polepiece and coil the value of the coil field B_{coil} at the poleface is highest and is added to the iron field B_{Fe}. At such excitation the contribution of B_{coil} at the poleface is reduced as the coil is shifted away and hence the poleface flux density, B_{pf} decreases. Consequently, the halfwidth W of the lens axial field distribution B_z in air increases with the increase of the distance of separation between the poleface and the coil centre-plane (figure 3.18). The broadening of B_z is caused by the movement of the peak flux density away from the poleface due to the movement of the coil. Thus, for the given excitation (NI = 60000 ampere-turns) the thin

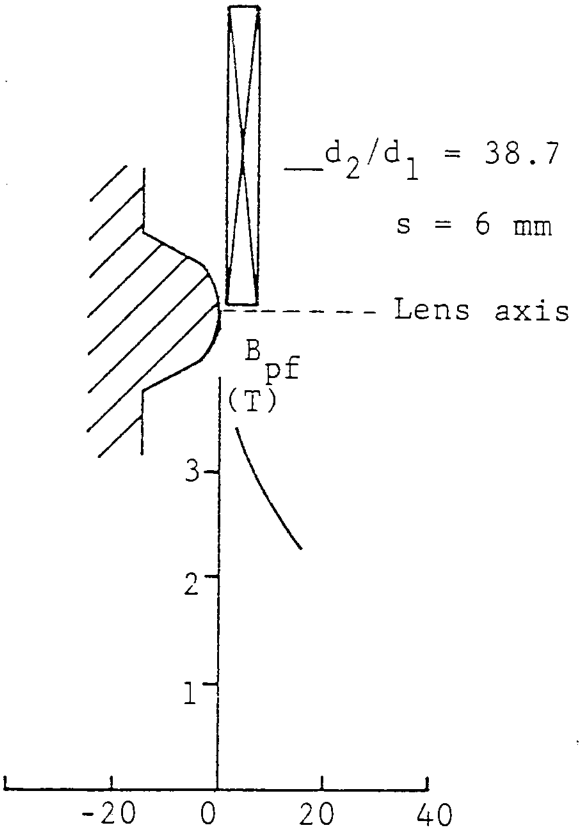

Distance between centre-plane of coil and poletip (mm)

Figure 3.17 The flux density B_{pf} at the tip of the spherical poleface of the zero-bore single polepiece test lens SP5 (figure 3.15) as a function of the distance between the coil centre-plane and the poletip. Only the upper half of the tape coil is shown. NI = 60000 ampere-turns and $\sigma = 19700$ A/cm^2.

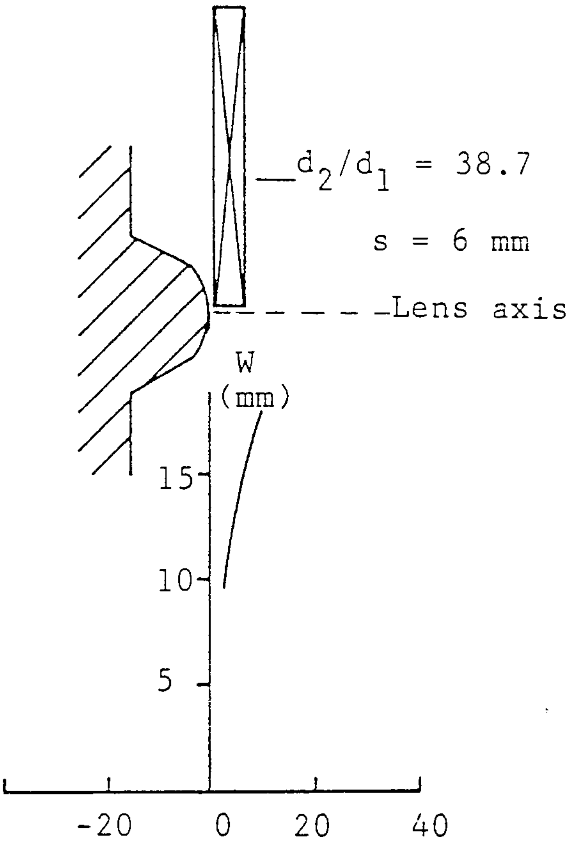

Distance between centre-plane of coil and poletip (mm)

Figure 3.18 The halfwidth W of the axial flux density distribution B_z of the test lens SP5 with a zero-bore single spherical-face truncated-cone polepiece as a function of the distance between the coil centre-plane and the poletip. Total halfwidth of the coil field = 18 mm, NI = 60000 ampere-turns and σ = 19700 A/cm^2. Only the upper half of the tape coil is shown.

coil placed in close proximity to the poleface gives the highest axial flux density peak at the poletip and the smallest halfwidth of the axial field B_z in air.

In order to compare the electron-optical properties of the flat-face and spherical-face truncated-cone polepiece at higher excitations it is important first to check any loss of ampere-turns due to flux leakage in the lenses shown above.

3.2 FLUX LEAKAGE

At high excitations, leakage of flux lines out of the iron circuit can be a serious problem leading to a marked loss of ampere-turns. To reduce unwanted flux leakage at the design stage, the thickness of the lens shroud should be adequate for the highest lens excitation required.. The position of the energizing coil can have an appreciable effect on loss of ampere-turns in the magnetic circuit.

In some computational work (Cleaver 1978) on test lenses, flux leakage was avoided by letting the magnetic material of the lens shroud have very high permeability. In a well-designed lens, the loss of ampere-turns in the external shell can be checked by setting the permeability of the iron shell to a high value and verifying that the axial field distribution is not thereby affected.

For the single polepiece test lenses investigated in this chapter, the thickness of the iron shell surrounding the coil was 13 mm while that of the plate at the back of the polepiece was 16 mm. The thickness of the screening iron plate, facing the poleface was 13 mm. For the test lens SP5 shown in figure 3.15, computations have shown that at excitation values up to 80000 ampere-turns no flux leakage was observed. The area under the axial flux density distribution was found to be consistent with the theoretical value. However, above 80000 ampere-turns flux leakage was apparent by the loss of ampere-turns. Figure 3.19 shows an example of the change in the area under the axial magnetic field before and after doubling the thickness of the iron shroud, computed at 161465 ampere-turns. With the original thickness of the iron shroud there was a loss of ampere-turns of 5.2% at an excitation of 161465 ampere-turns. The observed loss in area disappeared when the thickness of the shroud was doubled. At an excitation of 120000 ampere-turns flux leakage led to a loss of 1.7% of ampere-turns in the original lens field; this also disappeared when the thickness of the iron shroud was doubled.

When the thickness of the iron shroud was increased to double its original value, a maximum flux density of 7.2 Tesla in the region of the coil centre-plane was obtained at an excitation of 161465 ampere-turns. At this excitation the poletip is clearly saturated; the value of the field at the poleface due to iron is 2 Tesla and that at the lens poleface B_{pf} is 6.4 Tesla. These values indicate that at such excitation the coil field B_{coil} is dominant over B_{Fe}. In the lenses described in the following sections, care was taken to check the thickness of the iron shroud particularly for very high excitations.

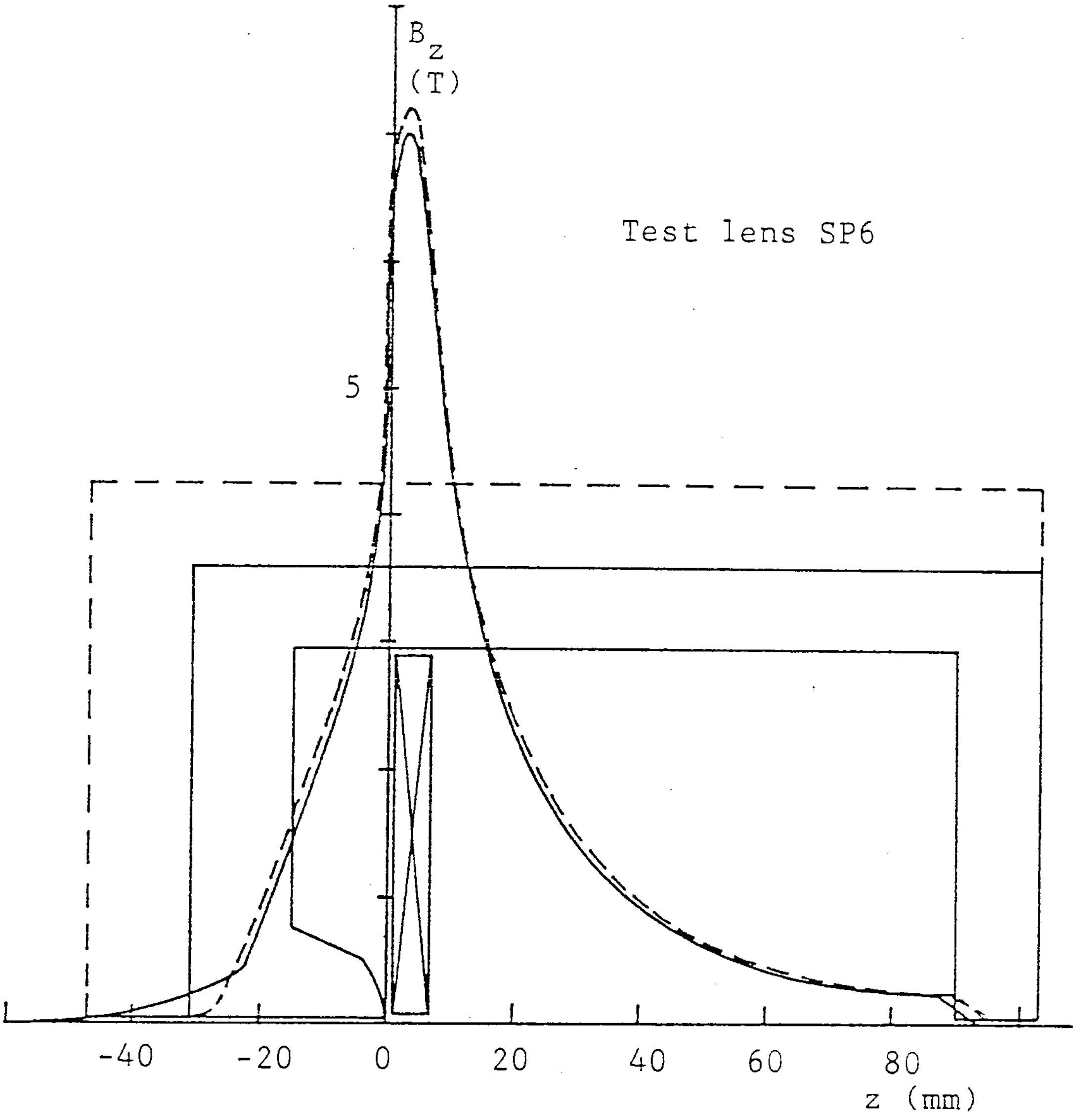

Figure 3.19 Change in the axial field B_z due to flux leakage before (solid line) and after (dotted line) doubling the thickness of the iron shroud, computed at 161465 ampere-turns. Only the upper half of the test lens SP6 and its energizing coil is shown.

3.3 COMPARISON BETWEEN FLAT-FACE AND SPHERICAL-FACE TRUNCATED-CONE POLEPIECES

With a conical polepiece the end of the conical section can either be flat or rounded off. A conical section polepiece rounded off in the form of a hemisphere is perhaps the simplest to analyze. In this section the electron-optical properties of these two pole shapes in single polepiece test lenses are compared.

Consider the test lenses SP3 and SP5 shown in figures 3.10 and 3.15 with single, zero-bore, truncated-cone polepieces of flat-face and spherical-face respectively. A comparison of their axial fields computed at constant excitation NI (60000 ampere-turns) and current density σ (19700 A/cm^2) shows that:

(a) The poleface flux density B_{pf} of the lens with a spherical-ended polepiece is higher than that with a flat-ended polepiece. For example, B_{pf} of the single spherical-face polepiece lens is 3.34 Tesla which is 8% higher than that with flat-face polepiece (B_{pf} = 3.07 Tesla).

(b) The peak flux density B_m of the lens with a spherical-face polepiece is situated at the poleface itself while that of the lens with a flat polepiece occurs away from the poleface but within the axial region occupied by coil.

(c) The halfwidth W (measured from the poleface) of the axial field of the lens with a spherical-face polepiece is smaller than that with a flat-face polepiece. For example, at the above values of NI and σ, the axial field halfwidth of the lens with a single spherical-face polepiece is 11.4 mm which is 7.3% smaller than that with a flat-face polepiece. Therefore, under these specific conditions of NI and σ, the axial flux density distribution of the lens with a single spherical-face polepiece is better than that with a flat-face polepiece due to its higher peak and smaller halfwidth.

To investigate the lenses shown in figures 3.10 and 3.15 at higher excitations, the thickness of the iron shroud was doubled so that no loss of ampere-turns occurs. Figures 3.20 and 3.21 show the axial field distributions of the two test lenses SP7 and SP8 under consideration. Each lens has a 1 mm diameter bore. The peak B_m of the axial field shown in figure 3.20 is situated at the poleface except at high excitations (NI $\geqslant$ 80000 ampere-turns) where the coil field B_{coil} becomes dominant over that due to iron magnetization, B_{Fe}. In this case the flux density peak occurs away from the poleface but within the axial region occupied by the thin coil. With the flat-face polepiece (figure 3.21) the peak of the axial field is always situated away from the poleface and it shifts further away as the excitation NI increases. At higher excitations (NI > 80000 ampere-turns) the peaks of the axial fields of both test lenses SP7 and SP8 (figures 3.20 and 3.21) have nearly equal values and occur within the axial region occupied by the coil. Therefore, the effect of the shape of the polepiece on the axial field becomes less significant due to the dominant effect of the coil field B_{coil} over that of iron B_{Fe}. However, in the linear and intermediate regions of the B-H magnetization curve the peak of the axial field of the lens with single spherical-face polepiece is always higher than that with single flat-face polepiece.

The values of the flux density peak, B_m of both lenses energized at high excitations are high and equal. For

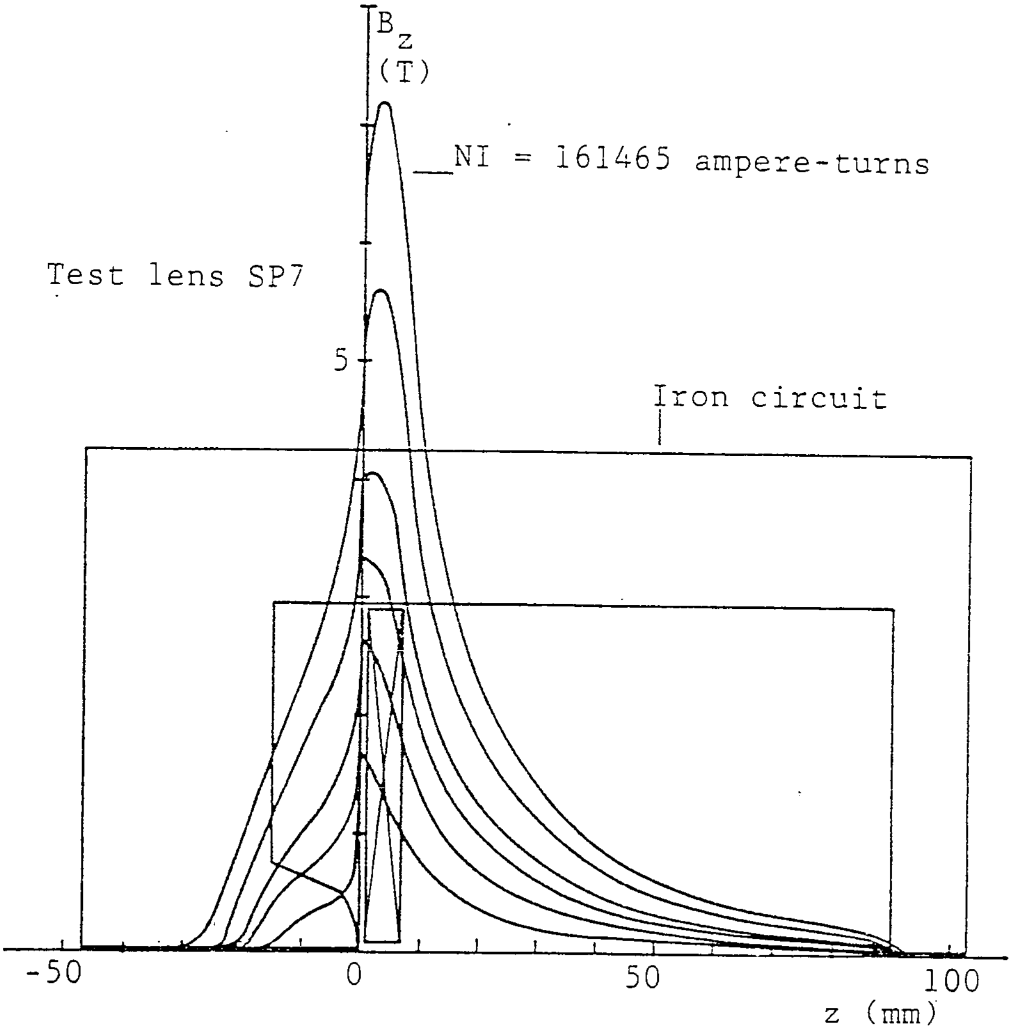

Figure 3.20 Axial flux density distributions in a single polepiece test lens SP7 with a soft iron spherical-face truncated-cone pole of 1 mm bore diameter. The fields are computed at NI = 20000, 40000, 60000, 80000, 120000 and 161465 ampere-turns which rise with increasing NI in the order shown. The coil dimensions are: s = 6 mm, d_1 = 3 mm and d_2 = 116 mm. Lens outer diameter = 170 mm. Only the upper half of the lens is shown.

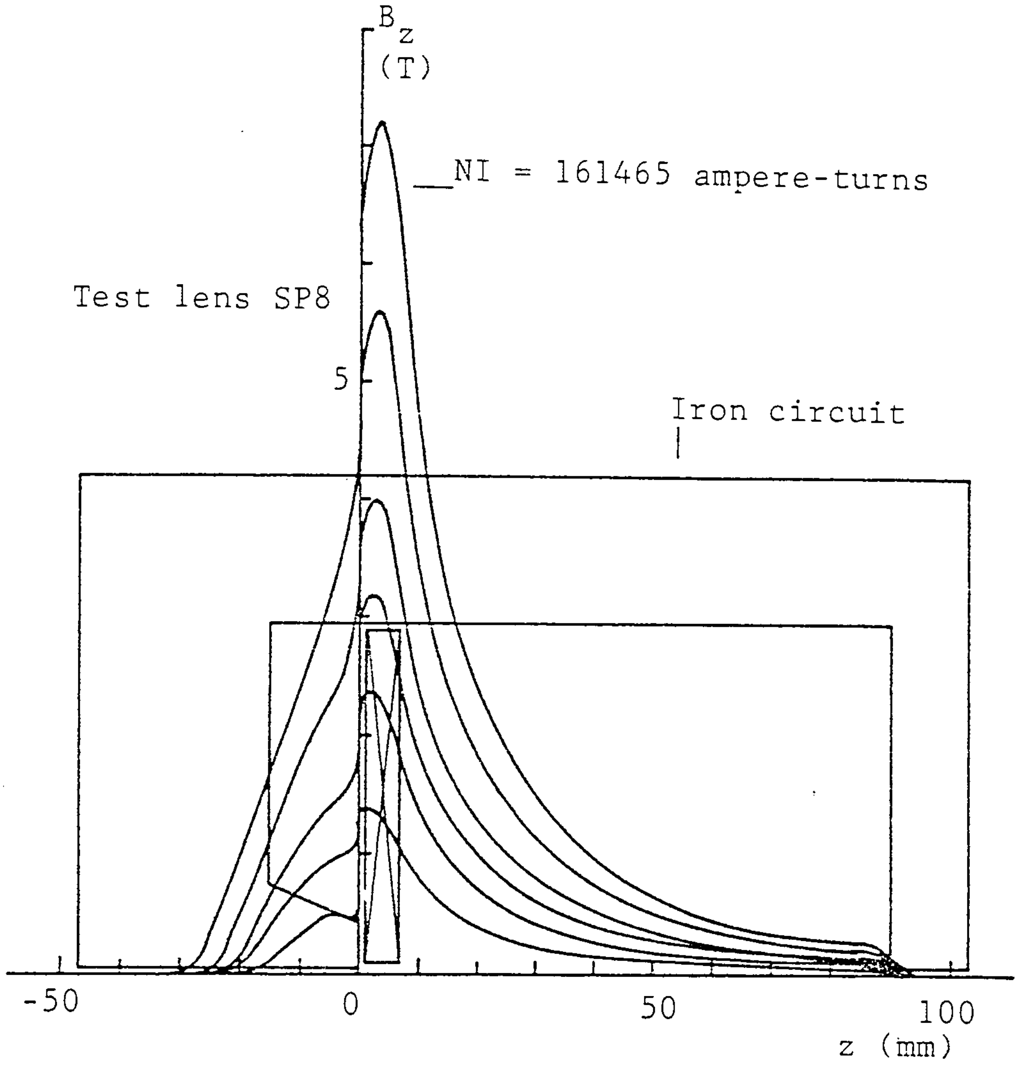

Figure 3.21 Axial flux density distributions in a single polepiece test lens SP8 with a soft iron flat-face truncated-cone pole of 1 mm bore diameter. The fields are computed at NI = 20000, 40000, 60000, 80000, 120000 and 161465 ampere-turns which rise with increasing NI in the order shown. The coil dimensions are: s = 6 mm, d_1 = 3 mm and d_2 = 116 mm. Lens outer diameter = 170 mm. Only the upper half of the lens is shown.

example, B_m = 7.2 Tesla at NI = 161465 ampere-turns. Such high flux density value may only be achieved at high current density (σ = 52900 A/cm^2) which requires superconducting coils. This region of the B_z peak can be the position of a specimen under investigation in analytical electron-optical instruments which require high flux densities.

Under non-saturation conditions, the energizing coil makes little contribution to the axial field B_z of the lens. Most of the lens field is produced by the magnetization of the iron polepiece. As the lens excitation is increased the polepiece begins to saturate. The maximum contribution of the iron field B_{Fe} is around 2 Tesla depending on the polepiece material. Figure 3.22 shows two examples of the B_{Fe} fields at different excitations of the test lens SP7 with a spherical-face polepiece (figure 3.22a) and of the test lens SP8 with a flat-face polepiece (figure 3.22b). At excitations less than 40000 ampere-turns the halfwidth W of the B_{Fe} fields remains constant; W is measured axially from the poleface where B_{Fe} is maximum to where B_{Fe} has dropped to half its maximum value. However, as the iron polepiece begins to saturate, the halfwidth W of the B_{Fe} field increases. Figure 3.22 shows that when the spherical and flat poletips are saturated (B_{Fe} at the poleface = 2 Tesla) the halfwidths of B_{Fe} fields remain constant with increase of the excitation NI. It should be noted that the halfwidth W of the B_{Fe} field due to the spherical-face polepiece is always smaller than that due to the flat-face polepiece at all excitations.

For the test lens SP7 with a spherical-face polepiece (figure 3.22a), the field due to iron magnetization under

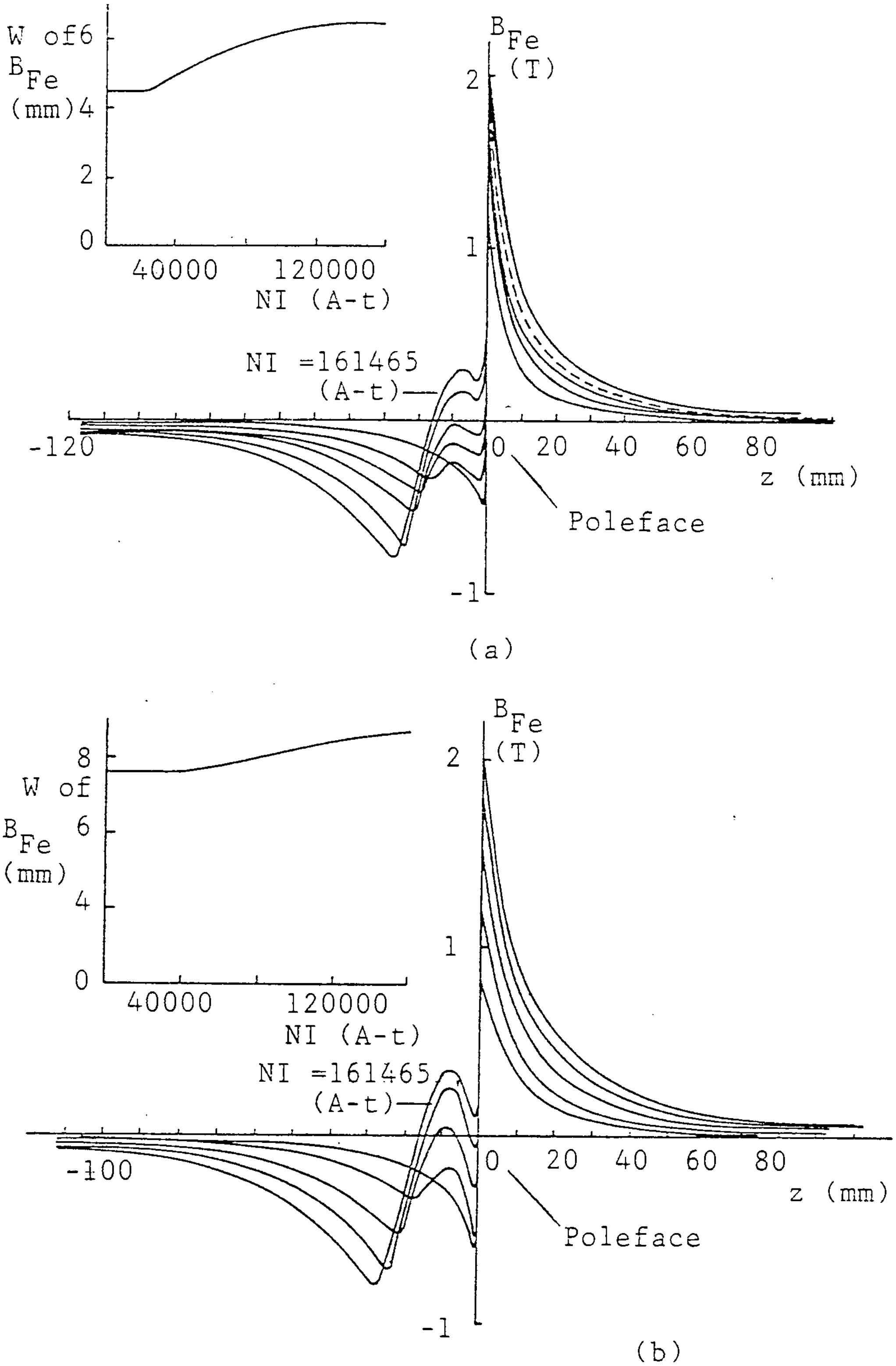

(a)

(b)

Figure 3.22 Axial fields B_{Fe} due to iron magnetization of the test lenses SP7 and SP8 shown in figures 3.20 and 3.21 respectively; (a) single polepiece test lens SP7 with spherical-face truncated-cone pole, (b) single polepiece test lens SP8 with flat-face truncated-cone pole. The halfwidth W of the field as a function of excitation NI is also plotted for the two lenses.

non-saturation conditions is found to be represented by the expression of the spherical-field model (see for example, Alshwaikh 1979)

$$(B_{Fe})_z = (B_{Fe})_m \left[\frac{3.847}{3.847 + (z/W)} \right]^3 \qquad (3.1)$$

where $(B_{Fe})_z$ = axial flux density due to iron magnetization outside the spherical polepiece.

$(B_{Fe})_m$ = maximum flux density due to iron magnetization at the poletip ($z = 0$).

W = halfwidth of the field due to iron magnetization measured from the poletip to where $(B_{Fe})_z = \frac{1}{2} (B_{Fe})_m$.

For the test lens SP8 with a single flat-face polepiece (figure 3.22b), the field due to iron magnetization under non-saturation conditions is found to be approximately represented by Glaser's bell-shaped field model

$$(B_{Fe})_z = (B_{Fe})_m / [\, 1 + (z/W)^2 \,] \qquad (3.2)$$

where $(B_{Fe})_z$, $(B_{Fe})_m$ and W are similar to those of equation (3.1). Equation (3.2) suggests that Glaser's expression is a good approximation for the iron magnetization field of a flat-end polepiece.

Under non-saturation conditions, the value of $(B_{Fe})_m$ of the spherical-face polepiece is always higher than that of the flat-face polepiece. For example, at 20000 ampere-turns, $(B_{Fe})_m$ due to the spherical-face polepiece is 1.15 Tesla while that of the flat-face polepiece is 0.83 Tesla. These properties are demonstrated in figure 3.23 under both saturation and non-saturation conditions. It is seen from the curves of B_{Fe} at the poleface that the magnetization of the spherical-face

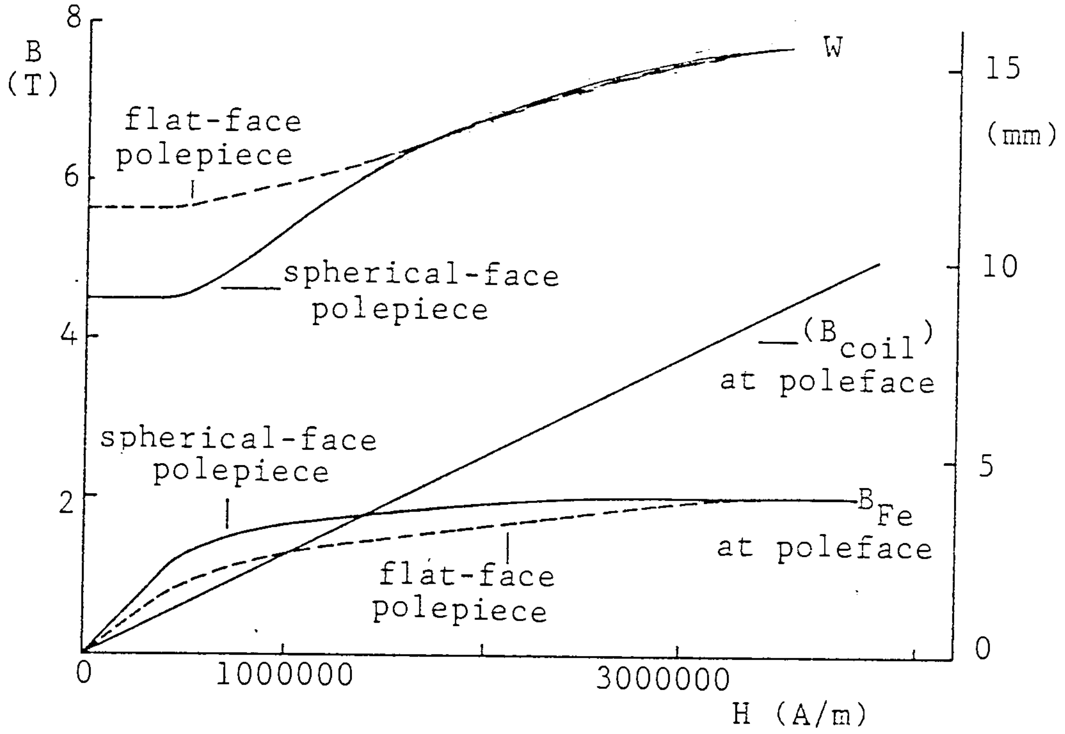

Figure 3.23 The axial field halfwidth W (determined from figures 3.20 and 3.21) and B_{Fe} at poleface (determined from figure 3.22) as functions of the magnetic field strength H. The flux density at the poleface due to the coil field is also plotted.

polepiece is better (i.e. dB/dH is higher) than that of the flat-face polepiece in the linear and intermediate regions of the B-H magnetization curves. Therefore, the B_{Fe} at the poleface contributed by the iron spherical-face polepiece to the lens axial field B_z is always higher than that of the flat-face in the linear and intermediate regions of the magnetization curve. At higher excitations where the iron is saturated (i.e. B_{Fe} remains constant with increasing H) the B_{Fe} contribution of both iron polepieces is the same (2 Tesla) i.e. at saturation B_{Fe} at the poleface is independent of polepiece shape. As one would excpect, the flux density at the poleface due to the coil field only is a linear function of H. The halfwidth W of the axial field distributions in air shown in figures 3.20 and 3.21 represents the axial distance between the two points on the distribution curve where $B_z = B_m/2$. The variation of the halfwidth W of the axial field B_z of the lenses shown in figures 3.20 and 3.21 with the magnetic field strength H is also plotted in figure 3.23. In the linear region of the magnetization curve the halfwidth W remains constant with the increase of H. At H > 500000 A/m where the B-H curve deviates from linearity (intermediate region), W increases with the increase of H. At the linear and intermediate regions, W of the lens with a spherical-face polepiece is always smaller than that with a flat-face polepiece. However, at saturation W becomes independent of the polepiece shape due to the dominance of B_{coil} over that of B_{Fe}.

From the above investigation concerning the effect of the pole-end shape on the electron-optical parameters of single polepiece lenses, it can be deduced that the polepiece shape has little effect on the electron-optical parameters of saturated high flux density single polepiece lenses. However, a truncated-cone polepiece with spherical-face is a favourable pole shape when the iron polepiece is energized in the linear and intermediate regions of its B-H curve where B_{Fe} at the poleface is less than 2 Tesla and poleface flux densities less than 4 Tesla. Under these conditions such pole shape produces the highest flux density at its poleface and the smallest halfwidth of the axial field for a specific value of H. It is, therefore, worthwhile investigating the effect of the coil position on B_z and B_{Fe} at the poleface at different excitations NI. Using the thin coil ($s = 6$ mm, $d_1 = 3$ mm and $d_2 = 116$ mm) of high ratio of outer to inner diameter ($d_2/d_1 = 38.7$) figure 3.24 shows the poleface flux density B_{pf} and that due to the iron magnetization B_{Fe} computed at different values of NI for four positions of the energizing coil measured from its centre-plane to the poleface. It is seen that the highest B_z and B_{Fe} at the poleface are achieved when the coil is as close as possible to the poletip. This is due to the combined effect of the coil field and the iron magnetization field at this coil position where B_{Fe} at the poleface reaches, as NI increases, its limit (2 Tesla) before those at other positions of the coil. Thus, for high poleface flux density, this position is favourable for such a coil. Figure 3.24 shows that at NI $\geqslant$ 150000 ampere-turns, B_{Fe} at the poleface is independent of the coil position since the iron is saturated. It also shows that a high poleface flux density ($\sim$ 7 Tesla) can be achieved with such coil and polepiece arrangement. In this case the polepiece shape will

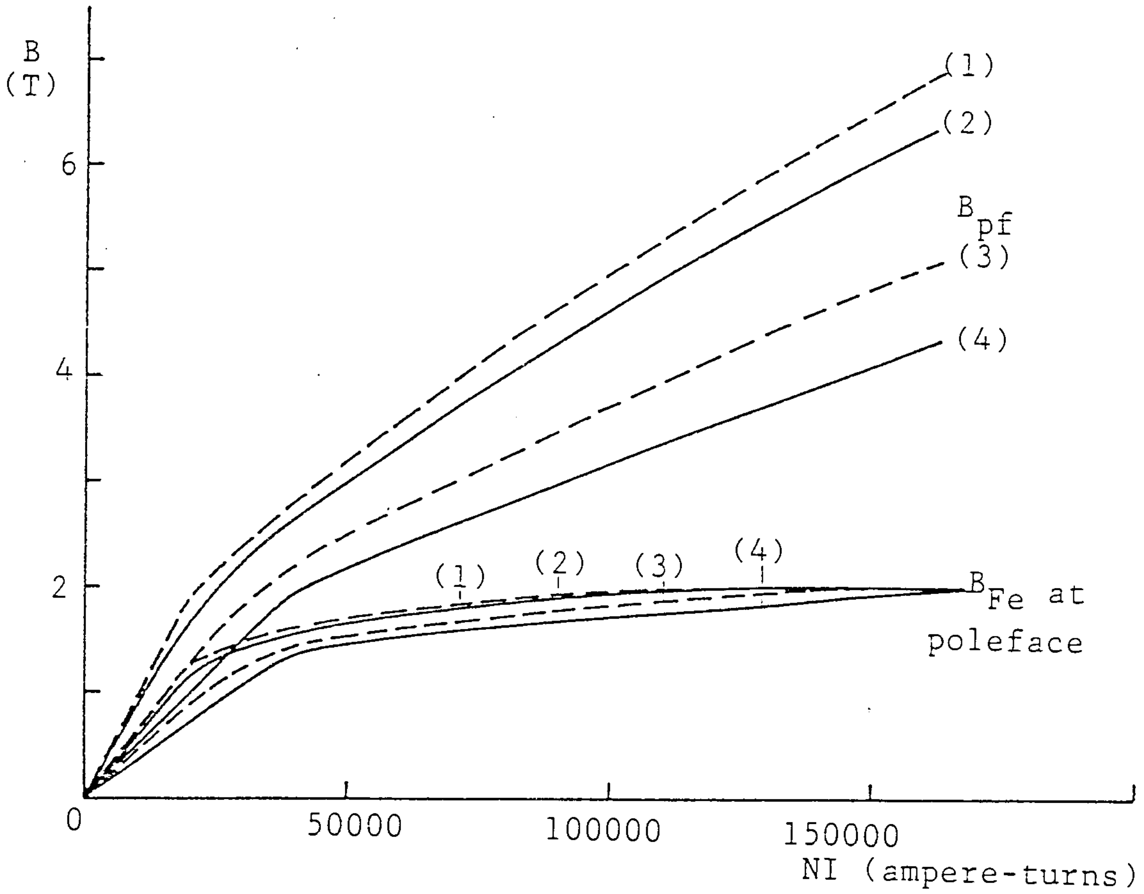

Figure 3.24 Poleface flux density B_{pf} due to the field of the single spherical-face polepiece lens and that due to the iron field, at four positions of the energizing coil ($s = 6$ mm, $d_1 = 3$ mm and $d_2 = 116$ mm), as functions of the excitation NI.

(1) Coil centre-plane 3 mm from poletip

(2) Coil centre-plane 4 mm from poletip

(3) Coil centre-plane 8 mm from poletip

(4) Coil centre-plane 12 mm from poletip

Note: The unconventional shape and position of the coil have strong effect on B_{Fe} at poleface.

no effect on such high flux density.

The focal properties, among other things, of single polepiece lenses have been investigated for the soft iron truncated-cone spherical-face pole. Such pole shape has been introduced for the design of new type of objective symmetrical double polepiece lenses which will be discussed in Chapter 4.

3.4 DESIGN OF COILS FOR SINGLE POLEPIECE LENSES

Even when the polepiece of an electron lens is saturated, a further increase in the total flux density B_z is still possible since an increase in the lens current will increase the coil field B_{coil}. The limiting factor to B_z is therefore the current density σ that can be supported by the energizing coil. Hence for a specific ratio d_2/d_1 of outer to inner diameter and s/d_m ratio of axial thickness to mean diameter the actual size of the coil and hence of a lens of given shape, will be decided by the current density in the windings, since in electron optics the excitation NI is usually a given quantity. It is thus important and worthwhile to consider this subject a little further.

Consider the coil previously shown in figure 3.1b whose outer diameter d_2 is 116 mm and inner diameter d_1 is 3 mm, i.e. d_m is 59.5 mm. By keeping the ratio d_2/d_1 (=38.7) constant, and allowing the axial thickness s of the coil to vary from 0.25 mm to 60 mm, a series of coils with a wide range of s/d_m values is obtained. These coils are allowed to energize the zero-bore single polepiece lens SP9 (figure 3.25) with a spherical-face on a truncated-cone. The end face of the coil is placed 1mm away from the poletip

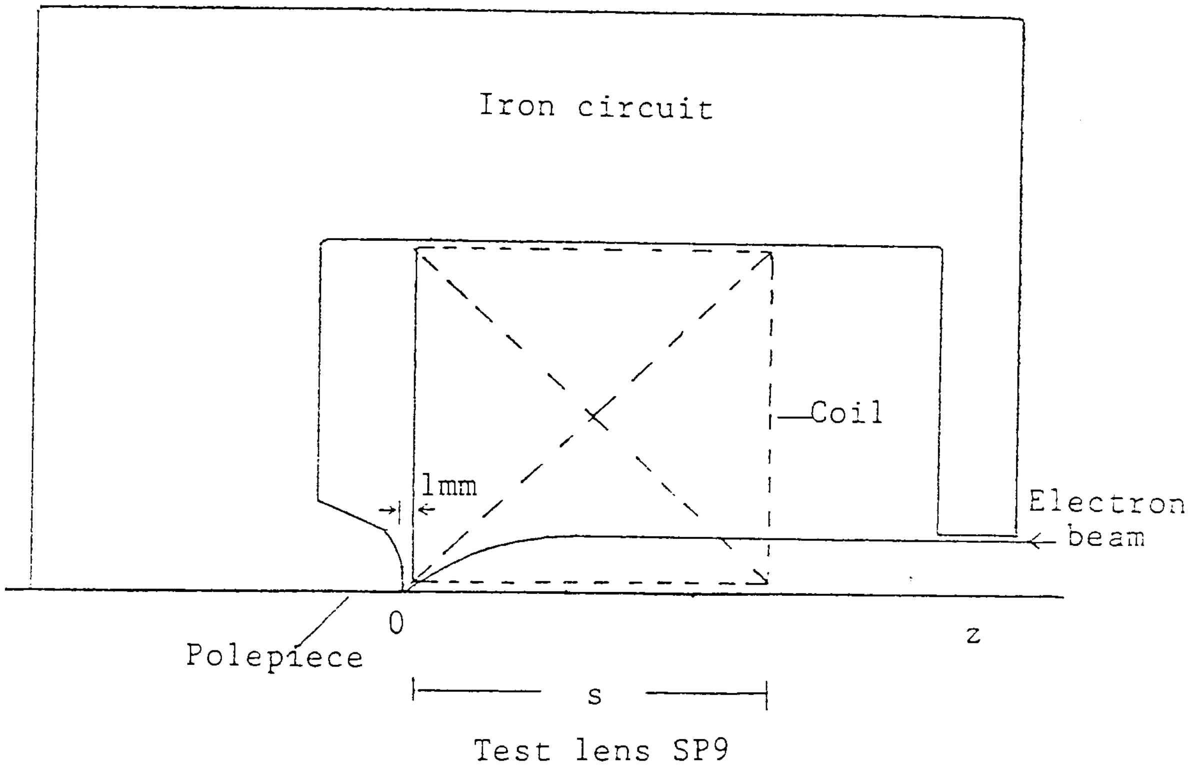

Figure 3.25 Cross-section of a zero-bore test lens SP9 with a single spherical-face truncated-cone polepiece energized by a coil of constant outer to inner diameter ratio ($d_2/d_1 = 38.7$). The coil is placed 1 mm away from the poletip. Only the upper half of the lens and its energizing coil is shown. The current density is constant ($\sigma = 20000$ A/cm^2). Note: s and d_m are varied to keep σ constant.

to allow room for the insertion of a specimen, positioned at $z_F = 0$ i.e. in contact with the poleface. The parallel incoming electron beam is brought to a focus on the specimen at this point. The coil was operated at a constant current density ($\sigma = 20000$ A/cm^2) and a relativistic accelerating voltage $V_r = 2$ MV. This means that the area and hence the size of the coil has to be adjusted for each value of s/d_m to satisfy the above conditions.

Figure 3.26 shows the computed focal properties at $V_r = 2000$ kV as a function of the ratio s/d_m. This shows that the spherical aberration coefficient C_s has a clearly defined minimum (1.83mm) at $s/d_m = 0.12$, corresponding closely to the position of the minimum value of the halfwidth W, though not to the maximum value $B_m = 2.7$ Tesla at $s/d_m = 0.24$ of the axial field distribution. This is an interesting result as it means that the restriction placed on the current density σ does not greatly alter the optimum value of $s/d_m = 0.1$ previously put forward by Marai (1977) for iron-free coils with an unlimited value of σ, and provisionally adopted in Chapter 3. The minimum chromatic aberration coefficient $C_c = 3.6$ mm occurs at $s/d_m = 0.32$. However, the C_c curve has a fairly shallow minimum so that the C_c value of 4 mm at the position of minimum C_s is only about 10% higher than the minimum C_c value. The minimum objective focal length $f_o = 5.5$ mm occurs at $s/d_m = 0.46$.

Figure 3.26 also shows that the outer diameter of the coil, and hence of the lens decreases inversely with $(s/d_m)^{0.6}$. Although the lens gets smaller when s/d_m approaches unity, its focal properties do not get better. Figure 3.26 also shows that the B_{Fe} value at the poleface in the important

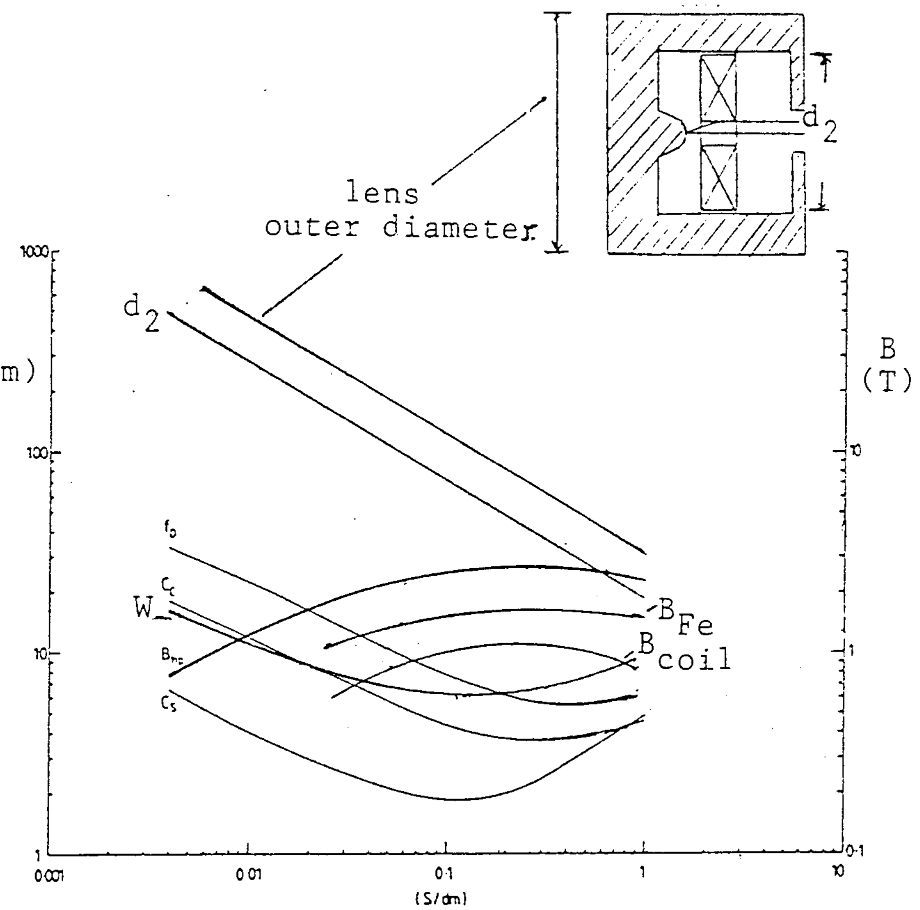

Figure 3.26 The electron-optical parameters of a combination of a coil and a spherical-face polepiece for constant focal distance ($z_F = 0$), current density ($\sigma = 20000$ A/cm^2) and accelerating voltage (V = 1 MV) as functions of coil geometrical ratio s/d_m of its axial thickness s to mean diameter d_m.

s/d_m range 0.1-0.3 is about 1.6 Tesla i.e. some 20% lower than the saturation value of 2 Tesla. This is a direct result of limiting the current density to 20000 A/cm^2. It will be shown later that an increase of about five times in current density would be needed to achieve saturation.

3.5 FOCAL PROPERTIES OF THE SINGLE POLEPIECE LENS

The test lens SP7 shown in figure 3.20 which has a small bore of 1 mm diameter was used to investigate the detailed focal properties of a single polepiece lens. The figure shows the axial flux density distributions B_z of the lens for different excitations NI. These B_z data were used for computing the focal properties C_s, C_c, f_o and focal distance z_F as a function of the relativistic voltage V_r. Each set of focal properties, at a given NI, is a function of V_r. The value of V_r at which $z_F = 0$ was noted, together with the associated C_s, C_c and f_o values corresponds to the specimen placed at the poletip of the single polepiece lens. These data may be transformed into data for a similar shape of lens operated at a desirable relativistic voltage $(V_r)_s$ by scaling the lens dimensions by a factor $k = [\ (V_r)_s/(V_r)_o\ ]^{\frac{1}{2}}$ where $(V_r)_o$ is the original value of V_r at which $z_F = 0$. The electron-optical parameters of the new lens will be scaled by the same factor. The value of flux density at corresponding points in the original and scaled lenses remains the same. This produces a family of lenses of different sizes, each having a different axial field distribution and hence a different peak flux density. The electron-optical characteristics of the family can be inferred from the B_z curves of figure 3.20 if use is made of the relevant scaling factor shown in table 3.1. For example the axial field distribution of the lens ($k = 0.1593$, $B_m = 7.2$ Tesla) at $V_r = 2000$ kV is obtained by multiplting the z scale of figure 3.20 by the factor 0.1593. This gives the halfwidth of this lens as 2.47 mm. The axial field distribution of the lens ($k = 1$, $B_m = 1.7$ Tesla) at V_r =2000 kV is correctly shown in the figure ($k = 1$). This lens has a halfwidth of 8.75 mm. It is therefore clear from table 3.1 that the focal properties of this family will improve steadily as the lenses are made smaller. However, the current density of the coil, as shown in table 3.1 increases rapidly as the size of the coil is reduced i.e. from $\sigma = 6500$ A/cm^2 for the largest lens to 332000 A/cm^2.

In order to investigate in more detail the properties of a single polepiece lens at various accelerating voltages, a value of σ of 20000 A/cm^2 was chosen as representing the the current density above which superconducting coils would certainly be needed. This choice is arbitrary but does not affect the general design principles involved.

When the lens shape, the object position, the current density and accelerating voltage are prescribed, the size of the lens is uniquely defined. Table 3.2 shows dimensions, and focal properties of three such lenses corresponding to the shape of the test lens SP7, and operating at 100 kV, 500 kV and 1000 kV accelerating voltage respectively. Table 3.2 shows that, for a fixed current density, the spherical and chromatic aberration coefficients C_s and C_c, the objective focal length f_o, and the size of the lens all increase with increasing accelerating voltage. This is to be expected since the lens must be made larger at higher voltages if σ is to be constant. The most significant

Table 3.1 Electron-optical characteristics of the family of six 1 MV single polepiece lenses similar in shape to that of lens SP7 (figure 3.20). The specimen is placed at the poleface ($z_F = 0$).

Scaling factor k	1	0.5464	0.39	0.302	0.21	0.1593
B_m (T)	1.7	2.65	3.34	4.06	5.607	7.2
σ (A/cm^2)	6500	23800	50000	86800	188000	332000
C_s (mm)	2.824	1.732	1.32	1.053	0.76	0.604
C_c (mm)	6.784	4.054	3.062	2.45	1.752	1.36
f_o (mm)	12.13	7.152	5.38	4.27	3.045	2.345
NI (A-t)	20000	21855	23400	24144	25116	25722
Lens outer diameter mm	196	107	76.5	59.2	41	31.2
W (mm)	8.75	5.57	4.6	3.93	3.08	2.47
B_{Fe} at the poleface(T)	1.15	1.565	1.712	1.85	2	2

Table 3.2 Electron-optical properties of three single polepiece test lenses similar in shape to that of test lens SP7 (figure 3.20) for current density $\sigma = 20000\ \mathrm{A/cm^2}$. The specimen is placed at the poleface ($z_F = 0$).

Voltage / Parameter	$V = 100$ kV $V_r = 110$ kV	$V = 500$ kV $V_r = 750$ kV	$V = 1000$ kV $V_r = 2000$ kV
B_{Fe} at the poleface (T)	1	1.32	1.5
B_{coil} at the poleface (T)	0.44	0.78	1
B_{pf} (T)	1.44	2.1	2.5
W (mm)	1.16	3.15	6.3
NI (A-t)	4711	12720	21500
Outer diameter (mm)	54.3	89.5	116
C_s (mm)	0.786	1.425	1.85
C_c (mm)	1.88	3.18	4.3
f_o (mm)	3.36	5.75	7.6
δ (nm)	0.363	0.1764	0.13

result shown in table 3.2 is that, although the peak flux density increases with increasing accelerating voltage, the halfwidth W increases more rapidly. This means that the improvement in lens performance due to increasing B, will be partly offset by the increase in halfwidth. This means that a restriction on σ will inevitably lead to higher aberrations. The variation of the 1 MV lens performance with σ is shown in table 3.1. When the lens is made smaller, the poleface flux density and σ increase and C_s, C_c, f_o and W decrease.

The resolution δ of each lens was calculated from the following relationship

$$\delta = 0.7\ (C_s\ \ \lambda^3)^{1/4} \tag{3.3}$$

where λ is the electron wavelength equal to $1.23/V_r^{\frac{1}{2}}$ in nm. As would be expected, δ improves with increasing voltage.

The flux density B_{Fe} at the poleface due to iron magnetization shown in table 3.2 is lower than the saturation value of 2 Tesla. This is a direct result of the large cross-section of the winding which has a limited current density (20000 A/cm^2). Table 3.1 shows that the B_{Fe} value at the poleface increases as the lens size is decreased. However, this calls for an increase in σ, keeping V and z_F constant. Therefore, at 1 MV accelerating voltage a five-times increase in current density ($\sigma = 10^5$ A/cm^2) would be needed to achieve poletip saturation (B_{Fe} = 2 Tesla) which would require a superconducting energizing coil. With such a lens of reduced size the following results could be achieved at an accelerating voltage of 1 MV.

C_s = 0.99 mm (compared with 1.85 mm)

C_c = 2.3 mm (compared with 4.3)

NI = 24230 A-t (compared with 21500 A-t)

B_{pf} = 4.2 Tesla (compared with 2.5 Tesla)

Therefore, improved focal properties are achieved as the polepiece tip saturates. The resulting improvement in resolution δ from 0.13 nm to 0.11 nm is small but significant at such high resolving powers. The lens outer diameter is however smaller with 55.2 mm against 116 mm, and would cause problems at the present stage of manufacturing technique.

3.6 MAGNETIZATION OF THE SINGLE POLEPIECE

Computations were carried out on the effect of the energizing coil arrangement on the magnetization of a saturated single polepiece lens. The lens had an outer diameter of 196 mm. As in the previous investigations, the radius of curvature of the spherical face of the single polepiece was kept constant (15 mm).

Figures 3.27, 3.28, 3.29 and 3.30 show the axial flux density distributions computed at different excitations NI of four zero-bore single polepiece test lenses SP10, SP11, SP12 and SP13 respectively with the same shape of magnetic circuit energized by four different coil arrangements (only the upper half of the lens is shown). Figure 3.28 shows that a flux density peak appears at high excitation in the region of the centre-plane of the coil due to the dominance of B_{coil} over B_{Fe}. Figure 3.30 shows that at excitations higher than 60000 ampere-turns the peak of the axial field shifts to the poletip due to the considerable effect of the thin coil.

Figure 3.31a shows the poletip B_{Fe}-H magnetization

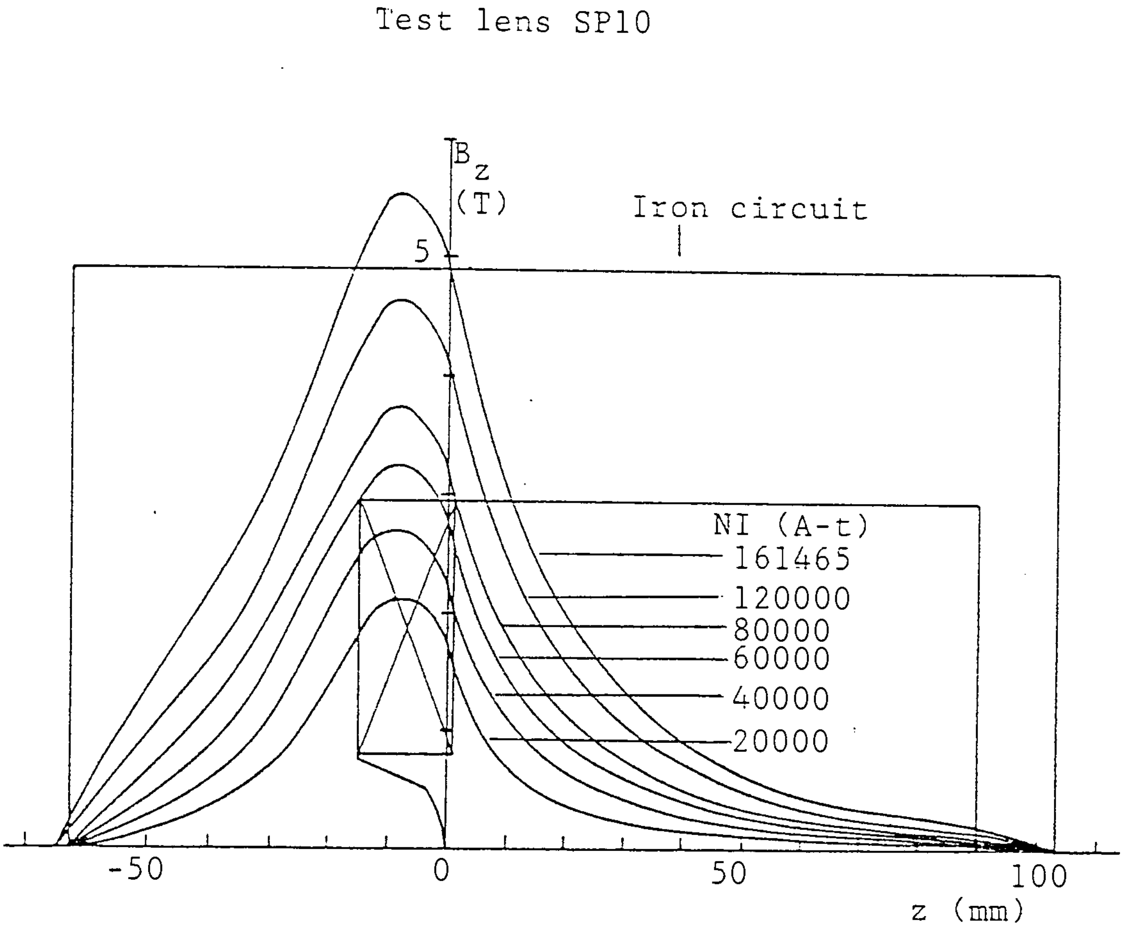

Figure 3.27 Axial flux density distributions of the zero-bore soft iron single polepiece test lens SP10 computed at different excitations NI. The energizing coil has an axial thickness s = 16 mm, inner diameter d_1 = 32 mm, outer diameter d_2 = 118 mm and s/d_m = 0.21, placed in the conventional position surrounding the single polepiece. Only the upper half of the lens and its energizing coil is shown. Lens outer diameter = 196 mm.

Test lens SP11

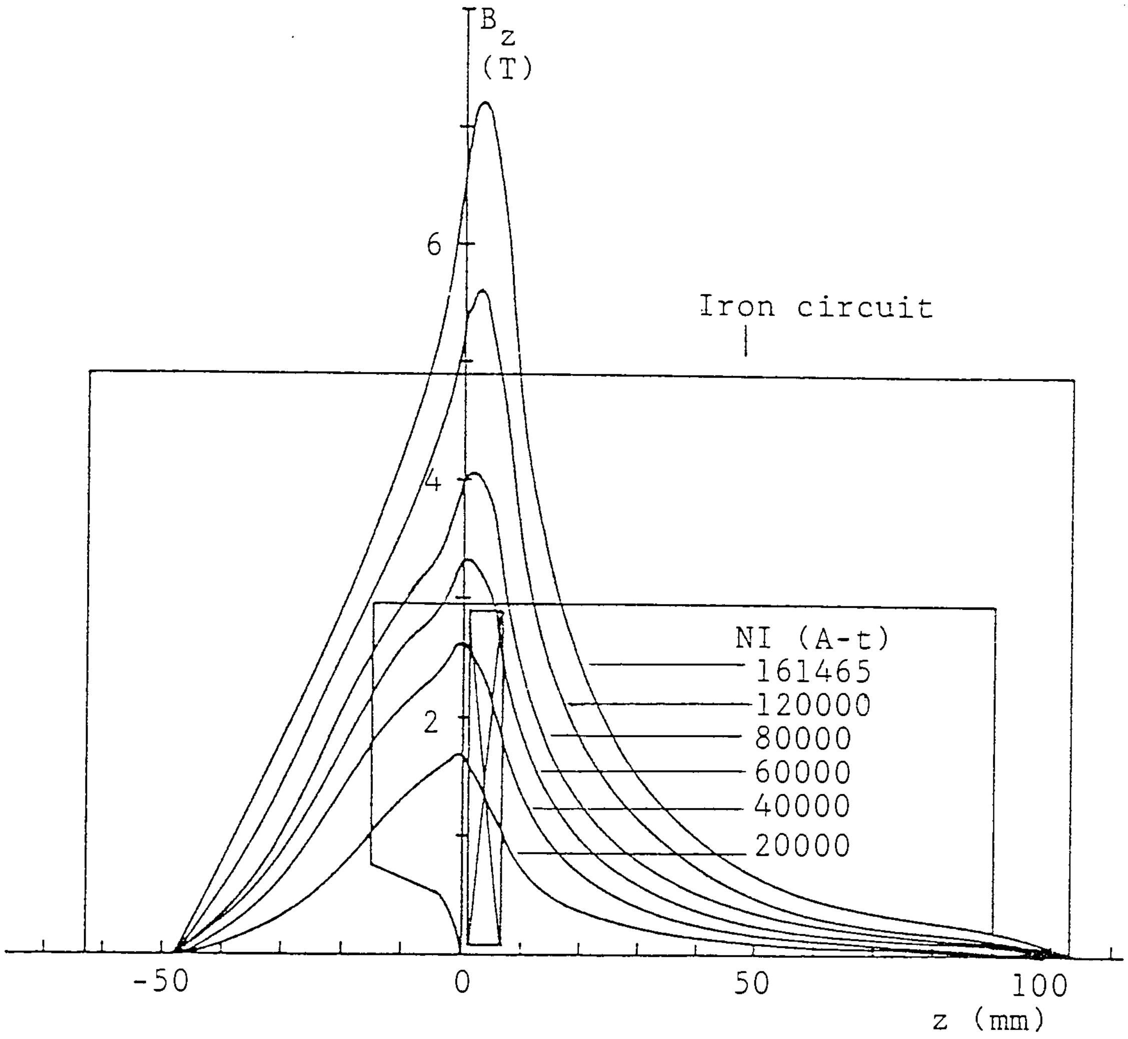

Figure 3.28 Axial flux density distributions of the zero-bore soft iron single polepiece test lens SP11 computed at different excitations NI. The energizing coil has an axial thickness s = 6 mm, inner diameter d_1 = 3 mm, outer diameter d_2 = 116 mm and s/d_m = 0.1, placed 1 mm away from the poletip. Only the upper half of the lens and its energizing coil is shown. Lens outer diameter = 196 mm.

Test lens SP12

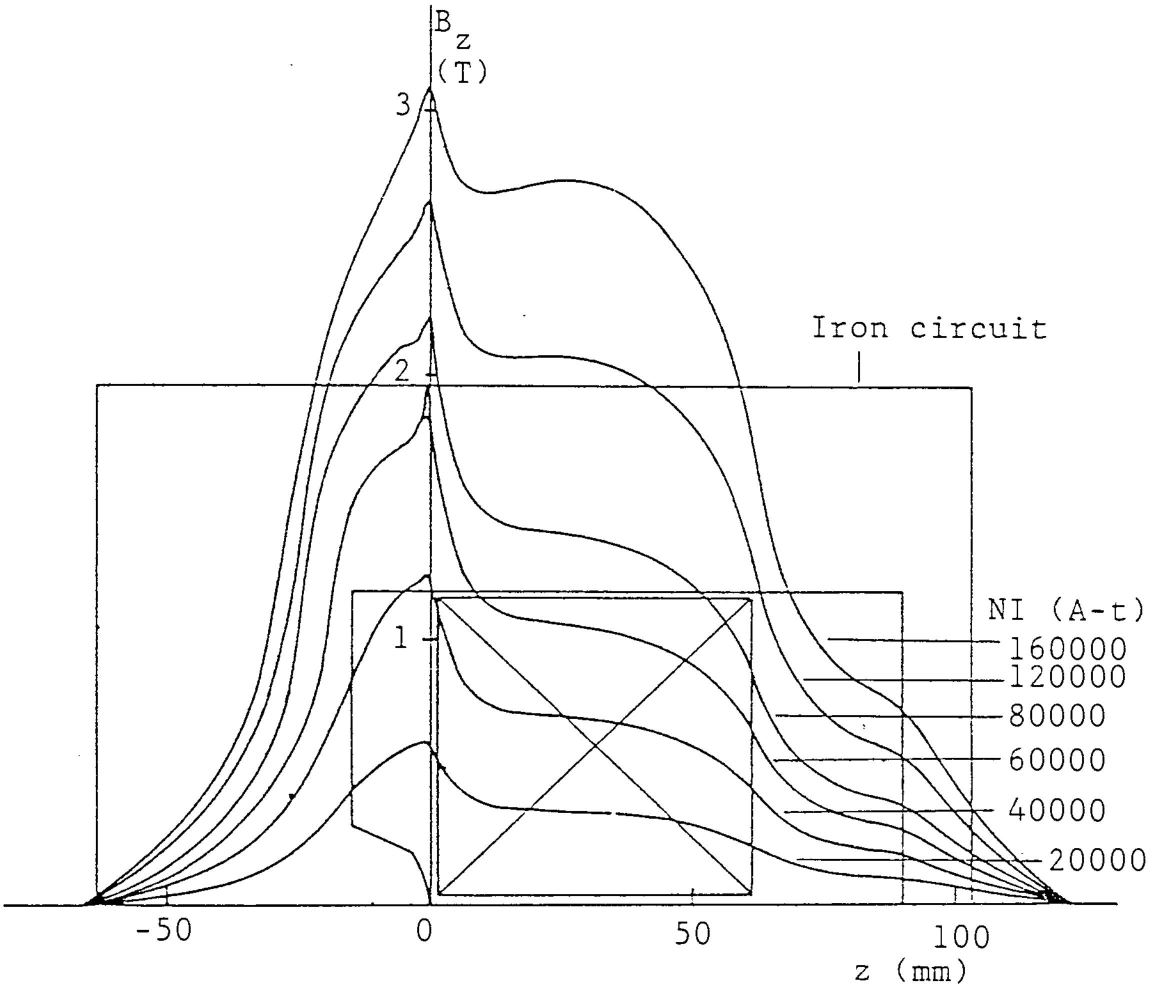

Figure 3.29 Axial flux density distributions of the zero-bore soft iron single polepiece test lens SP12 computed at different excitations NI. The energizing coil has an axial thickness s = 60 mm, inner diameter d_1 = 3 mm, outer diameter d_2 = 116 mm and s/d_m = 1, placed 1 mm away from the poletip. Only the upper half of the lens and its energizing coil is shown. Lens outer diameter = 196 mm.

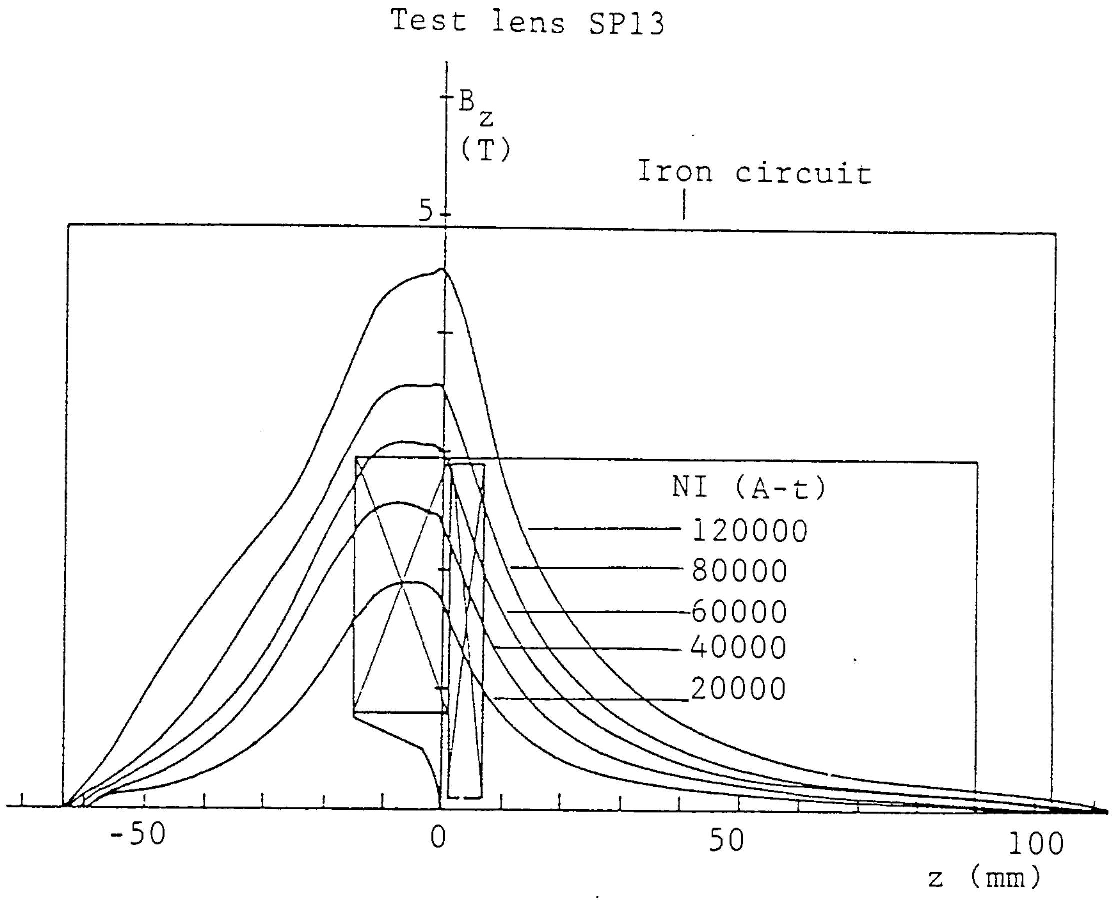

Figure 3.30 Axial flux density distributions of the zero-bore soft iron single polepiece test lens SP13 computed at different excitations NI. The lens is energized by a combination of the magnetizers of the lenses shown in figures 3.27 and 3.28. Only the upper half of the lens and its energizing coils is shown. Lens outer diameter =196 mm.

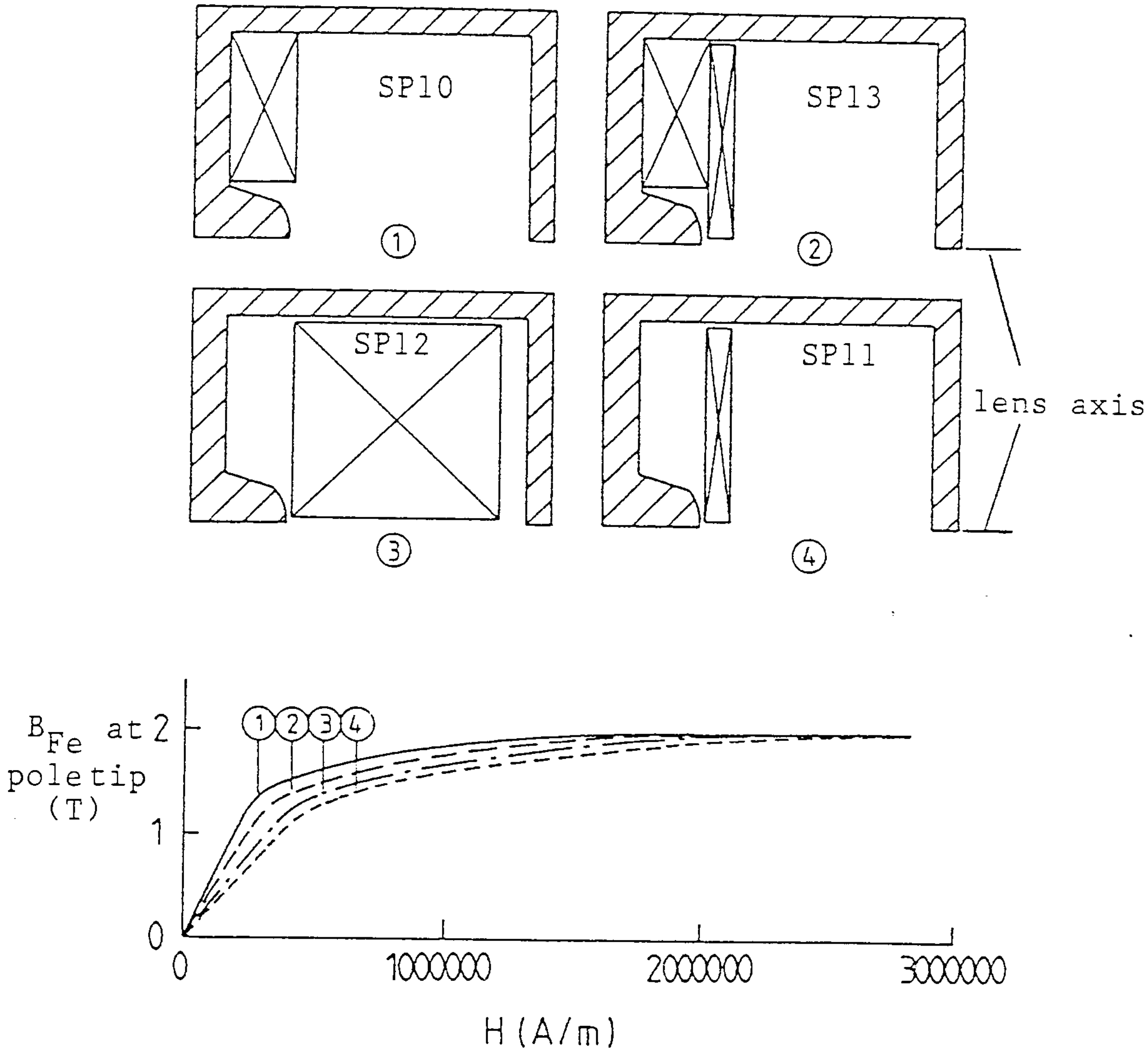

Figure 3.31a Poletip B_{Fe}-H magnetization curves of the four zero-bore single polepiece test lenses SP10, SP11, SP12 and SP13 energized by different coils. Only the upper half of the schematic cross-section of the lens is shown.

curves of the above four zero-bore single polepiece test lenses with the same shape of magnetic circuit energized by four different coil arrangements (only the upper half of the lens is shown). The maximum contribution of poletip magnetization is 2 Tesla (saturation flux density of soft iron). At magnetic field strength $H > 2000000$ A/m, the polepiece is saturated and the value of B_{Fe} at the poleface becomes independent of the energizing coil arrangement. The B_{Fe}-H curves do not depend on the size of the lens. Ideally, the poletip should reach magnetic saturation for the lowest possible values of field strength H and excitation NI. Figure 3.31a shows that dB_{Fe}/dH is highest when the lens is energized by a coil surrounding the polepiece and placed in the conventional position (see test lens SP10). Therefore, such a coil arrangement appears to be favourable as a magnetizer. However, the efficiency of each coil arrangement in producing a given value of H for the lowest excitation NI must also be considered, since in practice NI, rather than H, is prescribed in a given lens. Since the poleface is magnetized by the exciting coil, therefore a coil is needed that produces the highest magnetic field strength H. A thin coil near the poleface produces a higher value of H (for a given NI) than does a coil surrounding the polepiece. Figure 3.31b shows that coil arrangement in test lens SP11 is the best in this respect and so its axial field has the lowest halfwidth W4 for $NI>50000$ A-t and the highest flux density at poleface. In the vicinity of the polepiece the saturation flux density which is strongly located at the poletip is simply added to the field produced by the coil. In this type of lenses, there is no limit to the maximum flux density

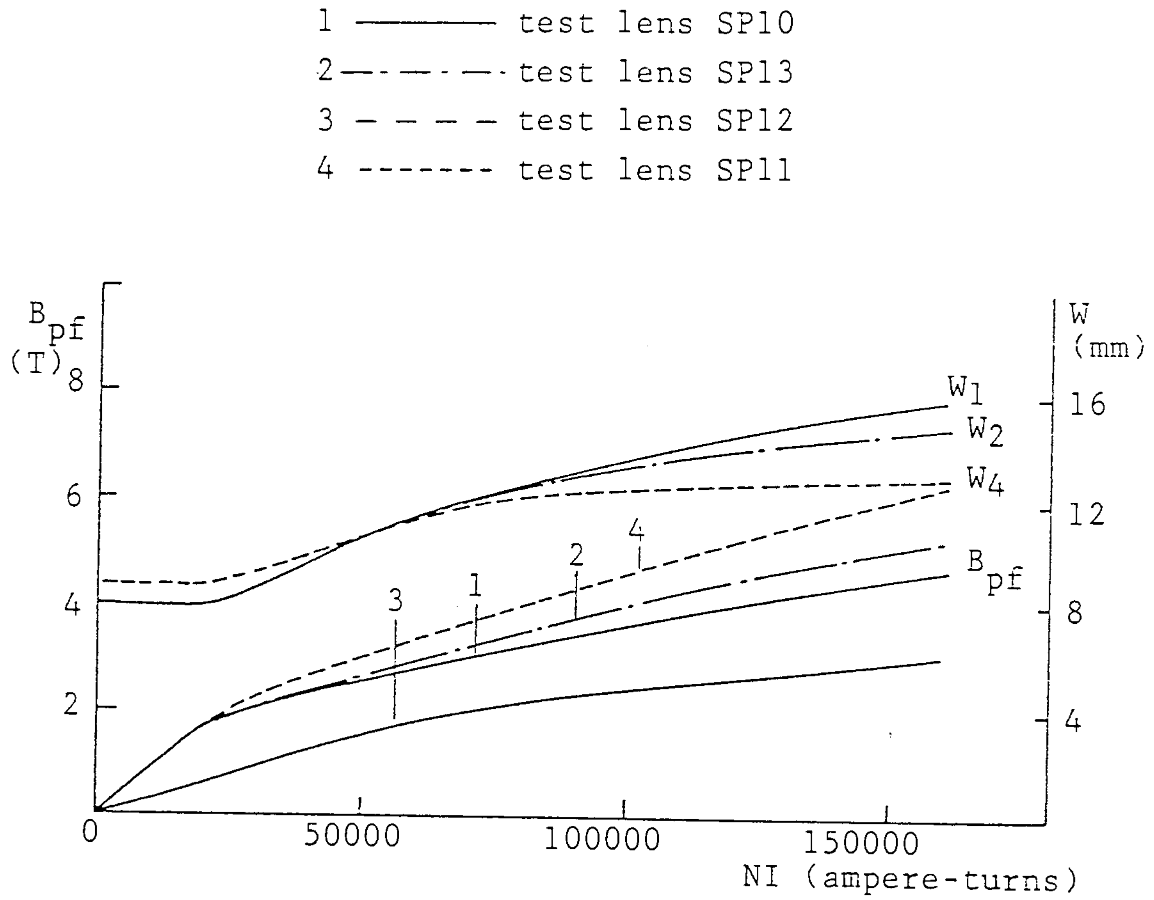

Figure 3.31b The halfwidth W of the axial field and the poleface flux density B_{pf} of the single polepiece test lenses SP10, SP11, SP12 and SP13 shown in figure 3.31a as functions of the excitation NI of the energizing coil. The axial fields of test lenses SP10, SP11, SP12 and SP13 are shown in figures 3.27, 3.30, 3.29 and 3.28 respectively.

that can be produced except that set by the maximum permissible current density in the exciting coil. The halfwidth W3 of the axial field of test lens SP12 has not been plotted in figure 3.31b since it is considerably larger as shown in figure 3.29.

Figure 3.31b shows that at high excitations NI test lenses SP11 and SP13 have higher B_{pf} and smaller W than those of test lenses SP10 and SP12. Such arrangements of energizing coils should be applicable to both spherical and flat ended polepiece shapes. The focal properties of the four single polepiece test lenses SP10, SP11, SP12 and SP13 will be investigated in the next section.

3.7 OBJECTIVE FOCAL PROPERTIES OF SINGLE POLEPIECE LENSES

The objective focal properties of test lenses SP10, SP11, SP12 and SP13 shown schematically in figure 3.31a will be plotted in terms of σ the current density in the windings, since this is the limiting factor for a saturated lens.

The computations have been carried out for an electron beam entering the lens field parallel to the optical axis with an energy of 1 MeV (i.e. relativistic accelerating voltage V_r = 2 MV). In this calculation, the beam intersects the optical axis at the poleface ($z_F = 0$), corresponding to a specimen placed in contact with the poleface. Figure 3.32 shows the objective focal properties of four families of 1 MV single polepiece lenses similar in shape to those of test lenses SP10, SP11, SP12 and SP13 as functions of σ . It is seen that as the current density σ increases (i.e. the lenses are made smaller) the focal properties of the test lenses improve steadily. Of the four families, the family of

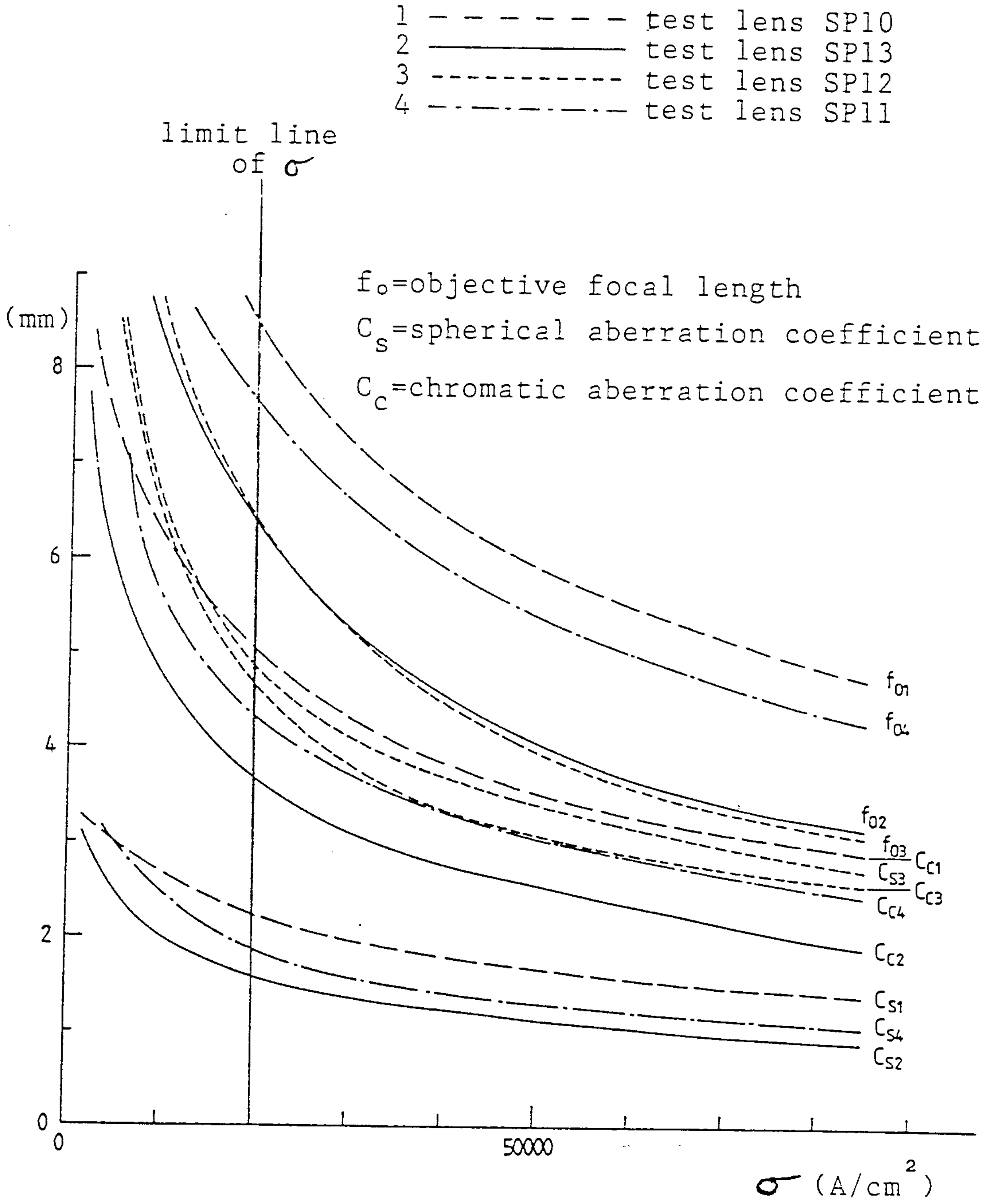

Figure 3.32 Objective focal properties of the four 1 MV single polepiece test lenses shown schematically in figure 3.31a computed as functions of the current density σ .

test lenses similar in shape to SP13 energized by a combination of two coils, has the lowest spherical aberration coefficient C_{s2} and chromatic aberration coefficient C_{c2}. The advantages of both coils have, therefore, combined to produce low aberrations. Thus test lenses similar in shape to SP13 arrangement are favourable for low spherical and chromatic aberration coefficients. At values of $\sigma < 10^5$ A/cm^2 the objective focal length f_{o_2} and f_{o_3} of test lenses similar in shape to SP13 and SP12 respectively are nearly the same and they are always lower than f_{o_1} and f_{o_4} of test lenses similar in shape to SP10 and SP11 respectively.

3.8 OBJECTIVE LENS DESIGN

From the focal properties of the four families of test lenses shown in figure 3.32 four test lenses were deduced operating at constant current density σ of 20000 A/cm^2. The electron-optical parameters of these four 1 MV test lenses SP14, SP14, SP16 and SP17 (figure 3.33) operated at σ = 20000 A/cm^2 are shown in table 3.3. Table 3.3 shows that test lens SP15 has the lowest aberration coefficients. The power required for operating this lens at σ = 20000 A/cm^2 and V = 1 MV is about 10 kW according to equation (1.4) using a water-cooled copper tape coil. The thickness of the copper tape is 0.125 mm and it is assumed that the coil temperature reaches 100 °C which is the boiling water temperature.

The values of flux density B_{Fe} at the poletip due to iron magnetization (table 3.3) show that the poletip of the four single polepiece test lenses do not saturate at such

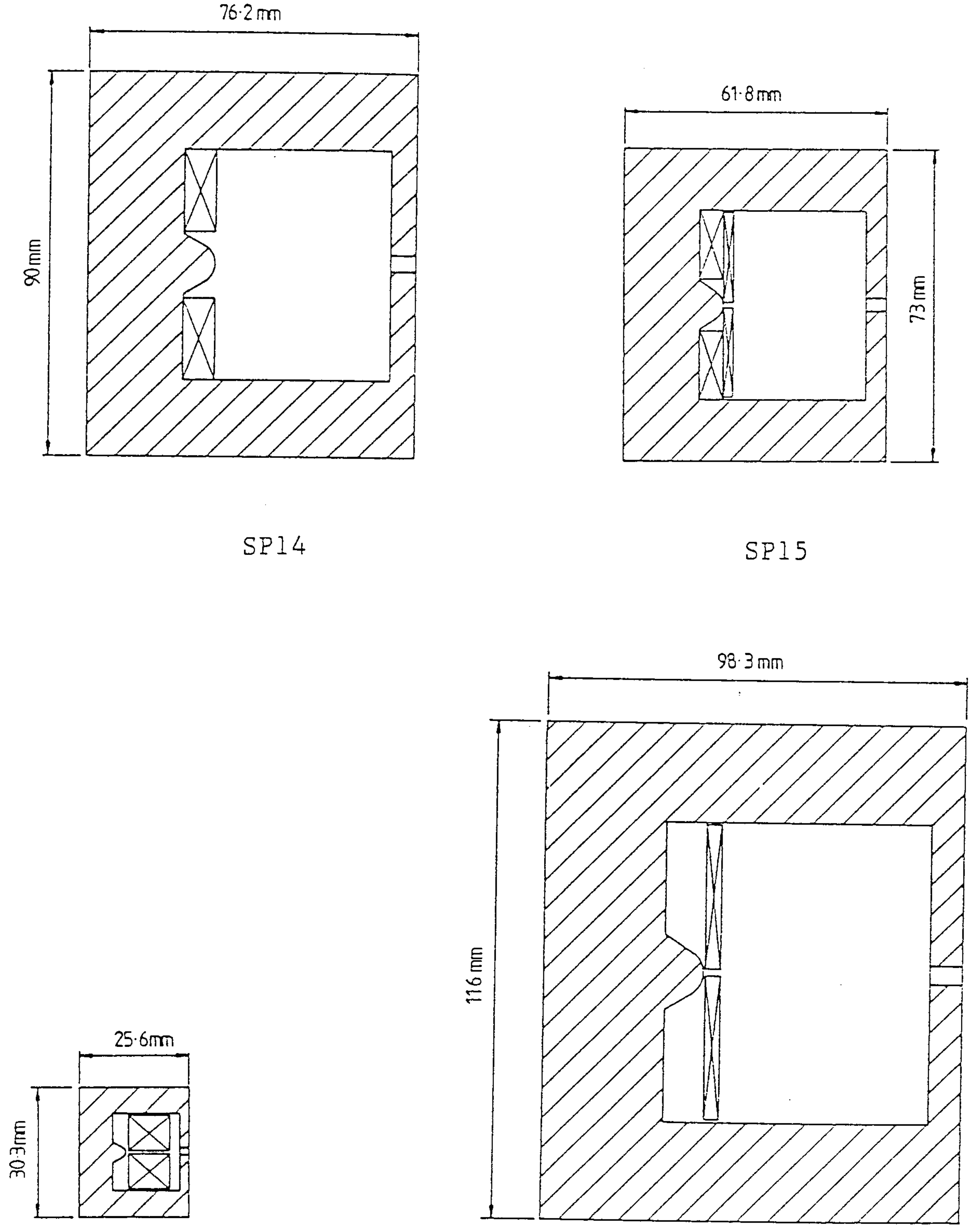

SP14

SP15

SP16

SP17

Figure 3.33 Cross-section of the four 1 MV zero-bore single polepiece test lenses operating at current density $\sigma = 20000\ A/cm^2$.

Table 3.3 Electron-optical parameters of four 1 MV single polepiece test lenses SP14, SP15, SP16 and SP17 shown in figure 3.33 operated at a constant current density σ of 20000 A/cm^2. The specimen is placed at the poleface ($z_F = 0$).

Parameter \ Test lens	SP14	SP15	SP16	SP17
B_{pf} (T)	2.7	3.2	2.3	2.5
B_{Fe} (T)	1.715	1.815	1.54	1.5
W (mm)	7	4.4	9	6.3
NI (A-t)	26650	25800	14307	21500
outer diameter (mm)	90	73	30.3	116
C_s (mm)	2.23	1.57	4.83	1.85
C_c (mm)	5	3.66	4.61	4.3
f_o (mm)	8.4	6.3	6.4	7.6
δ (nm)	0.137	0.125	0.166	0.13

current density. The value of B_{Fe} at the poletip of test lens SP15 is higher than those of the other lenses but it is less than the saturation value of 2 Tesla. At $\sigma = 30000$ A/cm^2 the poletip of a lens similar in shape to that of test lens SP15 will reach saturation. With this 50% increase in σ the following results of such a reduced size lens (60.2 mm outer diameter) could be achieved at an accelerating voltage of 1 MV and $z_F = 0$ compared with those of test lens SP15.

$C_s = 1.3$ mm compared with 1.57 mm
$C_c = 3.075$ mm compared with 3.66 mm
NI = 26150 A-t compared with 25800 A-t
$B_{pf} = 3.67$ Tesla compared with 3.2 Tesla
$\delta = 0.12$ nm compared with 0.125 nm

Therefore, improved focal properties are achieved as the poletip saturates.

Considering the present day figures of current density (for example $\sigma = 5000$ A/cm^2), the 1 MV single polepiece lens similar in shape to SP15 has the following parameters when $z_F = 0$:

$C_s = 2.45$ mm, $C_c = 5.8$ mm, $f_o = 10.1$ mm, $\delta = 0.14$ nm, NI = 22800 ampere-turns, $B_{pf} = 2.25$ Tesla and lens outer diameter = 137.7 mm.

For a 0.5 MeV electron beam entering the lens field parallel to the optical axis and focused at the poleface ($z_F = 0$), the outer diameter of the lens similar in shape to that of test lens SP15 becomes 56.4 mm when it is energized at a current density of 20000 A/cm^2. The electron-optical parameters of the 500 kV lens are:

$C_s = 1.15$ mm, $C_c = 2.7$ mm, $f_o = 4.7$ mm, $\delta = 0.167$ nm,

NI = 15290 ampere-turns and B_{pf} = 2.77 Tesla.

3.9 HIGH CURRENT DENSITY SATURATED SINGLE POLEPIECE LENSES

In the previous section the electron-optical properties of the different designs of single polepiece lenses have been investigated at current densities less than 10^5 A/cm^2. Single polepiece lenses operated at such current densities appear to have a favourable coil arrangement. It is, therefore, worthwhile to investigate single polepiece lenses energized at higher current densities by superconducting windings. Figure 3.34 shows the electron-optical properties of two families of 1 MV test lenses similar in shape to those of lenses SP13 and SP11 as functions of the current density σ for $z_F = 0$. It is seen that C_s, C_c, f_o and W of test lenses similar in shape to SP13 are less than those of test lenses similar in shape to SP11 at all values of σ. Furthermore, the flux density B_{pf} at the poleface of the lenses similar in shape to SP13 is higher than those similar in shape to SP11. The focal properties of the family of lenses similar in shape to SP13 are the smallest since their axial fields are characterized by the smallest W and highest B_{pf} at different values of σ as shown in figure 3.34.

Therefore, a combination of two coils similar to that of test lens SP13 is an optimum coil arrangement. This coil arrangement is applicable to spherical and flat face polepieces.

Figure 3.35 shows a log-log plot of the spherical and chromatic aberration coefficients of the two families of 1 MV lenses similar in shape to those of SP11 and SP13 as functions of the current density σ plotted linearly in

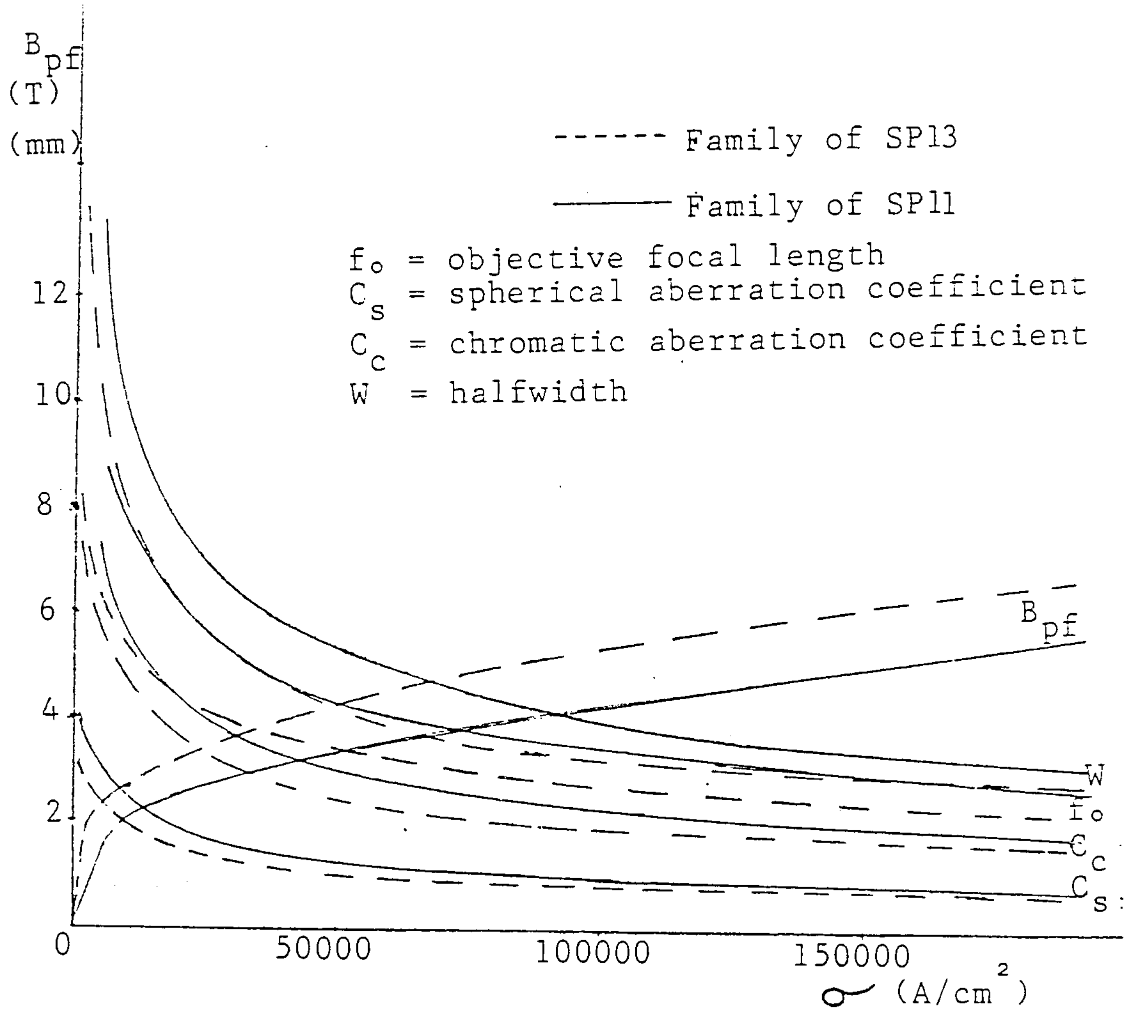

Figure 3.34 Electron-optical parameters of two families of 1 MV single polepiece test lenses similar in shape to SP13 and SP11 shown schematically in figure 3.31a plotted as functions of the current density σ for $z_F = 0$.

Solid lines: family of lenses similar to test lens SP11 energized by a thin flat coil.

Broken lines: family of lenses similar to test lens SP13 energized by two coils.

figure 3.34. This kind of plot shows the variation of the above coefficients more clearly than a linear plot can. The figure shows that the aberration coefficients vary inversely with σ^{n}. For the family of saturated single polepiece lenses similar in shape to test lens SP11 energized by a thin flat coil, the coefficients C_s and C_c improve as $\sigma^{-0.48}$. For the family of saturated single polepiece lenses similar in shape to test lens SP13 energized by a combination of two coils, the coefficients C_s and C_c improve as $\sigma^{-0.42}$.

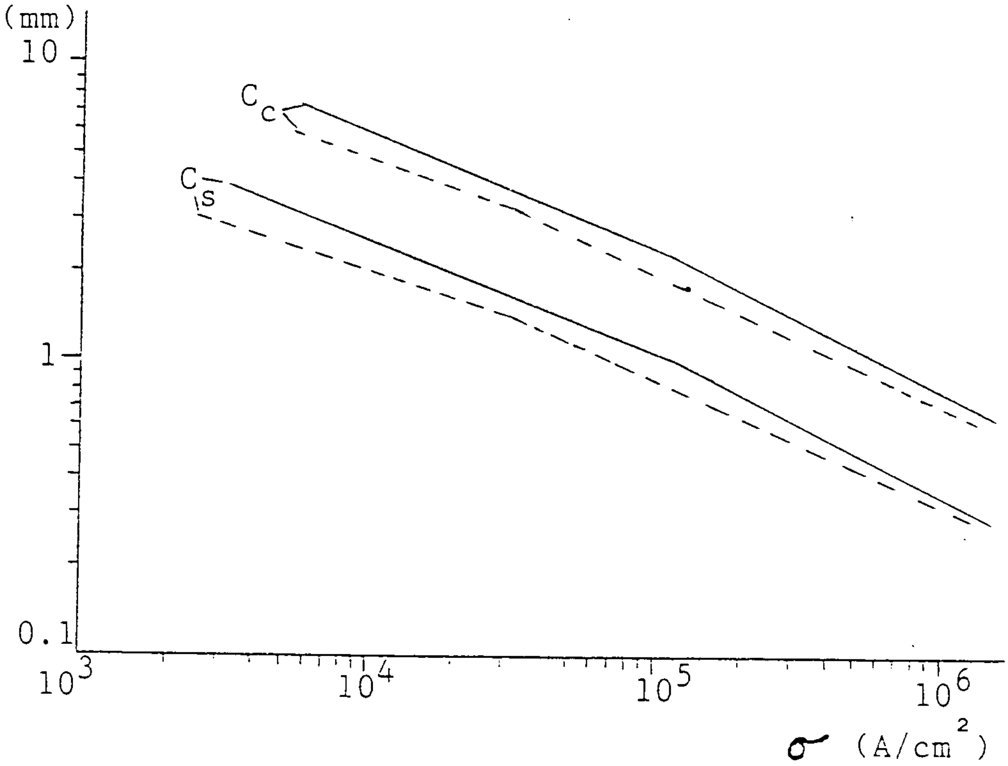

Figure 3.35 A log-log plot of the spherical and chromatic aberration coefficients as functions of the current density drawn linearly in figure 3.34.

Solid lines: family of lenses similar in shape to test lens SP11 energized by a thin flat coil.

Broken lines: family of lenses similar in shape to test lens SP13 energized by two coils.

4. DESIGN OF SATURATED SYMMETRICAL DOUBLE POLEPIECE OBJECTIVE LENS

The flat-face truncated-cone is usually adopted in conventional double polepiece lenses. In Chapter 3 it was shown that in the linear and intermediate regions of the iron magnetization curve the spherical-face truncated-cone polepiece is a favourable pole shape in single polepiece lenses. However, in saturated single polepiece lenses, the pole shape appears to be not critical. Till now, little has been published (Al-Nakeshli et al 1984a and b, Al-Nakeshli and Juma 1986) about the electron-optical properties of symmetrical double polepiece magnetic electron lenses with spherical-face poles (see Appendix 1). In the present chapter attention has therefore, been concentrated on the introduction of the spherical-face pole to symmetrical double polepiece objective lenses in order to achieve a favourable combination of the two polepieces and energizing coil.

4.1 DESIGN CONSIDERATIONS

The flat-ended and the spherical-face conical pole shapes in symmetrical double polepiece lenses are considered for comparison. The two designs of symmetrical double polepiece test lenses DP1 and DP2 shown in figures 4.1 and 4.2 have been studied. The dimensions of the polepieces and the inner diameter of the iron cylinder surrounding the coils are identical to those of the single polepiece lenses shown in figures 3.20 and 3.21. The air gap S separating the tips of the two polepieces is 8 mm wide in order to accommodate a thin flat coil of 6 mm thickness. Thus the coil is 1 mm

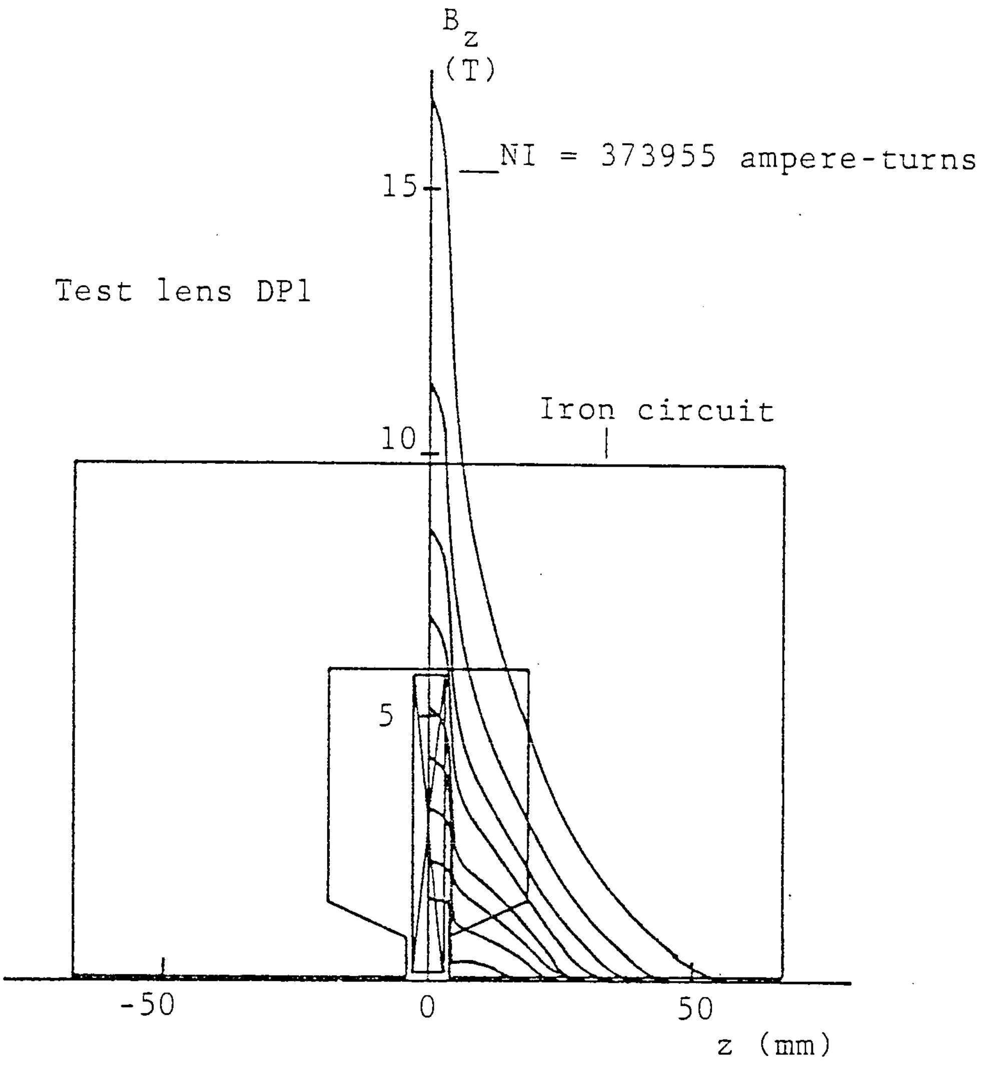

Figure 4.1 Axial flux density distributions B_z in a symmetrical double polepiece test lens DP1 with flat-face truncated-cone polepieces of 1 mm axial bore diameter and separated by an 8 mm air gap. Only the positive half of the fields and the upper half of the soft iron lens and its thin flat energizing coil ($s = 6$ mm, $d_1 = 3$ mm and $d_2 = 116$ mm) are shown. The axial fields are computed at excitations NI = 10000, 20000, 40000, 60000, 80000, 120000, 161465, 232282 and 373955 ampere-turns shown in an ascending order. Lens outer diameter = 196 mm.

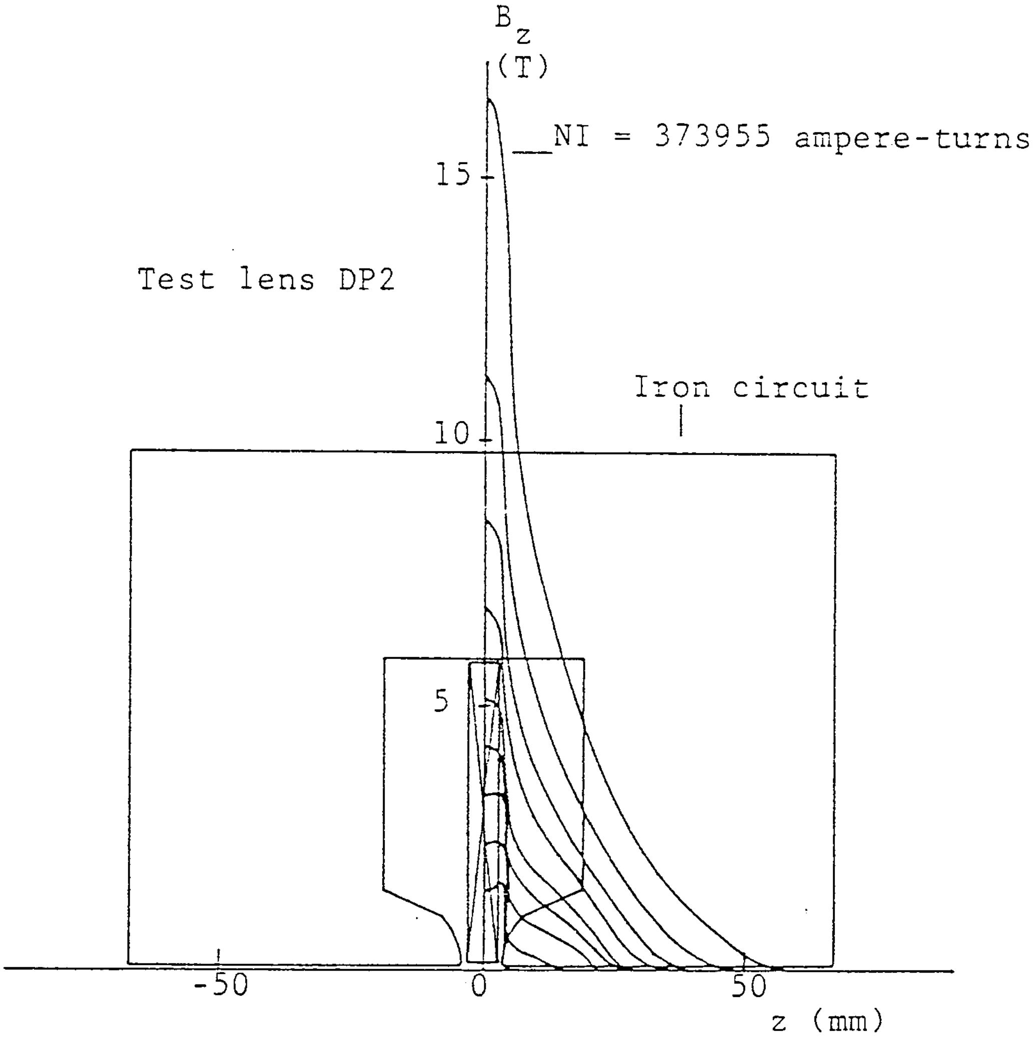

Figure 4.2 Axial flux density distributions B_z in a symmetrical double polepiece test lens DP2 with spherical-face truncated-cone polepieces of 1 mm axial bore diameter and separated by an 8 mm air gap. Only the positive half of the fields and the upper half of the soft iron lens and its thin flat energizing coil (s = 6 mm, d_1 = 3 mm and d_2 = 116 mm) are shown. The axial fields are computed at excitations NI = 10000, 20000, 40000, 60000, 80000, 120000, 161465, 232282 and 373955 ampere-turns shown in an ascending order. Lens outer diameter = 196 mm.

away from the tip of each polepiece. Each of the two double polepiece lenses has a 1 mm axial bore diameter to allow passage for the electron beam.

It should be mentioned that the lenses under consideration had thick iron shrouds. This is to avoid any unwanted loss of ampere-turns as the polepieces become saturated. For example, with a 16 mm thick iron plate at the back of each polepiece and a 13 mm thick cylinder around the coil (test lens DP3, figure 4.3) some loss of ampere-turns was observed as NI exceeded 60000 ampere-turns. This loss increased with increasing excitation. Figure 4.3 shows an example of the change in area (10%) as the thickness of the iron shroud is increased, computed at 161465 ampere-turns. For simplicity, only half the lens and its energizing coil and the positive half of the axial field are shown. At 373955 ampere-turns, the area under the axial field of the lens was 16% less than the theoretical value (μ_o NI). This loss decreased with increasing thickness of the shroud. It decreased to about 8% when the iron surrounding the lens was doubled. However, the loss in ampere-turns disappeared when the iron shroud was made three times its original thickness i.e. the iron plate at the back of each polepiece became 48 mm thick and the cylinder surrounding the coil became 39 mm thick as shown by the dotted shroud in figure 4.3. Flux leakage, as one would expect, is similar in the two test lenses DP1 and DP2 under consideration with different polepiece shapes.

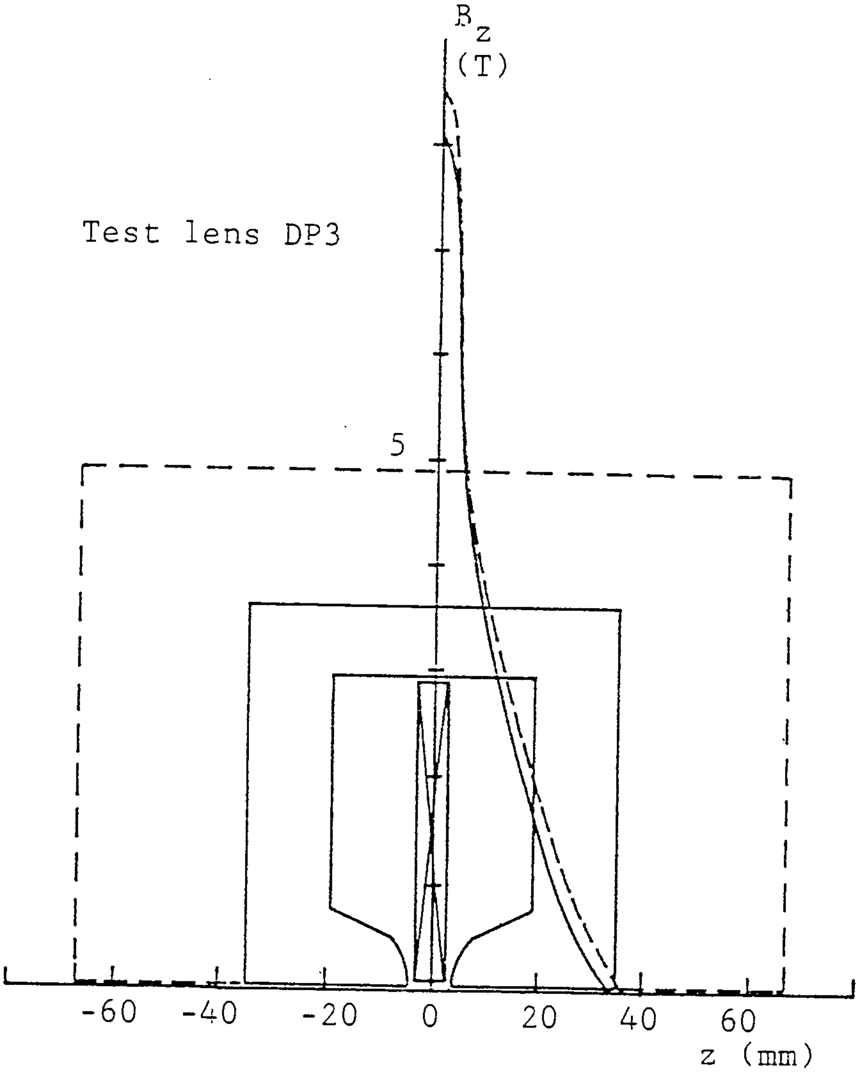

Figure 4.3 Change in the axial field B_z of the double spherical-face polepiece test lens DP3 due to flux leakage before (solid line) and after (dotted line) increasing the thickness of the iron shroud by three times, computed at NI = 161465 ampere-turns. Only the positive half of the field and the upper half of the lens and its thin flat energizing coil are shown.

4.2 COMPARISON BETWEEN FLAT-FACE AND SPHERICAL-FACE POLEPIECES IN SYMMETRICAL DOUBLE POLEPIECE LENSES

4.2.1 COMPARISON BETWEEN THE MAGNETIC FIELDS

Figures 4.1 and 4.2 show the two symmetrical double polepiece test lenses DP1 and DP2 of flat-face and spherical-face truncated-cone polepieces respectively together with their axial field distributions computed at different excitations NI. Due to the symmetry of the lenses and their axial fields, only the upper half of the cross-section of each lens and the positive half of its corresponding axial field distributions are shown. At any point along the optical axis of the two lenses the axial field B_z is the sum of the field B_{Fe} due to the magnetization of the iron polepieces and the field B_{coil} due to the energizing coil. Figures 4.1 and 4.2 show that at low excitations where the coil field is not dominant over that of B_{Fe}, the field at the centre of the lens with spherical-face polepieces is different from that with flat-face polepieces. At high excitations the axial field distributions become independent of the polepiece shape. This is largely due to the marked contribution of the coil to the lens field B_z. It is seen that a flux density of 16.6 Tesla at the centre of the air gap of both lenses can be achieved at 373955 ampere-turns.

The halfwidth W represents the axial distance between the two points on the axial flux density distribution B_z at which $B_z = B_m/2$, B_m being the maximum flux density. Figure 4.4 shows the variation of the axial field halfwidth W of the test lenses DP1 and DP2 as a function of the magnetic field strength H. It is seen that in the linear

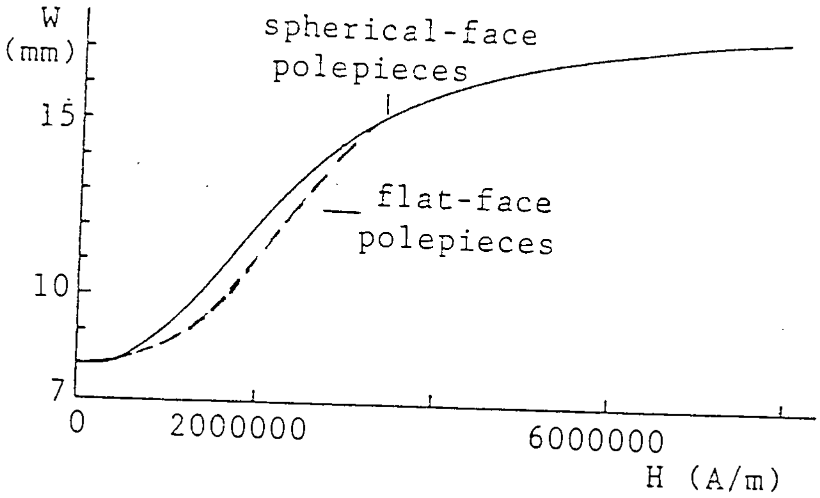

Figure 4.4 The halfwidth W of the axial fields shown in figures 4.1 and 4.2 as function of the magnetic field strength H.

region of the iron magnetization curve the halfwidth W is independent of both polepiece shape and H. The halfwidth at 10000 ampere-turns is equal to the air gap width S (8 mm) which is in good agreement with the value (7.8 mm) calculated from equation (1.7). In the linear region of iron B-H curve the maximum flux density B_m at the centre of air gap calculated from equation (1.5) is 1.57 Tesla which is in excellent agreement with the computed value (1.58 Tesla) achieved in the test lens DP1 with flat-face polepieces.

In the intermediate region of the iron B-H curve the axial field of both lenses broadens considerably, but the field halfwidth of the lens with flat-face polepieces is less than that with spherical-face polepieces. This is due to difference in the distribution of the axial fields in the region where the fields broaden. The field of the test lens DP1 with flat-face polepieces drops steeply from its maximum value at the lens centre. The halfwidth of the axial field lies within the steep field region. However, at the poleface and inside the bore the field broadens considerably. When the spherical-face polepieces (figure 4.2) are energized in the linear and intermediate regions, the axial field has two peaks in the air gap; each peak is situated in the region of the polepiece tip. In the middle of the air gap the field is slightly less than that of the two peaks. From the poletip region towards the bore, the field decreases gently and its halfwidth becomes broader than that of the flat-face polepieces whose field decreases sharply at first.

Figure 4.4 shows that at high values of the magnetic field strength H where the polepieces saturate, the polepiece shape has no effect on the halfwidth W. This is shown in the fields of figures 4.1 and 4.2 whose halfwidths at high excitations NI are not affected by the polepiece shape. As one would expect, the maximum value of W at very high excitations will be that of the coil field alone (18 mm).

Figure 4.2 shows that as the lens excitation is increased to the values (NI $\sim$40000 ampere-turns) at which the two peaks in the region of each polepiece tip disappear, the field between the two tips becomes nearly constant and the value of its halfwidth is slightly higher than the air gap width. To demonstrate the variations of the field at the air gap of the zero-bore double spherical-face polepieces lens, magnetic flux lines have been plotted as shown in figure 4.5. When the iron polepieces are not saturated (figure 4.5a) the flux lines are convex with respect to the lens optical axis which indicate that the field at the face

Figure 4.5 Magnetic flux lines distribution in the zero-bore symmetrical double polepiece lens with spherical poletip energized at different excitations NI by a thin flat coil placed within the air gap. Lens outer diameter = 196 mm.

lens B(T)	a	b	c
(B_z) centre	1.49	3.3	16.6
$(B_z)_{pf}$	1.68	3.1	12.14
$(B_{Fe})_{pf}$	1.4	2	2

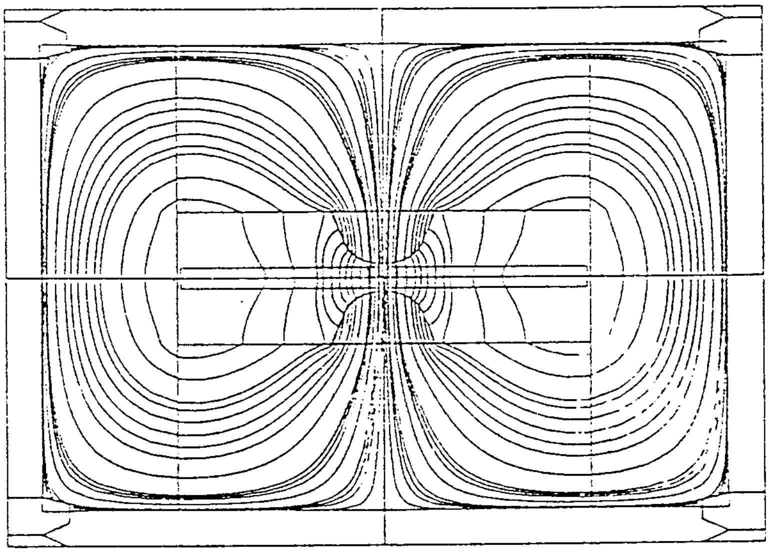

(a) NI = 10000 ampere-turns

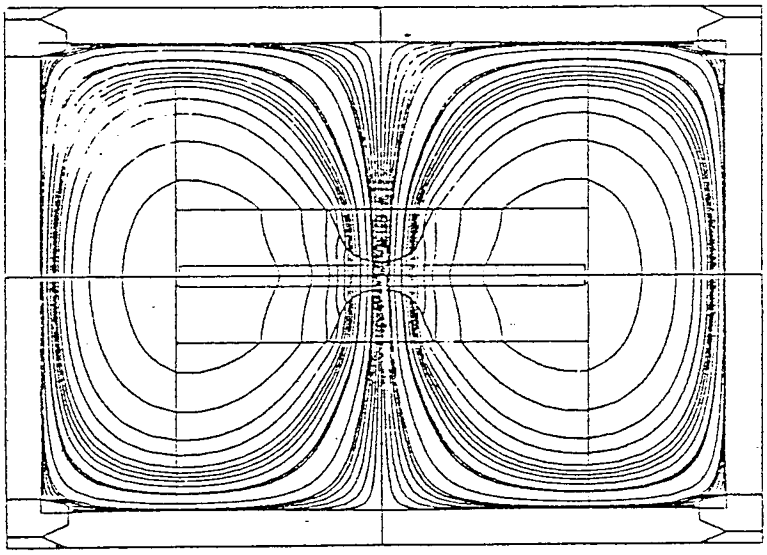

(b) NI = 40000 ampere-turns

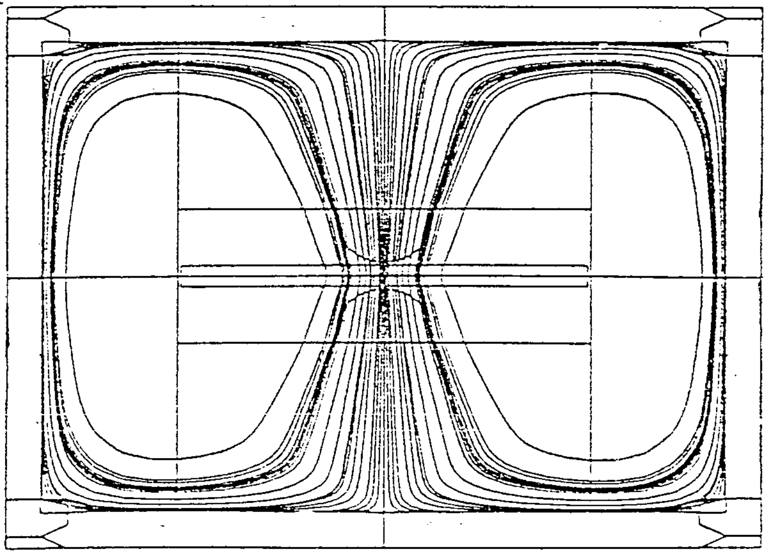

(c) NI = 373955 ampere-turns

of each pole is high. At higher excitations the field along the air gap begins to level off. It becomes nearly constant along the air gap width at NI $\sim$ 40000 ampere-turns where the flux lines are nearly parallel to the lens optical axis as shown in figure 4.5b. A field distribution of this kind is similar to that achieved in conventional lenses whose ratio of S/D is infinite and its field is represented by the square-top field which is characterized by its low chromatic aberration coefficient. At very high excitations, where the iron polepieces are saturated and the axial field has a peak at centre of the air gap , the flux lines are concave with respect to the optical axis (figure 4.5c).

The fields B_{Fe} due to the magnetization of iron in the double polepiece test lenses DP1 and DP2 are shown in figures 4.6 and 4.7 respectively at different excitations NI. For convenience, only half the fields is shown. The area of the positive and the negative parts of each B_{Fe} field agree within 1% accuracy. It is seen that from the poleface towards the axial bore the field drops abruptly. The field inside the bore of the spherical-face truncated-cone polepiece decreases continuously while that of the flat-face polepiece has a "shoulder". At the centre of the air gap, the value of the B_{Fe} field is little affected by the pole shape for a specific excitation. There is a B_{Fe} peak at the tip region for both polepiece shapes. The variation of B_{Fe} at the poletip is demonstrated by the B-H magnetization curve shown in figure 4.8. Before reaching the saturation limit of 2 Tesla, dB/dH of the spherical-face polepiece is higher than that of the flat-face polepiece. Therefore, the spherical-face polepiece reaches saturation magnetization at lower magnetic

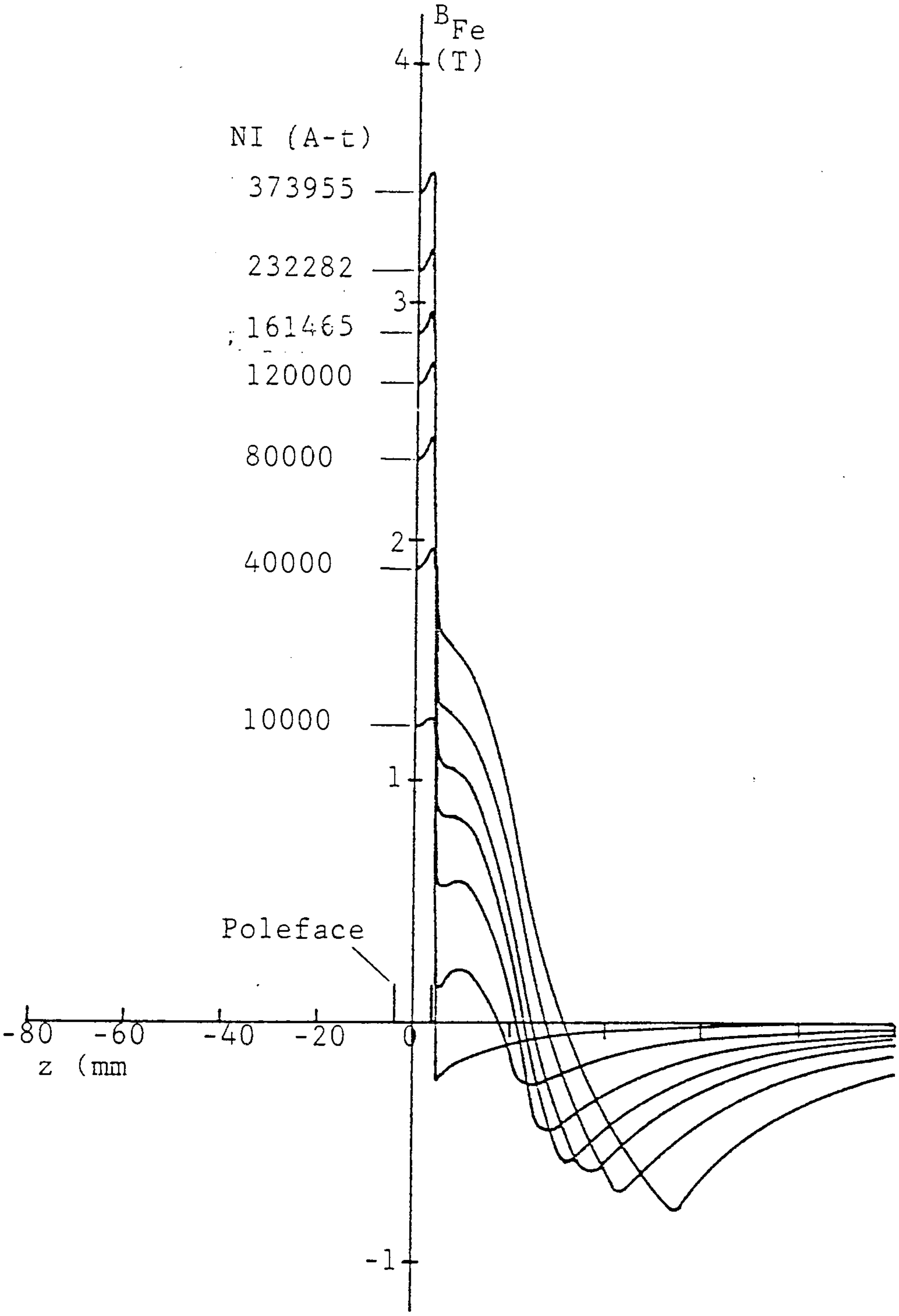

Figure 4.6 Axial flux density distributions B_{Fe} due to iron magnetization of the test lens DP1 with flat-face polepieces shown in figure 4.1, computed at different excitations NI. Only half the fields is shown.

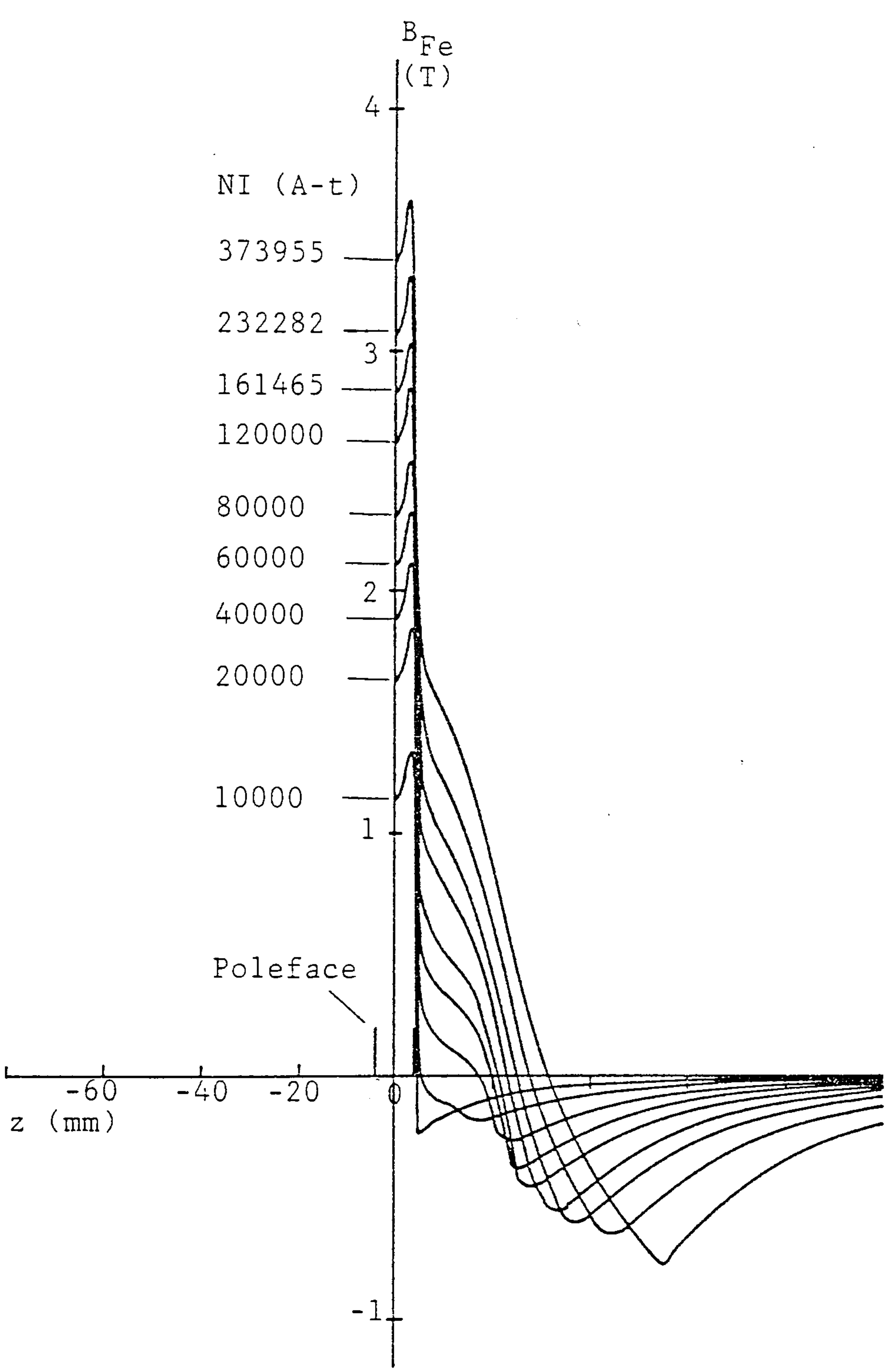

Figure 4.7 Axial flux density distributions B_{Fe} due to iron magnetization of the test lens DP2 with spherical-face polepieces shown in figure 4.2, computed at different excitations NI. Only half the fields is shown.

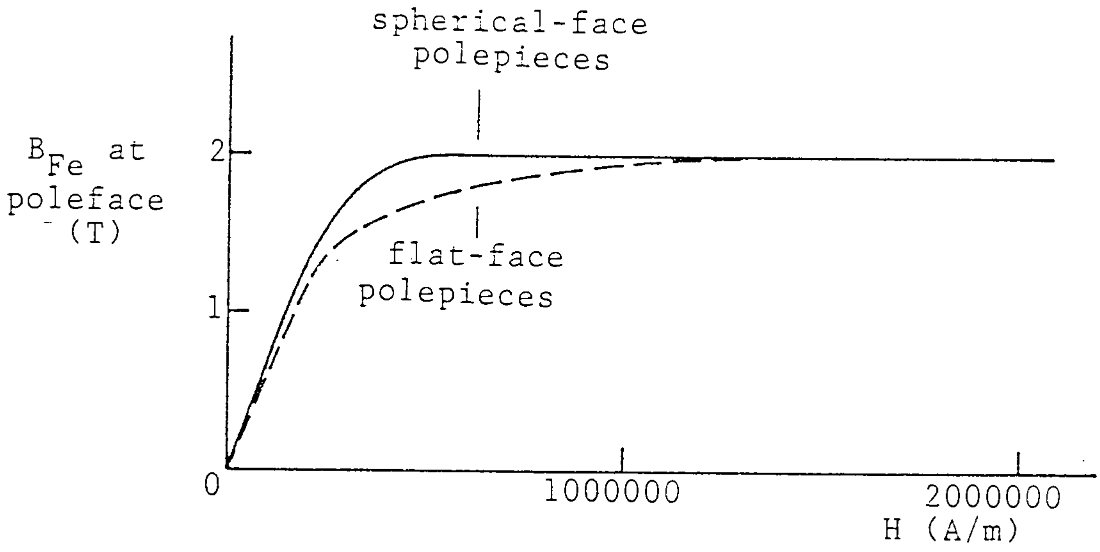

Figure 4.8 Poletip magnetization curves of the test lenses DP1 and DP2 shown in figures 4.1 and 4.2.

field strength H than that of the flat-face. However, figure 4.8 indicates that as H exceeds 1000000 A/m, the value of B_{Fe} at the poletip becomes independent of the shape of poleface.

4.2.2 COMPARISON BETWEEN THE FOCAL PROPERTIES

An objective lens in a high resolution TEM is often operated in the first telescopic mode, i.e. rays entering the lens field parallel to the axis converge at the specimen situated within the lens field and then diverge before emerging from the lens as a parallel beam. For unsaturated symmetrical double polepiece lenses, the excitation parameter $NI/V_r^{\frac{1}{2}}$ in the first telescopic mode depends weakly on the ratio S/D, varying from 23.2 for S/D = 0.25 to 19.1 for S/D = 3 (Kamminga et al 1968/69). Since in a symmetrical lens the specimen is at the centre of the air gap, a strong pre-field is created followed by an imaging field. A typical lens of this type is the strong condenser-objective lens of Riecke (1962) and Riecke and Ruska (1966).

Since the current density σ is an important limiting factor in saturated lenses, the objective focal properties of two families of lenses similar in shape to test lenses DP1 and DP2 operated in the first telescopic mode (condenser-objective) have been scaled for 1 MV accelerating voltage (similar to that for the single polepiece lens described in Chapter 3) and plotted as functions of σ. Figure 4.9 shows the variation of the objective focal length f_o, the chromatic aberration coefficient C_c, the spherical aberration coefficient C_s, the flux density at the lens centre B_{centre} and the halfwidth W with the current density σ for the two families of lenses of two different pole shapes. It is seen that at high coil current densities attainable only by superconducting windings, the shape of the saturated polepieces has no effect on the focal parameters. Furthermore, as σ exceeds 60000 A/cm^2 there is small improvement in the focal properties but can be significant for improving the resolving power.

At the current density $\sigma = 20000$ A/cm^2, C_s (2.6 mm) of the 1 MV test lens with two spherical-face polepieces is 24% less than that with two flat-face polepieces. Hence the resolution $\delta = 0.7\ (C_s\ \lambda^3)^{1/4}$ of the condenser-objective lens with spherical-face polepieces (0.142 nm) is 7% better than that with flat-face polepieces. Similarly, C_c (2.45 mm) and f_o (4.05 mm) are 8% and 5% respectively less than those of the flat-face polepiece lens. The halfwidth W of the lens with spherical-face polepieces

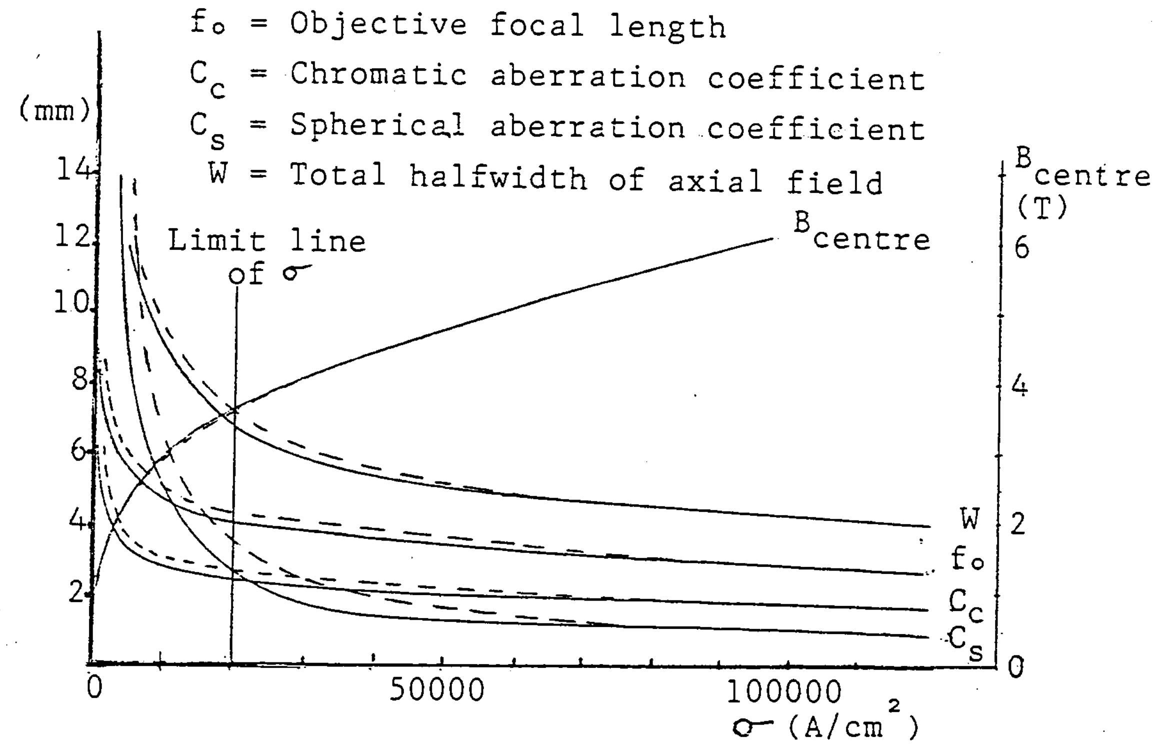

Figure 4.9 Electron-optical properties of the 1 MV condenser-objective symmetrical double polepiece lenses similar in shape to test lenses DP1 and DP2 shown in figures 4.1 and 4.2 as functions of current density σ.

Spherical-face polepiece: solid lines

Flat-face polepiece: broken lines

(6.7 mm) is 5.6% smaller than that with flat-face polepieces. In addition, the poleface flux density of the spherical-face polepiece is 5% higher than that (3.1 Tesla) of the flat-face polepiece. These differences in the electron-optical properties are attributed to the difference in the shape of the field and dimensions at such constant accelerating voltage and σ. Under these conditions the outer diameter (149 mm) of the test lens with spherical-face polepieces is smaller than that with flat-face pole-pieces (153 mm) and the maximum flux density at the centre-plane of the test lens with spherical-face polepieces (3.6 Tesla at NI = 34360 ampere-turns) is very slightly higher than that with flat-face polepieces (3.57 Tesla at NI = 35100 ampere-turns).

Therefore, at current densities attainable by suitably cooled copper-tape coils some improvement in the objective focal properties is achieved when the two polepieces in the symmetrical lens are in the form of a spherical-face truncated-cone. This result suggest that, at such range of current densities, a truncated-cone with a spherical-face is a favourable pole shape for symmetrical double polepiece lenses. Therefore, in the following investigation such pole shape will be taken into consideration.

It should be mentioned that at values of σ higher than 20000 A/cm^2 the values of the halfwidth W and the flux densities at the centre and at the poleface of the 1 MV test lenses are independent of the polepiece shape. However, both flux densities increase with increasing σ while W decreases. As σ increases the outer diameter of the 1 MV test lenses decreases in the same manner as the focal parameters and the halfwidth shown in figure 4.9.

Table 4.1 shows the electron-optical parameters of the three symmetrical condenser-objective test lenses similar in shape to that of test lens DP2 (figure 4.2) operating at 100, 500 and 1000 kV accelerating voltages for current density $\sigma = 20000$ A/cm^2. The specimen is situated at the centre of the air gap ($z_F = 0$). It can be seen that there is little increase in C_s with increasing accelerating voltage since an increase in B_{centre} is offset by the rapid increase in W. Table 4.1 shows that, for a fixed current density, C_c and f_o both increase with increasing V since the lens must be made larger at higher voltages if σ is to be constant. Therefore, a restriction on σ will lead to higher aberrations. At this constant σ of 20000 A/cm^2 the value of the flux density B_{Fe} at the poletip due to iron magnetization is 2 Tesla, the saturation value of soft iron.

The focal properties of the 100 kV test lens given in table 4.1 are better than those of the 100 kV iron-free superconducting lens ($C_s = 2.7$ mm, $C_c = 3.4$ mm) operated at the same current density of 20000 A/cm^2 described by Dietrich (1976). It is seen that it is possible to construct the small size saturated lens given in table 4.1 for a 100 kV electron microscope by energizing it with superconducting windings. However, table 4.1 shows that the best resolution is achieved at 1000 kV.

4.3 SINGLE POLEPIECE, SYMMETRICAL DOUBLE POLEPIECES AND IRON-FREE LENSES ENERGIZED BY A THIN FLAT COIL

When the current density is not limited the thin flat coil of high ratio of outer to inner diameter has many desirable electron-optical properties particularly when its axial

Table 4.1 Electron-optical properties of the three condenser-objective test lenses similar in shape to that of test lens DP2 (figure 4.2) for current density $\sigma = 20000\ \mathrm{A/cm^2}$. The specimen is placed at the centre of the lens ($z_F = 0$).

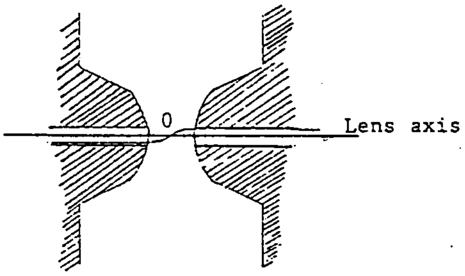

Parameter \ Voltage	V = 100 kV V_r = 110 kV	V = 500 kV V_r = 750 kV	V = 1000 kV V_r = 2000 kV
C_s (mm)	2.2	2.5	2.6
C_c (mm)	0.75	1.64	2.45
f_o (mm)	1	2.59	4
δ (nm)	0.404	0.204	0.142
B_{centre} (Tesla)	2.35	3.1	3.6
NI (A-t)	6700	20400	34360
Lens outer diameter (mm)	65	113.33	149
Halfwidth W (mm)	2.7	4.9	6.8

thickness is about one-tenth the mean diameter (Marai 1977). It is therefore, of interest to investigate the electron-optical properties of different types of lenses when energized by such a coil at different current densities.

To energize the single and double polepiece lenses effectively, the thin flat coil must be placed as close as possible to the polepieces, as shown for example in figures 3.20 and 4.2. The test lenses have polepieces in the shape of a spherical-face truncated-cone with a 1 mm axial bore diameter. The axial flux density distributions computed at different excitations NI shown in figures 3.20 and 4.2 have been used for computing the focal properties of these lenses. The symmetrical axial field due to the coil alone shown in figure 4.10 has also been used for computing the focal properties of the iron-free lens. Due the symmetry of their axial flux density distributions with respect to the coil centre-plane, the focal properties of the symmetrical double polepiece and iron-free lenses have been computed for a specimen at $z_F = 0$, the telescopic mode of operation (i.e. condenser-objective lenses). The focal properties of the single polepiece lens have been computed for a parallel electron beam on the open side of the lens crossing the optical axis at the poletip i.e. $z_F = 0$. The original computed focal properties of three families of test lenses similar in shape to those shown in figures 3.20, 4.2 and 4.10 have been scaled for 1 MV accelerating voltage and plotted in terms of the current density σ in the windings.

Figure 4.11 shows the spherical aberration coefficient C_s, chromatic aberration coefficient C_c and the objective focal length f_o of the three families of test lenses as

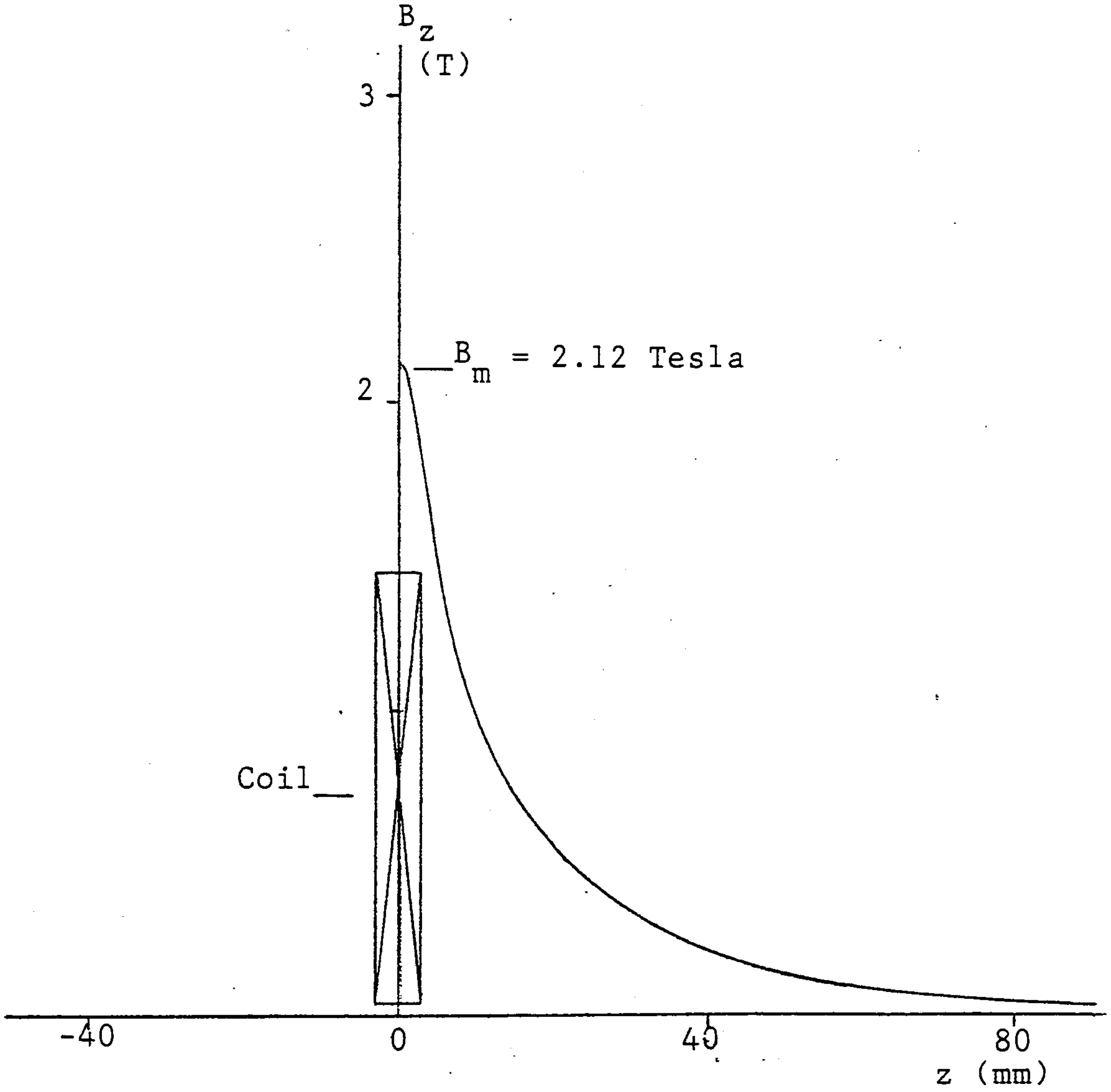

Figure 4.10 Computed axial flux density distribution B_z due to the thin flat coil (iron-free lens) of high outer to inner diameter ratio ($s = 6$ mm, $d_1 = 3$ mm, $d_2 = 116$ mm, $d_2/d_1 = 38.7$ and $s/d_m = 0.1$). The coil is energized at 60000 ampere-turns. Only the top half of the coil and the positive half of the axial field are shown.

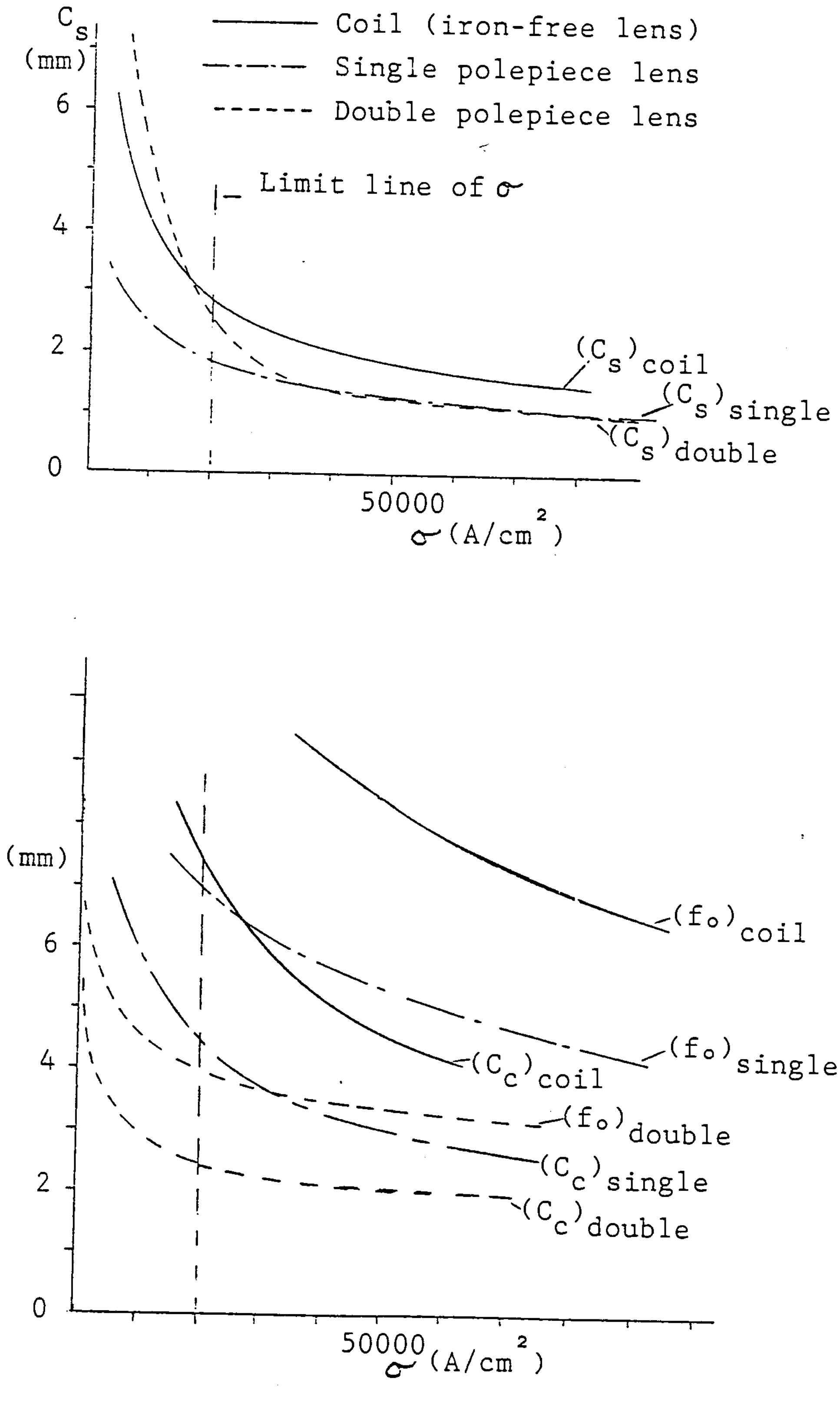

Figure 4.11 The focal properties of the 1 MV single polepiece, symmetrical double polepiece and iron-free lenses energized by a thin flat coil ($s/d_m = 0.1$) of high outer to inner diameter ratio ($d_2/d_1 = 38.7$), plotted in terms of the current density σ for $z_F = 0$.

functions of the current density σ. It is seen that the focal properties of the three lenses improve with increasing σ ; there is no optimum value for σ at which C_s, C_c or f_o is minimum. The lowest values of the focal properties are limited only by the technology of fabricating the energizing coil to make it capable of carrying very high current densities.

Imaging fields of low gradient dB_z/dz, high peak and small halfwidth are characterized by low C_s as in the case of single polepiece test lenses. It is seen that at high values of σ achieved by superconducting windings, the coefficient C_s of the single and that of the double polepiece families of lenses are identical since the size of the single polepiece lens is smaller than that of the double polepiece lens for a given value of $\sigma > 35000$ A/cm^2 and because the bore of the double polepiece lens is too small compared with its air gap width. At this range of current densities the high peak flux density and large halfwidth of double polepiece lenses are balanced by the lower peak flux density and smaller halfwidth of single polepiece lenses. Furthermore, some improvements in C_s are achieved as σ exceeds 35000 A/cm^2 which can be significant at high resolving powers. At the given range of σ shown in figure 4.11 the values of C_c and f_o of the family of symmetrical double polepiece test lenses are always lower than those of the single polepiece and iron-free lenses. This is due to the characteristic shape of the axial field of double polepiece lenses of very small bore and high gap-bore ratio which has steep boundaries i.e. the field gradient dB_z/dz is higher than those of the other two families of lenses. The axial field of symmetrical lenses of high S/D ratio are close in shape to the square-top fields which, particularly at low σ, are characterized by their low C_c and associated f_o. Out of the three families of test lenses, the iron-free test lenses have the highest C_c and f_o at the given values of σ. This demonstrates the importance of having an iron circuit in order to improve the focal properties. At current density $\sigma < 20000$ A/cm^2, C_s of the family of iron-free lenses is lower than those of the double polepiece test lenses since the fields of the latter have steep boundaries due to the high S/D ratio. Also at $\sigma \leqslant 35000$ A/cm^2, C_s of the family of single polepiece lenses is lower than those of the double polepiece lenses. However, as σ increases, C_s of the double polepiece lenses improves rapidly. Out of these two families of polepiece test lenses. the choice of a favourable lens design would, therefore, depend on the operational requirements and the value of σ at which the lens is energized.

Table 4.2 shows the electron-optical properties of the three 1 MV test lenses computed at a current density σ of 20000 A/cm^2 at $z_F = 0$. It is seen that, by keeping σ constant, the coil of the iron-free lens has about twice the excitation NI of the coil energizing the single polepiece lens. Therefore, the outer diameter of the iron-free coil (96 mm) is about $\sqrt{2}$ times as large as the outer diameter of the energizing coil of the single polepiece lens. At this current density, C_s of the single polepiece test lens is the lowest since its halfwidth and the size of coil are the smallest as shown in table 4.2. Furthermore, low values of C_s are associated with gently decreasing imaging fields of high peak and small halfwidth. The imaging field on the open side of the single polepiece test lens decreases

Table 4.2 Electron-optical properties of single polepiece, symmetrical double polepiece and iron-free test lenses energized at a constant current density σ of 20000 A/cm^2 by a long thin coil ($s/d_m = 0.1$, $d_2/d_1=38.7$). The 1 MV parallel electron beam is focused at $z_F = 0$ i.e. at the centre of the iron-free and double polepiece lenses and at the poletip of the single polepiece lens.

Lens Parameter	Single polepiece lens	Double polepiece lens	Iron-free lens
C_s (mm)	1.85	2.6	2.9
C_c (mm)	4.3	2.45	7.3
f_o (mm)	7.6	4.05	13
δ (nm)	0.13	0.142	0.146
B_z (Tesla)	at poleface 2.5	at centre 3.6	at centre 1.78
NI (ampere-turns)	21500	34360	41790
Lens outer diameter (mm)	116	149	96
Coil outer diameter in each lens (mm)	69	88	96
Power (kW)	11	22.5	25
Bore diameter (mm)	0.6	0.76	2.5
Halfwidth W (mm)	5.9	6.7	14.9

more gently (i.e. lower dB_z/dz, see figure 3.20) than the imaging field of the other two lenses (see figures 4.2 and 4.10). The values of C_c and f_o of the double polepiece test lens are the lowest since its imaging field decreases more steeply than the imaging field of the other two lenses. The highest flux density is that at the centre of the double polepiece lens which gives it the strong focusing action leading to small f_o. However, this high flux density is offset by the large halfwidth leading to high C_s. Table 4.2 shows that at this current density (20000 A/cm^2) the 1 MV test lens with a single spherical-face truncated-cone polepiece of small bore has the advantages of producing small C_s, hence improved resolution by consuming the lowest power supplied to a thin water-cooled copper-tape coil of high outer to inner diameter ratio operated at 100 °C.

4.4 ARRANGEMENT OF POLEPIECE AND COIL IN SYMMETRICAL DOUBLE POLEPIECE OBJECTIVE LENSES

It has been shown in the above sections that in the intermediate region of the iron B-H curve (figure 4.8) there is a favourable pole shape for double polepiece objective lenses. This shape is in the form of a spherical end cap joined to a conical section.

In order to achieve a favourable arrangement of polepiece and coil in symmetrical double polepiece lenses, various coil shapes have been considered here to magnetize the lens. The magnetization and the focal properties of the various arrangements are compared in order to determine a favourable design of a symmetrical double polepiece objective lens.

4.4.1 POLEPIECE MAGNETIZATION

Computations have been carried out concerning the effect of the energizing coil shape on the magnetization of soft iron conical polepieces terminated by spherical tips. The test lens DP2 shown in figure 4.2 which is energized by thin flat coil placed in the air gap, together with the test lenses DP4, DP5 and DP6 shown in figures 4.12, 4.13 and 4.14 respectively have been considered for investigating the polepiece magnetization. Only the upper half of the lenses and the positive half of the axial fields are shown. The test lenses are surrounded by a thick iron shroud to avoid flux leakage at high excitations. The air gap S separating the two polepieces was 8 mm wide and the bore diameter D was 1 mm.. Thus the test lenses are characterized by large ratio of S/D.

Figure 4.12 shows a section of the double polepiece test lens DP4 energized by two identical coils placed in the conventional position where each coil surrounds one polepiece. Each coil has an outer diameter d_2 = 118 mm, inner diameter d_1 = 32 mm and axial thickness s = 16 mm, i.e. $s/d_m \simeq 0.21$. It is seen that the flux density at the centre of the lens is less than that of the polepiece tip region even at high excitations such as 120000 ampere-turns unlike the axial fields of the test lens DP2 shown in figure 4.2 which tend first to level off with increasing excitation NI. Figure 4.13 shows a section of the double polepiece test lens DP5 energized by a bulk coil surrounding the polepieces and the air gap. The coil has an outer diameter d_2 = 118 mm, inner diameter = 32 mm and axial thickness s = 38 mm i.e. $s/d_m \simeq 0.507$. Figure 4.14 shows

Test lens DP4

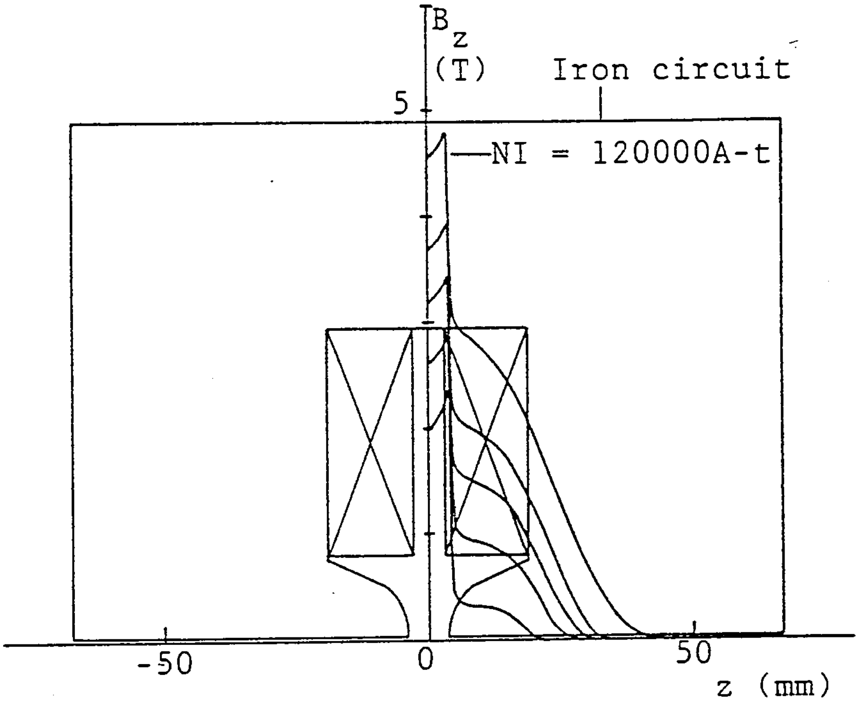

Figure 4.12 Axial flux density distributions B_z in the symmetrical double polepiece test lens DP4 with spherical-face truncated-cone polepieces of 1 mm axial bore diameter and separated by 8 mm air gap. Each of the two energizing coils (s = 16 mm, d_1 = 32 mm and d_2 = 118 mm) is placed in the conventional position. Only the positive half of the fields and the upper half of the soft iron lens and its two energizing coils are shown. The axial fields are computed at excitations NI = 20000, 40000, 60000, 80000 and 120000 ampere-turns shown in an ascending order.

Lens outer diameter = 196 mm.

Test lens DP5

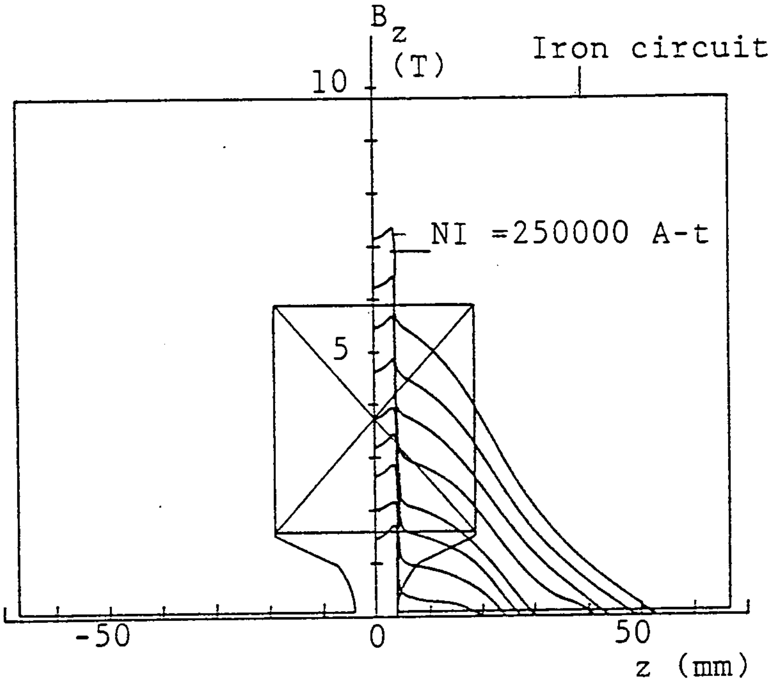

Figure 4.13 Axial flux density distributions B_z in the symmetrical double polepiece test lens DP5 with spherical-face truncated-cone polepieces of 1 mm axial bore diameter and separated by an 8 mm air gap. Only the positive half of the fields and the upper half of the soft iron lens and its thick energizing coil ($s = 38$ mm, $d_1 = 32$ mm and $d_2 = 118$ mm) are shown. The axial fields are computed at excitations NI = 10000, 20000, 40000, 60000, 80000, 120000, 160000, 200000 and 250000 ampere-turns shown in an ascending order. Lens outer diameter = 196 mm.

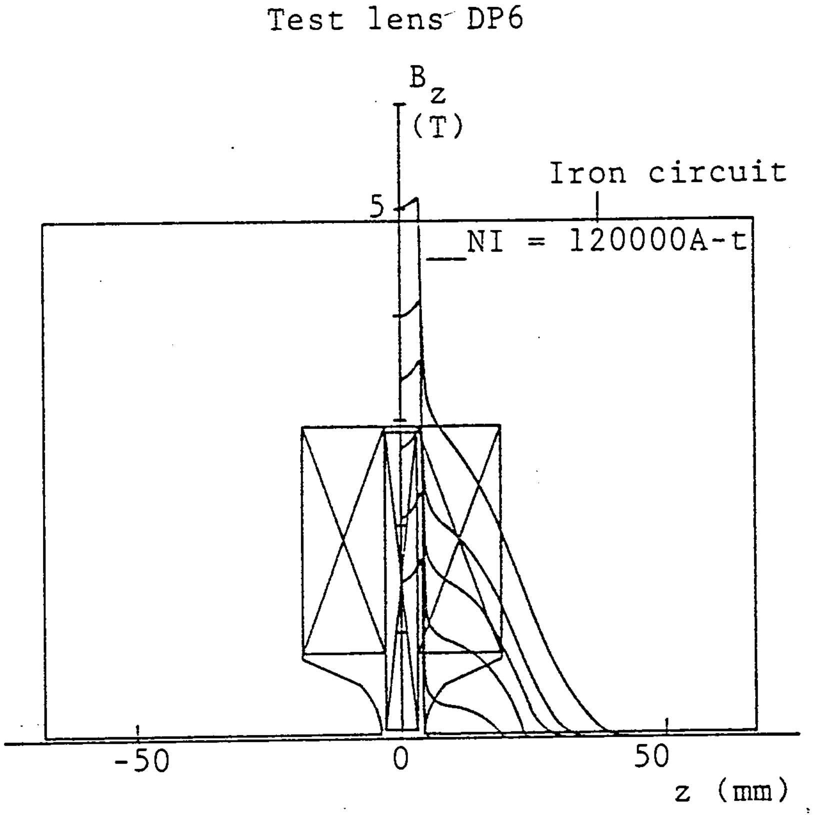

Figure 4.14 Axial flux density distributions B_z in the symmetrical double polepiece test lens DP6 with spherical-face truncated-cone polepieces of 1 mm axial bore diameter and separated by an 8 mm air gap. The lens is energized by a combination of the coils which separately energized the test lenses DP2 and DP4 shown in figures 4.2 and 4.12. Only the positive half of the fields and the upper half of the soft iron lens and its three energizing coils are shown. The axial fields are computed at 10000, 20000, 40000, 60000, 80000 and 120000 ampere-turns shown in an ascending order. Lens outer diameter = 196 mm.

a section of the double polepiece test lens DP6 energized by a combination of the coils which separately energized the test lenses DP2 and DP4. The axial fields of the four test lenses under consideration have been computed at different excitations NI.

Figure 4.15a shows the poletip B_{Fe}-H magnetization curves of four symmetrical double polepiece test lenses with the same shape of magnetic circuit energized by four different coil arrangements. The B_{Fe}-H curves do not depend on the size of the lens. Ideally, the poletip should reach magnetic saturation for the lowest possible value of magnetic field strength H and of excitation NI. Figure 4.15a indicates that as H exceeds 400000 A/m, the value of B_{Fe} at the poletip becomes independent of the coil arrangement and it shows that dB_{Fe}/dH is highest when the lens is energized by two identical coils surrounding the polepieces and placed in the conventional position. Therefore, such a coil arrangement appears to be favourable as a magnetizer. However, the efficiency of each coil arrangement in producing a given value of H for the lowest excitation NI must also be considered, since in practice NI, rather than H, is prescribed in a given lens. Since the poleface is magnetized by the exciting coil, therefore a coil is needed that produces the highest magnetic field strength H. A thin coil near the poleface produces a higher value of H (for a given NI) than a coil surrounding the polepiece. Figure 4.15b shows that coil arrangement in test lens DP2 is the best in this respect and so its axial field has the lowest halfwidth W4 and the highest flux density at the lens centre.

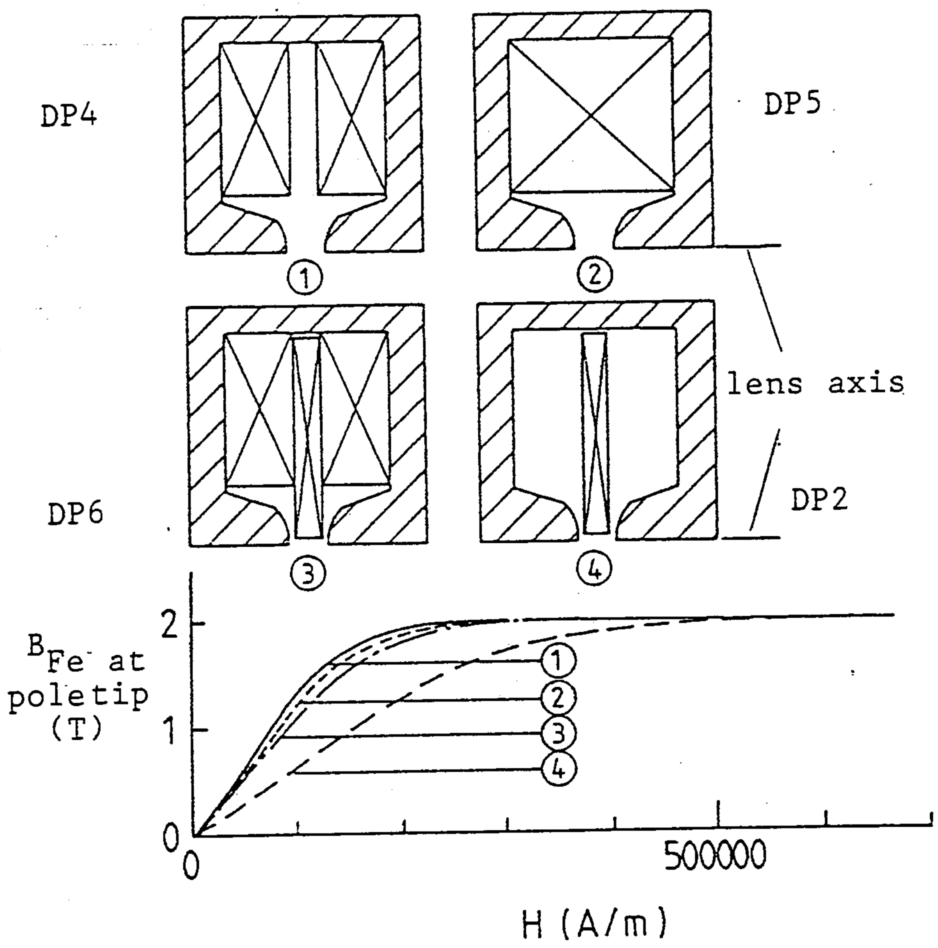

Figure 4.15a Poletip B_{Fe}-H magnetization curves of the four symmetrical double polepiece test lenses energized by different coils. Only the upper half of the schematic cross-section of each lens is shown.

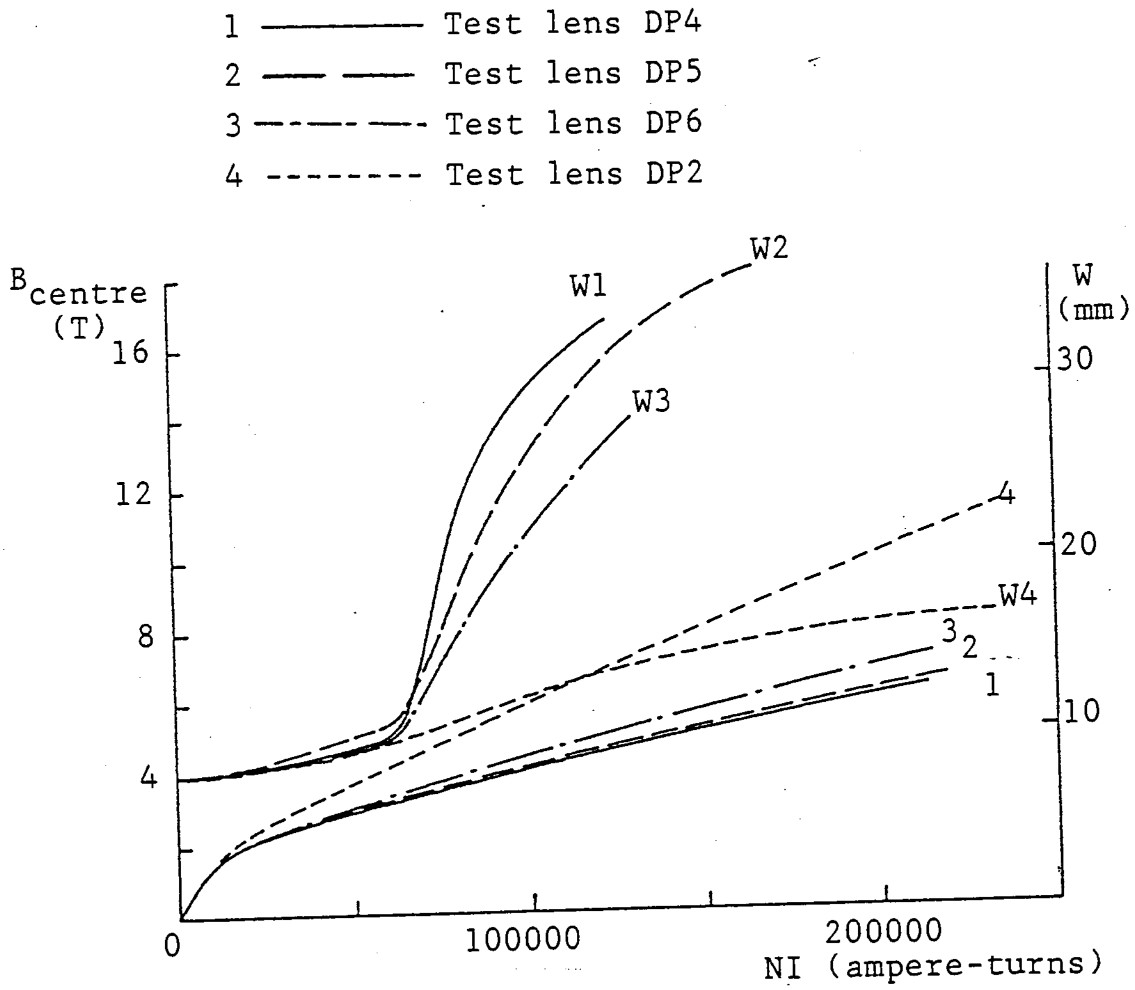

Figure 4.15b The halfwidth W of the axial fields and their corresponding flux density at the air gap centre of the four symmetrical double polepiece test lenses DP4, DP5, DP6 and DP2 in figure 4.15a (whose axial flux density distributions are shown in figures 4.12, 4.13, 4.14 and 4.2 respectively) as functions of the excitation NI.

The two types of magnetizers mentioned above, have been combined to energize the double polepiece test lens DP6. The value of dB_{Fe}/dH of this combination is higher than that of test lens DP2 and close to those of test lenses DP4 and DP5 (figure 4.15a). Furthermore, smaller halfwidth W and higher flux density at the air gap centre than those of test lenses DP4 and DP5 have been achieved as shown in figure 4.15b.

It should be noted from figure 4.15b that in the linear region of the iron magnetization curve, the halfwidth of the axial field and the maximum flux density at the air gap centre are not affected by the coil arrangement. Since the axial bore is very small, the value of the halfwidth and the air gap width (8 mm) are identical. In the intermediate region, the axial field of test lens DP5 energized by a bulk coil broadens more than those of test lenses DP4, DP6 and DP2. These broad fields are shown in figure 4.13.

4.4.2 OBJECTIVE FOCAL PROPERTIES

The axial flux density distributions computed at different excitations of the four double polepiece test lenses DP4, DP5, DP6 and DP2 which are shown in figures 4.12, 4.13, 4.14 and 4.2 respectively have been used for computing their objective focal properties. The focal properties of four families of test lenses similar in shape to DP4, DP5, DP6 and DP2 have been scaled for 1 MV accelerating voltage and plotted as functions of the current density σ. The computations have been carried out for an electron beam entering the lens field parallel to the optical axis; the beam intersects the optical axis at the specimen position at the centre of the air gap of the symmetrical double polepiece lens (telescopic mode of operation) i.e. $z_F = 0$.

Figure 4.16 shows the objective focal properties of the four families of 1 MV symmetrical double polepiece condenser-objective lenses of large S/D ratio similar in shape to those of test lenses DP4, DP5, DP6 and DP2 as functions of σ. It is seen that the focal properties improve with increasing σ. Of the four families, the family of lenses similar in shape to test lens DP6 energized by three coils has the shortest objective length f_{o3} and the smallest chromatic aberration coefficient C_{c3}. This family has also the smallest spherical aberration coefficient C_{s3} provided $\sigma < 35000$ A/cm^2. At current densities $\sigma > 35000$ A/cm^2, the family of the test lenses similar in shape to that of test lens DP2 energized by a thin flat coil has the smallest spherical aberration coefficient C_{s4}. At such high current densities the lenses should be energized by superconducting windings. It may therefore be deduced that the focal properties are sensitive to both coil arrangement and current density in the windings. So far as C_s is concerned, the arrangement of the three coils combination similar to that in test lens DP6 is favourable for symmetrical double polepiece lenses of high S/D ratio operated at current densities less than 35000 A/cm^2. One would not expect such an arrangement to be appreciably affected by the shape of the polepieces.

4.5 DESIGN OF A 1 MV SYMMETRICAL DOUBLE POLEPIECE LENS

The computed focal properties of the four families of test lenses similar in shape to those of test lenses DP4, DP5, DP6 and DP2 plotted in figure 4.16 for the telescopic mode of operation ($z_F = 0$) can be scaled at any desired

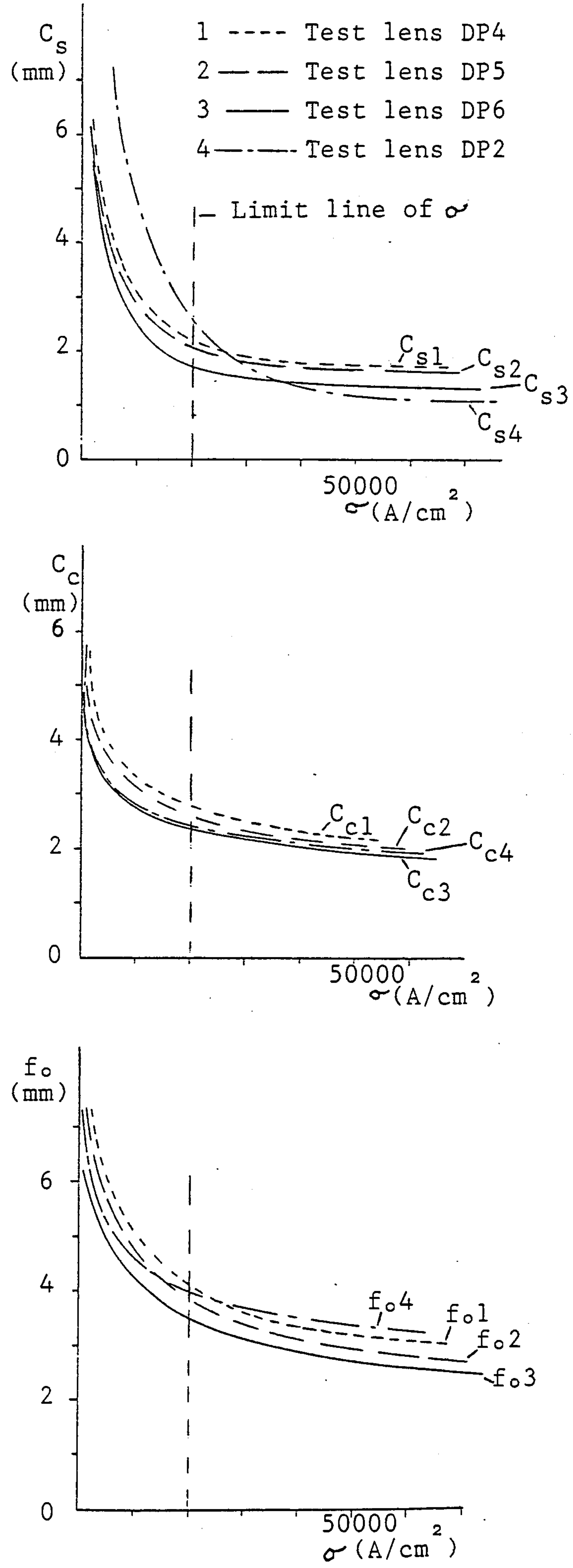

Figure 4.16 Objective focal properties of the four families of 1 MV condenser-objective symmetrical double polepiece lenses similar in shape to those of test lenses DP4, DP5, DP6 and DP2 shown schematically in figure 4.15a plotted as functions of the current density σ.

C_s = spherical aberration coefficient

C_c = chromatic aberration coefficient

f_o = objective focal length

accelerating voltage. The emphasis here is on the design of condenser-objective lenses for 1 MV electron microscopes which can be operated at a current density σ of 20000 A/cm^2.

The resulting size of the four symmetrical double pole-piece test lenses DP7, DP8, DP9 and DP10 which can be operated under the above conditions is shown in figure 4.17. Table 4.3 shows the electron-optical parameters of these four test lenses operated in the telescopic mode at 1 MV accelerating voltage and current density σ of 20000 A/cm^2. The flux density at the poletips of the four lenses due to iron magnetization is 2 Tesla, the saturation value of soft iron.

It is seen from table 4.3 that out of the four lenses, test lens DP9 has superior focal properties. It has the smallest values of the spherical and chromatic aberration coefficients C_s and C_c respectively and objective focal length f_o. At the above accelerating voltage and current density, test lens DP9 has the best resolving power and the highest flux density at the centre of the air gap. Furthermore, it requires the least power (10.4 kW) when energized by three water-cooled copper tape coils operated at 100 °C.

The condenser-objective focal properties of test lens DP9 has been compared with other lenses reported in literature. The symmetrical condenser-objective lens (S/D = 1.25) of Riecke and Ruska (Riecke 1972) has the following focal properties at 1 MV: C_s = 2.22 mm, C_c = 2.62 mm, f_o = 3.62 mm and δ = 0.137 nm. It is seen that test lens DP9 has lower focal properties and hence better resolving power. The value of C_s of test lens DP9 is

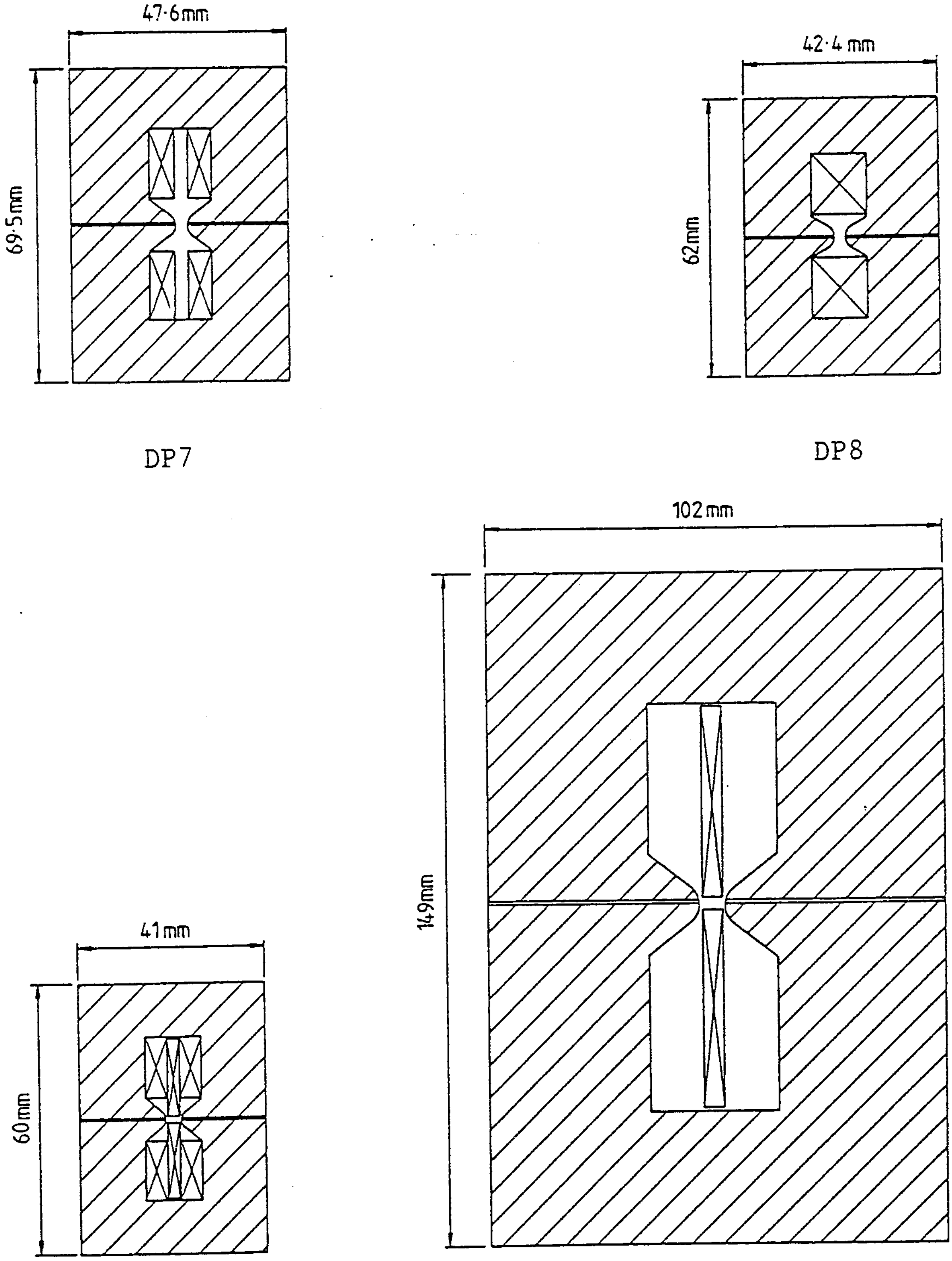

DP7 DP8 DP9 DP10

Figure 4.17 Cross-section of the four saturated 1 MV symmetrical double polepiece condenser-objective test lenses DP7, DP8, DP9 and DP10 operated at a current density of 20000 A/cm^2.

Table 4.3 Electron-optical parameters of the four 1 MV condenser-objective symmetrical double polepiece test lenses DP7, DP8, DP9 and DP10 shown in figure 4.17 operated at constant current density $\sigma = 20000$ A/cm^2.

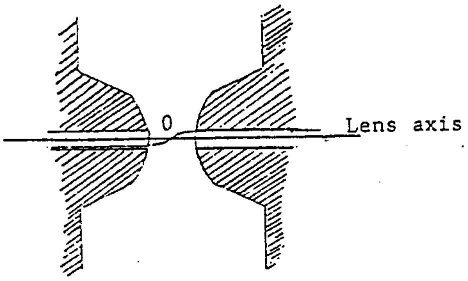

Test lens / Parameter	DP7	DP8	DP9	DP10
C_s (mm)	2.3	2.19	1.7	2.6
C_c (mm)	2.84	2.62	2.4	2.45
f_o (mm)	4.17	3.89	3.6	4.05
δ (nm)	0.138	0.136	0.128	0.142
B_{centre} (Tesla)	3.88	4.1	4.6	3.6
B_{Fe} at poleface (T)	2	2	2	2
Halfwidth W (mm)	8.8	7.8	6.8	6.8
NI (A-t)	31300	31365	32100	34360
Power (kW)	12	10.8	10.4	22.5
Lens outer diameter(mm)	69.5	62	60	149

comparable with the value 1.41 mm of 1 MV symmetrical condenser-objective lens (S = 5 mm and D = 3 mm) and better than that (2.66 mm) of the 1 MV asymmetrical condenser-objective lens (S = 15 mm, D_1 = 20 mm, D_2 = 3 mm) which have been proposed by Cleaver (1980). However, it is expected that C_c of test lens DP9 is smaller than those of the two proposed lenses of Cleaver due to its large S/D ratio. The minimum spherical aberration coefficient of the 1 MV asymmetrical saturated objective lens of Tsuno and Honda (1983) is 1.8 mm which is slightly higher than that of test lens DP9. Although the air gap width S and bore diameter D of test lens DP9 have not been optimized for C_s, its superior focal properties at such current densities in comparison with the condenser-objective lenses reported in literature suggests that the favourable arrangement of the coils can yield low aberrations and high resolving power. With further consideration of S, D and poleface radius of curvature of such lens,the spherical aberration C_s can be improved but probably at the expense of C_c. However, the choice of these dimensions will depend on the operational requirements. For example, in electron microscopes for biological studies and for investigating thick specimens the chromatic aberration coefficient C_c is very important while in those for investigating thin specimens in which only elastic scattering occurs, the spherical aberration coefficient C_s is the important limit.

For the same current density σ of 20000 A/cm^2, a scaled down version of test lens DP9 capable of operating at an accelerating voltage of 500 kV (V_r = 750 kV) in the condenser-objective mode has the following parameters:

C_s = 1.33 mm, C_c = 1.72 mm, f_o = 2.61 mm, δ = 0.174 nm, B_z at centre = 3.9 Tesla, NI = 21600 ampere-turns and an outer diameter of 51.8 mm. These focal properties are comparable with the values achieved by superconducting lenses operated at higher current densities ($\sim 10^6$ A/cm^2) and various accelerating voltages (Dietrich 1976, Dietrich et al 1977, Lefranc et al 1982). The size of this 500 kV lens suggests that it is possible in practice to construct such a lens. However, it might require energizing by superconducting windings. A 100 kV version of such a lens seems to be too small in size to be realised practically with the present technology and engineering.

4.6 HIGH CURRENT DENSITY SATURATED SYMMETRICAL DOUBLE POLEPIECE LENSES

In the above sections the design and the electron-optical properties of symmetrical double polepiece lenses have been investigated at current densities of the order of 10^4 A/cm^2. The properties of symmetrical double polepiece lenses operated at such current densities appear to be sensitive to the coil arrangement. Figure 4.18a shows the electron-optical properties of two families of 1 MV condenser-objective symmetrical double polepiece lenses similar in shape to those of test lenses DP6 and DP2 as functions of the current density σ. A log-log graph is plotted in figure 4.18b in order to show the variation of C_s and C_c with σ of figure 4.18a clearer. Figures 4.18a and 4.18b show that the aberration coefficients of both families of lenses improve with increasing σ. It is seen that when $\sigma < 35000$ A/cm^2 the spherical aberration

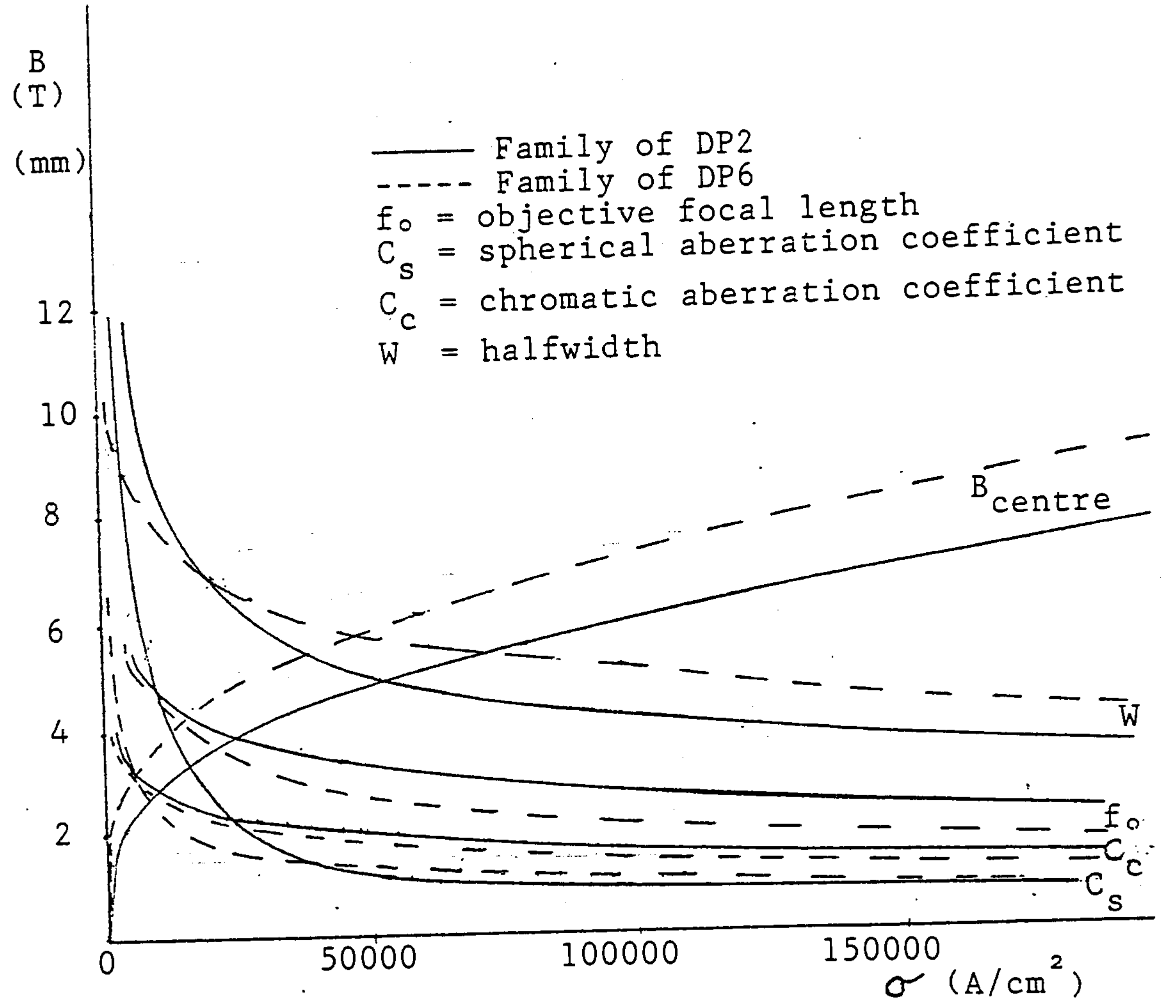

Figure 4.18a Electron-optical parameters of two families of 1 MV condenser-objective symmetrical double polepiece test lenses similar in shape to DP6 and DP2 shown schematically in figure 4.15a plotted as functions of the current density σ.

Solid lines: family of lenses similar to test lens DP2 energized by a thin flat coil.

Broken lines: family of lenses similar to test lens DP6 energized by three coils.

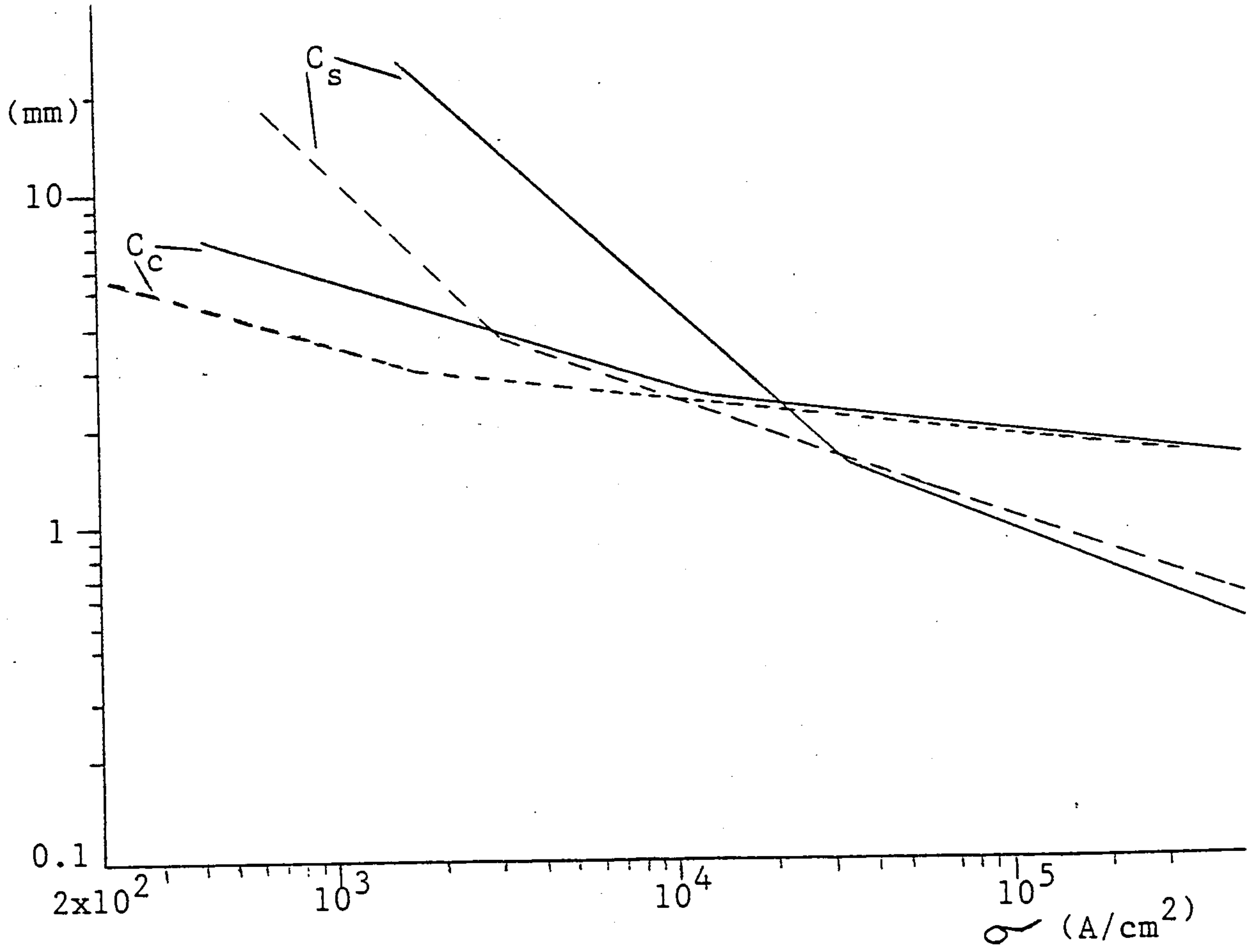

Figure 4.18b A log-log plot of the spherical and chromatic aberration coefficients as function of the current density drawn linearly in figure 4.18a.

Solid lines: family of lenses similar to test lens DP2 energizied by a thin flat coil.

Broken lines: family of lenses similar to test lens DP6 energized by three coils.

coefficient C_s of the lenses similar to DP6 is lower than that of the lenses similar to DP2. However, when σ exceeds 35000 A/cm^2, C_s of DP2 is better than that of DP6. Although the halfwidth W of the DP2 family is less than that of the DP6 family when $\sigma > 20000$ A/cm^2, the flux density B_{centre} at the centre of the air gap of the DP6 family is higher than that of the DP2 family at all current densities. The values of chromatic aberration coeffiecient C_c and the objective focal length f_o of the family of test lenses similar in shape to DP6 are less than those of test lenses similar to DP2 at all values of σ. Therefore, a combination of three superconducting coils similar to those of test lens DP6 is a favourable coil arrangement at current densities less than 35000 A/cm^2. Such arrangement of energizing coils should be applicable to both spherical and flat ended polepiece shapes.

Figure 4.18b shows that there is progressive improvement in C_s and C_c with increasing σ. However, the improvement may not be worthwhile in practice for current densities greater than about 10^5 A/cm^2. At high current densities, it is seen that the improvement in C_c is not sensitive to coil arrangement; C_c improves as $\sigma^{-0.12}$. However, C_s is slightly affected by the coil arrangement. For lenses similar in shape to test lens DP2, C_s improves as $\sigma^{-0.4}$ and for lenses similar in shape to test lens DP6, C_s improves as $\sigma^{-0.35}$.

Figure 4.18b also shows that as σ exceeds 10^4 A/cm^2 the improvement in C_s is better in lenses similar to DP2 energized by a thin flat coil. It should be noted, however, computations carried out on thin flat iron-free coil (figure 4.10) have shown that C_s and C_c improve at a constant rate as $\sigma^{-0.5}$. Therefore, the iron-free coil can in principle provide lower aberration coefficients at very high current densities than are possible with a combination of iron polepiece and energizing coil.

4.7 IMPROVED DESIGN OF SATURATED DOUBLE POLEPIECE LENSES

Figure 4.19a shows three test lenses in cross-section designed to work at 1 MV accelerating voltage (V_r = 2000 kV) in the telescopic mode ($z_F = 0$) and the same current density (σ = 15000 A/cm^2). The corresponding axial flux densities are shown in figure 4.19b. The three lenses are characterized by a spherical polepiece joined to a cone. Lens DP2 has a gap of 6.9 mm, bore diameter 0.9 mm and a radius of curvature of the polepiece 12.9 mm; lens DP6 has a gap of 3 mm, bore diameter 0.4 mm and a radius of curvature of the polepiece 5.7 mm; whereas lens DPH (Yin 1985) has a gap of 4.3 mm, bore diameter 2.1 mm and a radius of curvature of 32 mm. The cross-sections of the exciting coils are approximately the same.

Lens DPH was designed towards the end of the investigation making full use of the experience gained with the design of lens DP2. The actual computations were carried out by Mrs H. C. Yin in collaboration with the author and another colleague Mrs K. Tahir. The author is grateful to Mrs Yin for agreeing to allow her calculations to appear here before any other publication.

It is seen from figure 4.19b that the field of the test lens similar to DPH is characterized by the desired properties of high peak flux density and narrow width. Although the axial field of the lens similar in shape to DP2 is of high peak flux density, it however broadens considerably. This field broadening leads to offset the

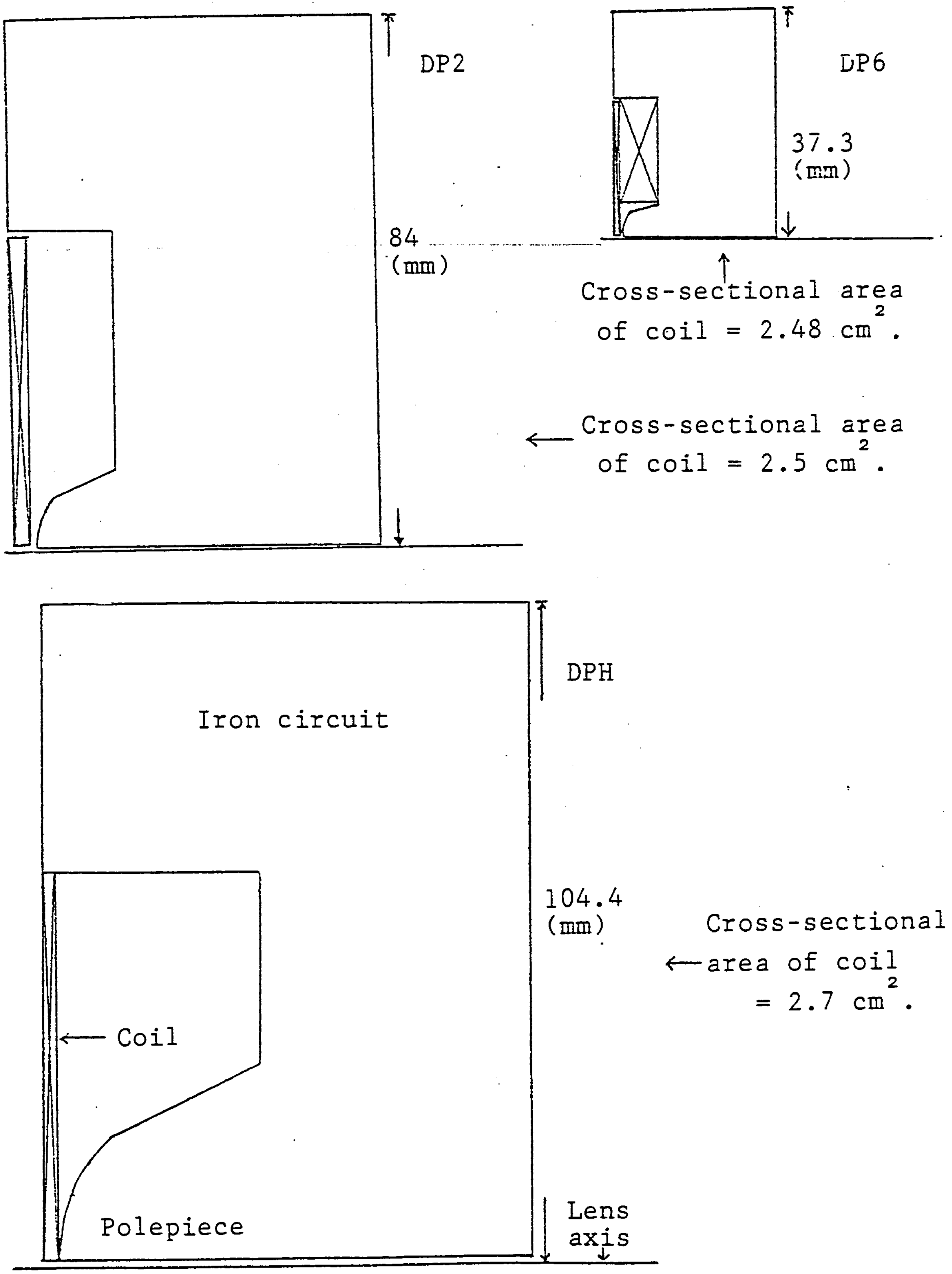

Figure 4.19a Cross-section of the upper quarter of the three double polepiece test lenses similar in shape to test lenses DP2, DP6 and DPH designed to operate at 1 MV accelerating voltage in the telescopic mode ($z_F = 0$) and the same current density ($\sigma = 15000$ A/cm^2).

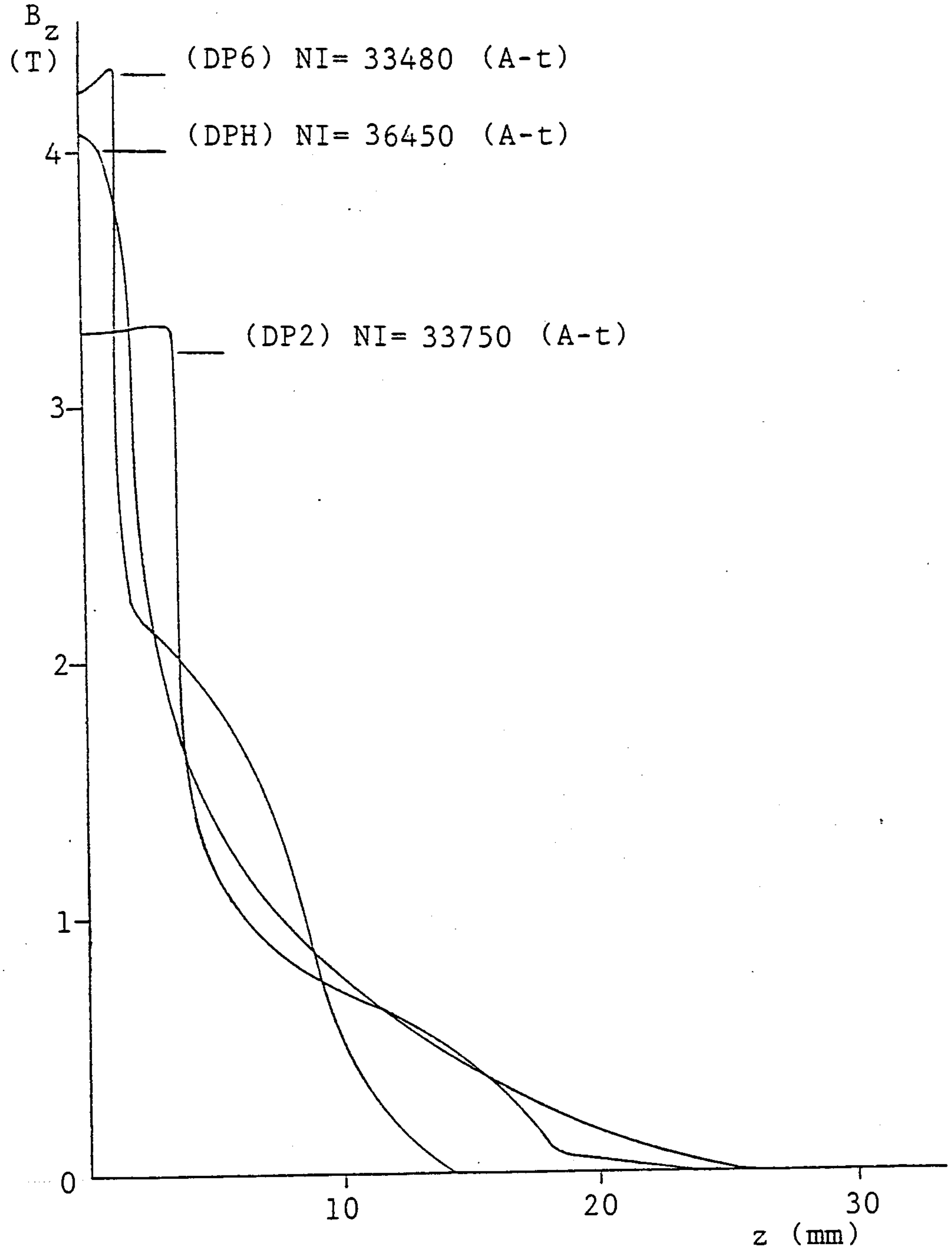

Figure 4.19b Axial flux density distributions of the three double polepiece test lenses shown in figure 4.19a operated at the same current density σ of 15000 A/cm^2. Only the positive half of the axial magnetic fields is shown.

advantages of the high peak flux density by increasing the aberration coefficients. The small size of test lens DP6 led to high peak and narrow halfwidth.

Figure 4.20a shows a log-log plot of the spherical aberration coefficients of three families of test lenses similar in shape to those of DP2, DP6 and DPH as functions of the current density σ. Figure 4.20b shows a log-log plot of the chromatic aberration coefficients of three families of lenses similar in shape to those of DP2, DP6 and DPH as functions of the current density σ. This kind of plot shows the variation of the above coefficients more clearly than a linear plot can. It is seen that both the spherical C_s and chromatic C_c aberration coefficients of the three families of lenses decrease with increasing σ. However, the family of test lens DPH has the lowest spherical aberration coefficient. Interestingly it also has the lowest chromatic aberration coefficient at low σ. The family of test lens DP2 has the highest spherical aberration coefficient at low σ. The difference in aberration coefficients between the various curves tend to get less with increasing σ. At high current densities the aberration coefficients of the families of test lenses DP2 and DP6 improve considerably with increasing σ; those of the family of DPH, on the other hand are not so sensitive to the effect of σ. This indicates that the polepiece dimensions and design are critical in lenses operating at high flux density, even for chromatic aberration.

The dashed lines in figures 4.20a and 4.20b designated $(C_s)_{DP2}$, $(C_s)_{DP6}$ and $(C_c)_{DP2}$, $(C_c)_{DP6}$ respectively show the C_s and C_c of the lenses similar to DP2 and DP6. The values

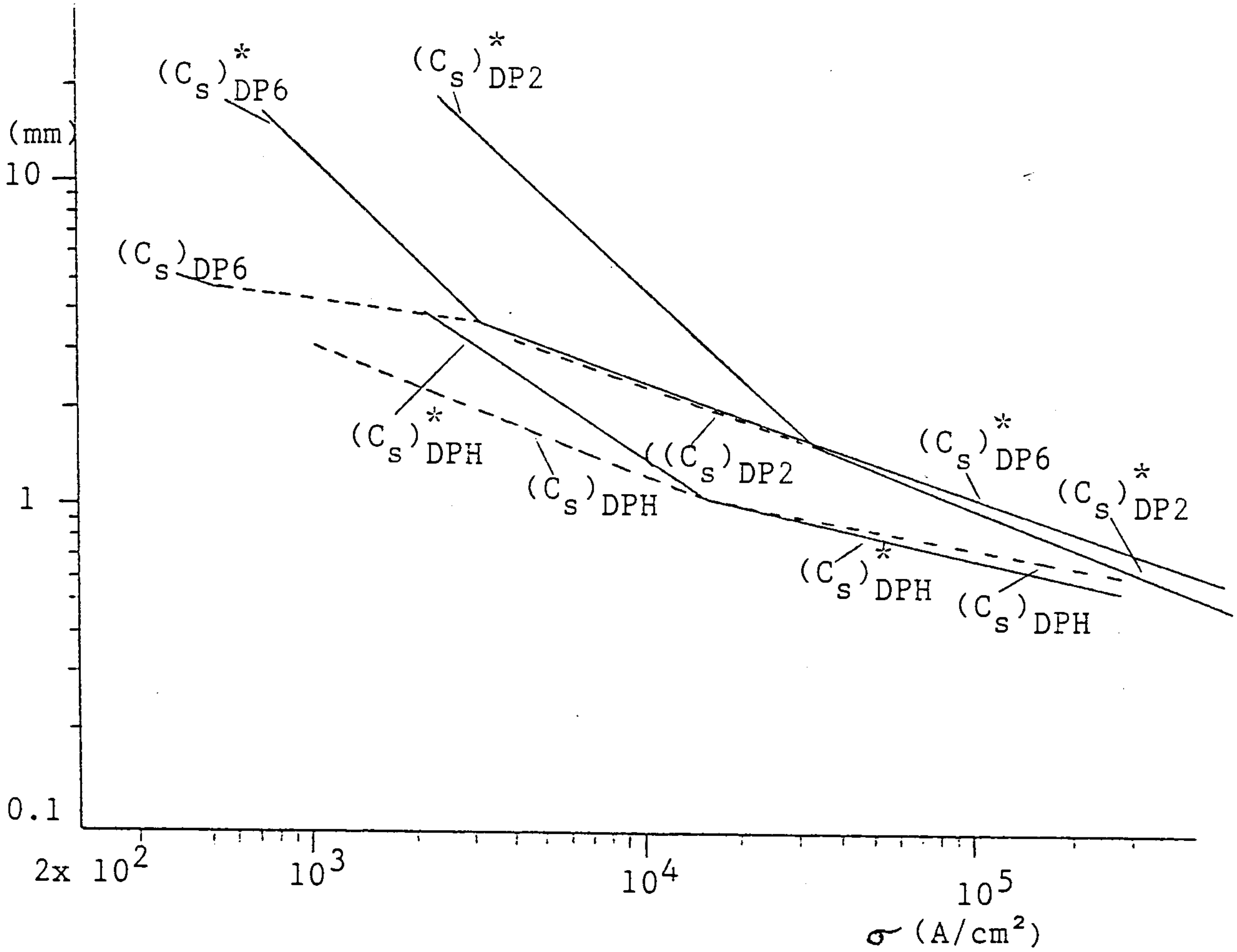

Figure 4.20a The spherical aberration coefficient C_s of three families of 1 MV condenser-objective symmetrical double polepiece test lenses, similar in shape to those of DP2, DP6 and DPH, as functions of the current density σ.

$(C_s)^*_{DPH}$ (solid line) spherical aberration coefficient of DPH family with zero-bore,

$(C_s)_{DPH}$ (dashed line) spherical aberration coefficient of DPH family with S/D = 2 (large bore),

$(C_s)^*_{DP2}$ and $(C_s)^*_{DP6}$ (solid lines) spherical aberration coefficients of DP2 and DP6 families respectively with very small bore,

$(C_s)_{DP2}$ and $(C_s)_{DP6}$ (dashed lines) spherical aberration coefficients of DP2 and DP6 families respectively estimated from the limiting values for lenses of S/D = 1 given by Fert and Durandeau (1967).

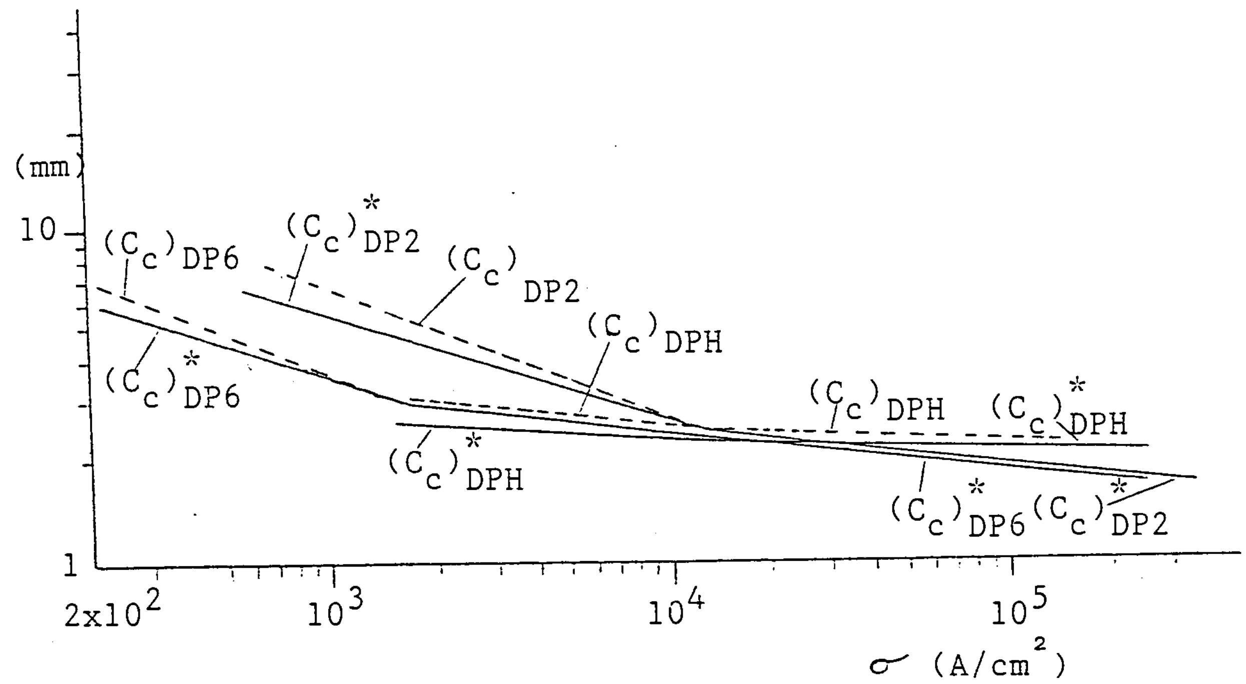

Figure 20b The chromatic aberration coefficient C_c of three families of 1 MV condenser-objective symmetrical double polepiece lenses, similar in shape to those of DP2, DP6 and DPH, as functions of the current density σ.

$(C_c)^*_{DPH}$ (solid line) chromatic aberration coefficient of DPH family with zero-bore,

$(C_c)_{DPH}$ (dashed line) chromatic aberration coefficient of DPH family with S/D = 2 (large bore),

$(C_c)^*_{DP2}$ and $(C_c)^*_{DP6}$ (solid lines) chromatic aberration coefficients of DP2 and DP6 families respectively with very small bore,

$(C_c)_{DP2}$ and $(C_c)_{DP6}$ (dashed line) chromatic aberration coefficients of DP2 and DP6 families respectively estimated from the limiting values for lenses of S/D = 1 given by Fert and Durandeau (1967).

are estimated from the limiting values for lenses of $S/D = 1$ given by Fert and Durandeau (1967). These curves show the considerable improvement , at low values of σ , in C_s in the presence of a large bore; however C_c is thereby slightly increased.

It can readily be seen from figures 4.19a and 4.19b why lens DPH is superior in performance. The relatively thicker outer casing ensures the minimum loss of excitation in the external iron circuit. In addition the spherical part of the polepiece is continued for about five gap widths away from the poleface before merging into the conical part. In addition, for a given inner bore diameter, the ratio d_2/d_1 of the coil is greater than in lens DP2 or DP6. Lenses DP2 and DP6 suffer from several defects. The radius of the spherical tip seems to be too low in relation to the gap width S. This defect is accentuated by the premature terminating of the sphere where it joins the conical part of the polepiece. In spite of all these short comings, however, their performance is quite reasonable at high current densities where the chromatic aberration coefficient of both lenses becomes smaller than that of DPH. This is due to the shape of their field distribution (figure 4.19b) which becomes too much like a square top field and hence producing small chromatic aberration and relatively high spherical aberration. Nevertheless, they cannot be recommended as a serious design since they have no advantages over the lens DPH so far as the spherical aberration is concerned. The high peak and the narrow width of the field (hence small aberrations) of the lens similar to DPH means that there is no need to operate this lens at high current densities as it is essential for the lenses similar to DP2 and DP6 in order to achieve low aberrations.

In order to improve the field of the DP2 and DP6 type of lenses, the taper angle of the polepiece should be increased to 60° to add more iron and hence avoid high flux densities in the inside parts of the polepiece which cause the field broadening and the considerable waste of ampere-turns at the expense of the peak region in the air gap. Therefore, in designing lenses it is important to check the flux density distribution in the polepiece region and to vary the polepiece shape, including the bore diameter to be sure that an optimum has been achieved. Since the optimum S/D ratio of the polepieces varies, albeit slowly, with the value of σ it is advisable to check the design at low values of σ (high permeability region) and at high values of σ (low permeability region). It is fortunate that the optimum design is not very sensitive to small variation of its parameters, so it is worth while to spend some effort in finding this optimum.

5. CONCLUSION

With the aid of the computer programs of Munro and Lencová it appears that, by carefully choosing the number and layout of meshes in the finite element method, it is possible to investigate computationally the design of conventional and unconventional lenses with sufficient accuracy for design purposes well before fabrication for experimental confirmation.

In iron-shrouded lenses, it was found that eliminating flux leakage in the external lens shell, was as important as the design of the polepieces themselves. The iron shroud of saturated polepiece lenses may therefore appear usually thick compared with that of a conventional polepiece lens.

The current density σ that can be supported by the coil windings is, effectively, the chief factor that limits the design and hence the electron-optical properties of magnetic lenses. The electron-optical properties of the lenses investigated showed that for a fixed accelerating voltage and a fixed specimen position, the objective focal properties of the various test lenses improved continuously with increasing current density. The performance of the worst test lenses in fact improved even more rapidly with increasing σ than did the best lenses. It was found that there is no limit to the improvement of a lens except that set by the maximum permissible current density σ in the coil windings. Improvement of a lens is, therefore, largely limited by the technology and engineering of high current density windings. However, the present investigation has shown that although increasing the current density in the coil windings progressively reduces the aberration coefficients, the improvement may not be worthwhile in practice for current densities greater than about 10^5 A/cm^2. The aberration coefficients of magnetic lenses improve with σ^{-n}; the value of n depends on the type of lens. However, since an iron-free coil improves at a constant rate as $\sigma^{-0.5}$ and hence can in principle provide lower aberration coefficients than are possible with an iron polepiece lens since all other iron polepiece lenses improve at not better than $\sigma^{-0.48}$ for saturated single polepiece lenses and $\sigma^{-0.4}$ for saturated double polepiece lenses. Since there are many critical geometrical and physical factors affecting the design of high flux density magnetic lenses for high voltage electron microscopes, the choice of a favourable design would depend on the operational requirements.

The results of this investigation not only prove the possibility of designing magnetic electron lenses capable of yielding high flux densities, low aberrations and high resolution in theory but also give encouragement to the possibility of building in practice objective lenses of sizes much smaller than the conventional ones so much needed for high voltage and high resolution electron microscopes. It is likely that one can design an entirely new unconventional electron-optical column by computer-aided-design that is greatly superior to conventional columns currently in use.

APPENDIX 1: PUBLICATIONS

(a) 202-206

High flux density single polepiece electron lenses

I S Al-Nakeshli, S M Juma and T Mulvey

Electron Microscopy and Analysis 1983

Edited by P Doig

(Inst. Phys. Conf. Ser. No. 68)

pp 475-478

1984

(b) 207-209

Unconventional saturated objective lenses for high voltage high resolution electron microscopes

I S Al-Nakeshli, S M Juma and T Mulvey

Electron Microscopy 1984 vol. 1

Editors: A' Csanády, P Röhlich and D Szabo'

(Budapest: Programme Committee of the Eighth European Congress on Electron Microscopy)

pp 21-22

1984

(c) 210-214

Computations on the electron-optical parameters of saturated objective lenses

I S Al-Nakeshli and S M Juma

Electron Microscopy and Analysis 1985

Edited by G T Tatlock

(Inst. Phys. Conf. Ser. No. 78)

pp 125-8

1986

Electron Microscopy and Analysis, 1983

Proceedings of The Institute of Physics Electron Microscopy and Analysis Group conference held at the University of Guildford, 30 August–2 September 1983 (EMAG 83)

Edited by P Doig

Conference Series Number 68

The Institute of Physics
Bristol and London

ELECTRON MICROSCOPY 1984

VOLUME 1

INSTRUMENTATION
PHYSICS AND MATERIALS SCIENCE
APPLICATIONS I

Proceedings of the

EIGHTH EUROPEAN CONGRESS
on
ELECTRON MICROSCOPY

Budapest, Hungary
August 13—18, 1984

Editors: Á. Csanády, P. Röhlich and D. Szabó

Published by the Programme Committee of the Eighth European
Congress on Electron Microscopy

Budapest, 1984

Electron Microscopy and Analysis, 1985

Proceedings of The Institute of Physics Electron Microscopy and Analysis Group conference held at the University of Newcastle upon Tyne, 2–5 September 1985 (EMAG 85)

Edited by G J Tatlock

Institute of Physics Conference Series Number 78
Adam Hilger Ltd, Bristol and Boston

APPENDIX 2: COMPUTATION IN PROGRAM M21

The method used for Program M21 is as follows. The paraxial electron trajectories r(z) are computed numerically, using a fourth-order Runge-Kutta formula to integrate the paraxial ray equation

$$r'' + \frac{\eta}{8V_r} B_z^2 r = 0 \qquad (A2.1)$$

where η is the ratio of charge to rest-mass of the electron and the primes denote the differentiation of r with respect to z. The paraxial ray equation gives a solution for a constant magnetic field in an interval of small width. The spherical and chromatic aberration coefficients, referred to the object plane z_o or the image plane z_i, are computed numerically by using Simpson's rule to evaluate the following aberration integrals

$$C_s = \frac{\eta}{128V_r} \int_{z_o}^{z_i} [\frac{3\eta}{V_r} B_z^4 r_\alpha^4(z) + 8B_z'^2 r_\alpha^4(z) - 8B_z^2 r_\alpha^2(z) r_\alpha'^2(z)] dz \qquad (A2.2)$$

$$C_c = \frac{\eta}{8V_r} \int_{z_o}^{z_i} B_z^2 r_\alpha^2(z) dz \qquad (A2.3)$$

where $r_\alpha(z)$ is the solution of the paraxial ray equation with initial conditions $r_\alpha(z_o) = 0$ and $r_\alpha'(z_o) = 1$ if the aberration coefficients are referred to z_o, or $r_\alpha(z_i) = 0$ and $r_\alpha'(z_i) = -1$ if the aberration coefficients are referred to z_i. For low or high magnification conditions, the magnification is calculated from the formula $M_o = \alpha_o/\alpha_i$ where α_o and α_i are the convergence angles of the trajectory at z_o and z_i respectively. The output produced by Program M21 is a table of the computed objective properties.

APPENDIX 3: POSSIBLE LAYOUTS OF MESH DISTRIBUTION FOR FIGURE 2.12 (LENS SP7, CHAPTER 3)

Mesh layout for a single polepiece lens with a spherical tip on a conical polepiece.

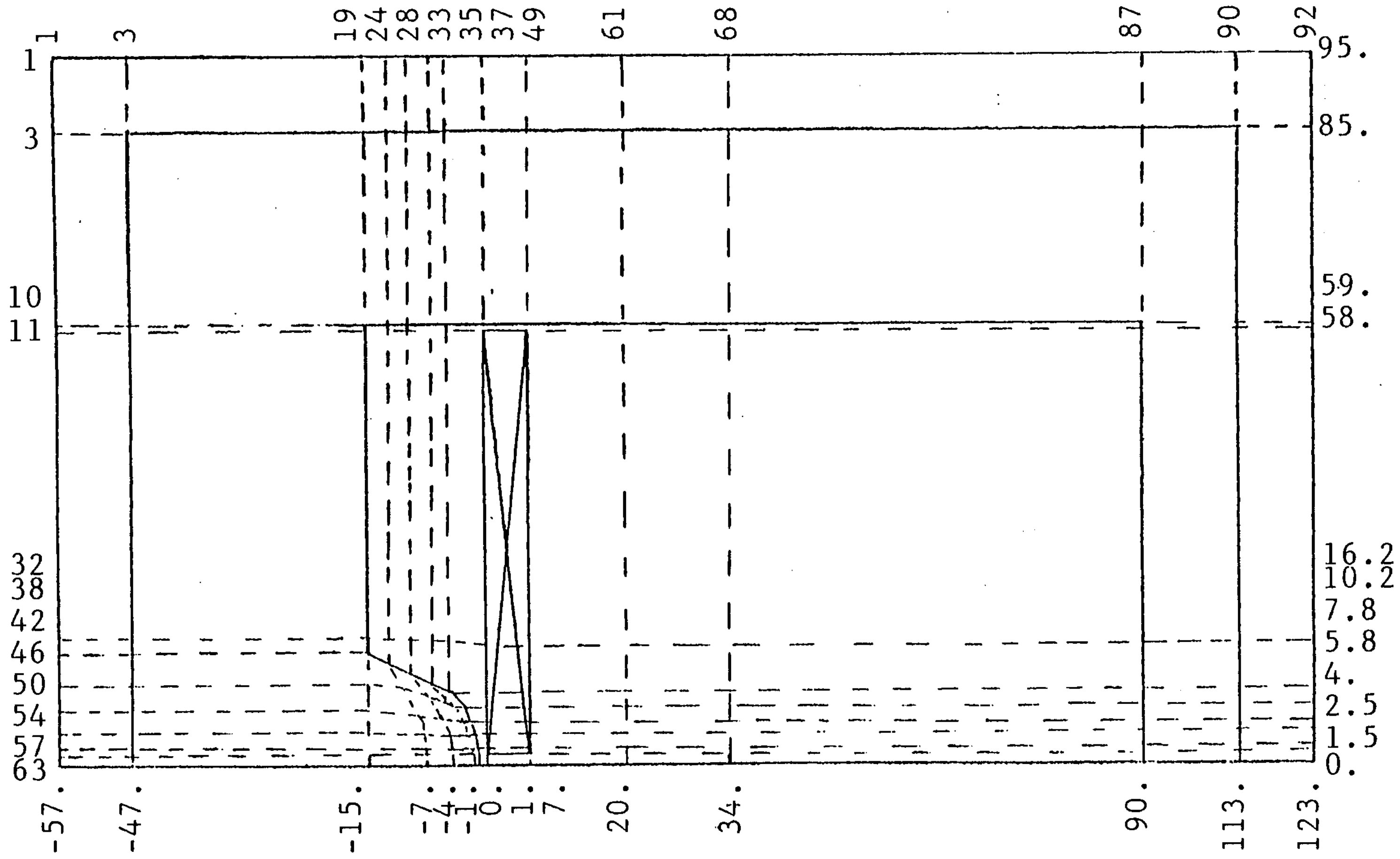

Alternative mesh layout for a single polepiece lens in which the conical polepiece and its spherical end is replaced by a series of steps (staircase) to permit a rectangular mesh to be used.

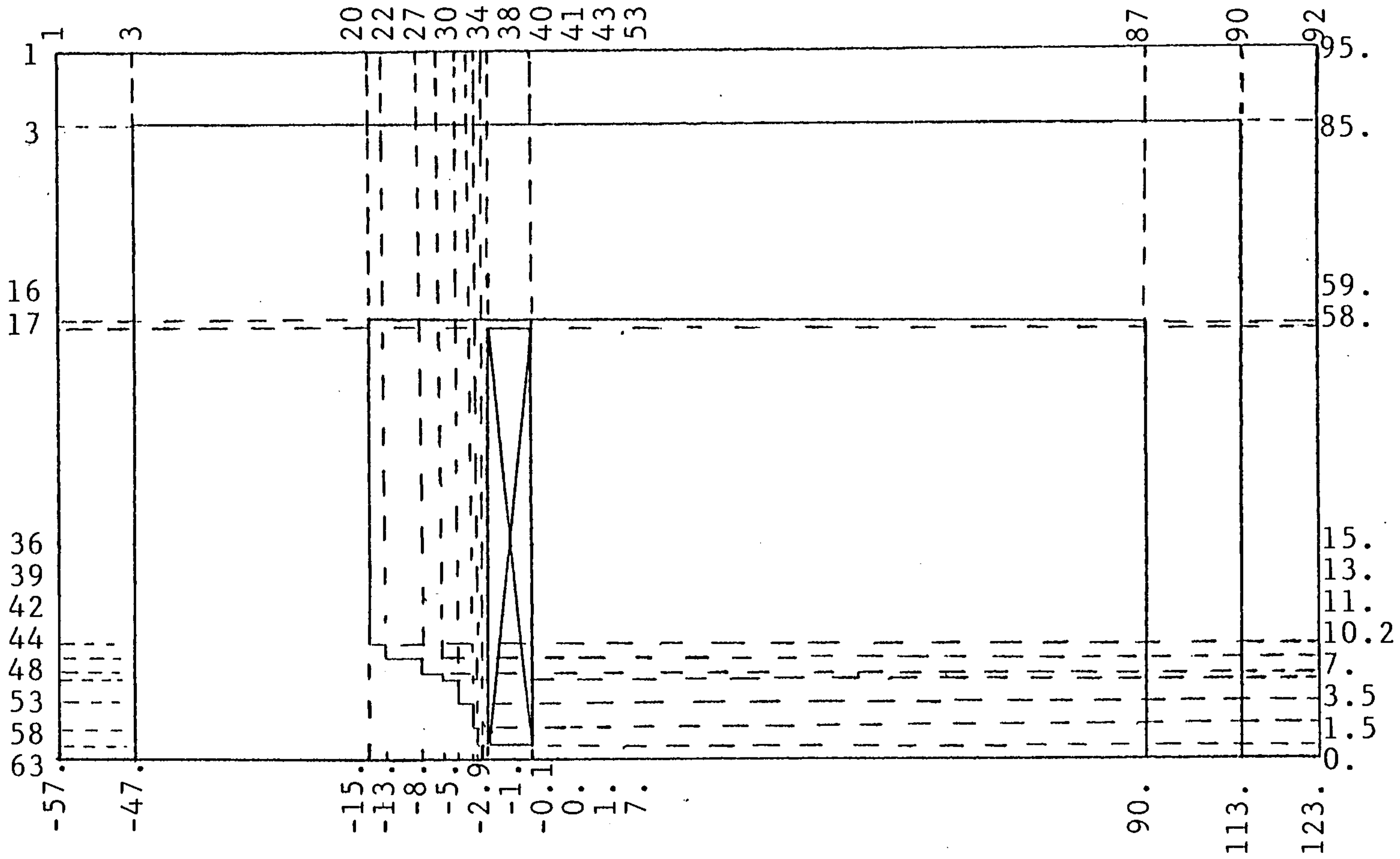

REFERENCES

Al-Hilly S M and Mulvey T 1982 Wide-angle projector systems for the TEM
Electron Microscopy and Analysis 1981 ed. M J Goringe (Inst. Phys. Conf. Ser. No. 61) pp 103-6

Al-Nakeshli I S and Juma S M 1986 Computations on the electron-optical parameters of saturated objective lenses
Electron Microscopy and Analysis 1985 ed. G T Tatlock (Inst. Phys. Conf. Ser. No. 78) pp 125-8

Al-Nakeshli I S, Juma S M and Mulvey T 1984a High flux density single polepiece electron lenses
Electron Microscopy and Analysis 1983 ed. P Doig (Inst. Phys. Conf. Ser. No. 68) pp 475-8

Al-Nakeshli I S, Juma S M and Mulvey T 1984b Unconventional saturated objective lenses for high voltage high resolution electron microscopes
Electron Microscopy 1984 eds. A Scanády, R Röhlich and D Szabó (Programme Committee of the Eighth European Congress on Electron Microscopy, Budapest) pp 21-2

Alshwaikh A A 1979 Magnetic electron lenses based on the uniformly magnetized ellipsoid
PhD Thesis, University of Aston in Birmingham, UK

Alshwaikh A and Mulvey T 1977 The magnetised iron sphere, a realistic theoretical model for single-polepiece lenses
Electron Microscopy and Analysis 1977 ed. D L Misell (Inst. Phys. Conf. Ser. No. 36) pp 25-8

Bassett R and Mulvey T 1969 Flat helical electron-optical lenses
Z. Angew. Phys. 27 142-5

Cleaver J R A 1978 Some optical characteristics of the saturated symmetrical condenser-objective lens
Optik 49 413-31

Cleaver J R A 1980 The choice of pole piece shape and lens operating mode for magnetic objective lenses with saturated pole pieces
Optik 57 9-34

Dietrich I 1976 Superconducting electron-optic devices
(New York and London: Plenum)

Dietrich I, Fox F, Knapek E, Lefranc G, Nachtrieb K, Weyl R and Zerbst H 1977 Improvements in electron microscopy by application of superconductivity
Ultramicroscopy 2 241-9

Dietrich I, Herrmann K -H and Passow C 1975 A proposal for a high voltage electron microscope with superconducting microwave linear accelerator and superconducting lenses
Optik 42 439-62

Dietrich I, Koller A and Lefranc G 1972 Feldverteilung in eisenfreien supraleitenden Linsen
Optik 35 468-78

Dugas J, Durandeau P and Fert C 1961 Lentilles électroniques magnétiques symétriques et dyssymétriques
Rev. Opt. 40 277-305

Dupouy G 1968 Electron microscopy at very high voltages
Adv. Opt. Electron Micros. 2 167-250

Durandeau P and Fert C 1957 Lentilles électroniques magnétiques
Rev. Opt. 36 205-34

Fert C and Durandeau P 1967 Magnetic electron lenses
Focusing of Charged Particles vol. 1 ed. A Septier
(New York: Academic) pp 309-52

Hawkes P W 1972 Electron Optics and Electron Microscopy
(London: Taylor and Francis)

Hawkes P W and Valdré U 1977 Superconductivity and electron microscopy
J. Phys. E: Sci. Instrum. 10 309-28

Hill R and Smith K C A 1982 The single-pole lens as a scanning electron microscope objective
Scanning Electron Microscopy 1982 Part II ed. O Johari
(Chicago: IITRI) pp 465-71

Juma S M, Al-Nakeshli I S and Khaliq M A A 1983a Pole design in single pole piece projector electron lenses
J. Phys. E: Sci. Instrum. 16 171-6

Juma S M, Khaliq M A and Antar F H 1983b Some properties of single pole piece objective electron lenses
J. Phys. E: Sci. Instrum. 16 1063-8

Juma S M and Yahya A A 1984 Characteristics of the axial magnetic field of asymmetrical electron lenses
J. Phys. E: Sci. Instrum. 17 398-404

Kamminga W 1976 Properties of magnetic objective lenses with highly saturated pole pieces
Optik 45 39-54

Kamminga W, Verster J L and Francken J C 1968/69 Design consideration for magnetic objective lenses with unsaturated pole pieces
Optik 28 442-61

Kasper E 1982 Magnetic field calculation and the determination of electron trajectories
Magnetic Electron Lenses ed. P W Hawkes (Berlin: Springer) pp 57-118

Kunath W, Riecke W D and Ruska E 1966 Spherical aberration of saturated strong objective lenses
Electron Microscopy 1966 vol. 1 ed. R Uyeda (Tokyo: Maruzen) pp 139-40

Lefranc G, Knapek E and Dietrich I 1982 Superconducting lens design
Ultramicroscopy 10 111-24

Lenc M and Lencova' B 1984 Saturated single polepiece objective lenses
Electron Microscopy 1984 eds. A Csanády, R Röhlich and D Szabo' (Programme Committee of the Eighth European Congress on Electron Microscopy, Budapest) pp 27-8

Lencova' B 1977 On the use of finite element method for the computation of electron optical elements
Proc. VI Int. Conf. Magnet Technology, Brotislava pp 813-9

Lencova' B 1984 Program AMAG
Private communication, Czechosl. Acad. Sci., Brno

Lencova' B and Lenc M 1984 The computation of open electron lenses by coupled finite element and boundary integral methods
Optik 68 37-60

Lenz F 1982 Properties of electron lenses
Magnetic Electron Lenses ed. P W Hawkes (Berlin: Springer) pp 119-61

Liebmann G 1955a The field distribution in asymmetrical magnetic electron lenses
Proc. Phys. Soc. B 68 679-81

Liebmann G 1955b A unified representation of magnetic electron lens properties
Proc. Phys. Soc. B 68 737-45

Marai F Z 1977 Electron-optical properties of single-pole magnetic electron lenses
PhD Thesis, University of Aston in Birmingham, UK

Mulvey T 1953 The magnetic circuit in electron microscope lenses
Proc. Phys. Soc. B 66 441-7

Mulvey T 1972 Improvements in or relating to magnetic lenses
British Patent Application 40888/72

Mulvey T 1974a Mini-lenses and the SEM
Scanning Electron Microscopy 1974 Part I ed. O Johari
(Chicago: IITRI) pp 43-50

Mulvey T 1974b Imaging systems for conventional electron microscopes
Electron Microscopy 1974 vol. 1 eds. J V Sanders and
D J Goodchild (Canberra: Australian Academy of Sciences)
pp 16-7

Mulvey T 1982 Unconventional lens design
Magnetic Electron Lenses ed. P W Hawkes (Berlin: Springer)
pp 359-412

Mulvey T 1984 Magnetic electron lenses II
Electron Optical Systems for Microscopy, Microanalysis and Microlithography (Proc. 3rd Pfefferkorn Conf.) eds. J J Hren,
F A Lenz, E Munro and P B Sewell (SEM Inc., AMF O'Hare,
Chicago, IL 60666-0507, U.S.A.) pp 15-27

Mulvey T and Nasr H 1981 An improved finite element method for calculating the magnetic field distribution in magnetic electron lenses and electromagnets
Nucl. Instrum. Meth. (Proc. 1st. Conf. on Charged Particle Optics, 1980) ed. H Wollnik (Amsterdam: North Holland Pub. Co.) pp 201-8

Mulvey T and Newman C D 1973 New electron-optical systems for SEM and STEM
Scanning electron microscopy: systems and applications 1973 (Inst. Phys. Conf. Ser. No. 18) pp 16-21

Mulvey T and Newman C D 1974 New experimental lens designs for high voltage electron microscopes
High Voltage Electron Microscopy eds. P R Swann, C J Humphreys and M J Goringe (London: Academic) pp 98-102

Mulvey T and Wallington M J 1973 Electron lenses
Repts. Prog. Phys. 36 347-421

Munro E 1971 Computer-aided-design methods in electron optics
PhD Thesis, University of Cambridge, UK

Munro E 1973 Computer-aided design of electron lenses by the finite element method
Image Processing and Computer-Aided Design in Electron Optics ed. P W Hawkes (London: Academic) pp 284-323

Munro E 1975 A set of computer programs for calculating the properties of electron lenses
University of Cambridge, Department of Engineering Report CUED/B-Elect TR45

Munro E 1976 Some techniques and applications of the finite element method for solving magnetic field problems
Proc. COMPUMAG Conf. on Computation of Magnetic Fields
ed. C W Trowbridge (Rutherford Lab., Chilton, Didcot, Oxon, UK) pp 35-46

Nasr H 1981 A critical assessment of the finite element method for calculating electric and magnetic fields
PhD Thesis, University of Aston in Birmingham, UK

Ozasa S, Sakitani Y, Katagiri S, Kimura H, Sugata E, Fukai K, Fujita E, Fujita H and Ura K 1970 Development of 3 MeV electron microscope column
microscopie électronique 1970, résumés des communications présentées au septième congrès international, Grenoble, ed. P Favard vol. 1 (Société Française de Microscopie Electronique, Paris) pp 123-4

Riecke W D 1962 Ein Kondensorsystem für eine starke objektivlinse
Electron Microscopy vol. 1 ed. S S Breese, Jr (New York and London: Academic) KK-5

Riecke W D 1972 Objective lens design for transmission electron microscopes-A review of the present state of the art
Electron Microscopy 1972 (Inst. Phys. Conf. Ser. No. 14) pp 98-103

Riecke W D 1982 Practical lens design
Magnetic Electron Lenses ed. P W Hawkes (Berlin: Springer) pp 163-357

Riecke W D and Ruska E 1966 A 100 kV transmission electron microscope with single-field condenser objective
Electron Microscopy 1966 vol. 1 ed. R Uyeda (Tokyo: Maruzen) pp 19-20

Ruska E 1962 What is the theoretical resolution limit of the electron microscope and when will it be reached?
Electron Microscopy vol. 1 ed. S S Breese, Jr (New York and London: Academic) A-1

Schiske P 1956 Die untere Grenze des Farbfehlers magnetischer Linsen bei vorgeschriebener Maximalfeldstärke
Optik 13 502-5

Sugata E, Fukai K, Fujita H, Ura K, Tadano B, Kimura H, Katagiri S and Ozasa S 1970 Project for construction and application of 3 MeV electron microscope
microscopie électronique 1970, résumés des communications présentées au septième congrès international, Grenoble, ed. P Favard vol. 1 (Société Française de Microscopie Electronique, Paris) pp 121-2

Tahir K 1985 A critical assessment of the finite element method for calculating magnetic fields in electron optics
PhD Thesis, Aston University, UK

Thomson, Sir William (Lord Kelvin) 1872 Reprints of papers on electrostatics and magnetism
(London: MacMillan) esp. p. 564

Tsuno K and Harada Y 1983 Design procedure for a high resolution electron microscope objective lens
J. Electron Microsc. 32 289-98

Tsuno K and Honda T 1983 Magnetic field distribution and optical properties of asymmetrical objective lenses for an atomic resolution high voltage electron microscope
Optik 64 367-78

Yin H C 1985 Improvement of the resolution of double polepiece lenses energized by low current density coil
Private Communication, Mathematics and Physics Department, Aston University